TRANSCEND

Transformative Science and Engineering for Nuclear Decommissioning

Combining electro-kinetic remediation with colloidal silica grouting in radioactively contaminated soils

Dr Arianna Gea Pagano, University of Strathclyde

Theme 2 – Site decommissioning and remediation

01/11/2022
Glasgow

Energy
For a Low Carbon Future

TRANSCEND

Transformative Science and Engineering for Nuclear Decommissioning

University of Strathclyde Glasgow

Prof Becky Lunn

Dr Grainne El Mountassir

Dr Arianna Gea Pagano

University of Southampton

Prof Andy Cundy

Dr Frances Burrell

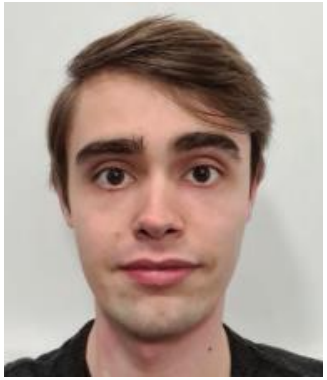

Shaun Hemming

What is colloidal silica?

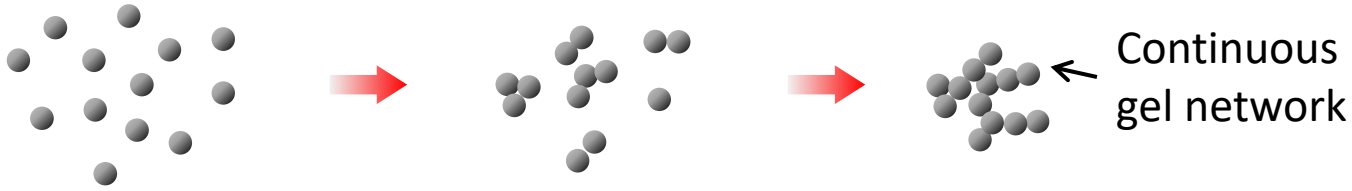

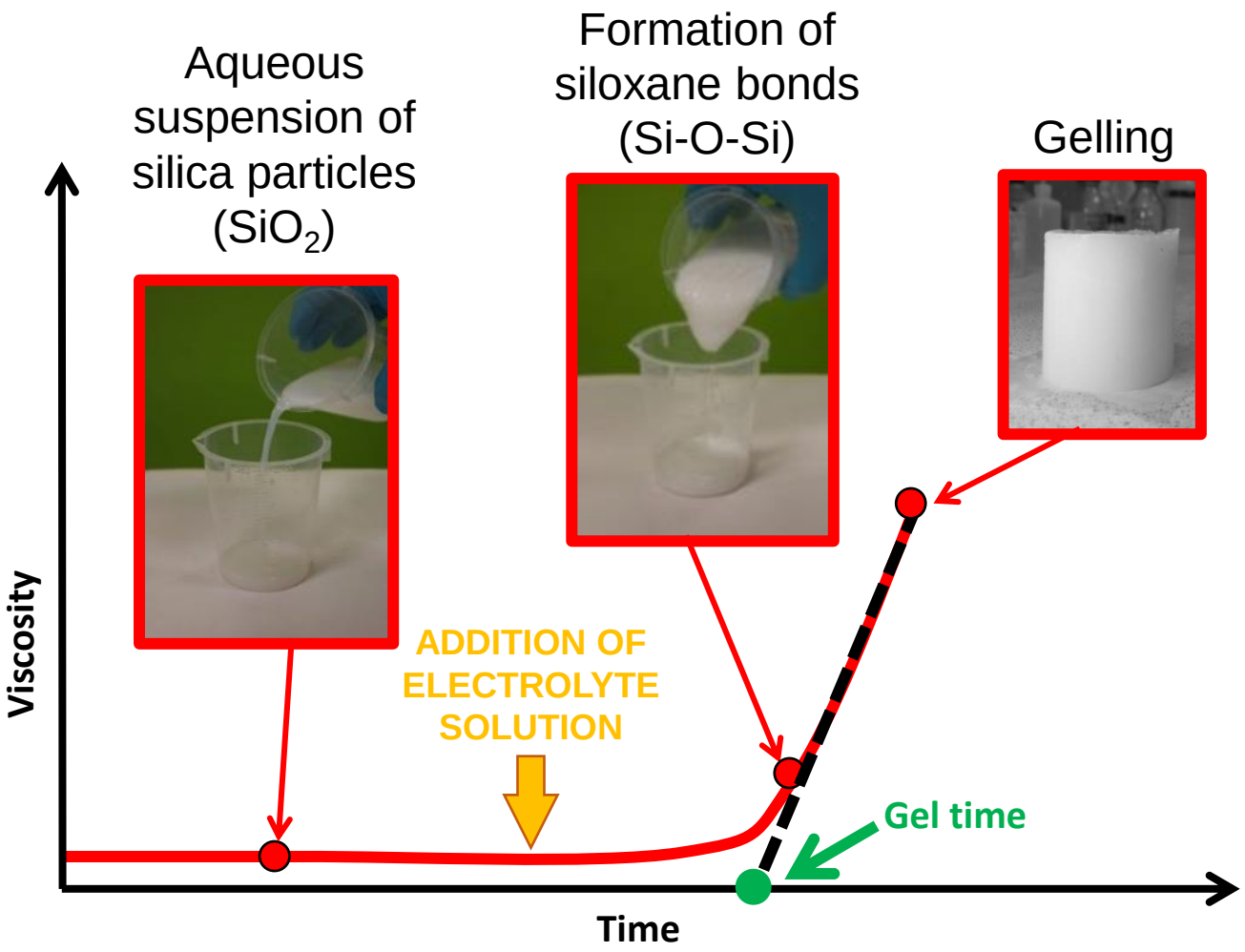

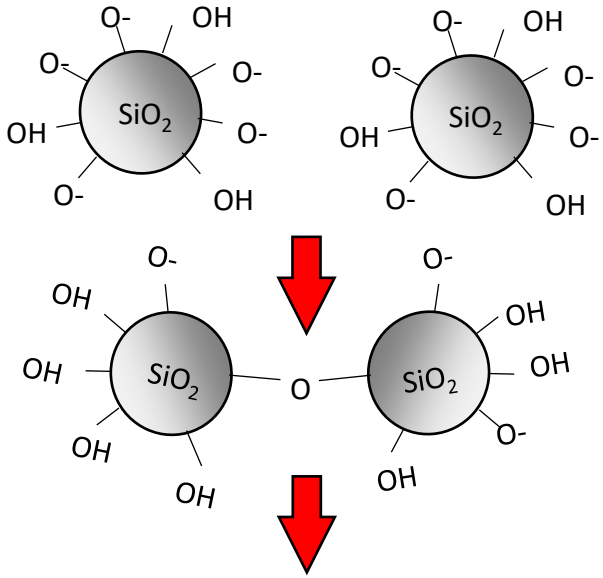

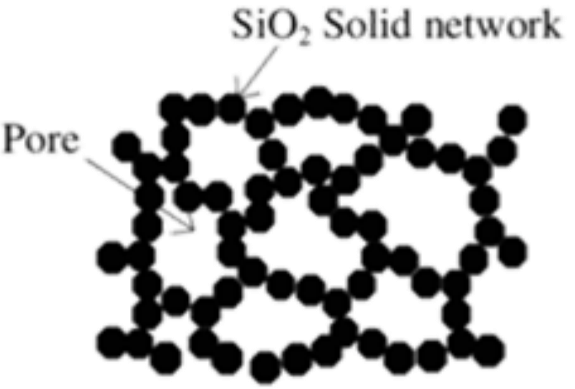

Soil grouting with colloidal silica

- Turns loose soil into ‘cohesive’ soil
- The grout gains strength overtime as the gelation process evolves -> grouted soils gain strength overtime
- Lowers soil permeability (gel permeability: 10^{-17} to 10^{-18} m^2)
- Enhances sorption capacity -> beneficial effect towards radionuclide retention

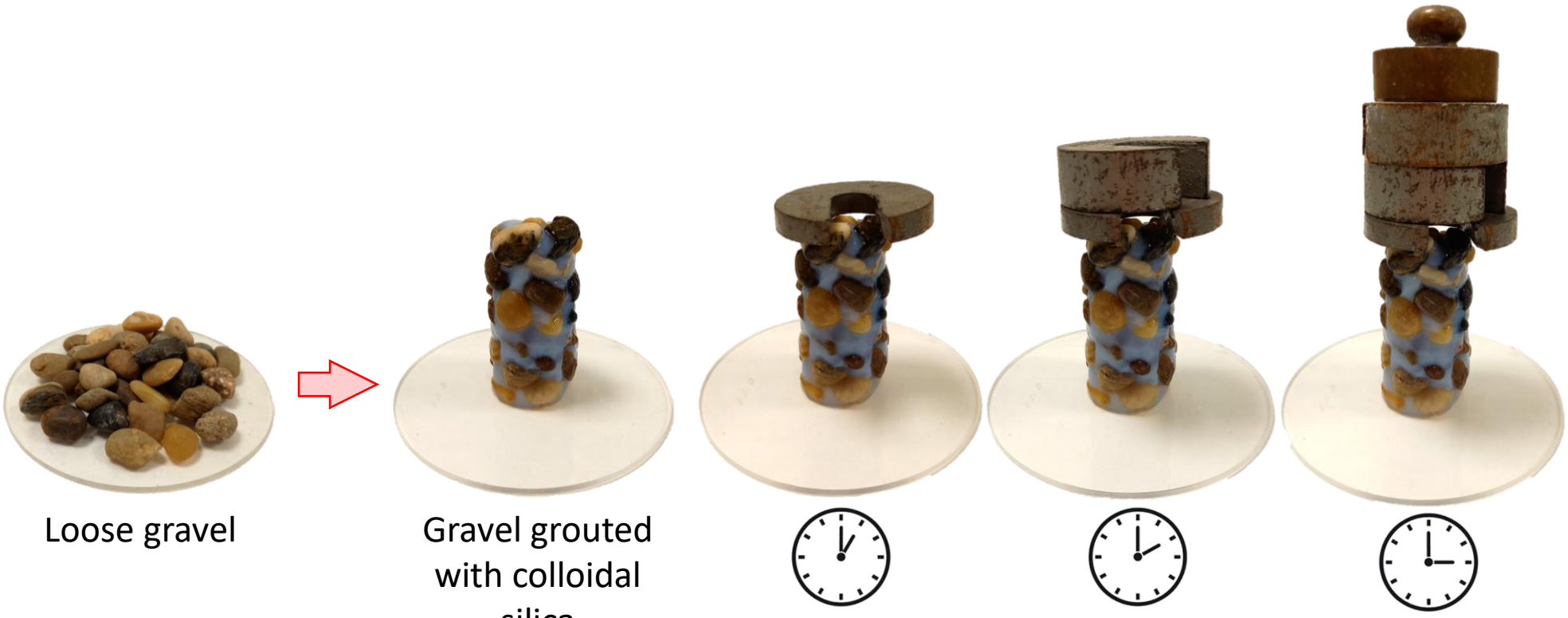

Loose gravel

Gravel grouted with colloidal silica

Soil grouting with colloidal silica

- Turns loose soil into ‘cohesive’ soil
- The grout gains strength overtime as the gelation process evolves -> grouted soils gain strength overtime
- Lowers soil permeability (gel permeability: 10^{-17} to 10^{-18} m^2)
- Enhances sorption capacity -> beneficial effect towards radionuclide retention

Colloidal silica grout is a promising material for nuclear decommissioning application

Electro Kinetic Remediation (EKR) of radioactively contaminated soils

Electro-kinetic remediation: remediation technique using a low-voltage, direct-current electric field applied across a section of contaminated soil to move contaminants.

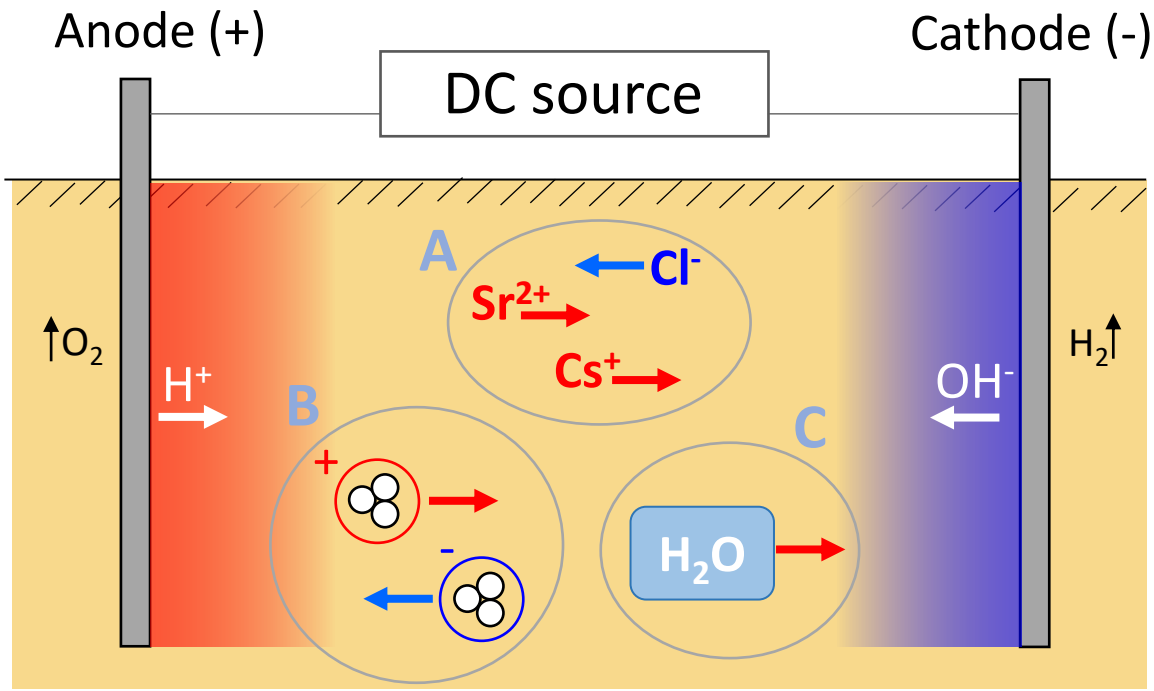

A: Electro-migration

B: Electrophoresis

C: Electro-osmosis

Electro Kinetic Remediation (EKR) of radioactively contaminated soils grouted with colloidal silica

'Purge & trap' concept

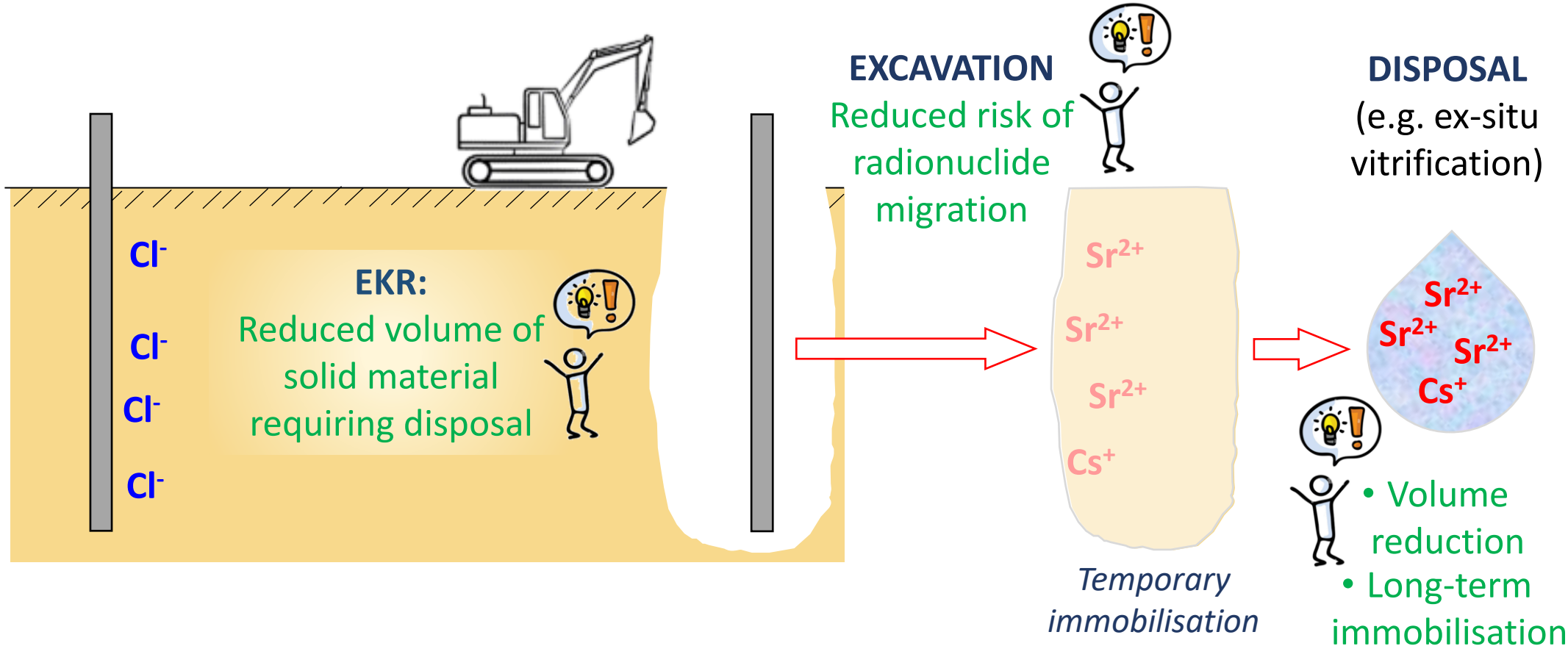

Experimental trials

Electrokinetic cells

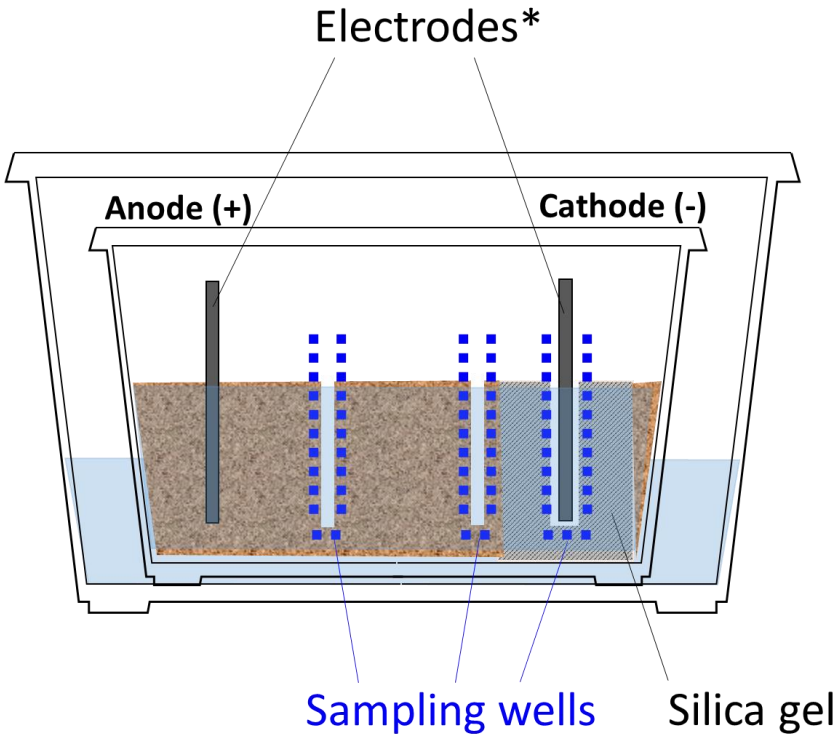

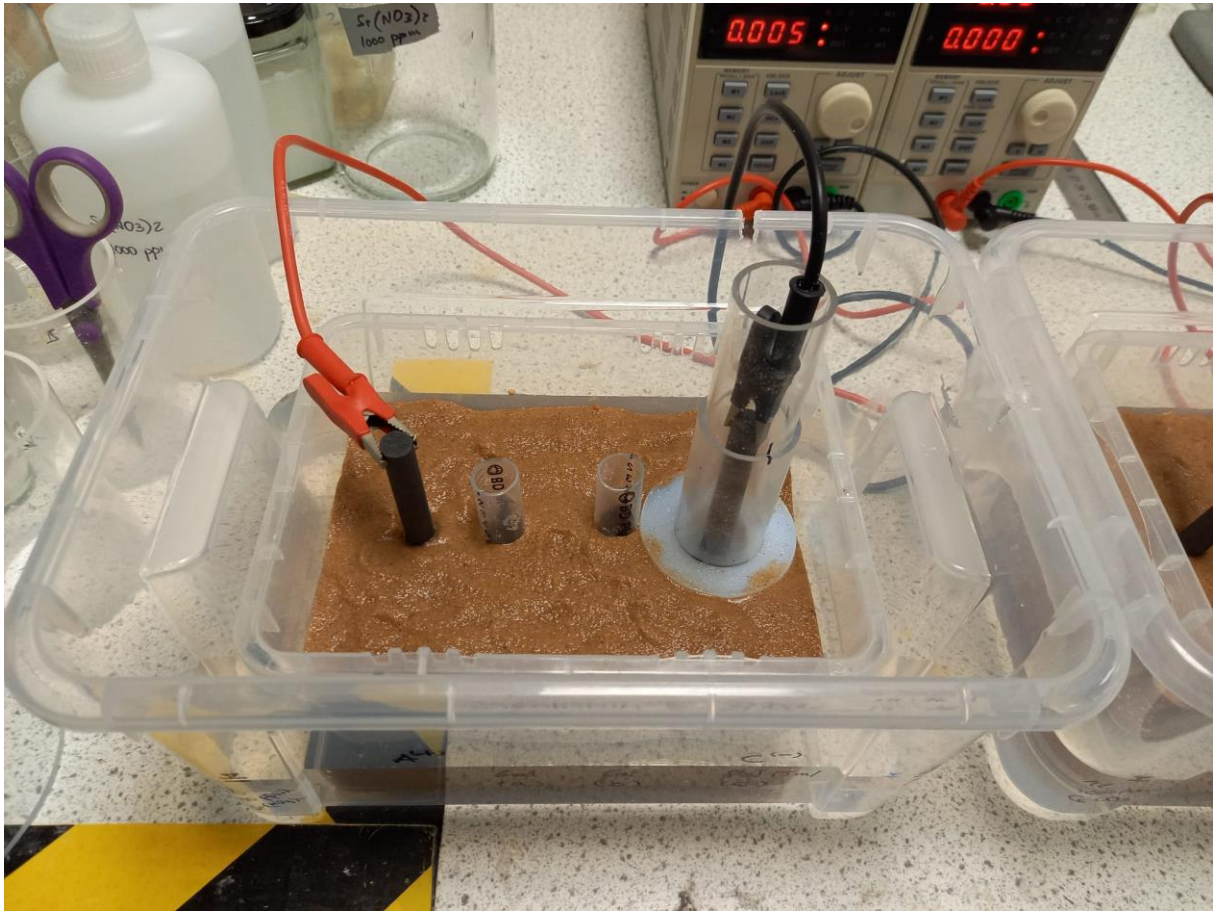

Experimental trials (1)

Electrokinetic cells

1. Strontium-contaminated soils

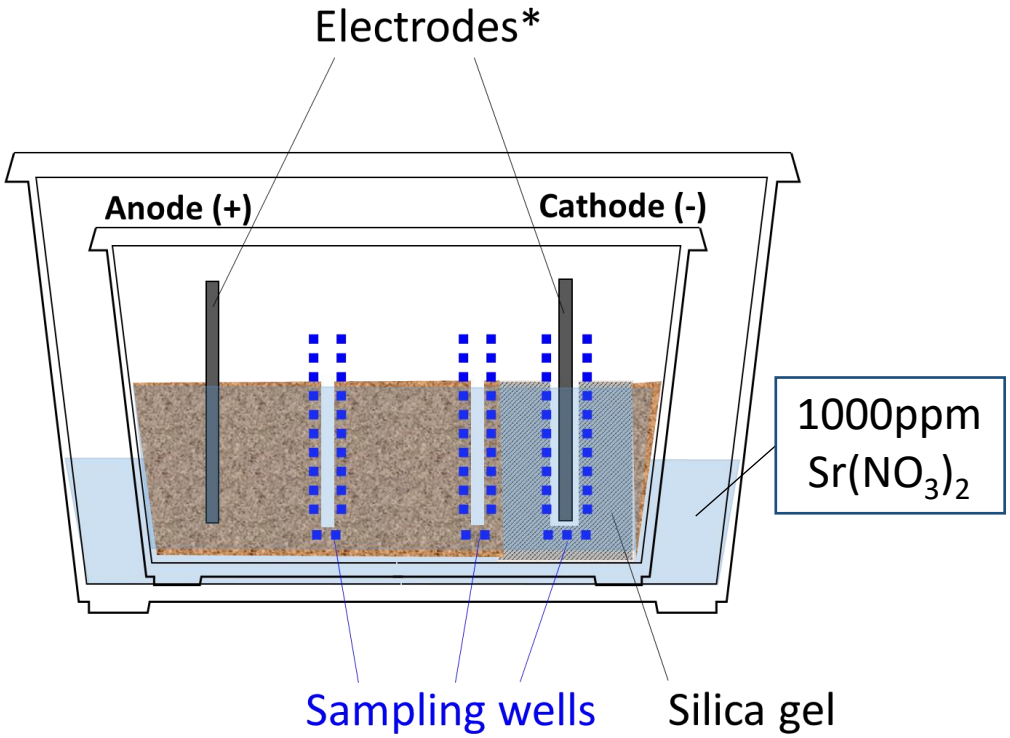

2. Caesium-contaminated soil

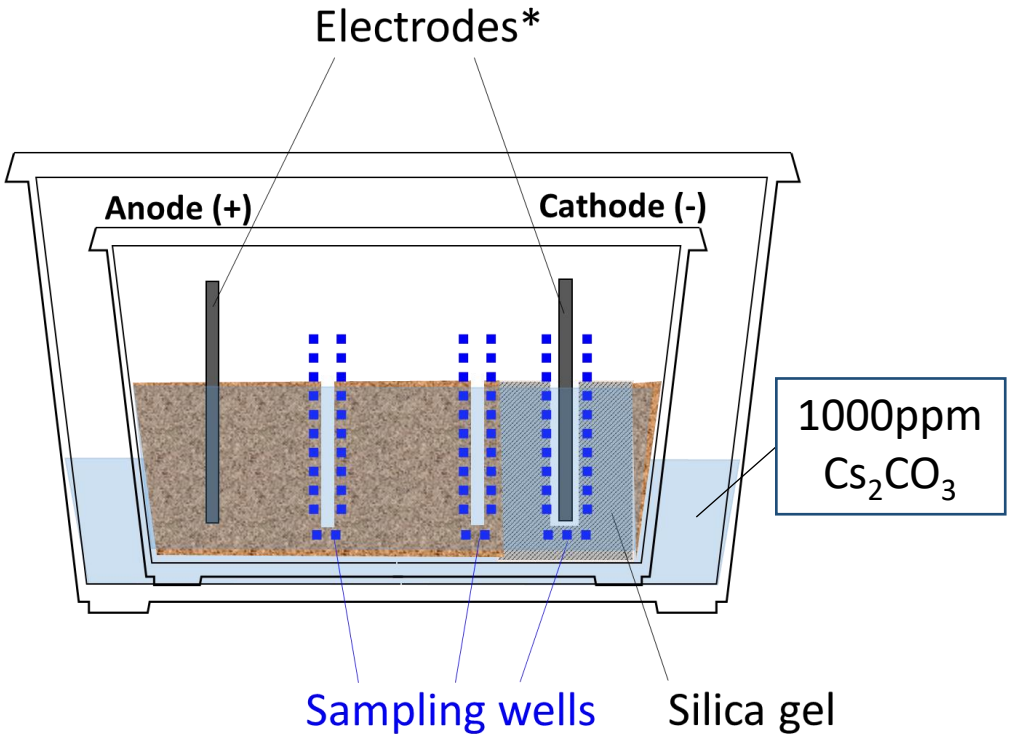

*EKR run for 4 days (**96 hours**) at **1 V/cm**

Experimental trials (1)

Sampling procedure

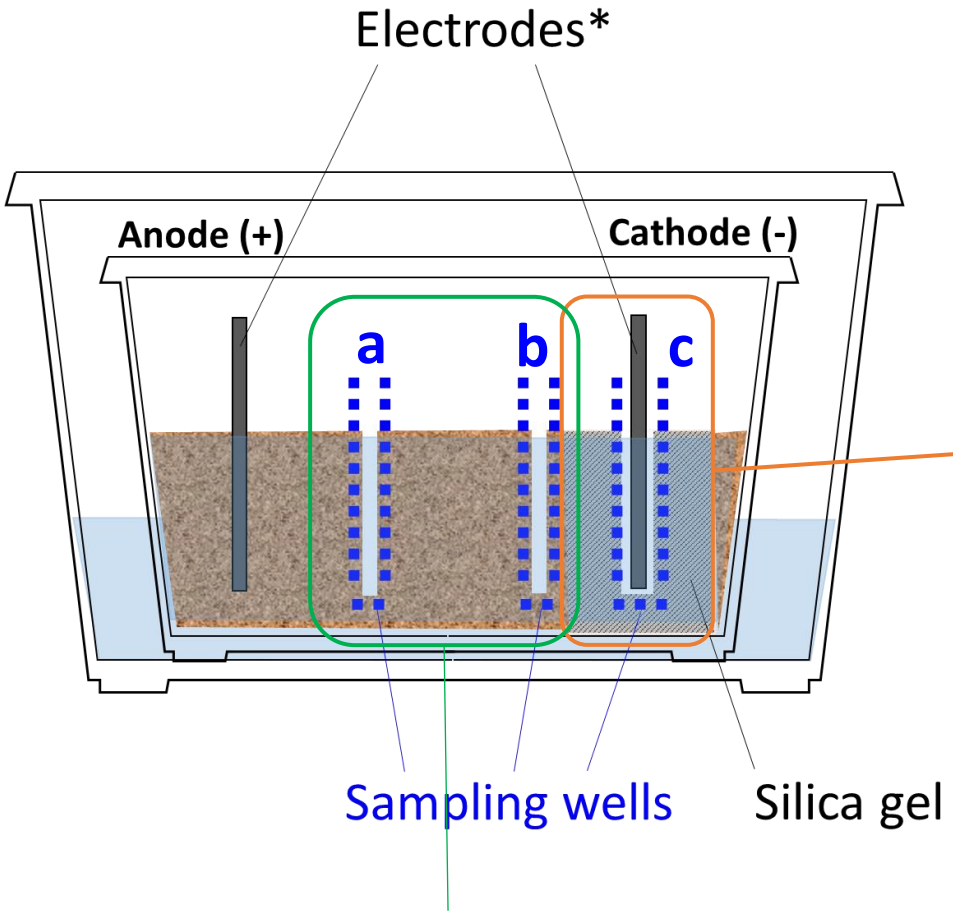

Sampling well 'a' and 'b':

Whole volume sampled once after 96 hours

Sampling well 'c'

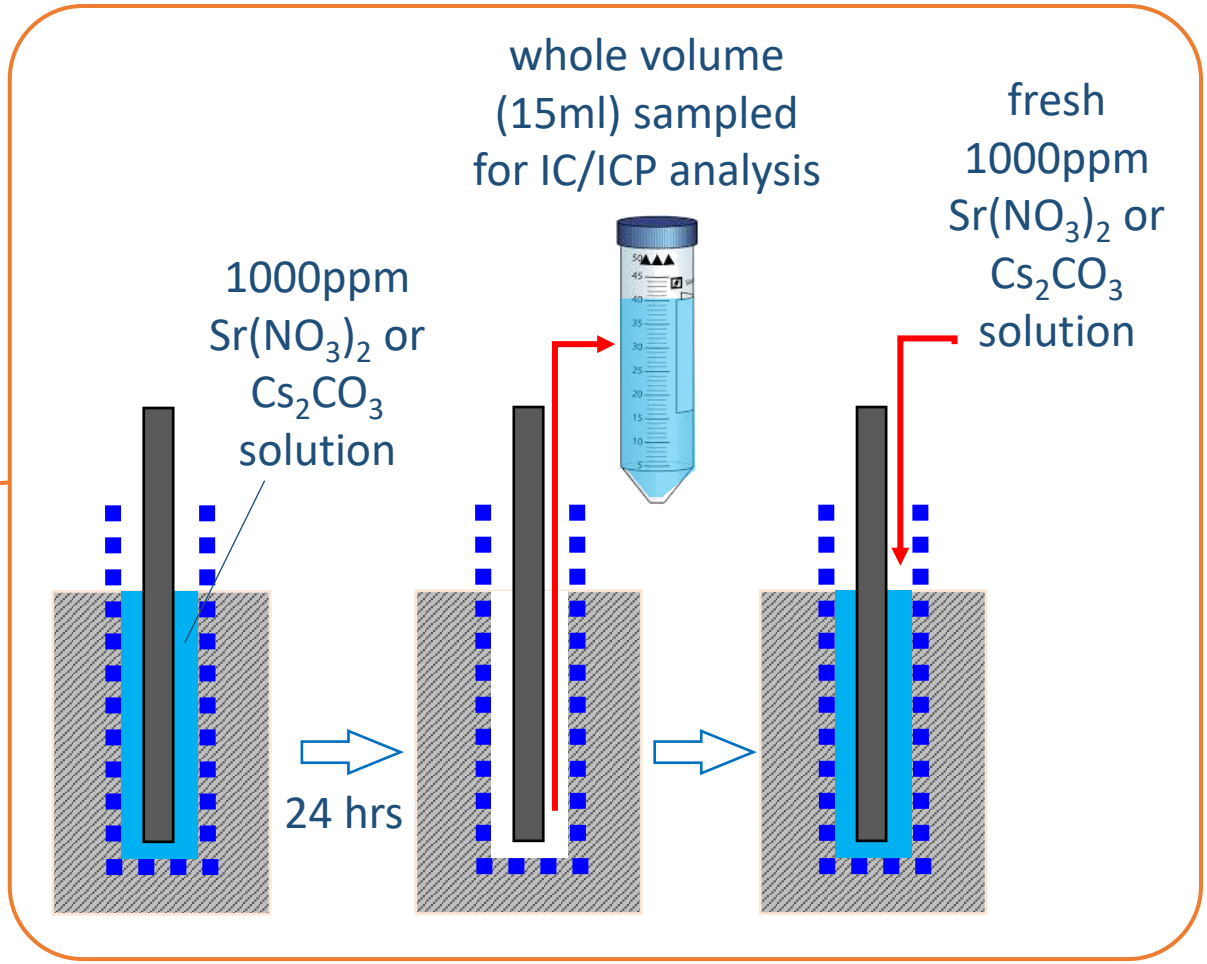

Experimental trials (1)

Results: silica dissolution

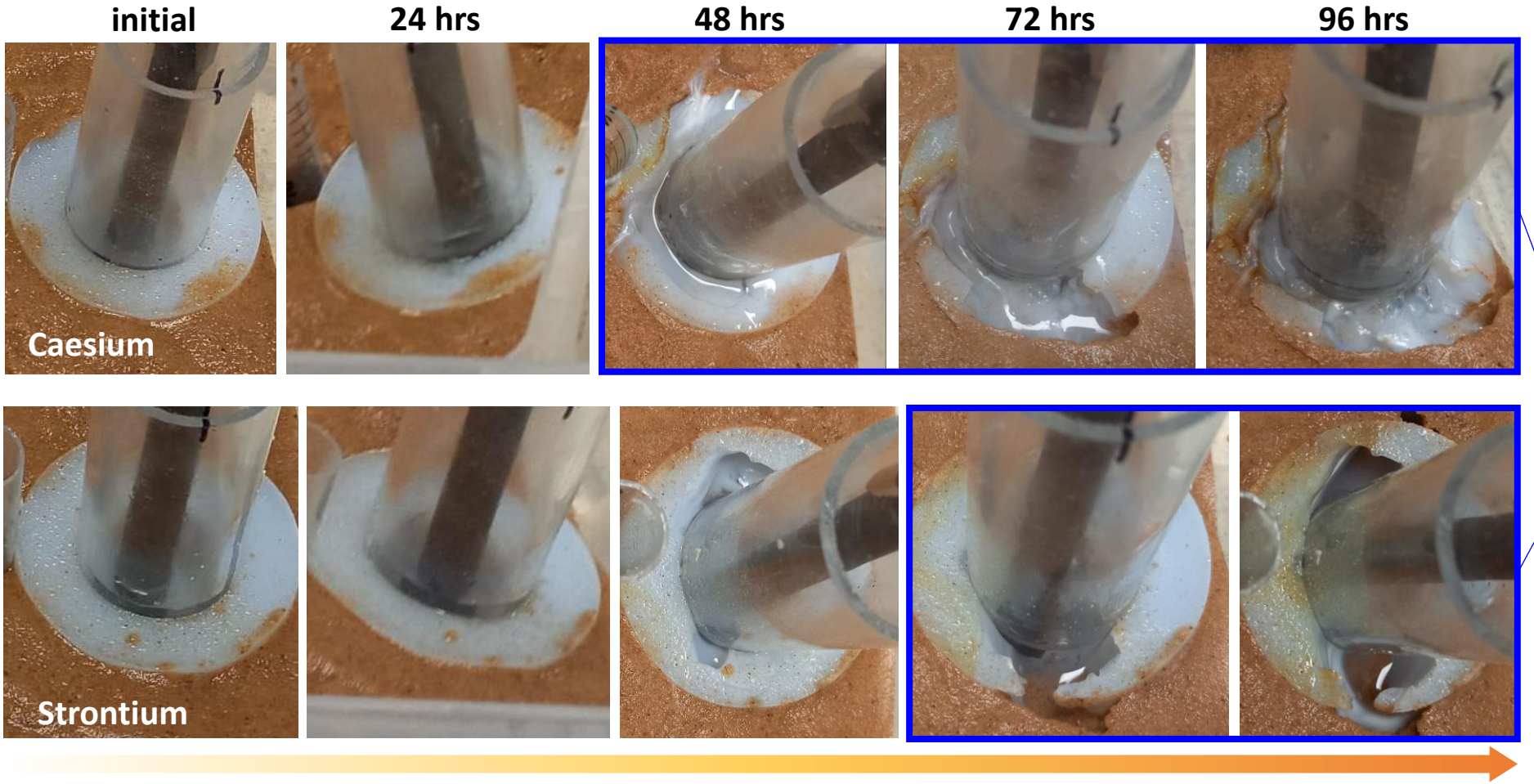

Experimental trials (1)

Results: ion mobility

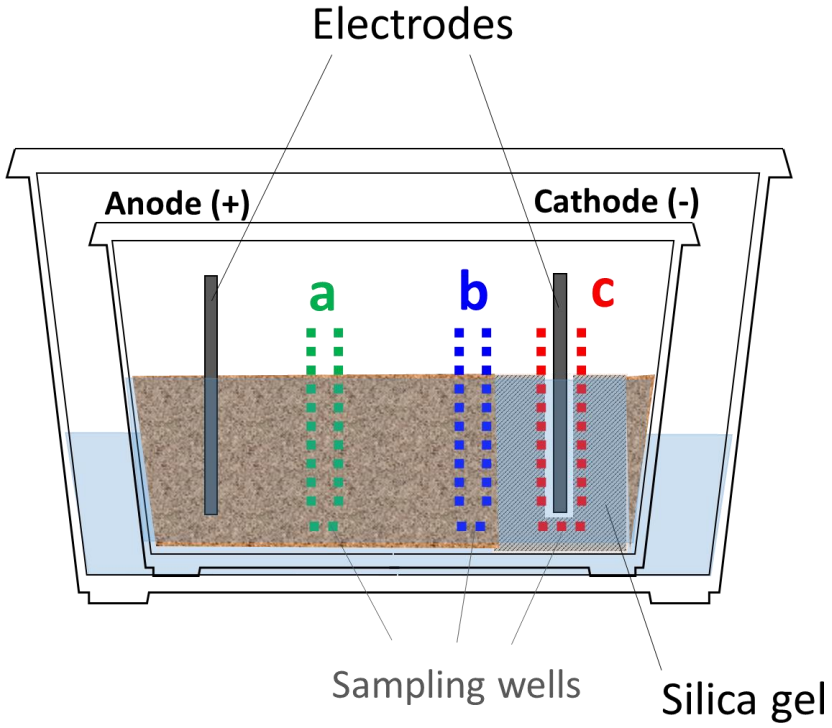

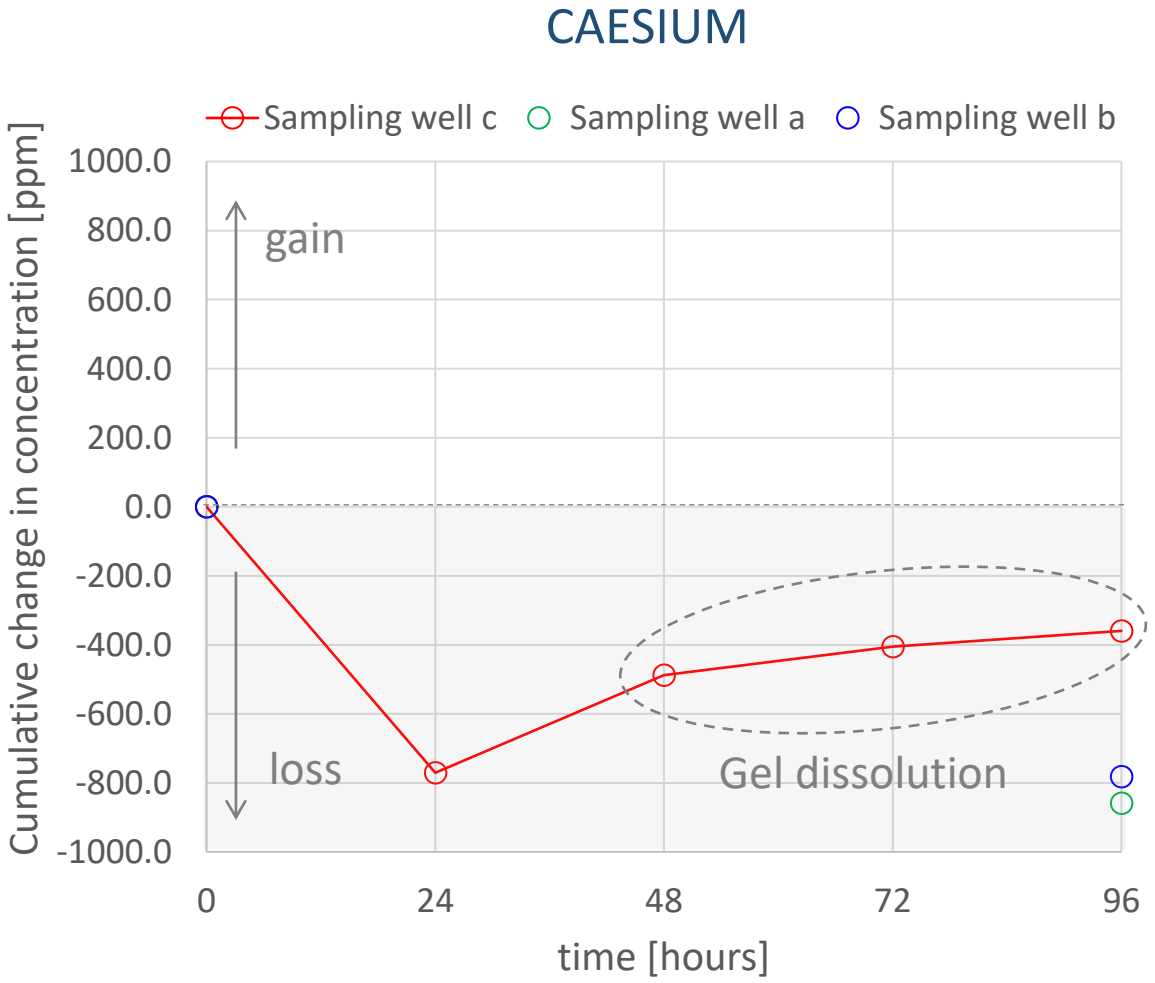

*EKR run for 4 days (**96 hours**) at **1 V/cm**

Experimental trials (1)

Results: ion mobility

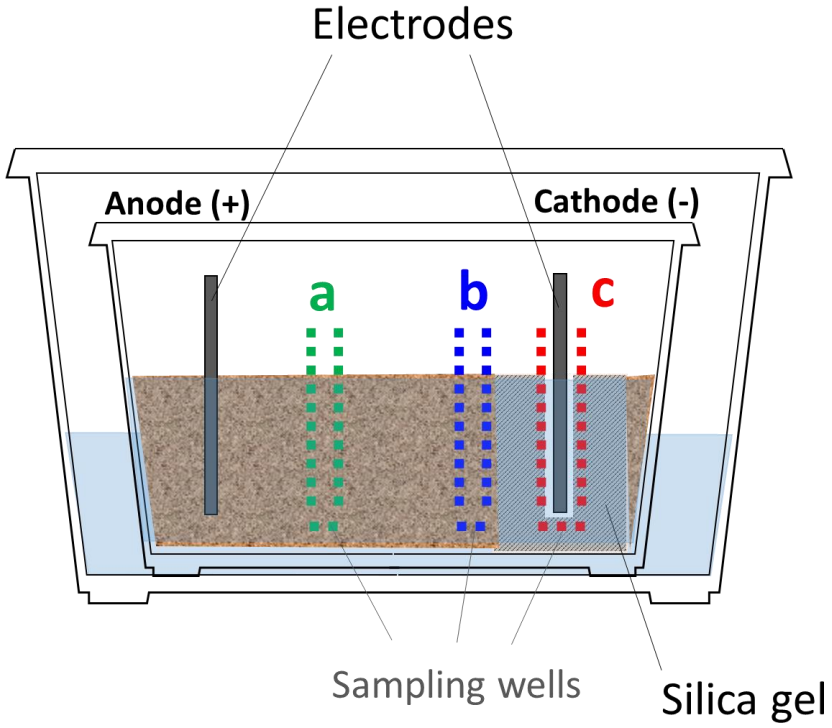

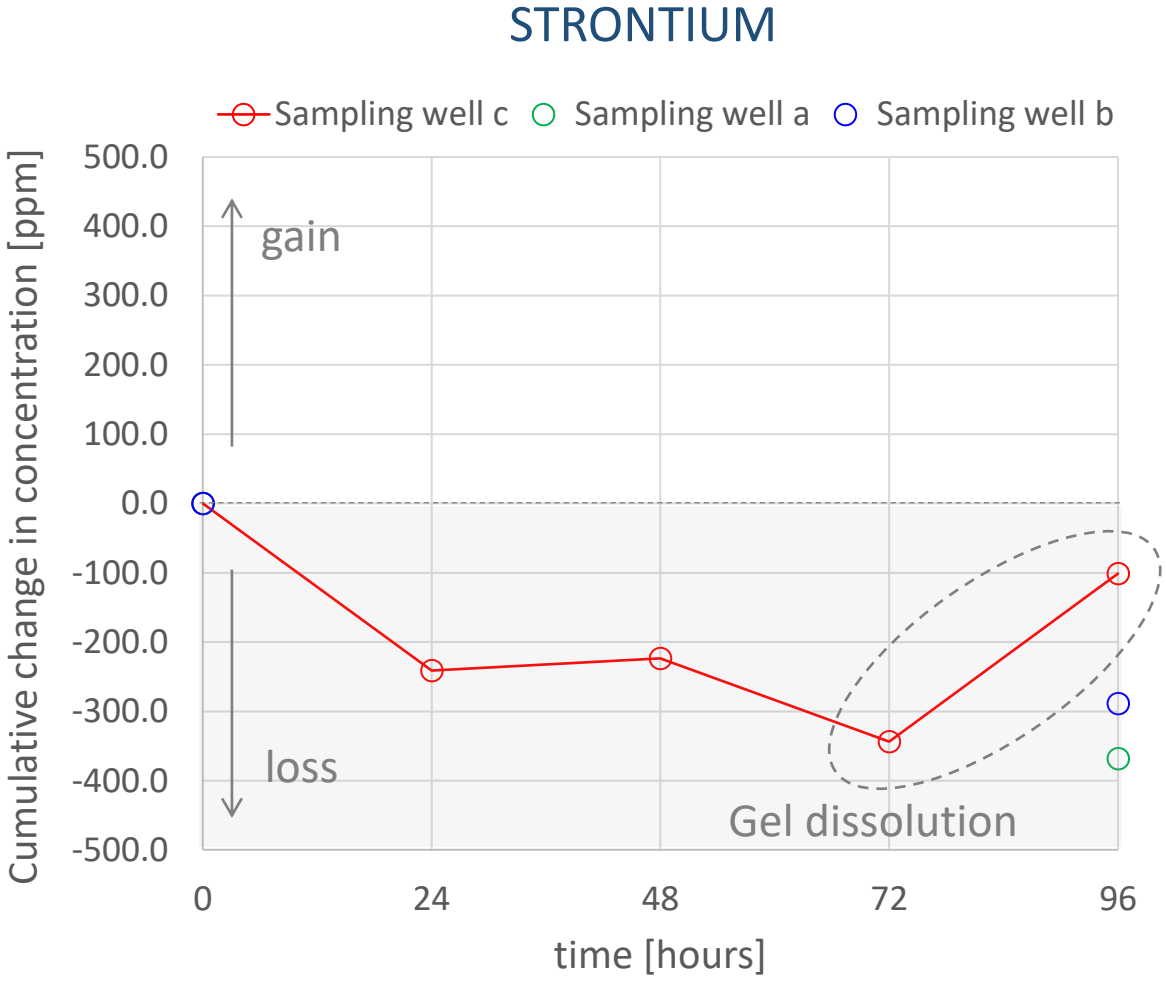

*EKR run for 4 days (**96 hours**) at **1 V/cm**

Experimental trials (1)

Electro-migration vs diffusion

Initial condition:

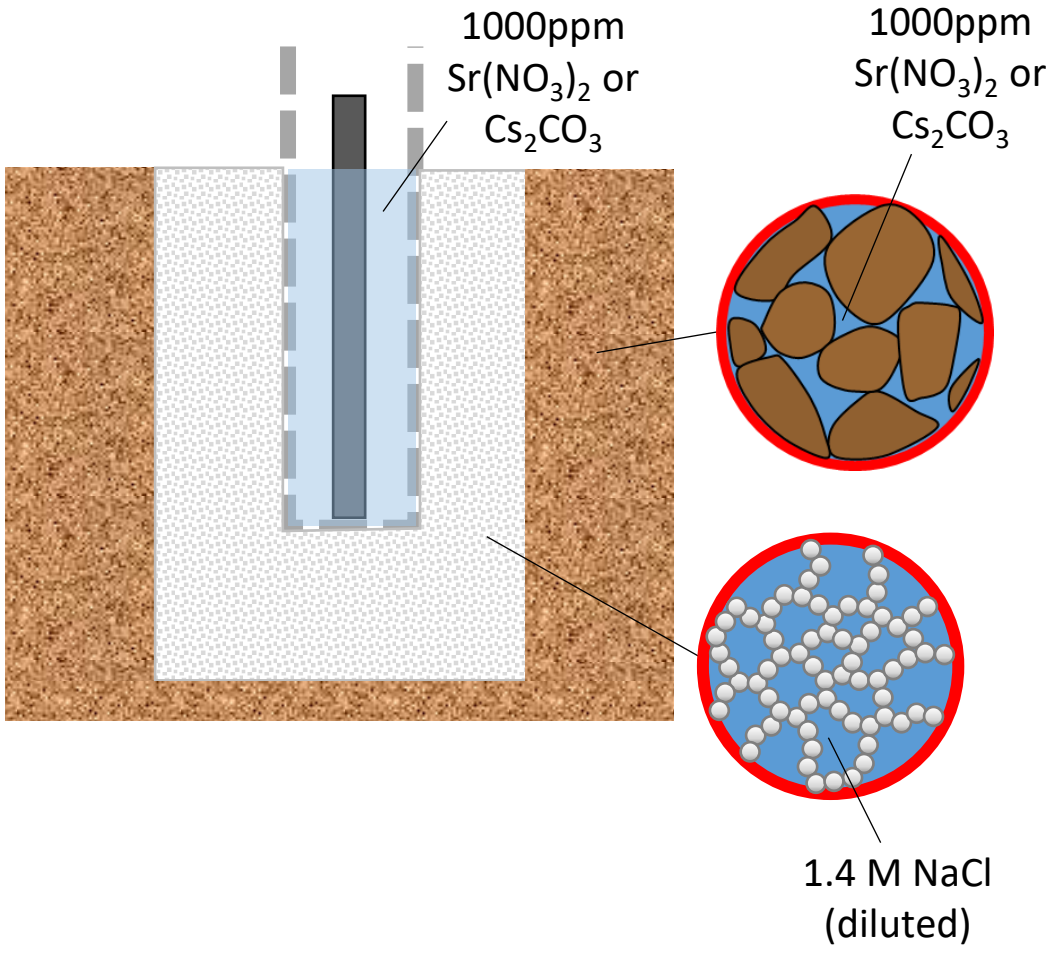

Potential mechanisms of ionic transport:

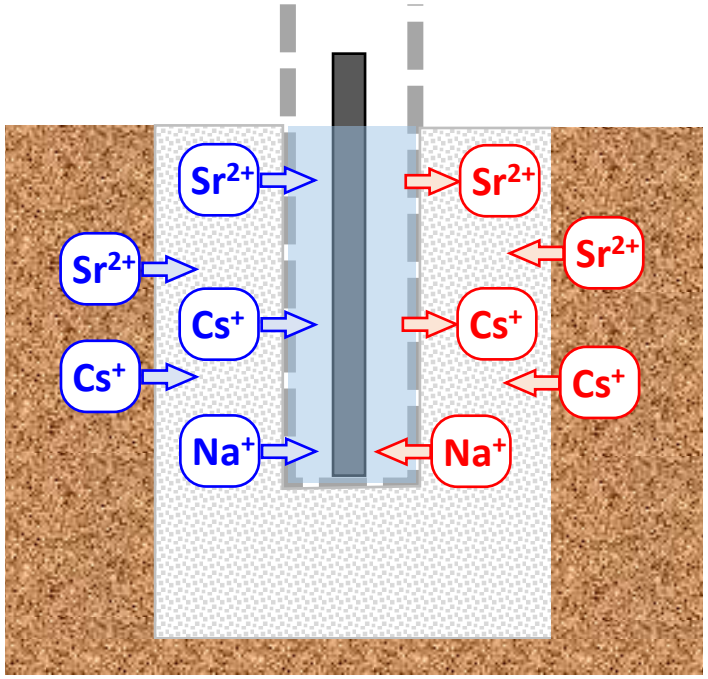

Electro-migration

Diffusion

Competing mechanisms!

Experimental trials (2)

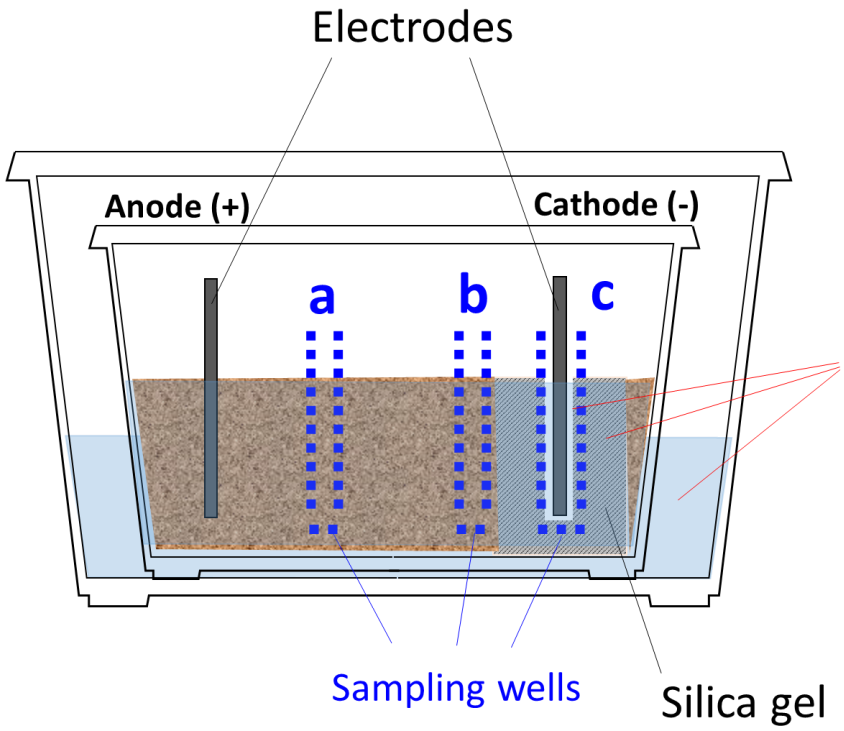

0.17M $CaCl_2$ in 1000ppm Cs_2CO_3 / 0.17M $CaCl_2$ in 1000ppm $Sr(NO_3)_2$

Sampling solution, silica gel pore-water and sand pore-water have the **same initial composition** to **avoid diffusion**

EKR run for 6 days (**144 hours**) at **0.5 V/cm**

EKR run at half the V/cm to avoid **silica dissolution**

Experimental trials (2)

Sampling procedure

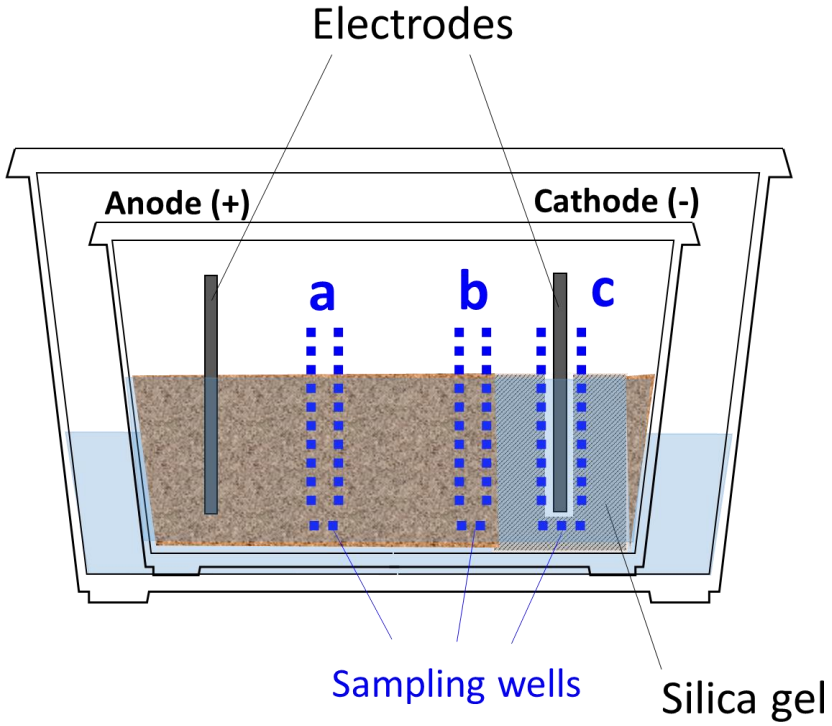

EKR run for 6 days (**144 hours**)
at **0.5 V/cm**

Sampling well 'c'

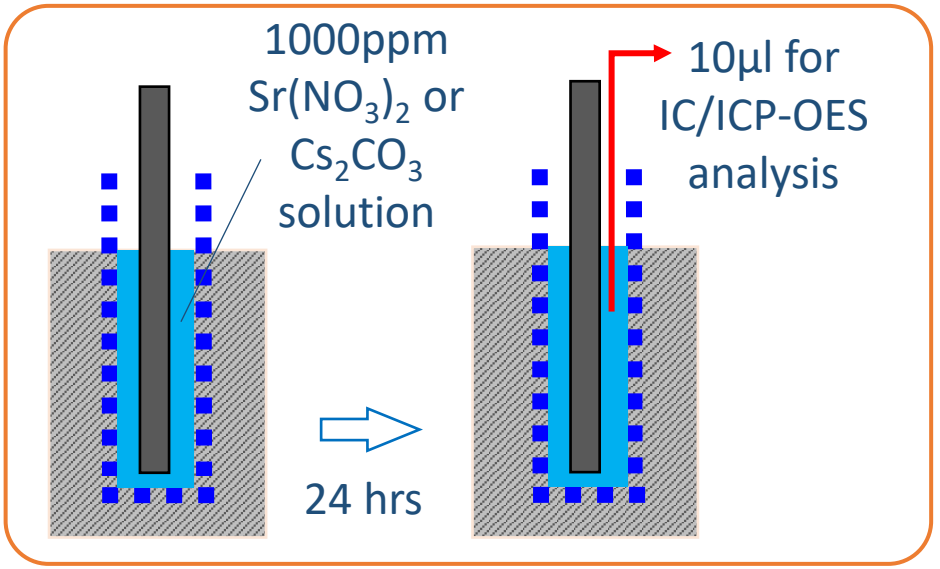

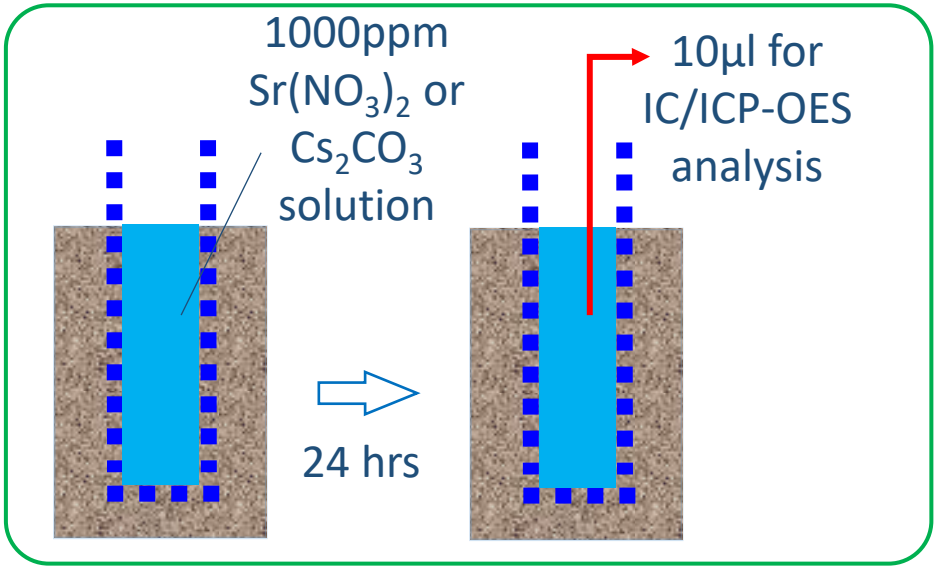

Sampling well 'a' and 'b'

Experimental trials (2)

Results

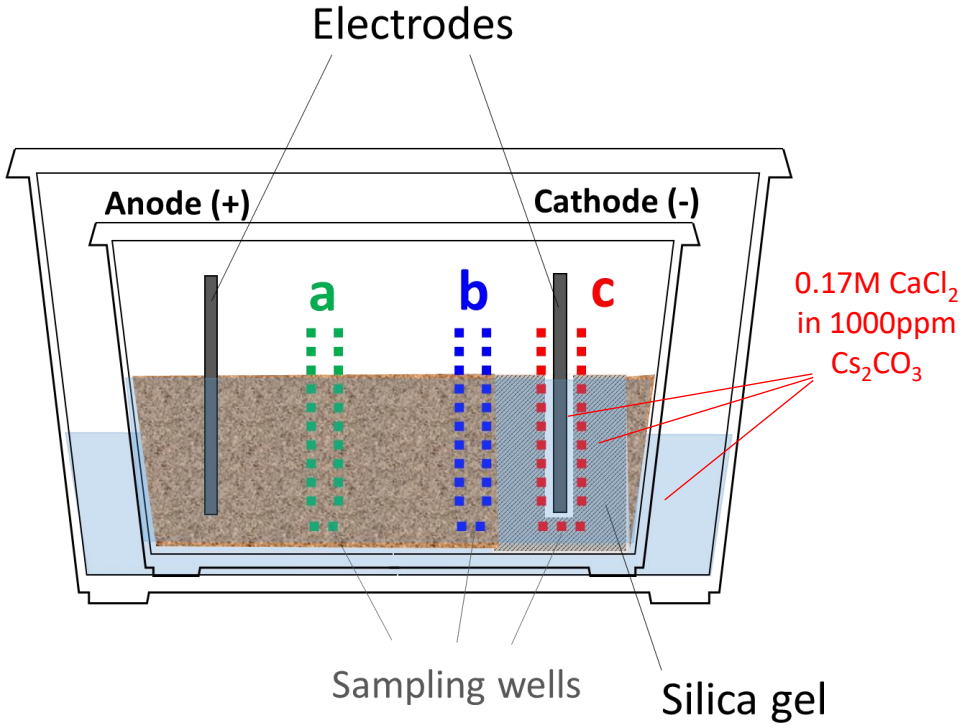

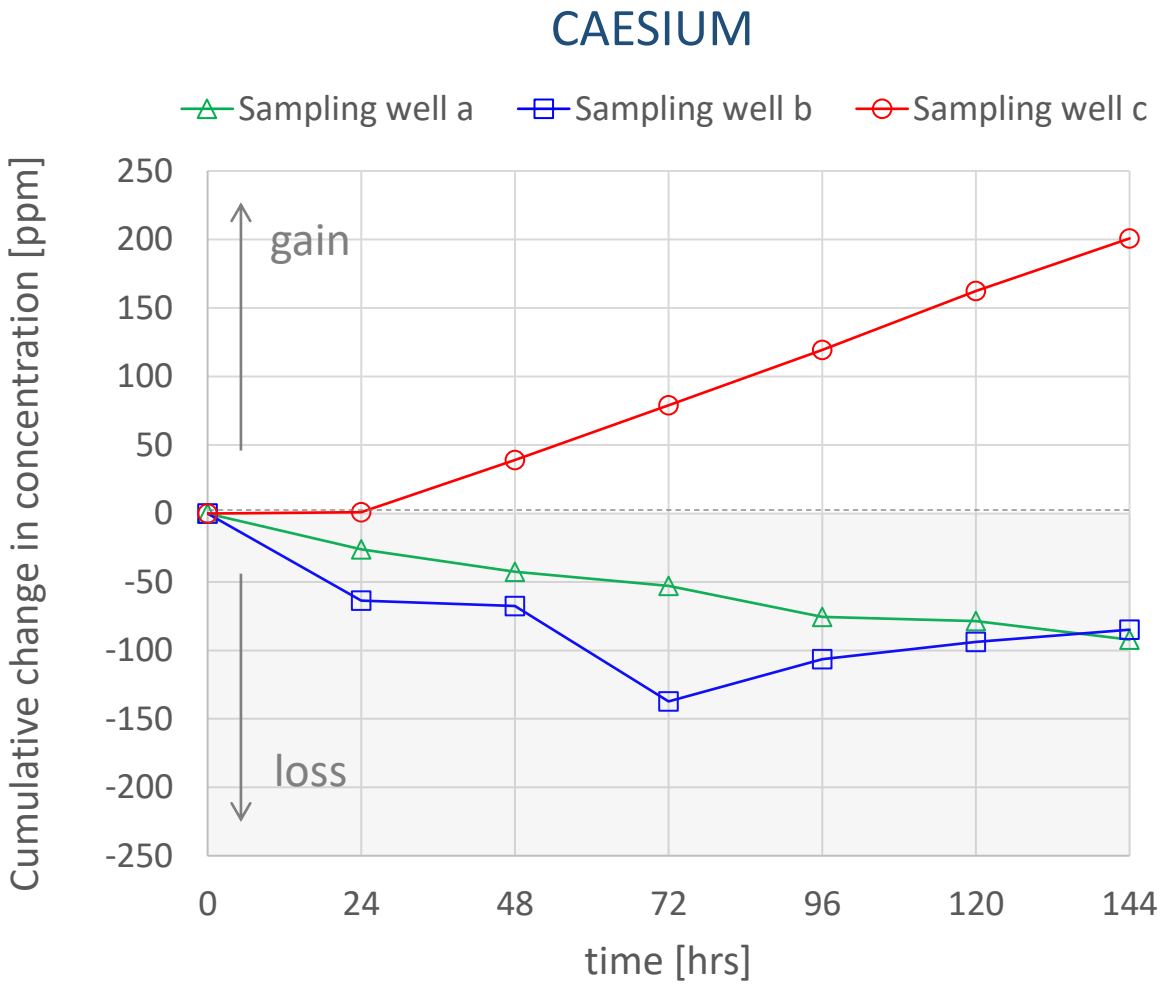

EKR run for 6 days (**144 hours**)
at **0.5 V/cm**

Experimental trials (2)

Results

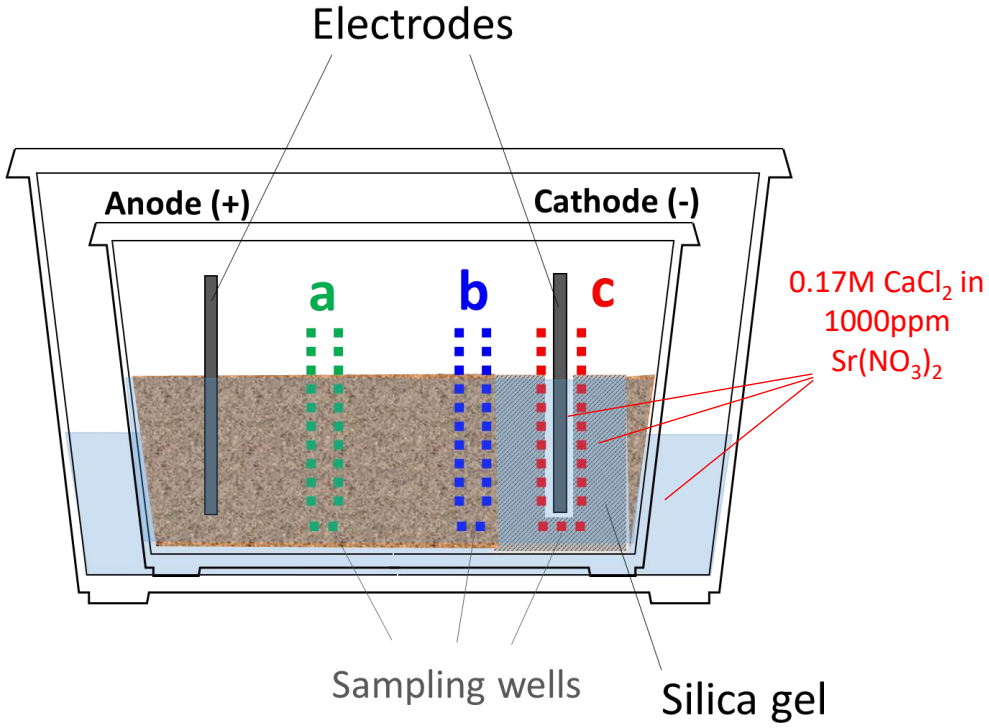

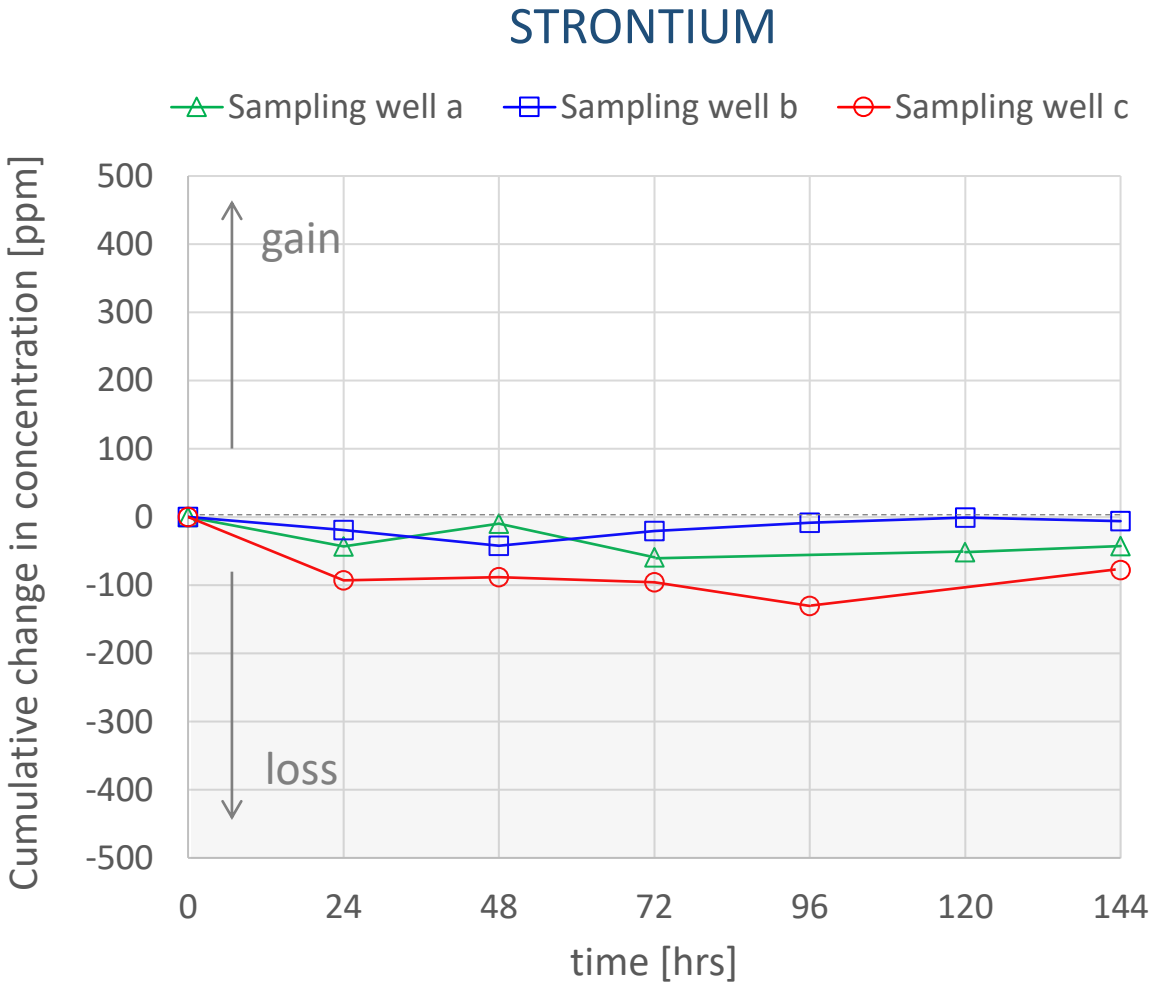

EKR run for 6 days (**144 hours**)
at **0.5 V/cm**

Experimental trials (3)

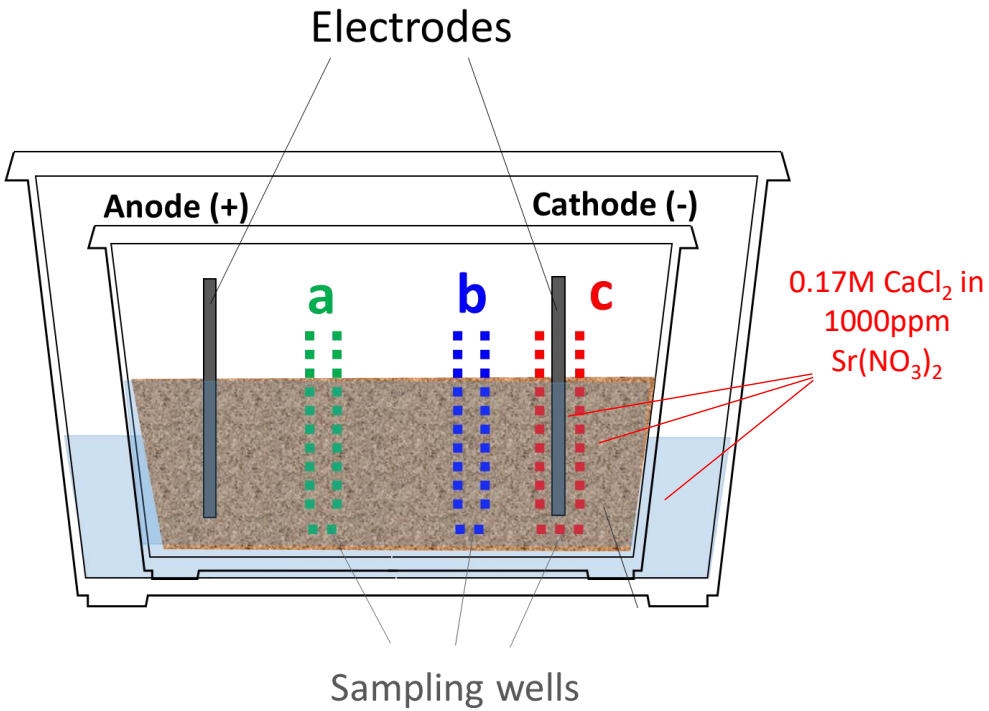

EKR run for 6 days (**144 hours**) at **0.25 V/cm**

EKR run at half the V/cm to avoid **Sr precipitation**

Experimental trials (3)

Results

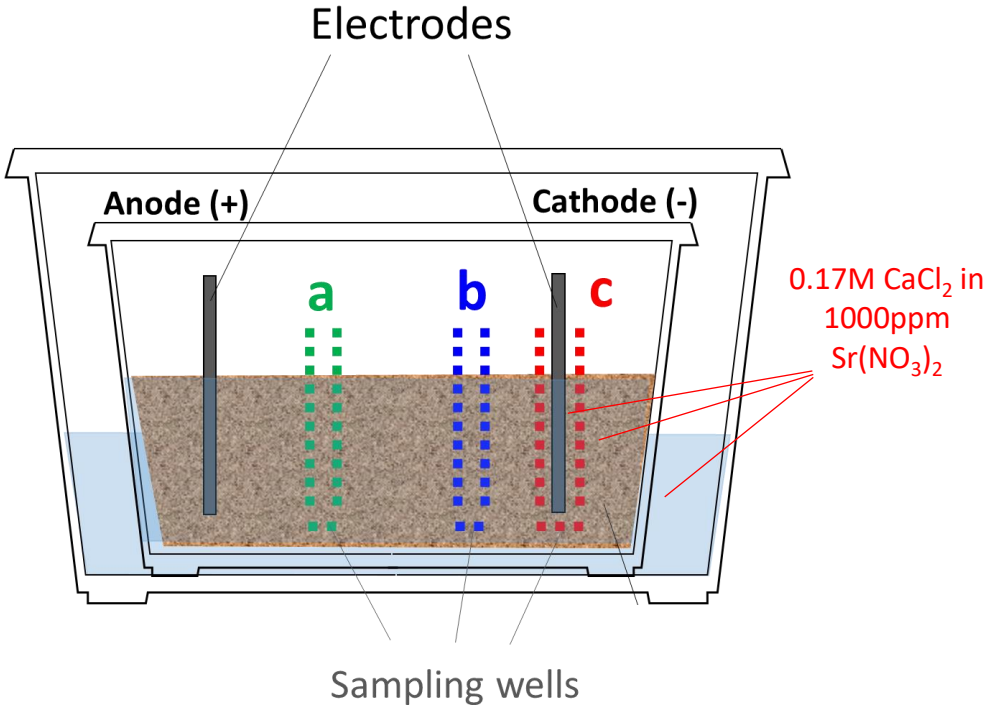

EKR run for 6 days (**144 hours**)
at **0.25 V/cm**

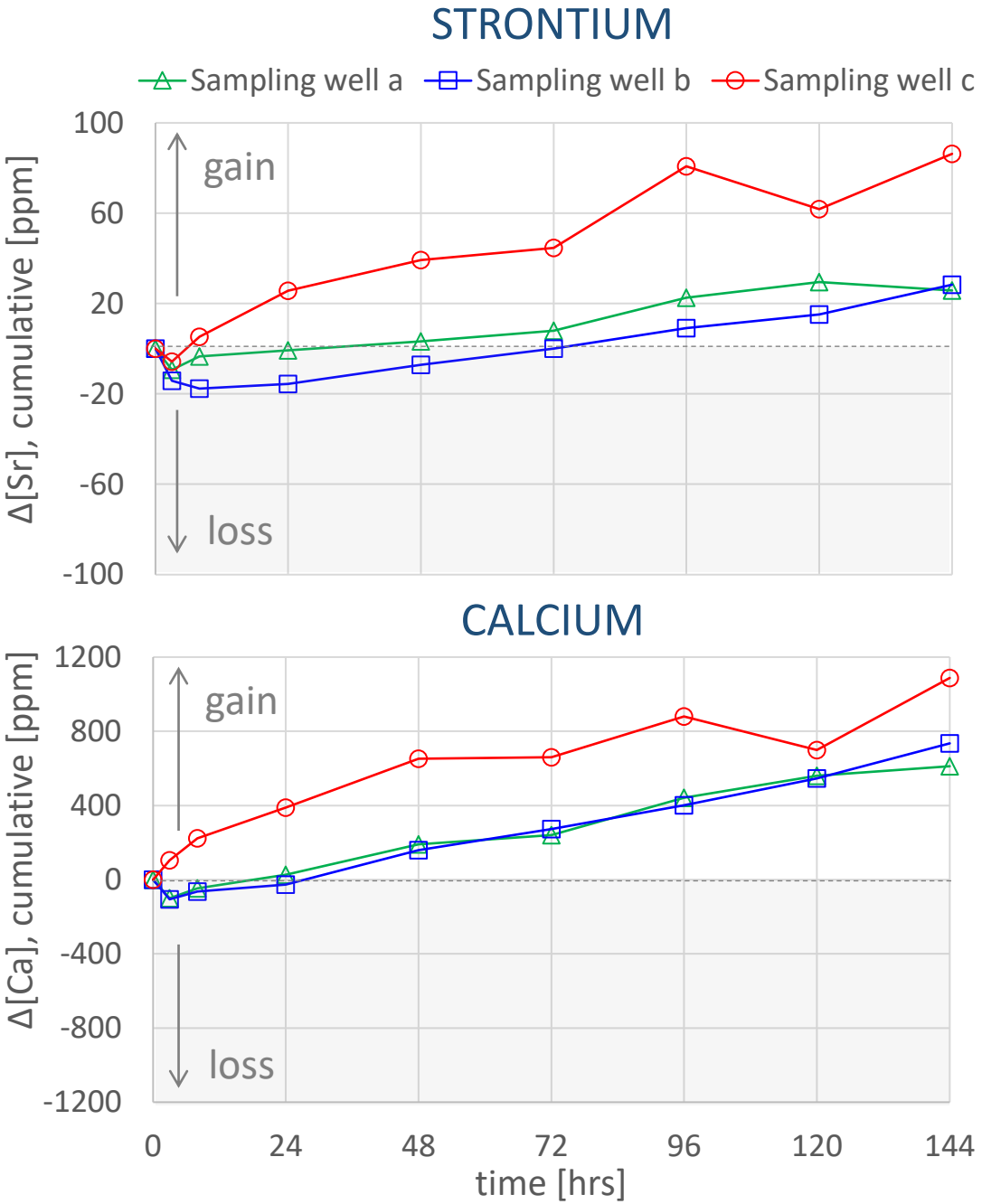

Conclusions

- Colloidal silica grout combined with electro-kinetic remediation provides a valuable 'purge and trap' technology for radioactively-contaminated land remediation
- Experimental trials were carried out in lab-scale electro-kinetic cells to explore the mobility of Cs and Sr ions through a plug of colloidal silica hydrogel:

  - the highly alkaline pH front produced at the cathode resulted in the dissolution of the silica hydrogel after 48 hours at 1 V/cm; reducing the voltage to 0.5 V/cm successfully prevented silica gel dissolution over a duration of 6 days
  - a further voltage reduction down to 0.25 V/cm allowed to prevent the precipitation of Sr salts at the cathode, while still allowing the mobilisation of Sr ions through the silica gel
  - Further experiments will explore the mobility of different ions (+ve and –ve), in sand and sand+clay samples.

TRANSCEND

Transformative Science and Engineering for Nuclear Decommissioning

arianna.pagano@strath.ac.uk

Understanding caesium's effect on the CAS system due to vitrification

Lucas-Jay Woodbridge[1], Daniel Bailey[1]and Russell Hand[1]

The University of Sheffield

[1]*Immobilisation Science Laboratory, University of Sheffield, Department of Materials Science and Engineering, Sir Robert Hadfield Building, Mappin Street S1 3JD, UK*

Transcend annual meeting – 1st & 2nd August 2022

*lwoodbridge1@Sheffield.ac.uk

Chemical system of TiO_2-Na_2O-SiO_2

- Well known glass formers
- Pristine series created
- Reasons for selection of sample

Pristine sample CAS 50 10 40

	C28Al12Si60	C42Al12S46	C42.4A15.5S42.1	C50Al10Si40	C35Al10Si55
Oxide	Mol%	Mol%	Mol%	Mol%	Mol%
CaO	28	42	42.4	50	35
Al2O3	12	12	15.5	10	10
SiO2	60	46	42.1	40	55
Total	100	100	100	100	100

Glass series chemistry in Mol%

Crystalline phases labelled for the phase diagram divisions

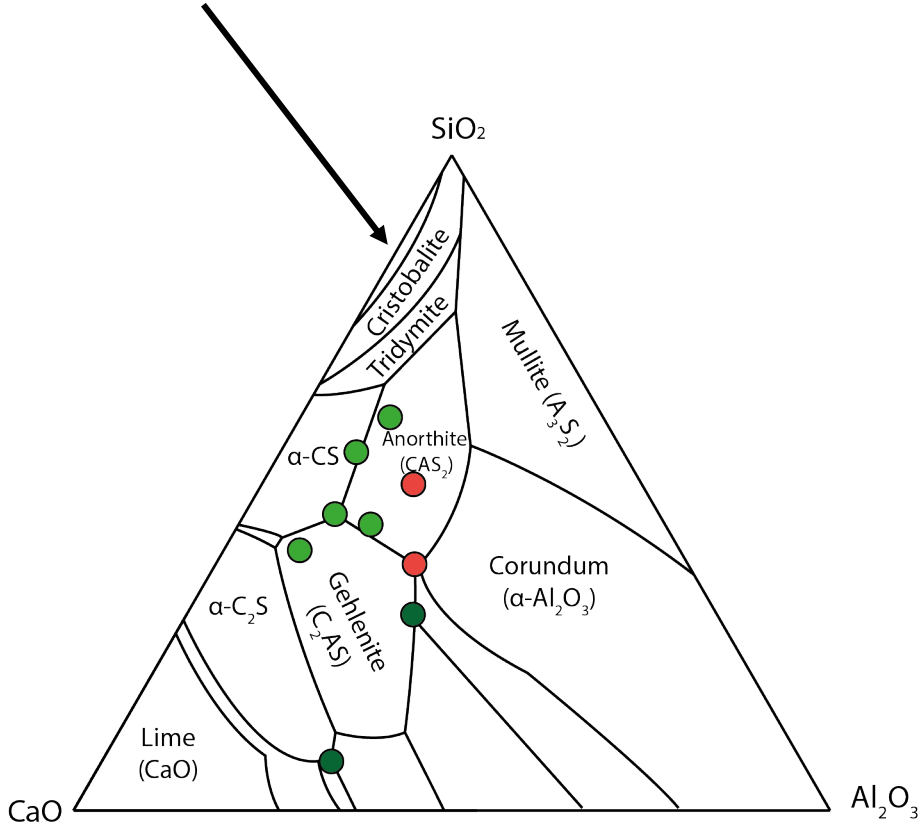

CaO, Al_2O_3, SiO_2 phase diagram with samples plotted
Edited from Khadilkar et al 2015.

*lwoodbridge1@Sheffield.ac.uk

[1]Glass formation in silicates: Insights from composition – Pascal Richet, Mathieu Roskosz & Jacques Roux – 2006

Proof of a proven concept… or not

- Next step was Cs loading of these pristine glasses

Very uninspiring batch sandcastles

*lwoodbridge1@Sheffield.ac.uk

Scope melt process

- For the interest of time scoping melts were undertaken
- Attempt to find the right temperature
- Attempt to see what the problem is

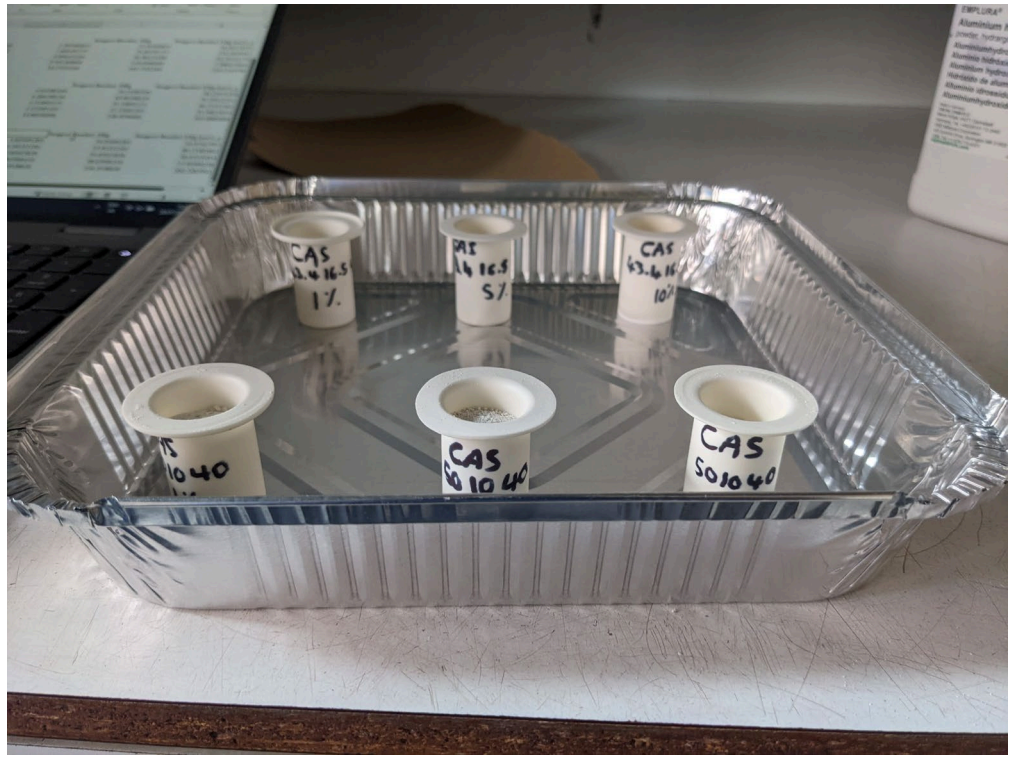

10g melt alumina crucibles to do 6 melts at a time

*lwoodbridge1@Sheffield.ac.uk

Scope melt process

- Issues still found at max muffle furnace temperature
- Alkalis a problem across the board?
- Is it a size issue?

10g melt alumina crucibles most of which didn’t melt

*lwoodbridge1@Sheffield.ac.uk

Scope melt process

- Li, Na and K all perfect at loading level and temperature
- Rb not perfect but better than Cs
- Pollucite might be the important

Left- CAS 35 10 55 with 1 Mol% Cs and right 1, 5 and 10 Mol% K in CAS 50 10 40

*lwoodbridge1@Sheffield.ac.uk

The University Of Sheffield.

NucleUS
Immobilisation Science Laboratory

XRD of glasses

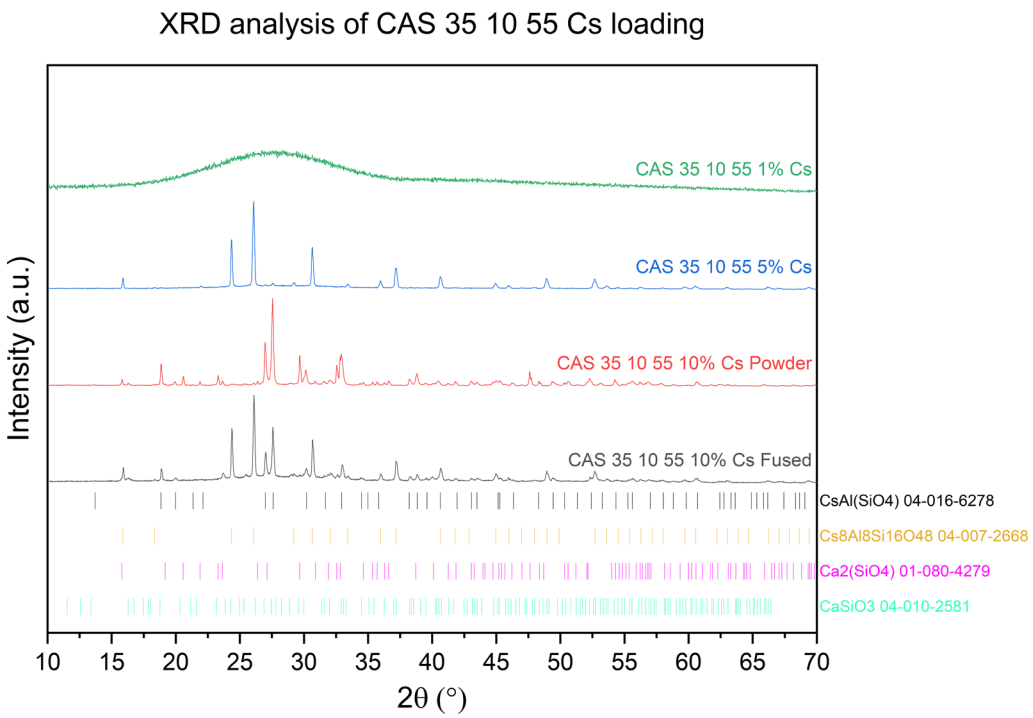

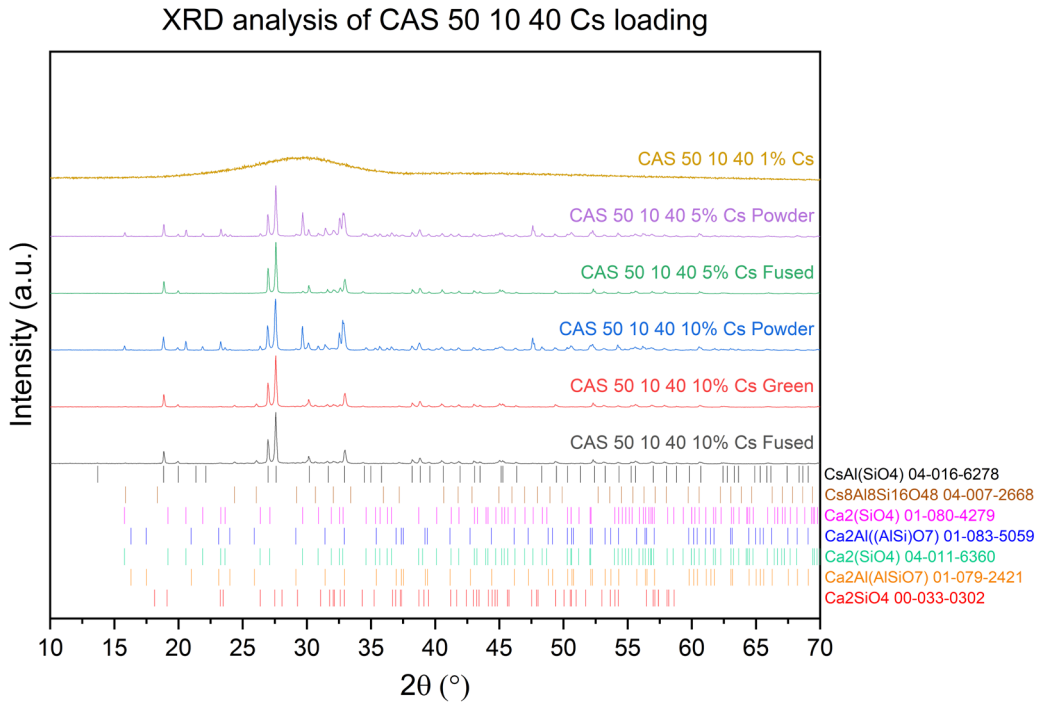

@ISL_Sheffield

The University Of Sheffield.

NucleUS
isation Science Laboratory

XRD of glasses

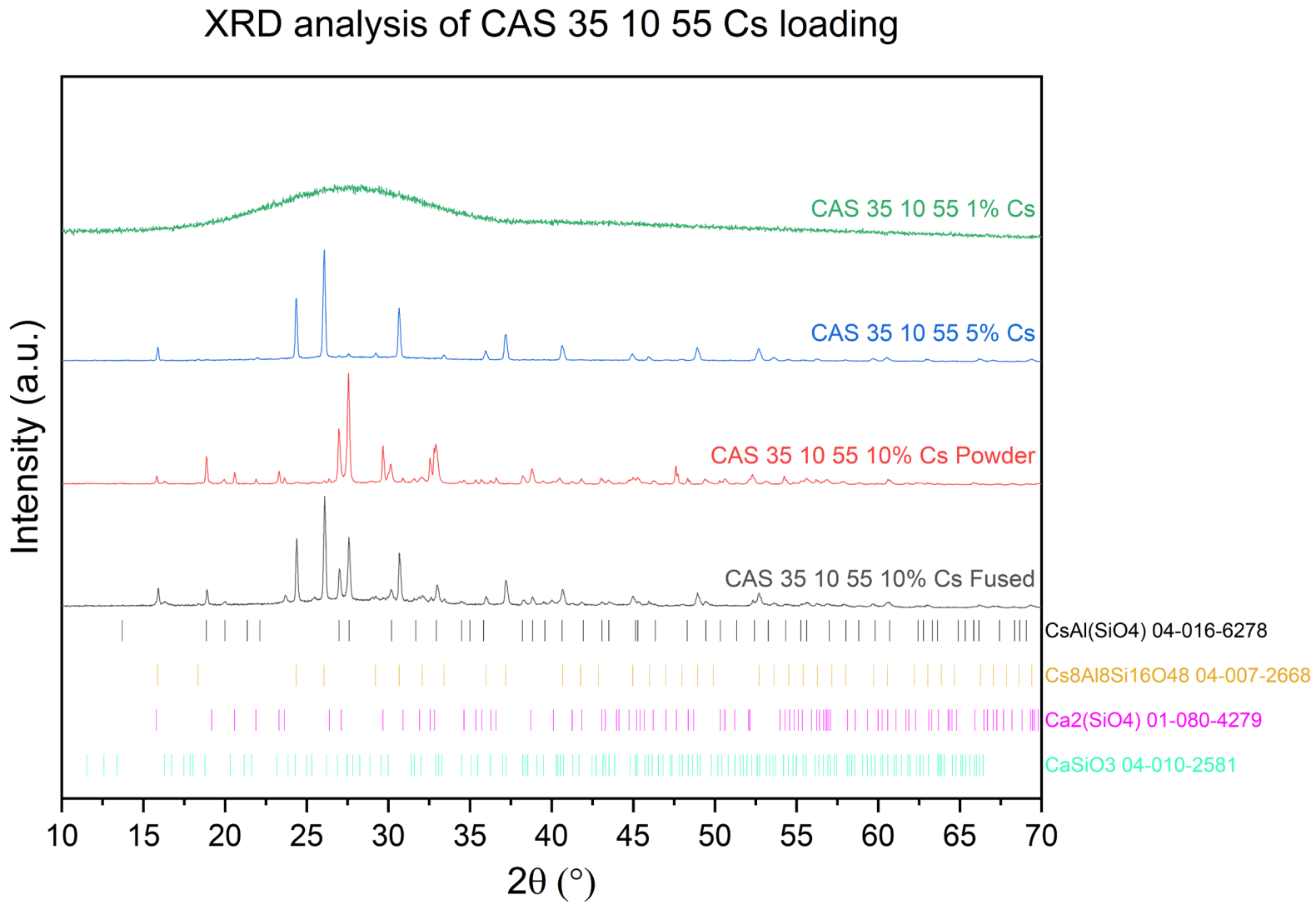

@ISL_Sheffield

XRD of glasses

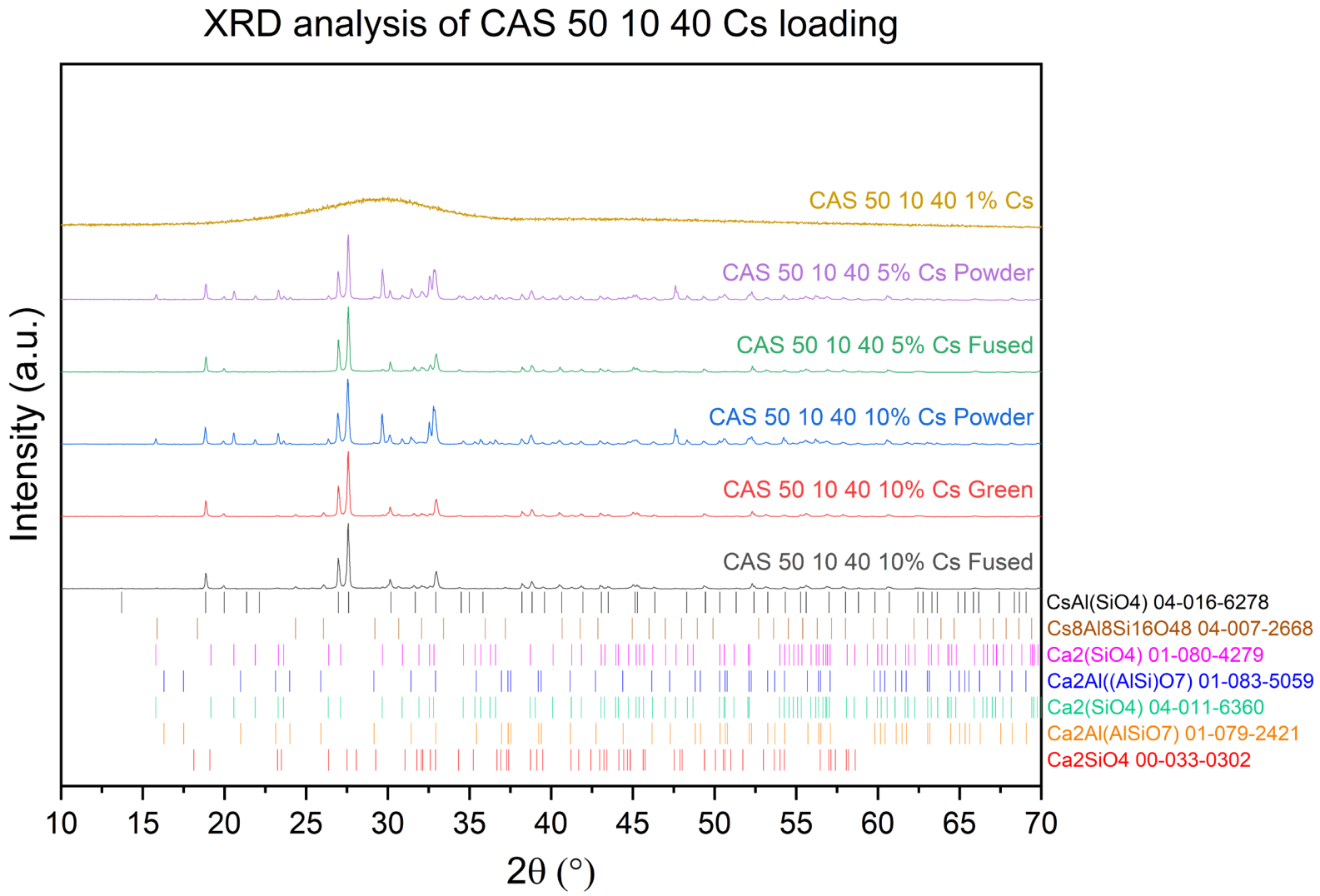

@ISL_Sheffield

The University Of Sheffield.

NucleUS
Immobilisation Science Laboratory

XRD of glasses

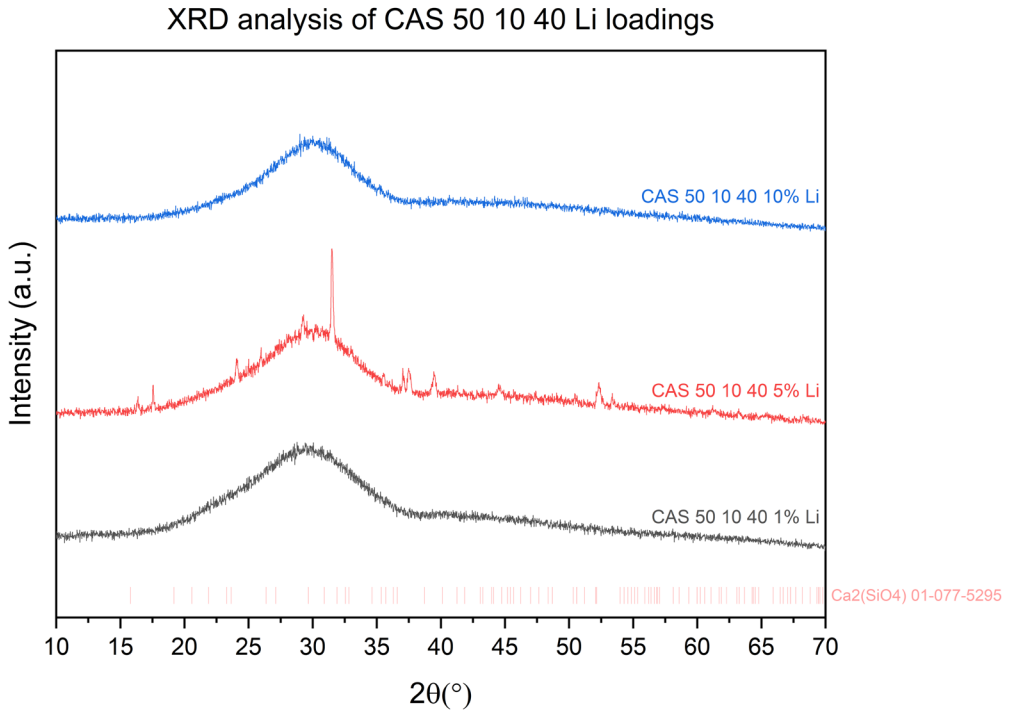

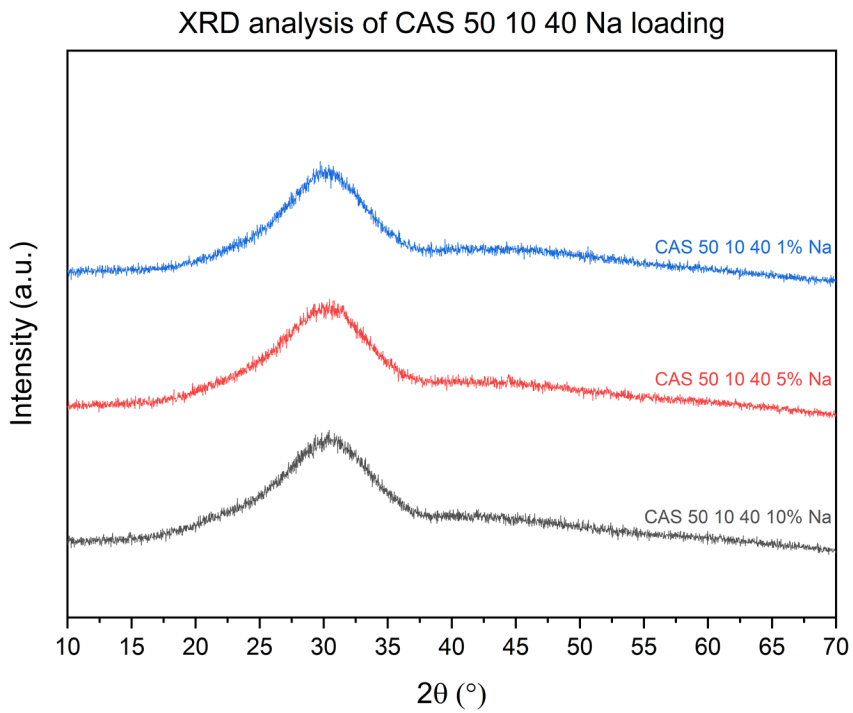

@ISL_Sheffield

The University Of Sheffield.

NucleUS
mobilisation Science Laboratory

XRD of glasses

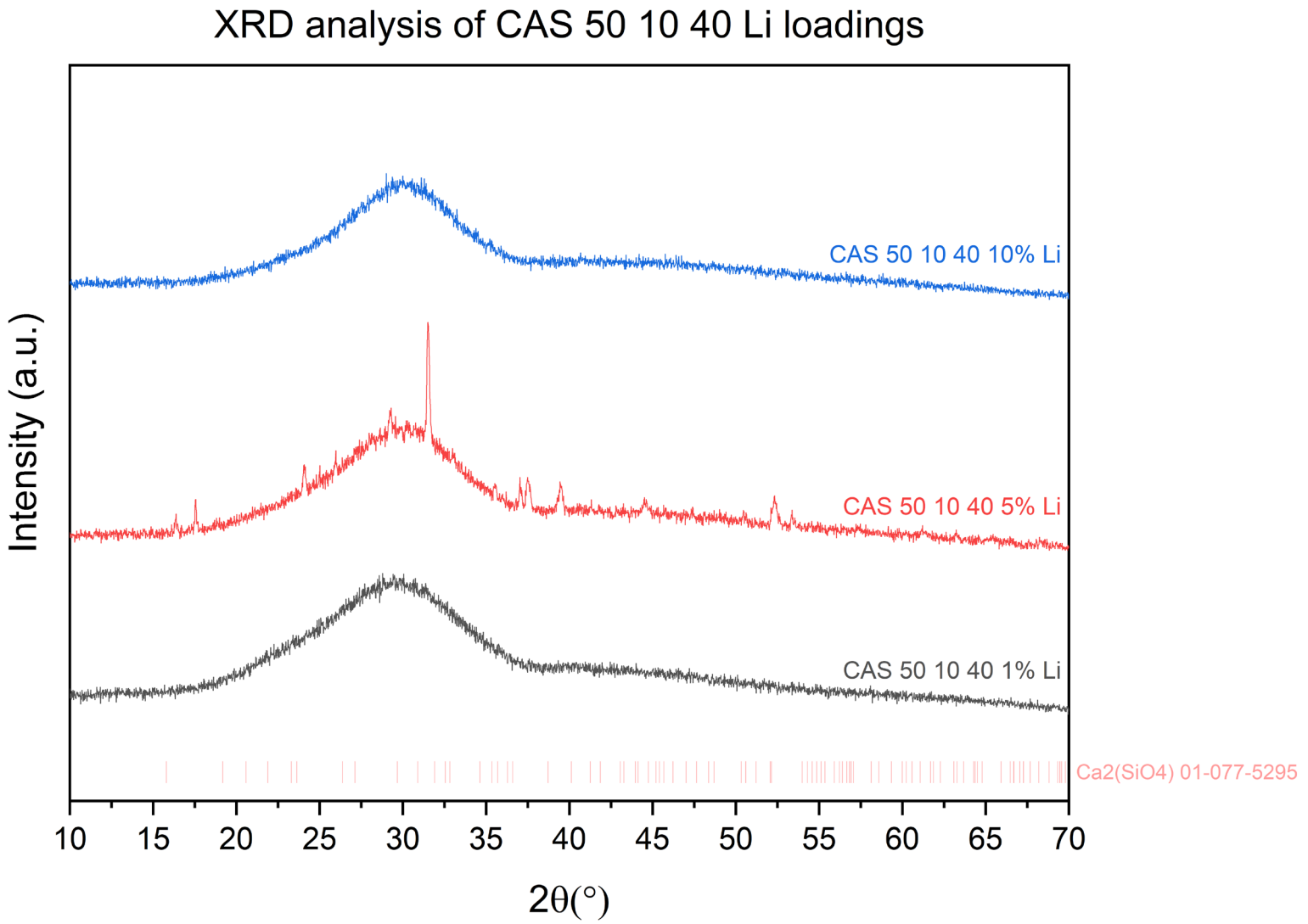

@ISL_Sheffield

The University Of Sheffield.

NucleUS
Immobilisation Science Laboratory

XRD of glasses

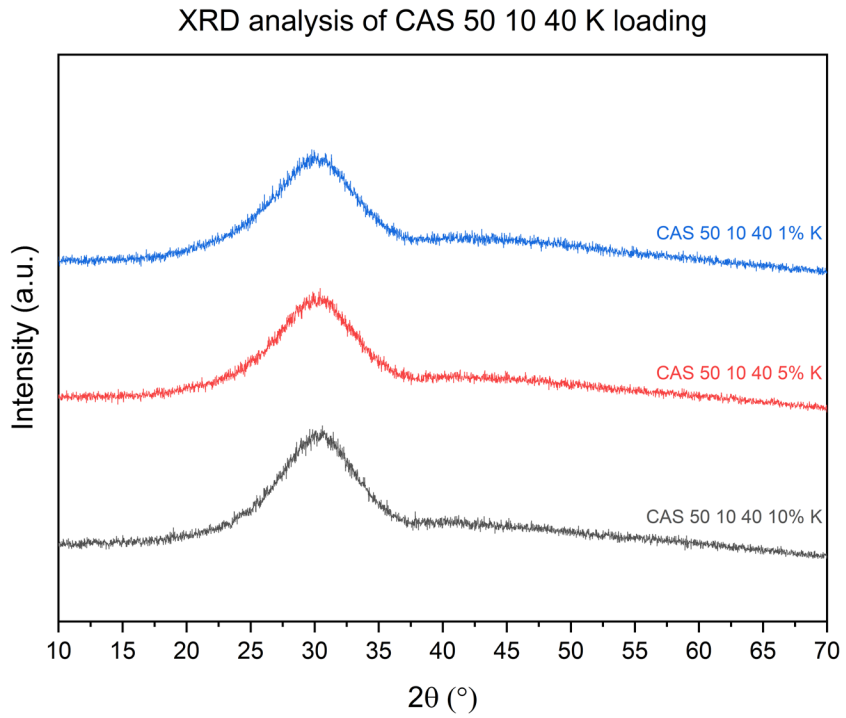

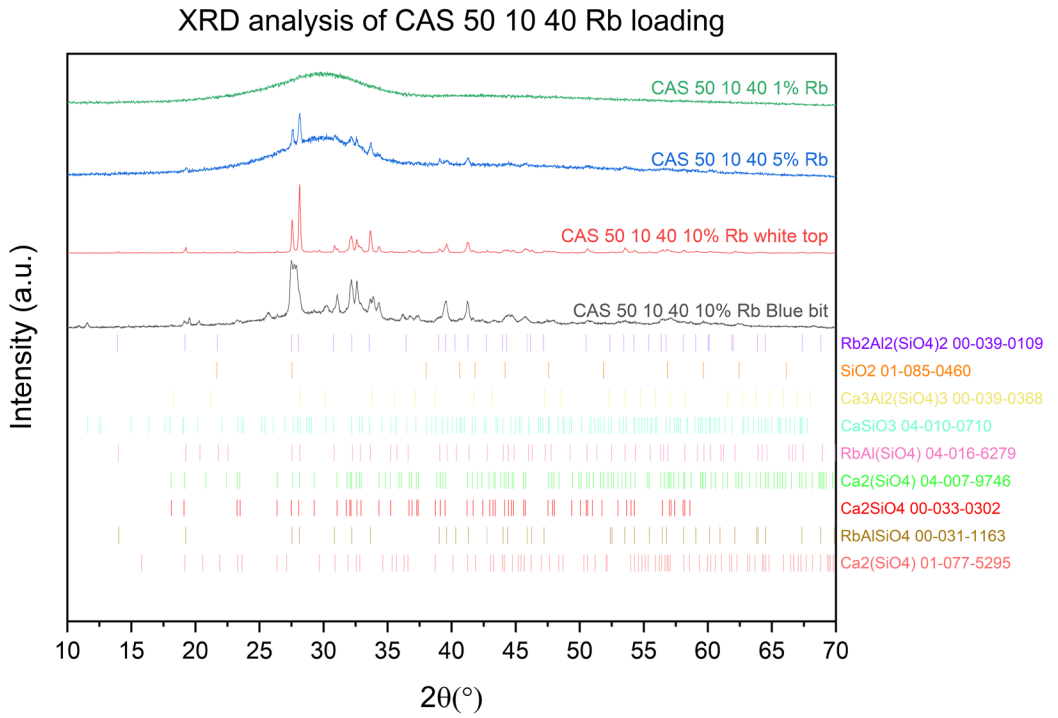

@ISL_Sheffield

XRD of glasses

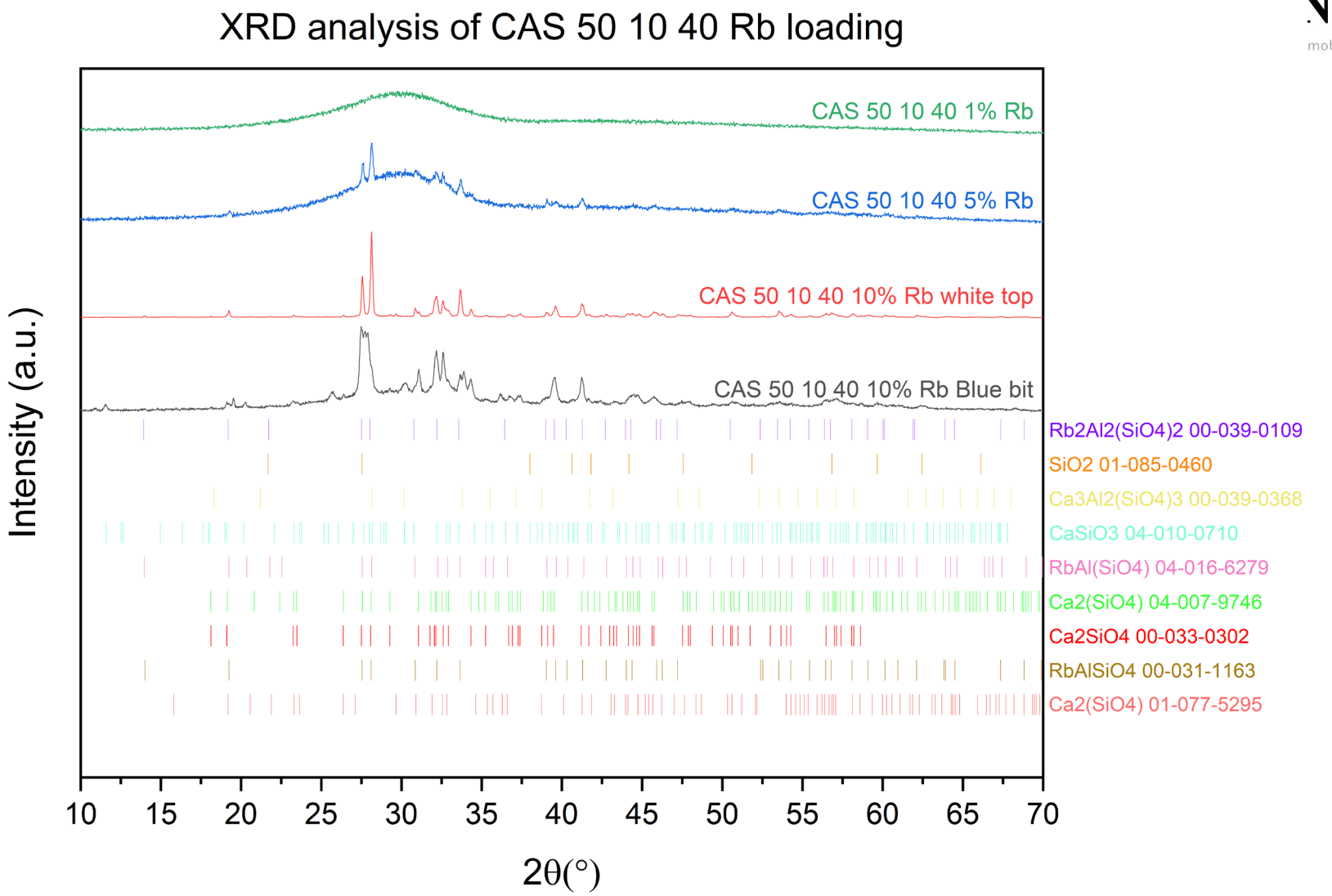

@ISL_Sheffield

Scope melt process

- In order to see where the alkalis sit in the network each loading level ideally fully vitreous
- Re-do the scopes at 1600°C to try and achieve this

*lwoodbridge1@Sheffield.ac.uk

XRD of glasses

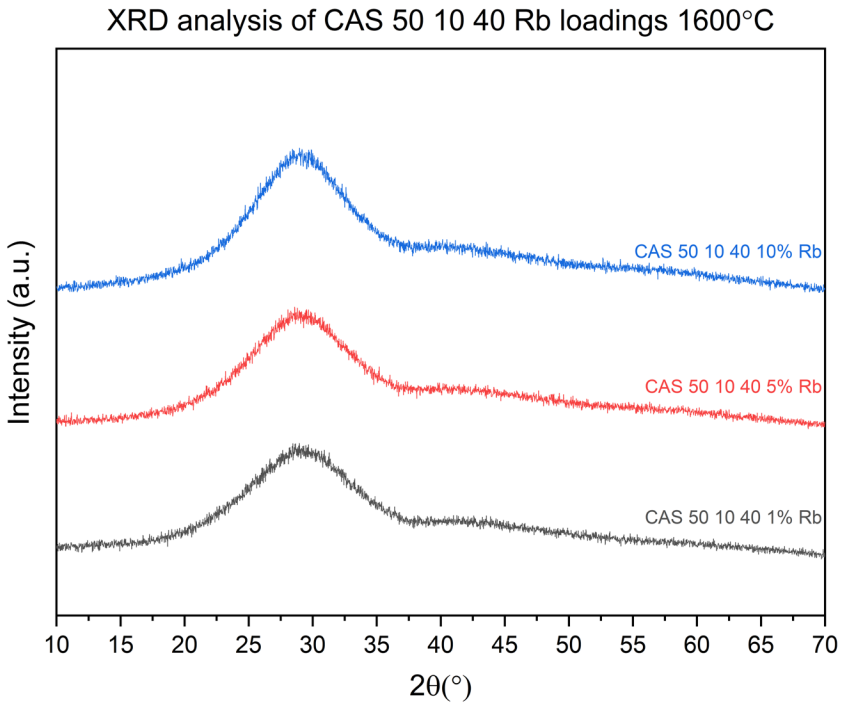

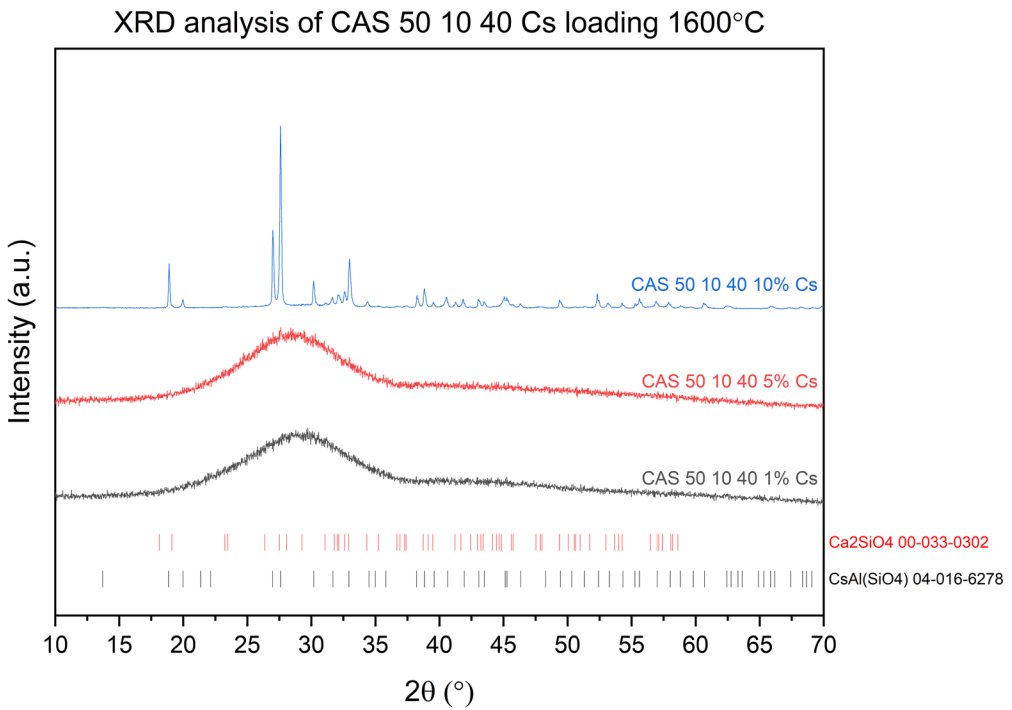

@ISL_Sheffield

The University Of Sheffield.

NucleUS
mobilisation Science Laboratory

XRD of glasses

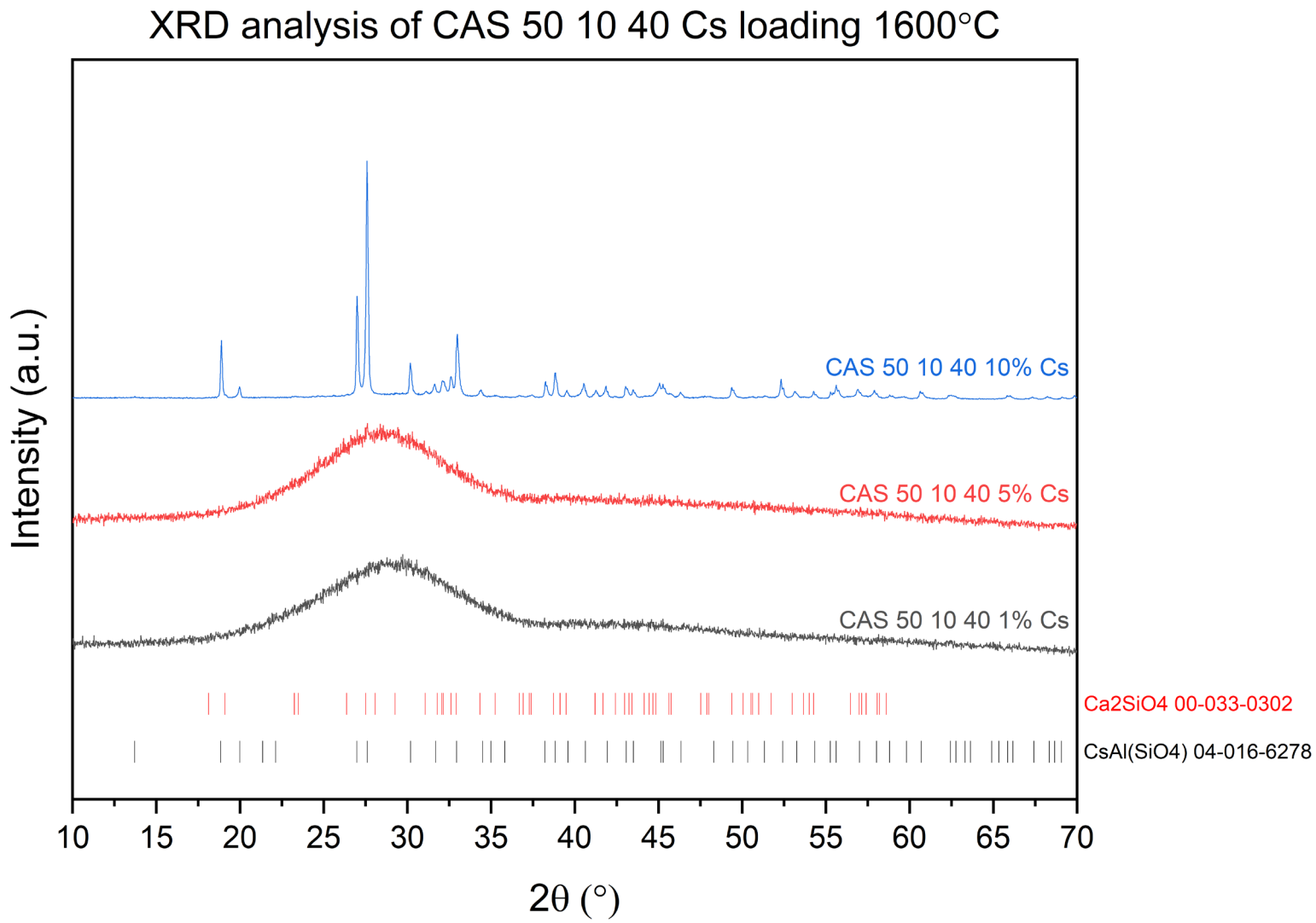

@ISL_Sheffield

Scope melt process

- Evidence from the literature that in other fields Li and Na are known to decrease viscosity and K increases it (Chang and Ejima 1987, Sukenaga et al 2006)
- Can you flux Cs into melt with Li or Na additions?

5% Li 5% Cs

3% Na 7% Cs

3% Na 7% Cs

*lwoodbridge1@Sheffield.ac.uk

The University Of Sheffield.

NucleUS
mobilisation Science Laboratory

XRD of glasses

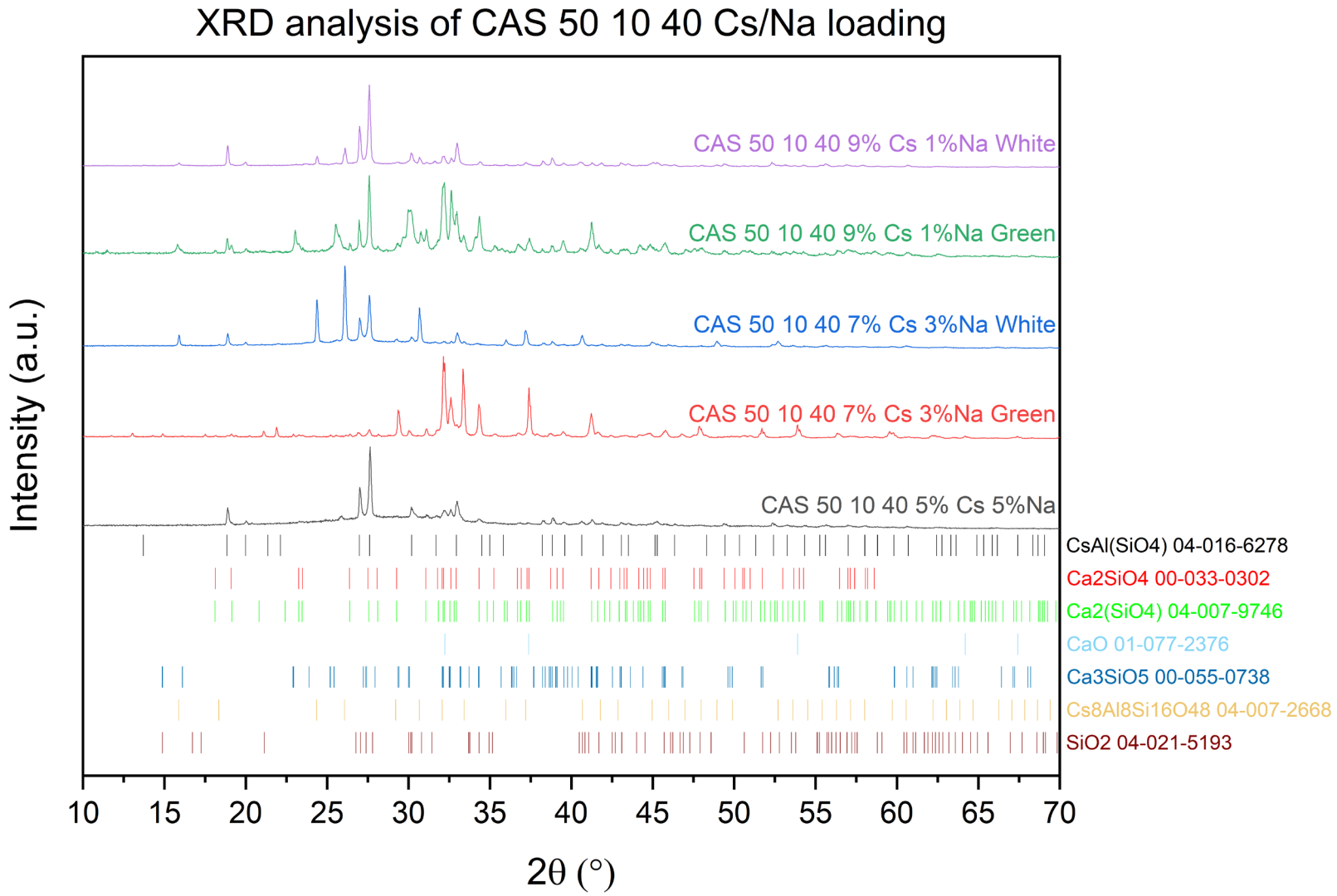

@ISL_Sheffield

The University Of Sheffield.

NucleUS
Immobilisation Science Laboratory

Raman of glasses

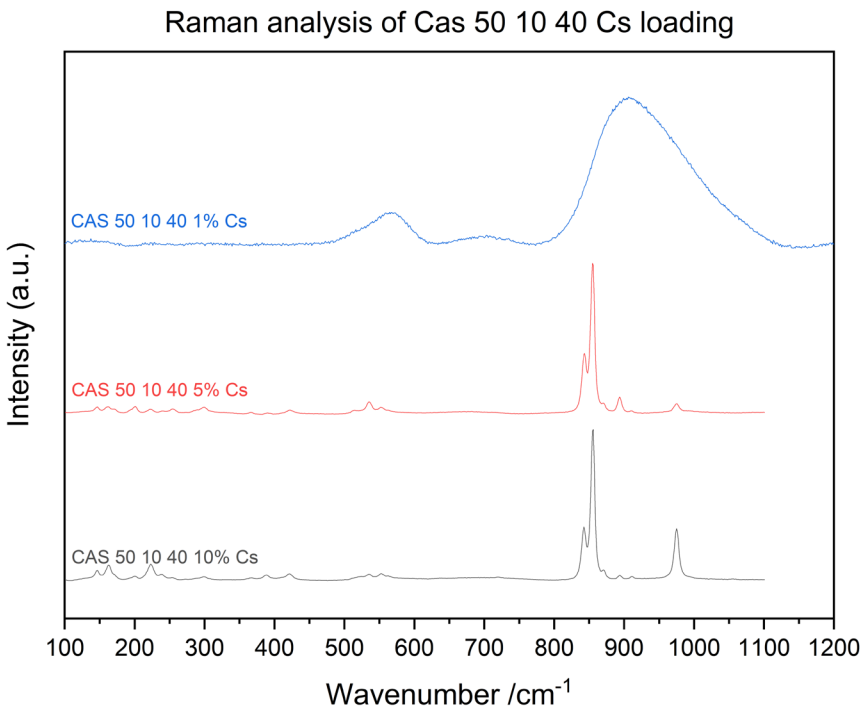

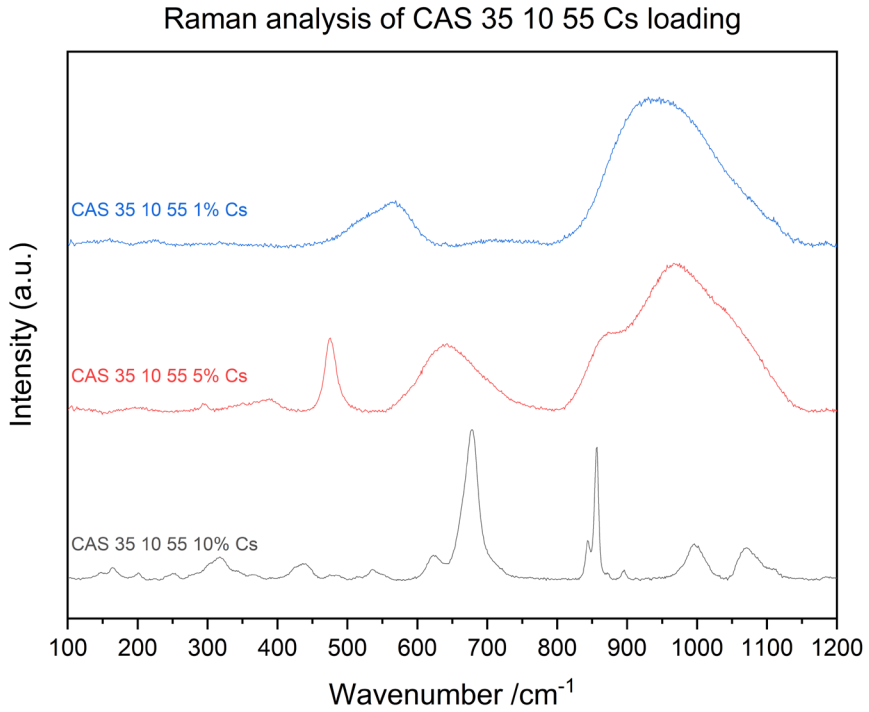

@ISL_Sheffield

The University Of Sheffield.

NucleUS
Immobilisation Science Laboratory

Raman of glasses

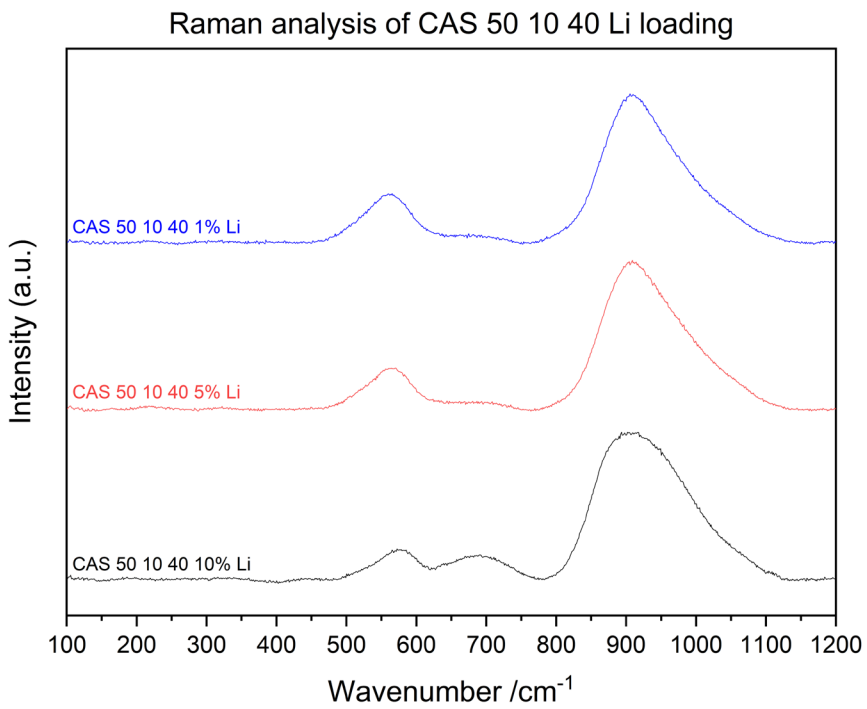

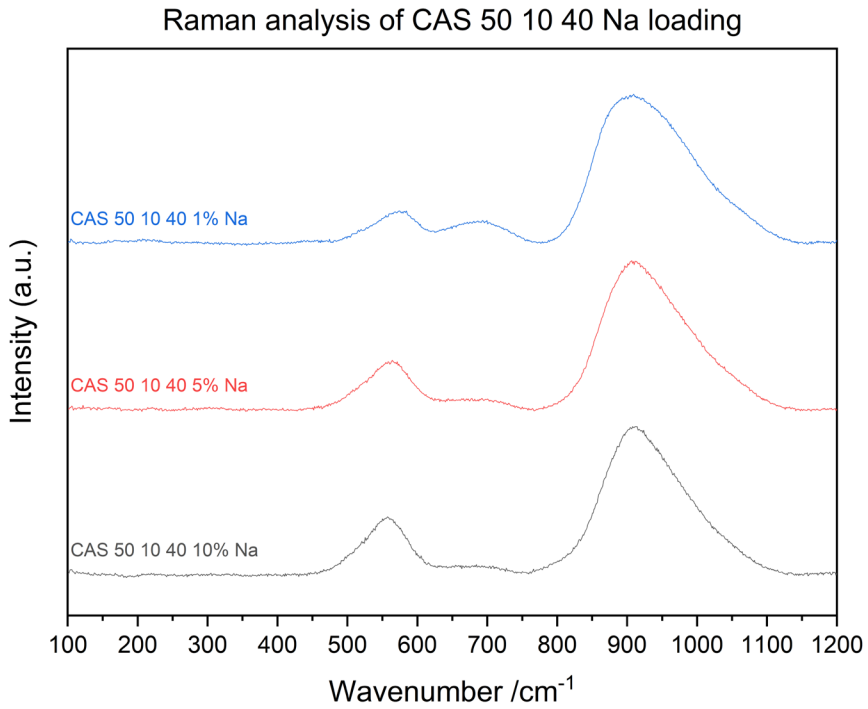

@ISL_Sheffield

The University Of Sheffield.

NucleUS
Immobilisation Science Laboratory

Raman of glasses

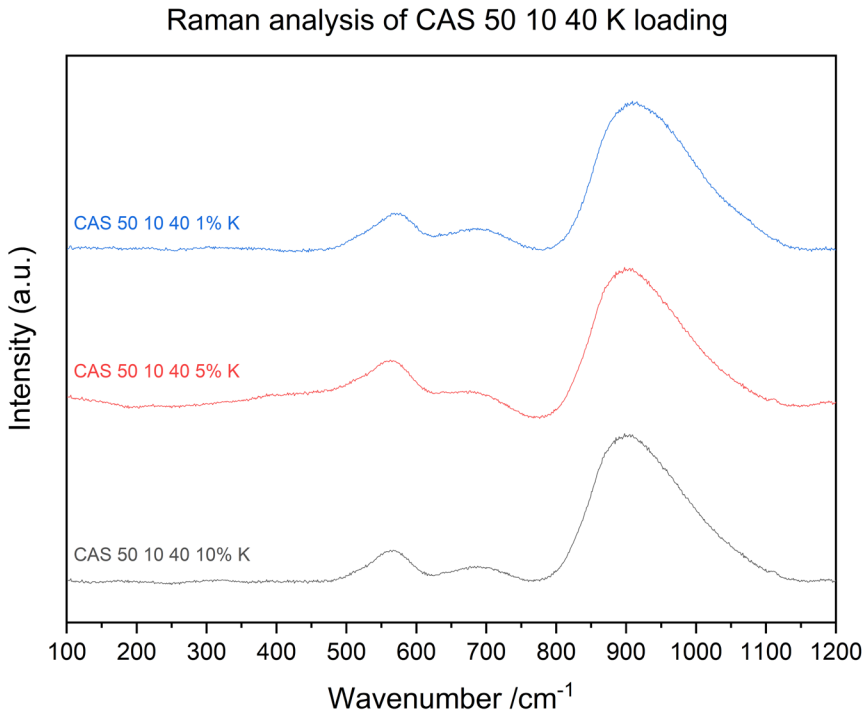

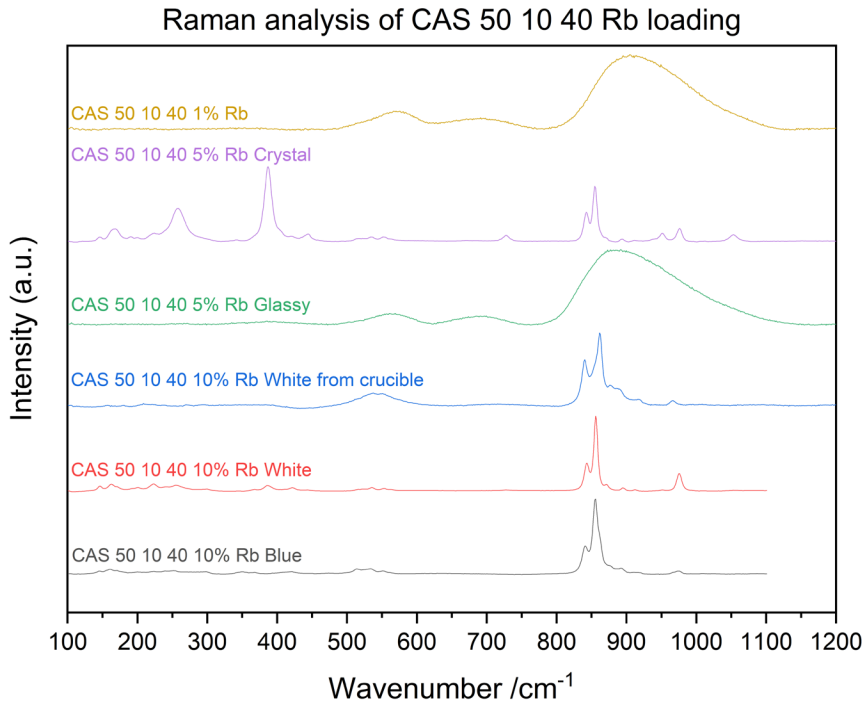

@ISL_Sheffield

The University Of Sheffield.

NucleUS
Immobilisation Science Laboratory

Raman of glasses

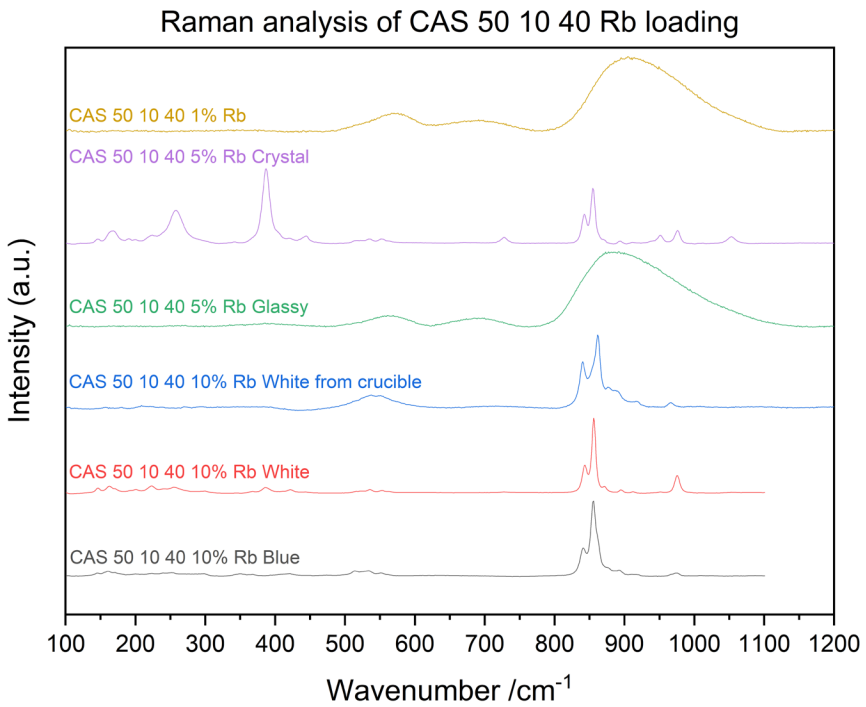

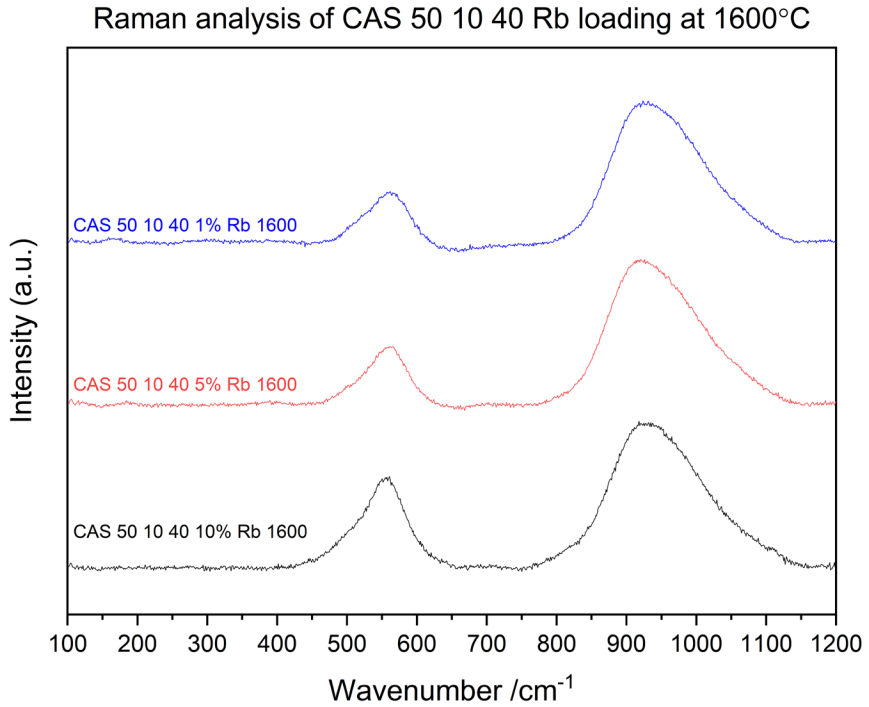

@ISL_Sheffield

The University Of Sheffield.

NucleUS
Immobilisation Science Laboratory

Raman of glasses

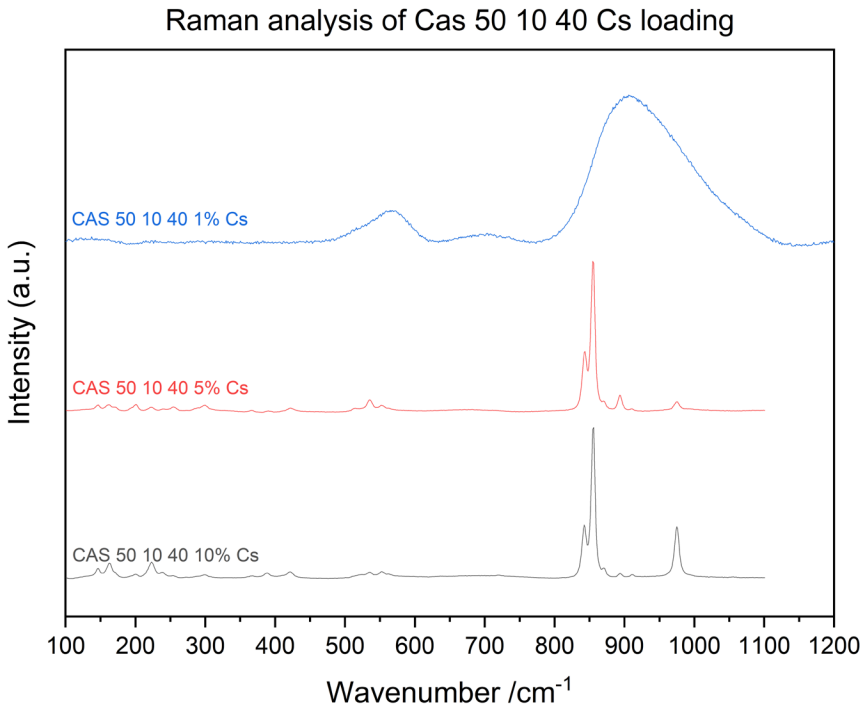

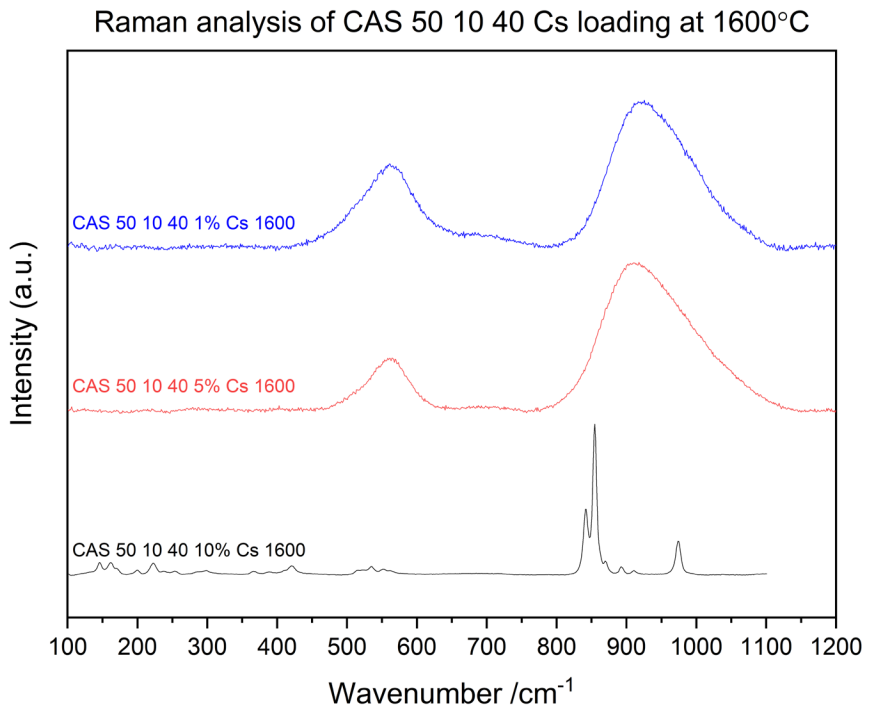

@ISL_Sheffield

Raman of glasses

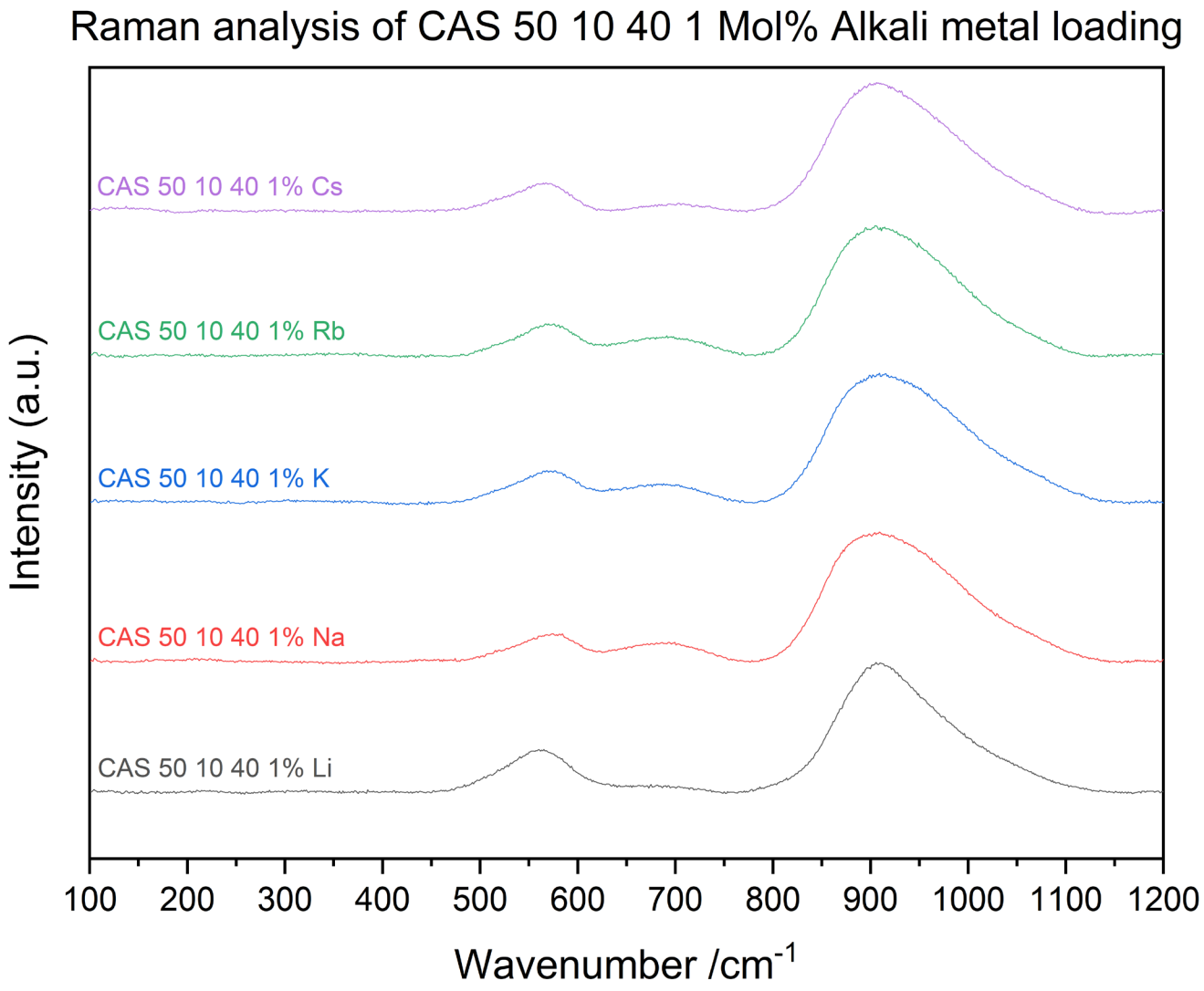

@ISL_Sheffield

The University Of Sheffield.

NucleUS
ilisation Science Laboratory

Raman of glasses

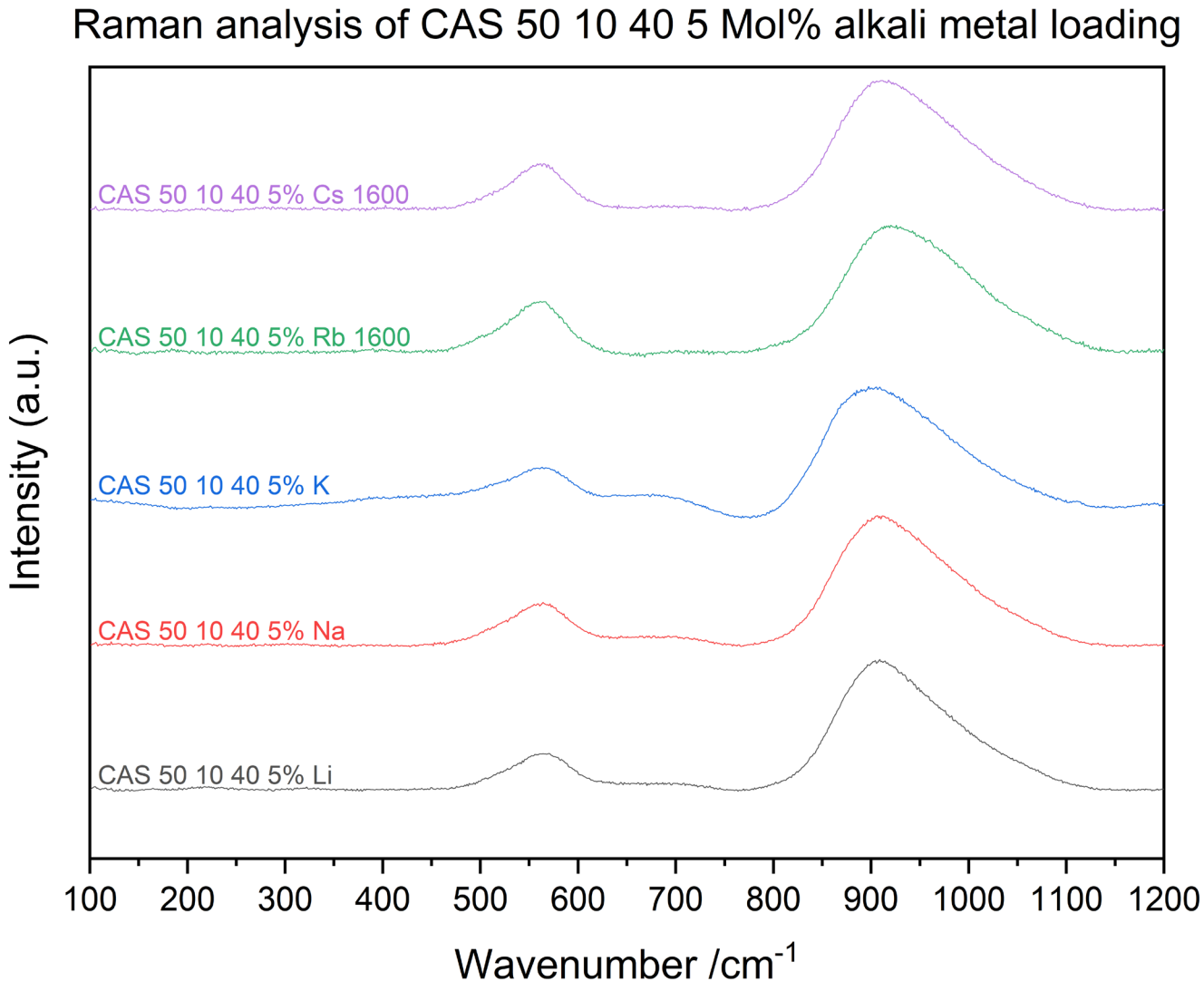

@ISL_Sheffield

The University Of Sheffield.

NucleUS
ilisation Science Laboratory

Raman of glasses

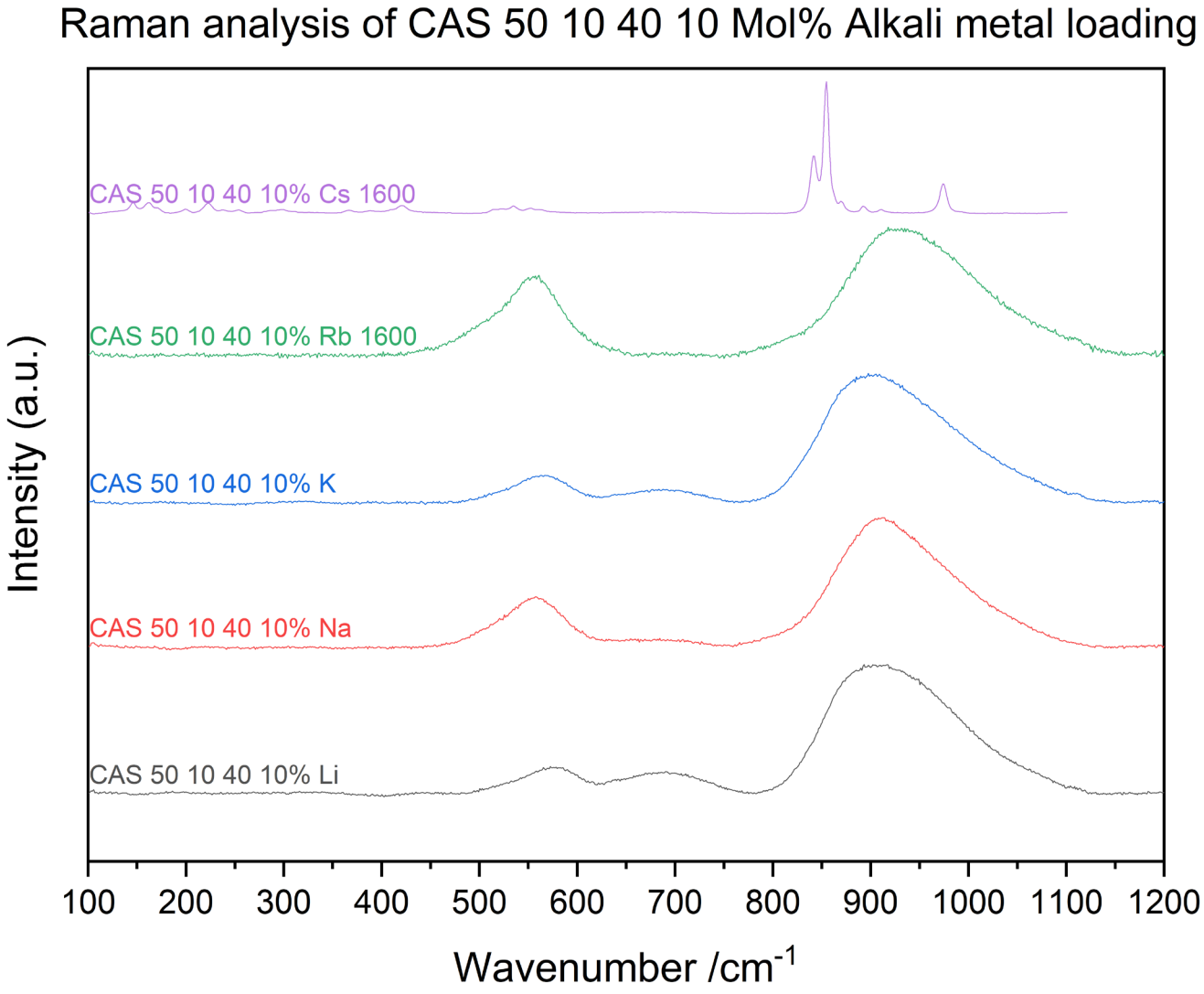

@ISL_Sheffield

The University Of Sheffield.

NucleUS
Immobilisation Science Laboratory

Further work

- Achieve a 10 Mol% Cs fully amorphous sample
- Get SS-NMR at warwick on CAS 10% alkalis and 1, 5 10% Cs
- Potential beamline data to support Raman and NMR
- Compositional data to see volatile retention
- Do melts of loaded Clino

@ISL_Sheffield

Acknowledgements

This research utilised the HADES/ MIDAS facility at The University of Sheffield established with financial support from EPSRC and BEIS, under grant EP/T011424/1.

Special thanks to:

Russell Hand
Daniel Bailey
Lisa Hollands
Martin Stennett
ISL group members

@ISL_Sheffield

"This research utilised the HADES / MIDAS facility at The University of Sheffield established with financial support from EPSRC and BEIS, under grant EP/T011424/1."

TRANSCEND

Transformative Science and Engineering for Nuclear Decommissioning

Improving *in situ* acoustic characterisation of suspensions with machine learning methods

Joseph Hartley, University of Leeds

TRANSCEND Annual Meeting 2022

02/11/2022
Technology and Innovation Centre, Glasgow

Energy
For a Low Carbon Future

TRANSCEND

Transformative Science and Engineering for Nuclear Decommissioning

Research Challenge

ILW legacy sludge at Sellafield needs to be processed for disposal.

Characterisation data on the sludge is difficult to collect.

A remote online monitoring system is needed to determine concentration and particle size.

Figure 13: Composition of ILW by waste group

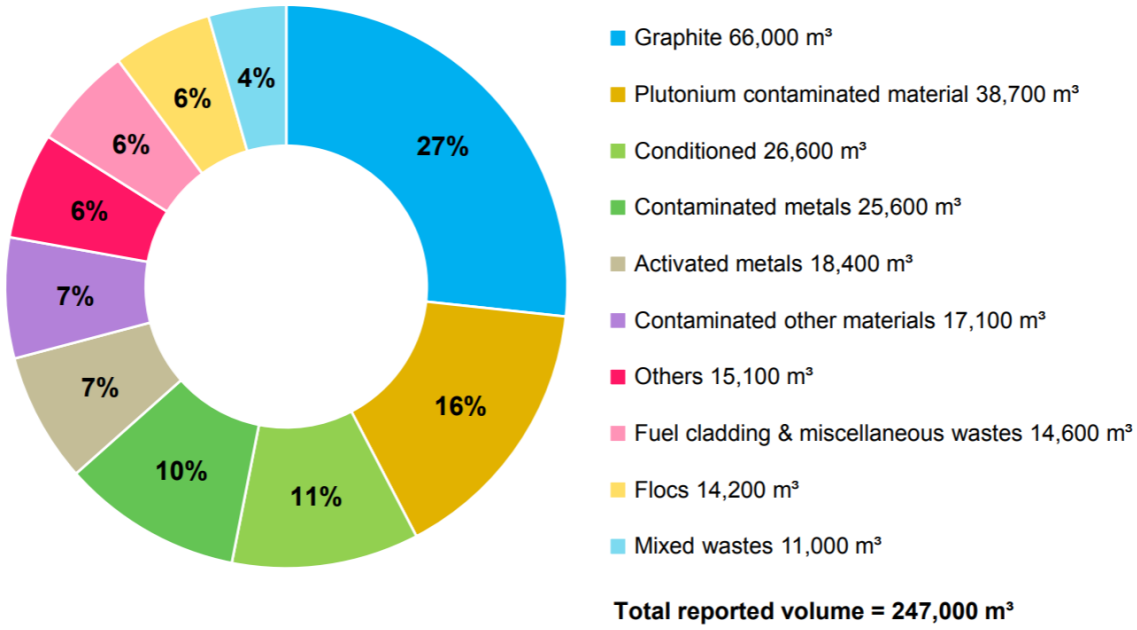

https://ukinventory.nda.gov.uk/wp-content/uploads/2020/01/2019-Waste-Report-Final.pdf

https://www.youtube.com/watch?v=Yu7-D37SKOY&ab_channel=SellafieldLtd

Acoustics

Acoustics has been used to characterise sediments in eaustrine environments and recently in nuclear decommissioning processes.

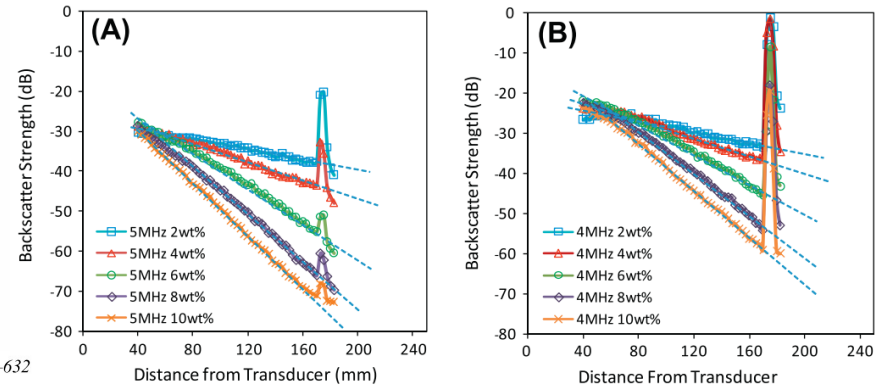

P.D. Thorne, D.M. Hanes / Continental Shelf Research 22 (2002) 603–632

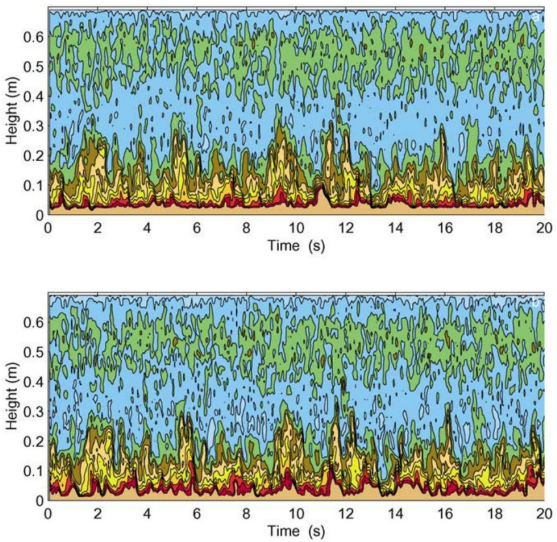

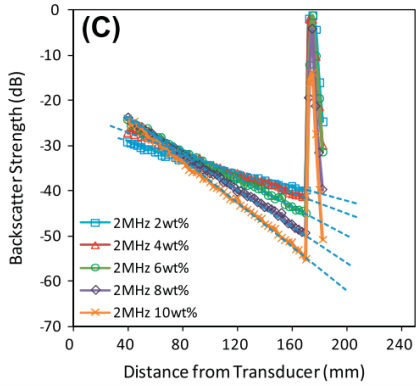

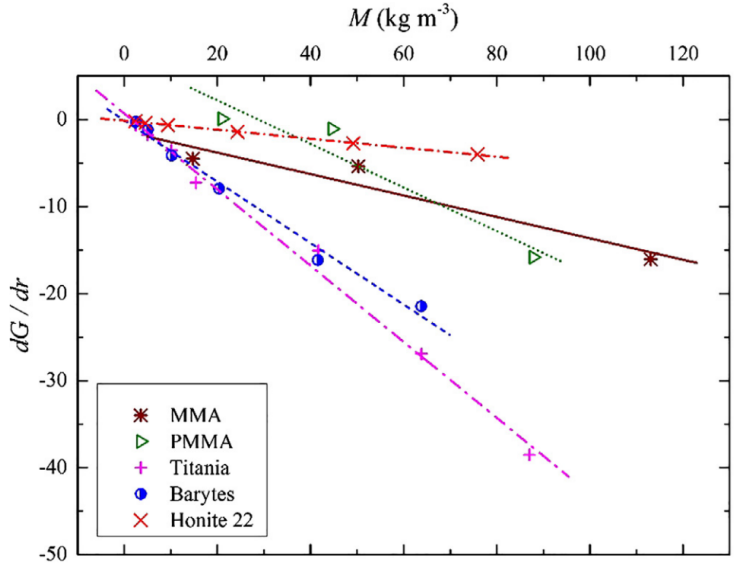

Thorne, Hanes; *A reveiw of acoustic measurement of small-scale sediment processes*

DOI:10.1016/j.mineng.2011.12.003

DOI: 10.1016/j.apacoust.2018.10.022

Research Aims

- Size Characterisation of virgin vs. sieved size fractions and bimodal size fraction mixtures of spherical glass particles.

- Development of Machine Learning code to characterise size and concentration of spherical glass particles.

- Application of aforementioned research to flocculated systems.

Acoustic theory – viscous & scattering losses

Two types of attenuation mechanisms; dependent on particle size, namely scattering and viscous elastic losses.

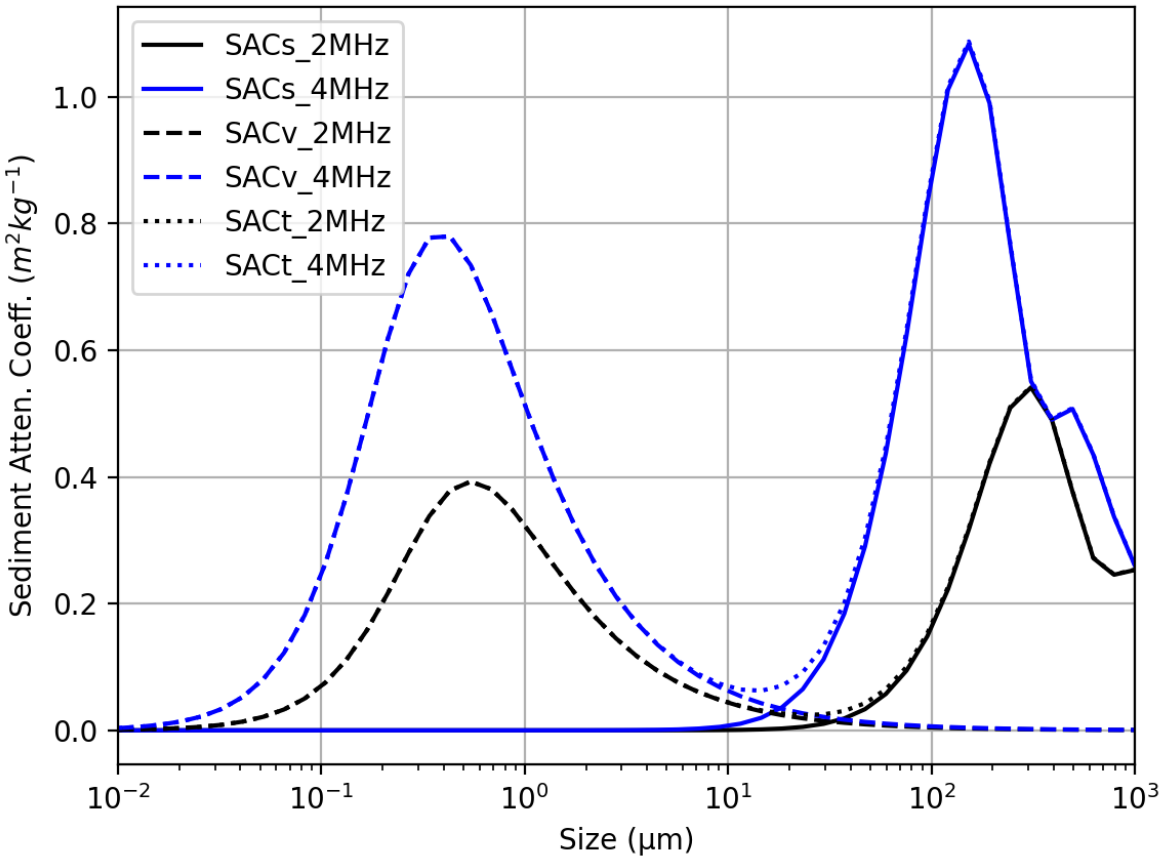

$$\xi = \frac{3(\chi_{ss} + \chi_{sv})}{4\rho a_s}$$

$$\chi_{ss} = \frac{0.24\varphi x^4}{0.7 + 0.3x + 2.1x^2 - 0.7x^3 + 0.3x^4}$$

$$\varphi = 1 - 0.4e^{-\left(\frac{x-5.5}{2.5}\right)^2} \qquad x = ka_s = \frac{2\pi}{\lambda}a_s$$

$$\chi_{sv} = \frac{2}{3}x(g-1)^2\left[\frac{s}{s^2 + (s+\delta)^2}\right]$$

$$g = \frac{\rho_s}{\rho_0} \qquad s = \frac{9}{4\beta a_s}\left(1 + \frac{1}{\beta a_s}\right)$$

$$\delta = \frac{1}{2}\left(1 + \frac{9}{2\beta a_s}\right) \qquad \beta = \sqrt{\frac{\omega}{2v_0}}$$

Methodology – Acoustic theory

$$V_{RMS} = \frac{k_t k_s}{\Psi r} M^{0.5} e^{-2r(\alpha_w + \alpha_s)}$$

V_{RMS} – backscatter voltage
k_s – sediment specific backscatter constant
k_t – transducer specific backscatter constant
Ψ –near field correction factor, taken as 1
r – distance from transducer
M – concentration of sediment (g/l)
α_w, α_s – attenuation due to water and sediment respectively

$$G = \ln(\Psi r V) = \ln(k_t k_s) + \frac{1}{2} lnM - 2r(\alpha_w + \alpha_s)$$

ξ^m – concentration independent sediment attenuation coefficient (SAC)

$$\alpha_s = M\xi^m$$

Methodology – Acoustic theory

$$\xi^m = -\frac{1}{2}\frac{d}{dM}\left[\frac{d}{dr}[\ln(\Psi r V)]\right] = -\frac{1}{2}\frac{d^2G}{dMdr}$$

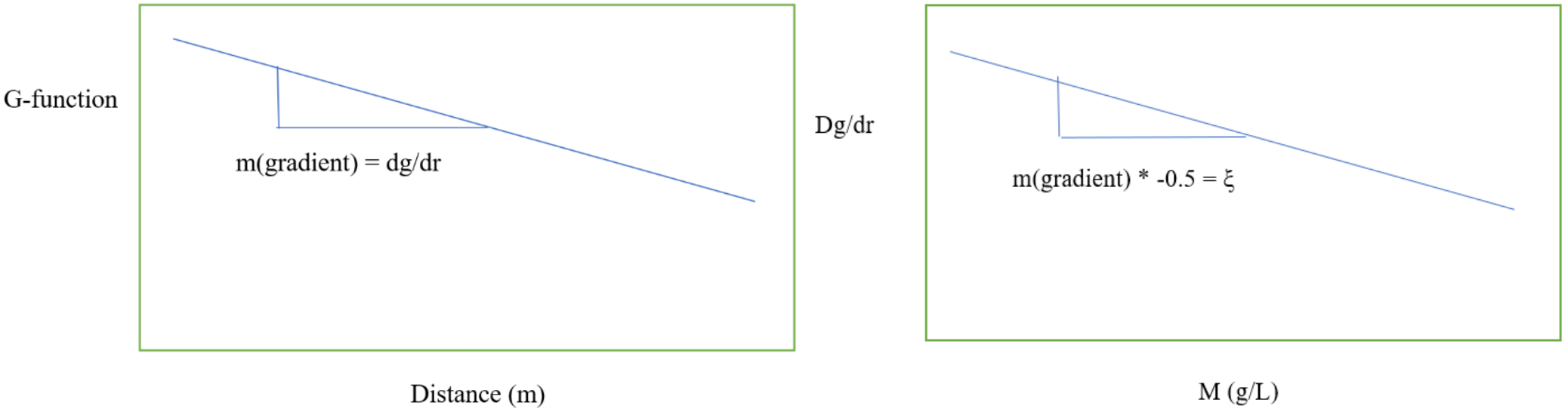

Setup

To speed up data collection, only in situ acoustic probes were utilised.

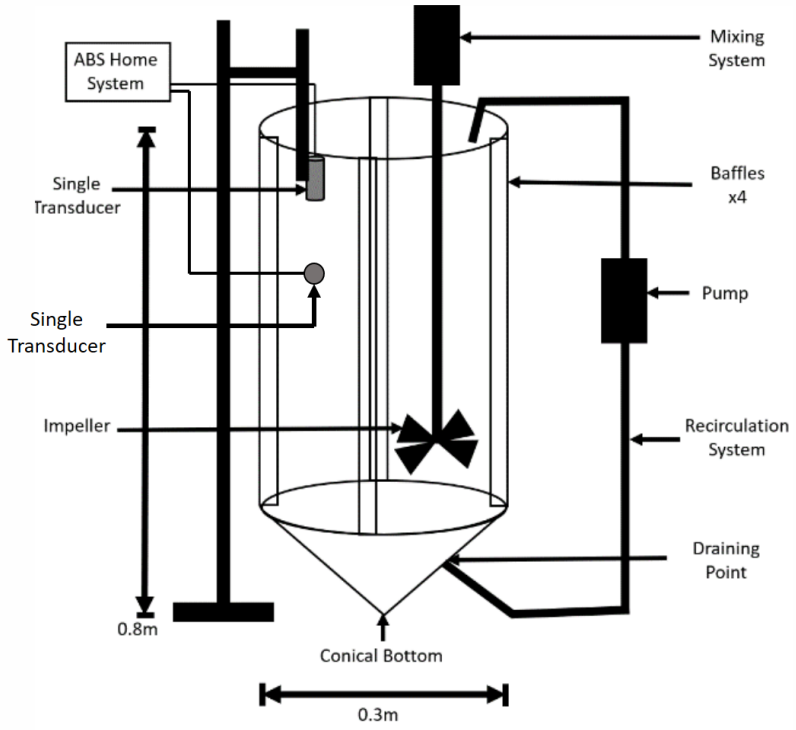

Mastersizer – PSD of bi-modal mixes

Large: Small Wt.%	μ (μm)	σ (μm)	C_v = σ/μ
0 : 100	37.6	8.8	0.23
25 : 75	44.9	14.8	0.33
50 : 50	64.1	25.3	0.39
75 : 25	81.2	28.6	0.35
100 : 0	86.4	15.4	0.17

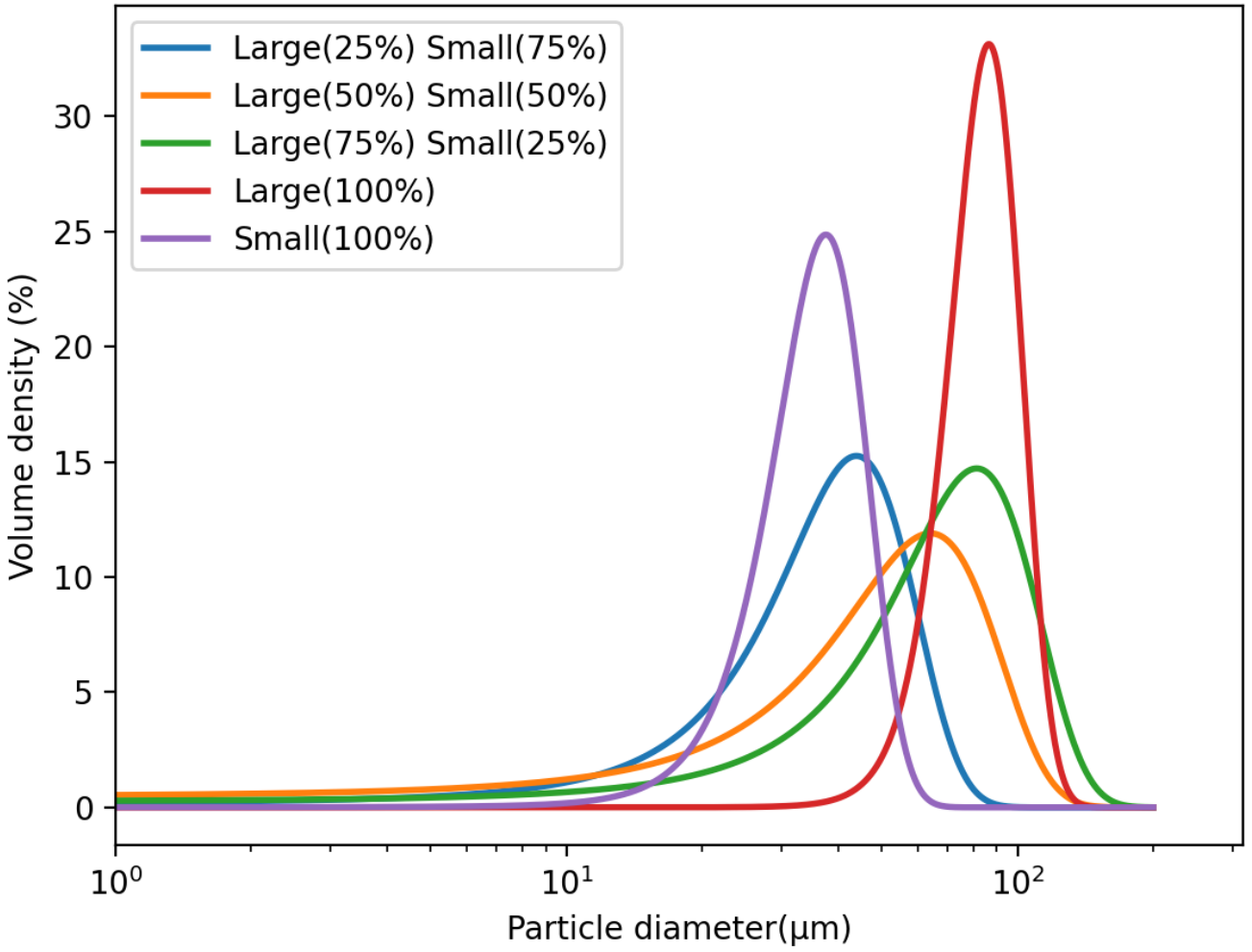

UVP Data – 2MHz – Large:Small - 25:75 and 50:50 wt.% mixes

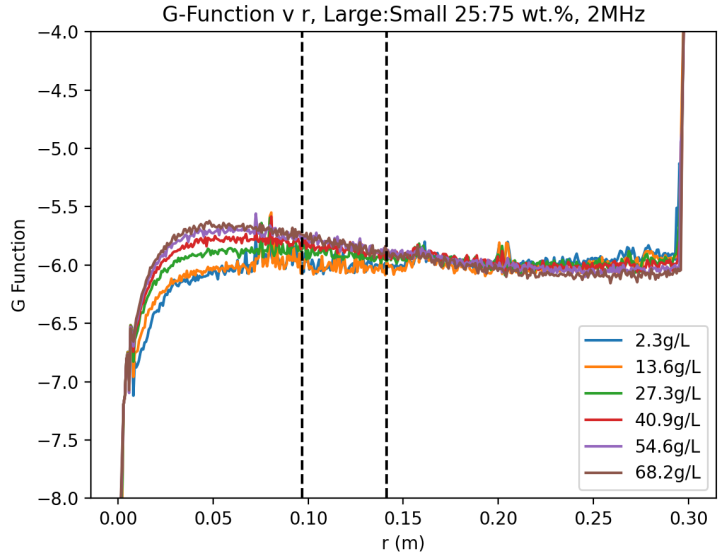

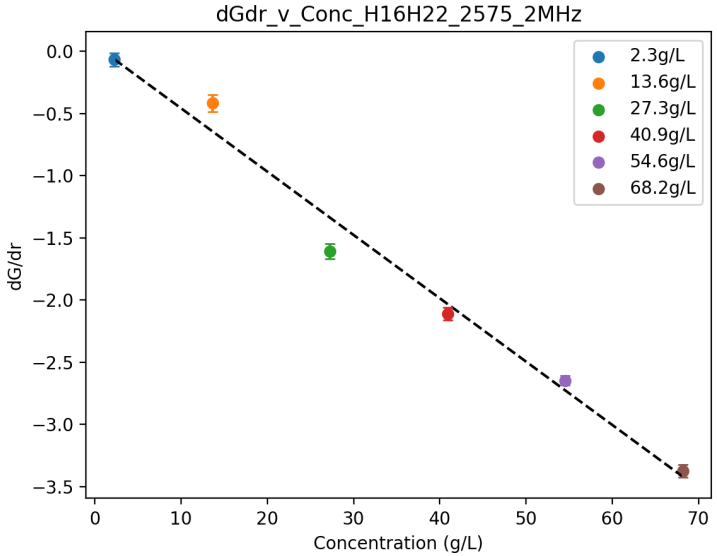

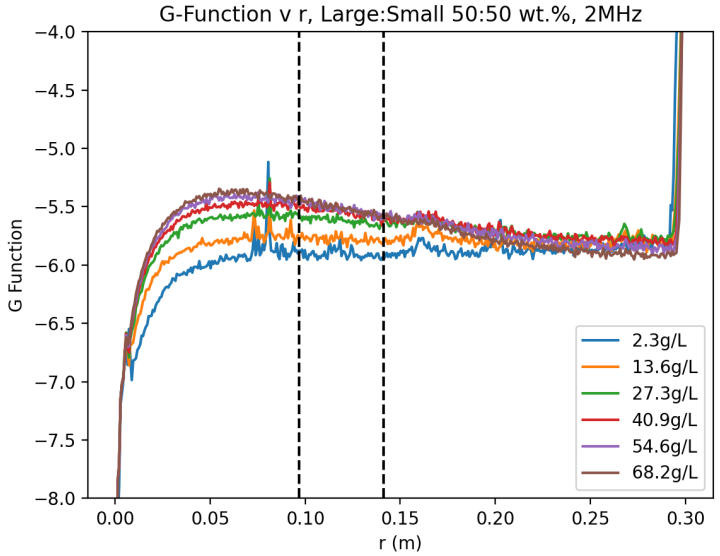

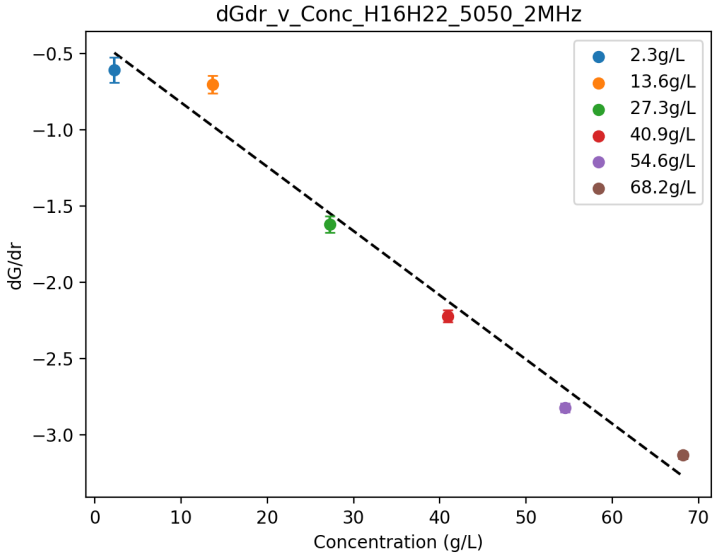

UVP Data – 4MHz – Large:Small - 25:75 and 50:50 wt.% mixes

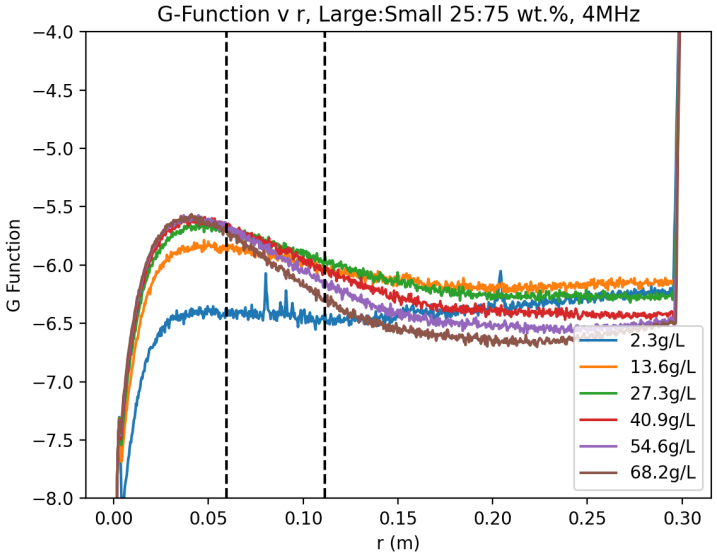

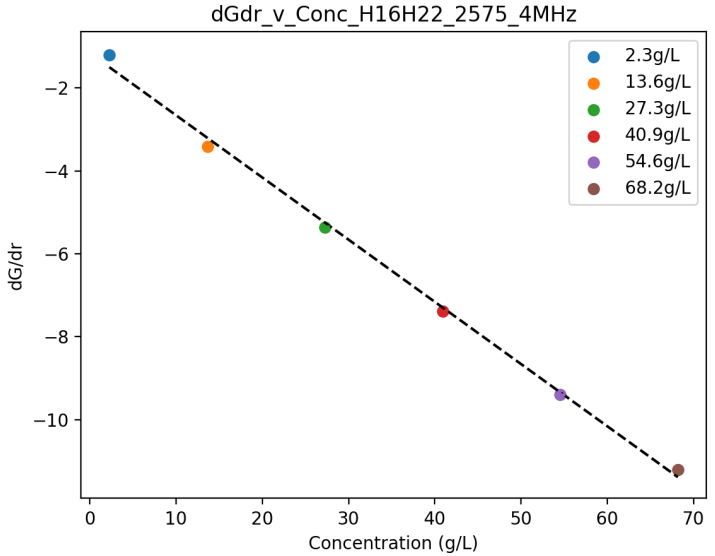

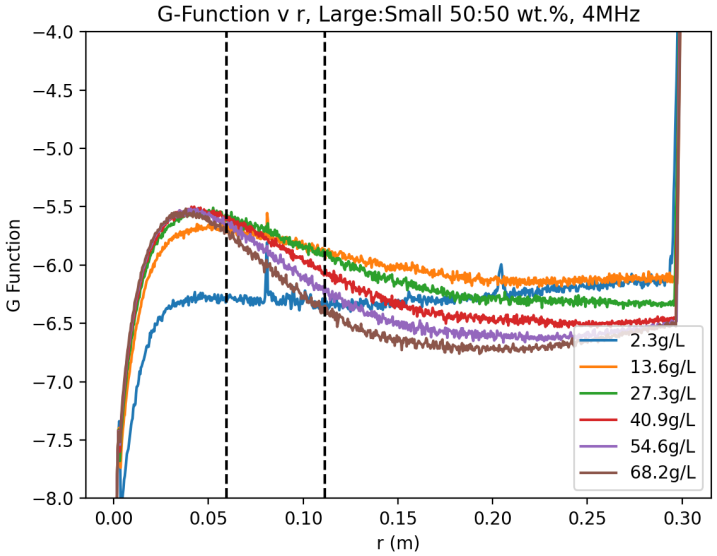

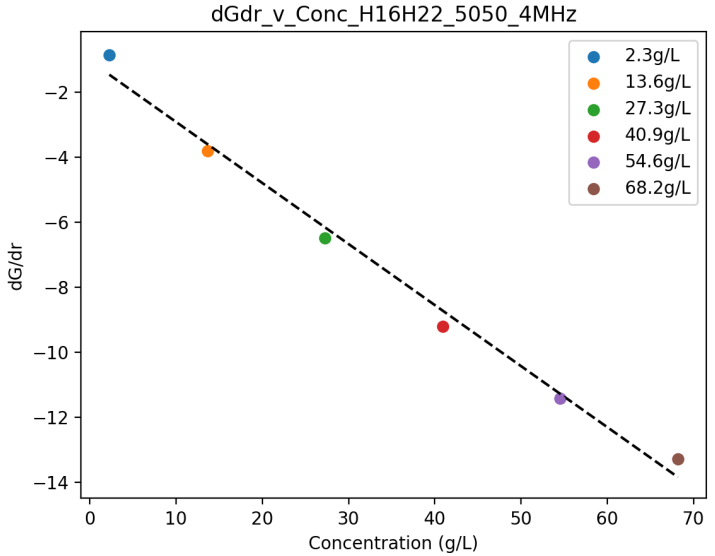

Sediment Attenuation Coefficient

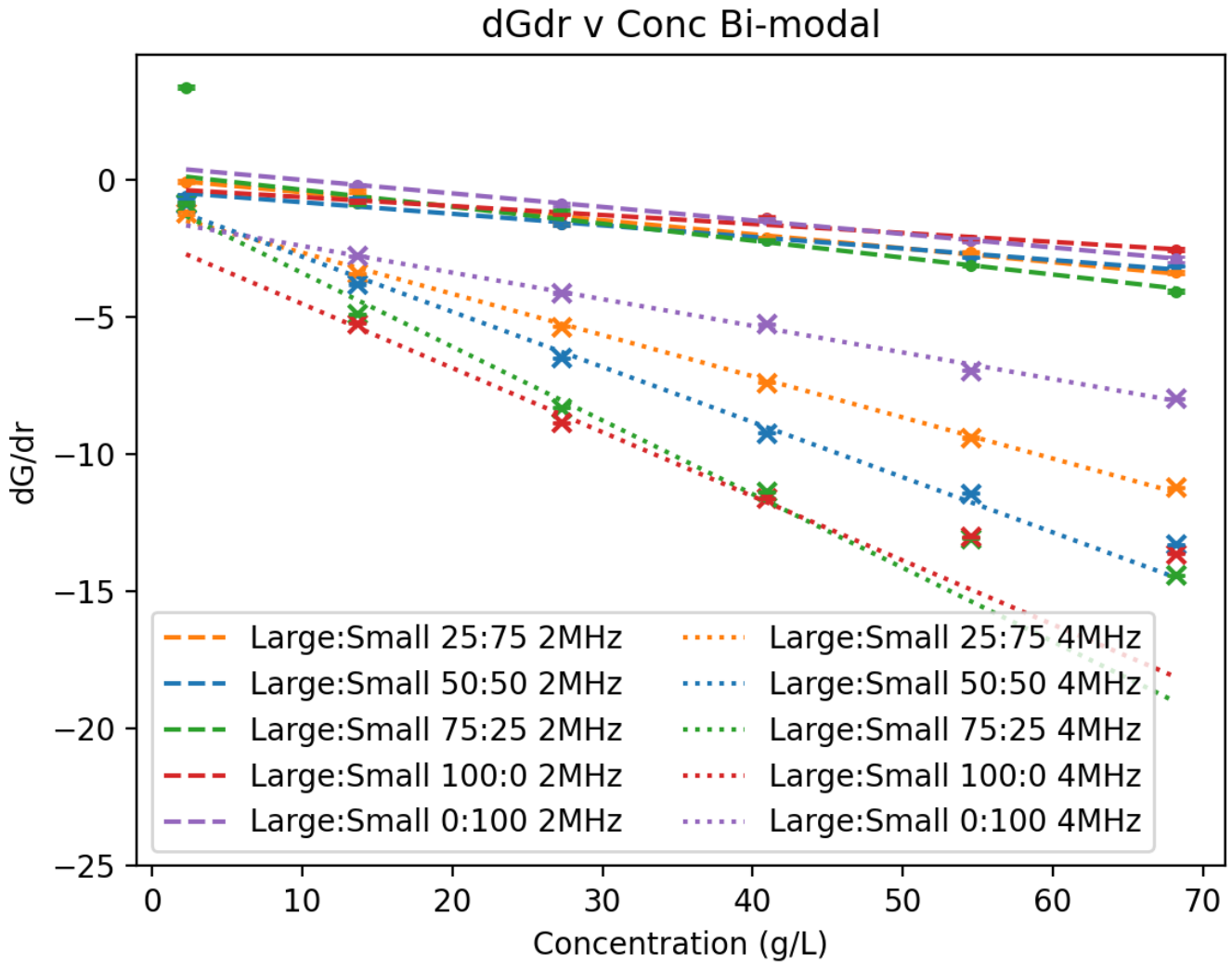

Sediment Attenuation Coefficient

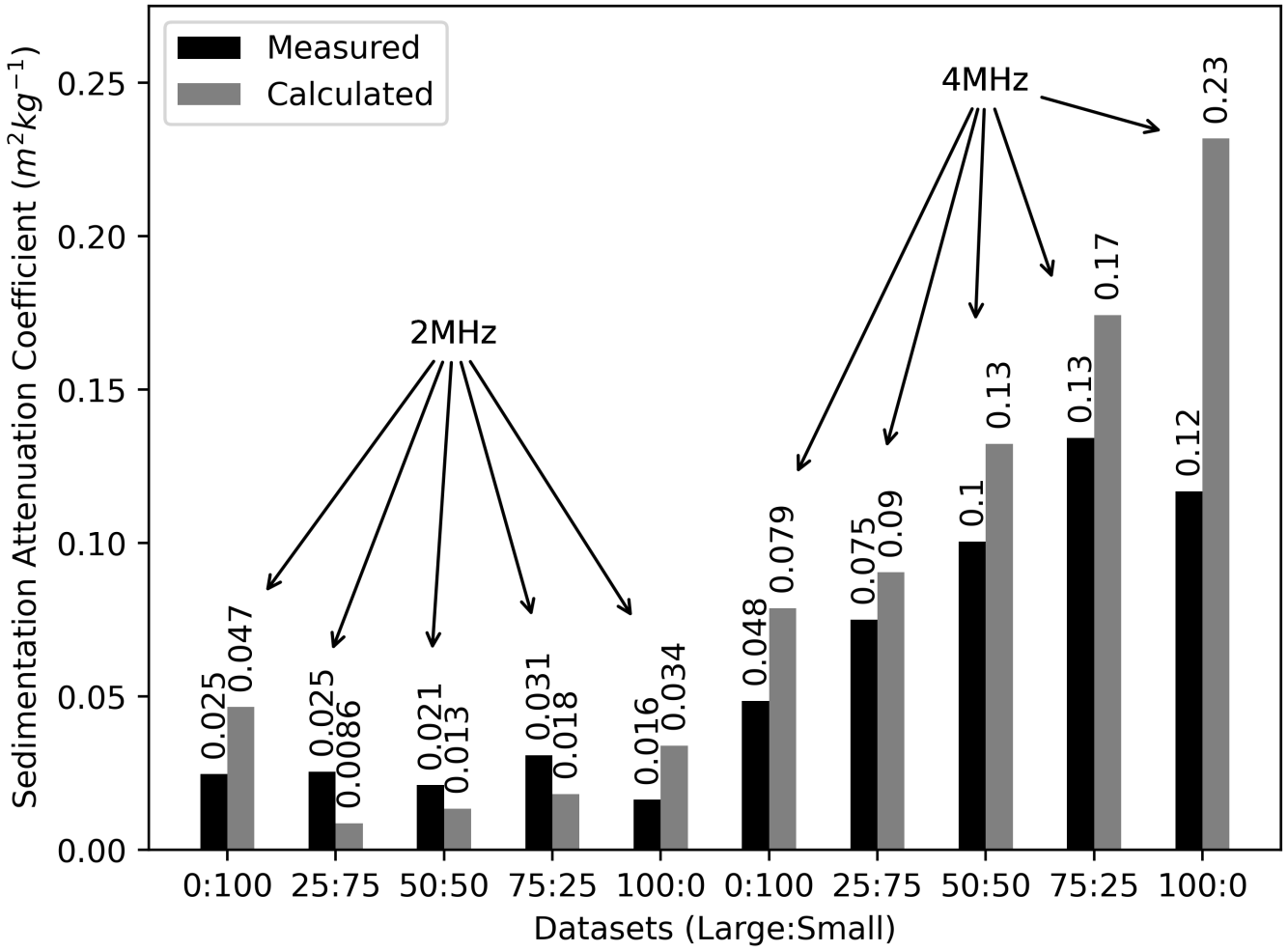

SAC calculations with size integral

- Current equation used to express SAC uses only a single mean value:

$$\alpha_s = \frac{3M(\chi_{ss} + \chi_{sv})}{4\rho a_s}$$

- Vergne et al (20) expressed the SAC which incorporates an integral over a range of particle sizes:

$$\alpha_s = \frac{3M\int_0^\infty a^2(\chi_{sv} + \chi_{ss})n(a)da}{4\rho_s\int_0^\infty a^3 n(a)da}$$

- Where the n(a) term describes the distribution using the mean and standard deviation of the distribution:

$$n_v(a) = \frac{1}{a\sigma\sqrt{2\pi}}e^{-((\log_e(a)-\mu)^2/2\sigma^2)} \qquad \mu = \log_e(a_0)$$

DOI:10.1029/2021wr029589

Bimodal mixes – volume v number

Acoustic models are built on principle of scattering events

Bimodal PSD is characterised by acoustic backscatter the signal will be a number average.

Number distributed mixes at same ratios need testing

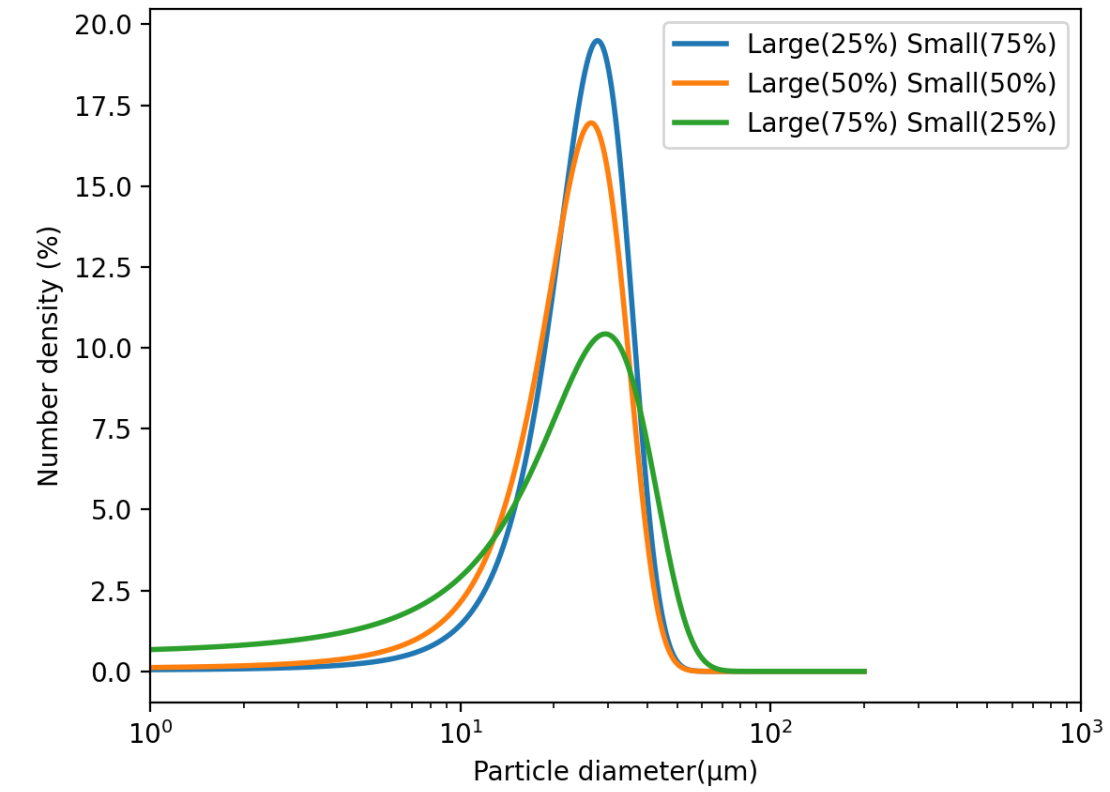

Future work

- Repeat acoustic data collection with number distributed mixes.
- Gather acoustic data on sieved material and as-received material at same concentrations.
- Apply integral sediment attenuation coefficient calculation method and incorporate weighted coefficients for two-peak PSD.
- Draft a machine learning method for determining SAC and particle size from acoustic data.

Future work – NPL work from ARF

Active work to be completed with a visit to NPL:

- Characterisation of acoustic probe with NPL's hydrophone beam plotting facility:
  - Electrical impedance measurements;
  - Axial beam-profiling;
  - Detailed 2D raster scans, carried out at the last-axial maximum and close to the transducer face (< 3 mm).
  - Reporting the pulse-echo response of the transducer using a standard reflecting target.
  - The above measurements to be performed at two drive voltages such that propagation of ultrasound through the water is under linear and nonlinear conditions ("low" and "high" drive conditions).
- Irradiate probes up to 1 MGy.
- Repeat characterization to determine if the exposure to radiation has affected the probe.

TRANSCEND

Transformative Science and Engineering for Nuclear Decommissioning

NUCLEAR ENGINEERING
University of Leeds

NATIONAL NUCLEAR LABORATORY

Thank you

Email:
pmjha@leeds.ac.uk

MANCHESTER 1824
The University of Manchester

Reactions of NO and H_2O on the PuO_2 {111} surface: a DFT study

Xiaoyu Han
Nikolas Kaltsoyannis

Department of Chemistry, The University of Manchester
Glasgow, 2022

TRANSCEND

MANCHESTER 1824
The University of Manchester

Background

The Sellafield nuclear reprocessing site in Cumbria © Redharc Images/Alamy

UK has the world's largest stockpile of the PuO_2.

- Sellafield in Cumbria
- 2 "Magnox" research sites and 10 nuclear power stations

Only one container detected **H_2**
The **N_2** and **O_2** ratio is not the same ratio as in air.

Inside of the PuO_2 storage container, **water** and other small molecules (**NO**) might interact with PuO_2

However, there are limited approaches to fully investigate this material due to the high restrict regulation and difficulty in preparing and handling this material.

Calculation details

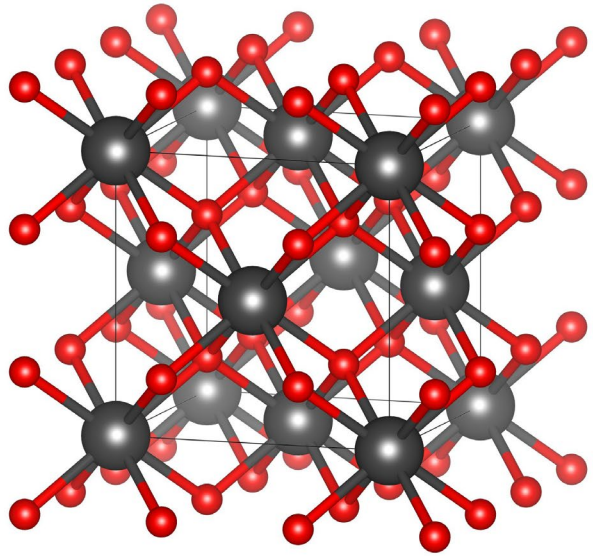

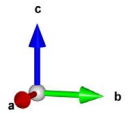

- Periodic condition DFT: VASP;
- DFT+U: Dudarev approach;
- E cutoff 10^{-5} and F cutoff 0.01 eV/Å;
- Grimme-D3 method for vdW
- G-type AFM magnetic ordering for both bulk and surface;
- 3 X 3 with 6 repeated layer supercell for the surface;
- The reaction free energy ΔG calculated at 300K

$$\Delta G = \Delta E_{DFT} + \Delta E_{ZPE} - T\Delta S$$

- The energy barriers are calculated using Ci-NEB method

MANCHESTER 1824
The University of Manchester

Outline:

- Section I: U factor
- Section II: NO and H_2O individually reacts on PuO_2 (111) surface
- Section III: Sequence reactions

Section I: Choices on the Hubbard U

- The experimental data on lattice parameter, **bandgap**, bulk modulus, etc.

1) **1.8 eV**; electron activation energy(1964);[1]
   - Calcined plutonium oxalatc; 20-1000 C; linear fitting for intrinsic bandgap.
2) **2.80 eV**; optical band gap (2013);[2]
   - PAD thin film; RT
3) **4.1 eV;** Ultraviolet Photoelectron Spectra (UPS)+ Inverse Photoemission Spectroscopy (IPS) (2021).[3]

(A) The form of the sample
(B) The technic of the measurements

- A linear response approach to the calculation of the effective interaction parameters in the DFT+U method

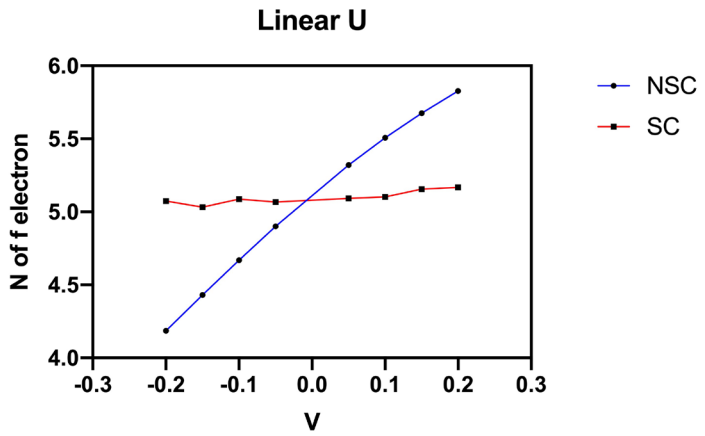

a small added potential on f electron (0.2 eV) could change the number of f electron by nearly 2 e.

Revisiting the U effect on PuO_2 is needed!

- The redox reaction from the experiment

[1]C.E. McNeilly, J. of Nuclear Materials, 11, 53, (1964)
[2] T. Mark McCleskey, J. of Appl. Phys. 113, 013515 (2013);
[3] P. Roussel, AJ Bishop, AF Carley, Surf. Sci. 714 12191(2021)

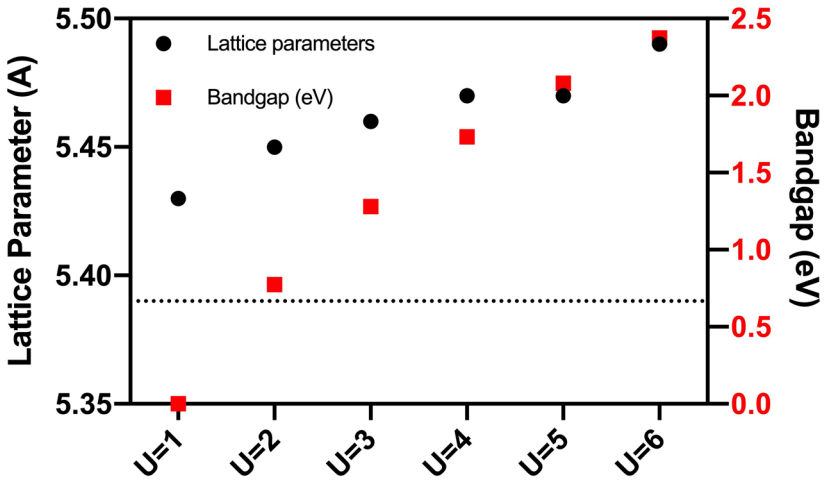

The dash line is the lattice parameter from exp.

- +U overestimates the lattice parameter but opened the bandgap
- U values doesn't affect on lattice parameter that much;
- Larger U, bigger the bandgap

Which U could mimic the electronic character?

MANCHESTER 1824
The University of Manchester

PuO_2 in-between

A Mott insulator ⟷ A charge-transfer insulator

bandgap between bands alike

bandgap between anion and cation states

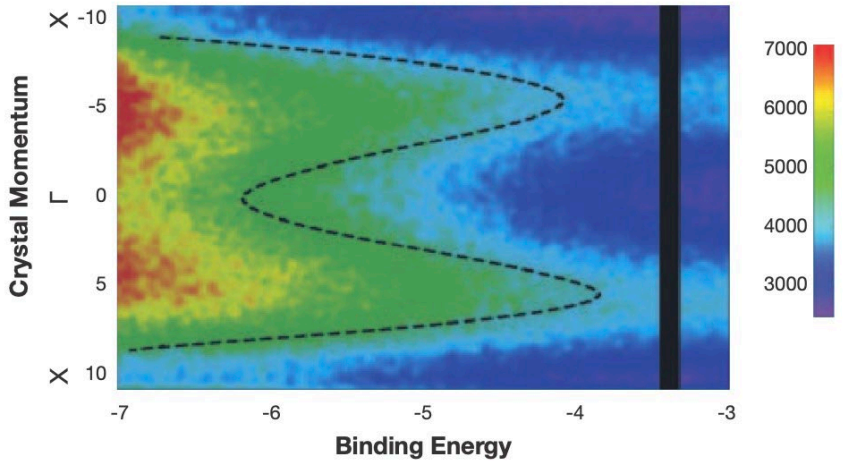

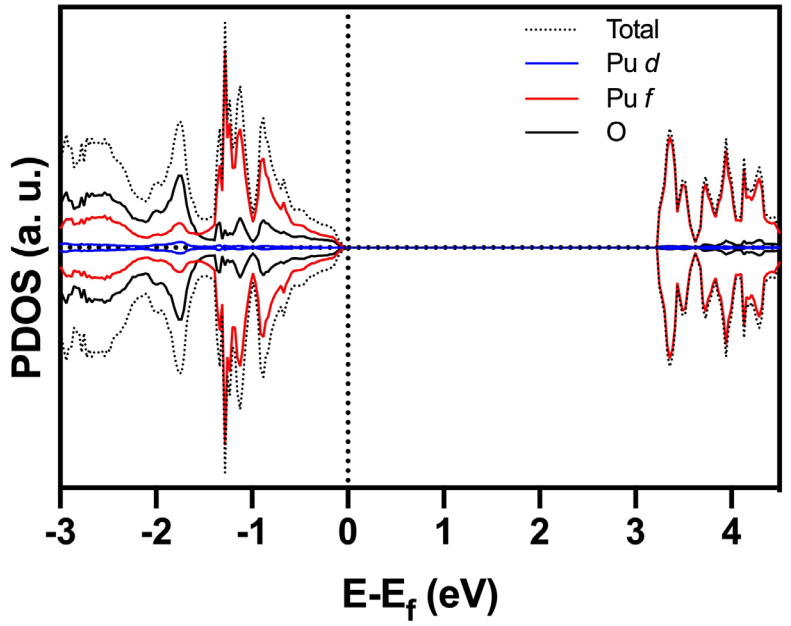

the degeneracy of the plutonium 5f and oxygen 2p bands

ARPES for PuO_2 on a PAD film at 40.8 eV (enhance 5f character)*

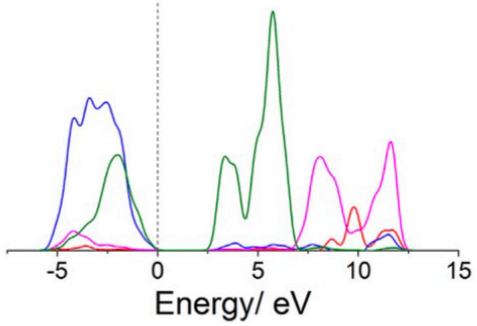

Fig. 4. PDOS of bulk AnO_2 (An = U (top), Np, Pu (bottom)) modelled as $An_{16}O_{32}$ clusters with the PEECM and the PBE0 functional. Vertical line shows the Fermi level. Vertical scale in arbitrary units.

Pu 5f **hybridization** with O 2p orbital at valence band is the KEY.

*LANL Research Quarterly, Issue 1, page 25, 2014

**Journal of Nuclear Materials 482 (2016) 124-134

5f-2p hybridization and peaks distance

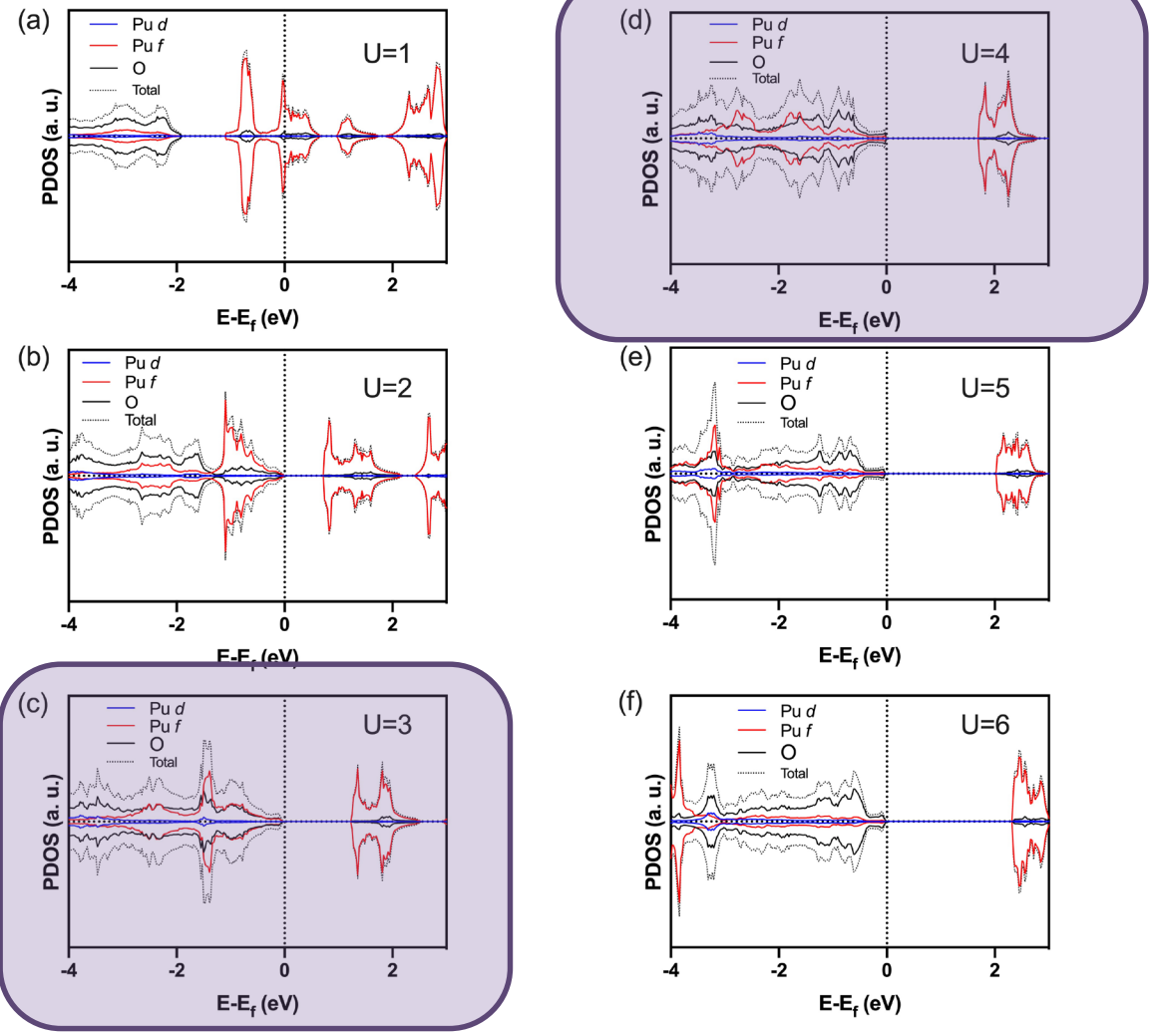

The O 1s XES :Two shoulders with width of 1.8 eV

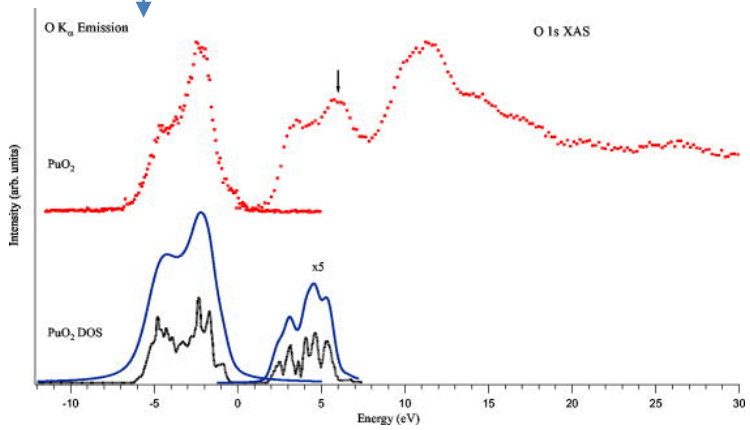

- Small U leads to metallic;
- a charge-transfer insulator in large Hubbard U;
- a Mott insulator in small Hubbard U
- Peaks distance is **0.51 eV** and 0.37 eV for U=3 and 4, respectively

U=3 preserved the **hybridization** and closer to XES data of **the peaks distance**

PuO_2 (111) work function

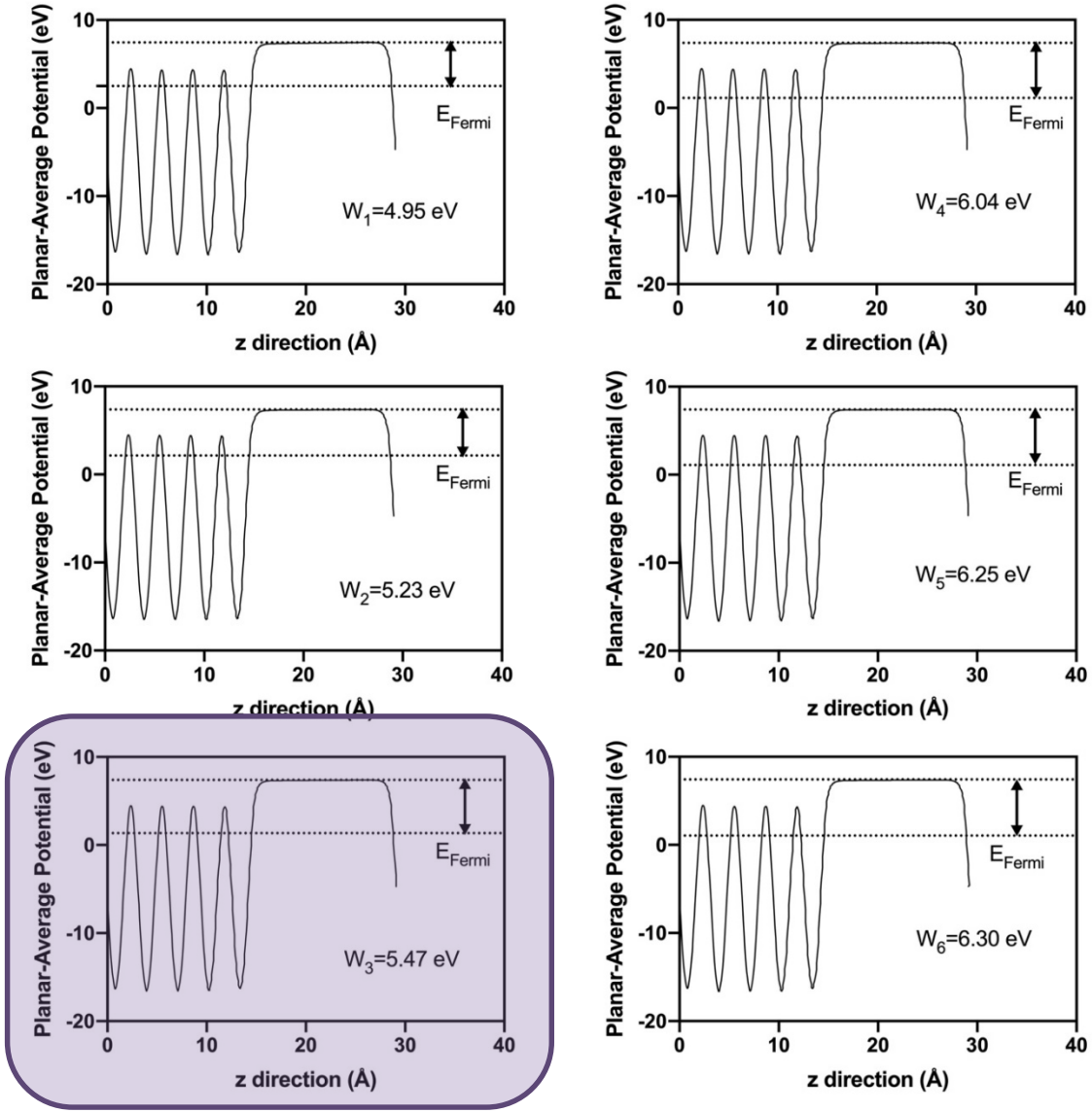

W: How hard to remove an electron from the surface

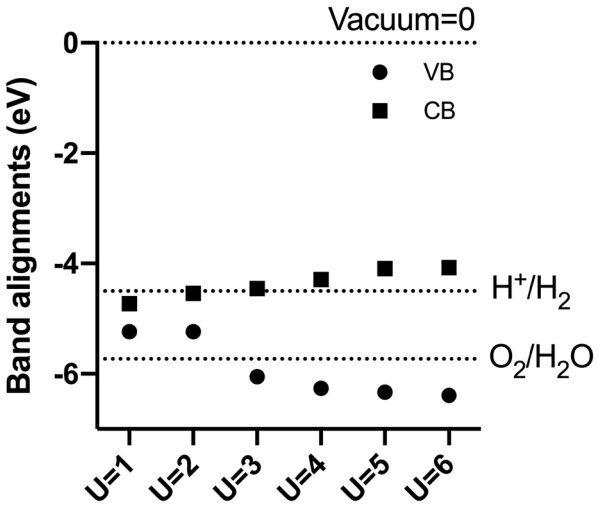

exp. data: 5.6 ±0.1 eV [1]

U=3 is the winner!

For larger U, the band alignments of PuO_2(111) surface is favorable for water redox reaction.

A carefully selected U is essential.

[1] P. Roussel, AJ Bishop, AF Carley, Surf. Sci. 714 12191(2021)

The effective charge

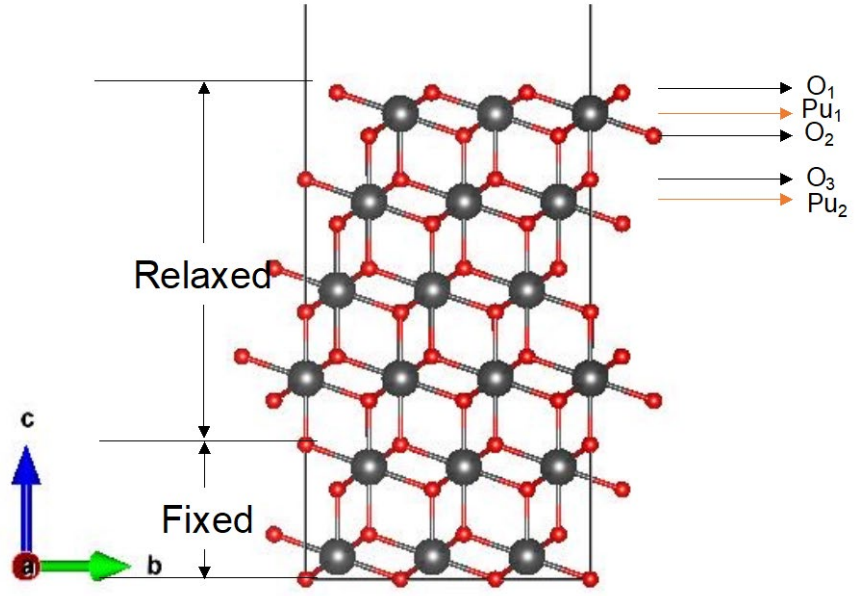

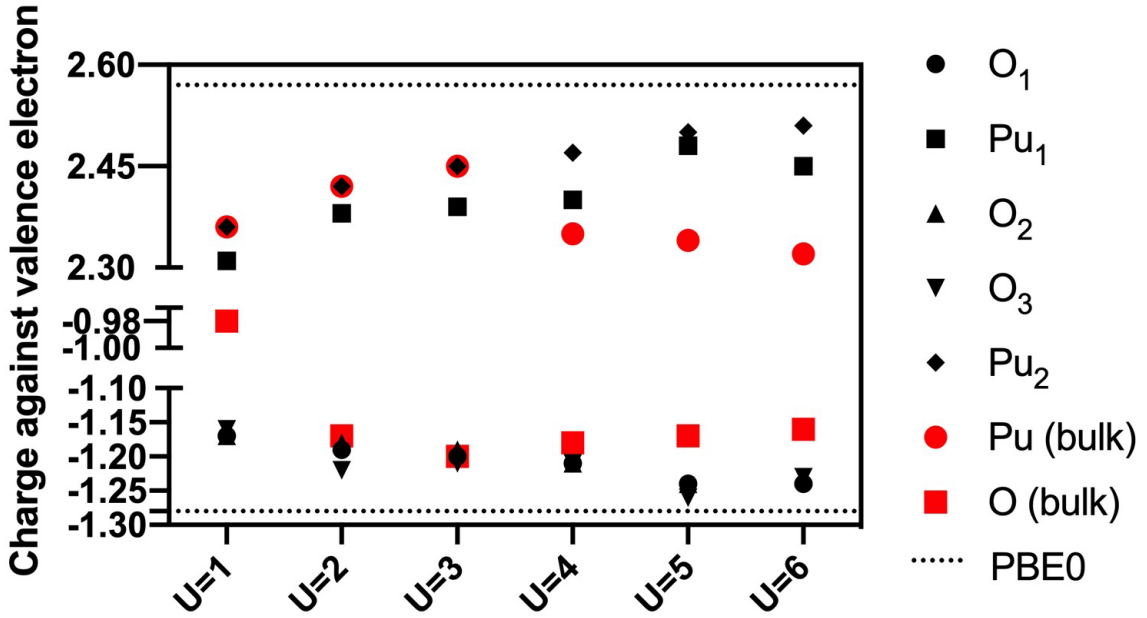

- DFT+U results are overall underestimated the oxidation states of Pu
- **U=3** is closer to the results from PBE0 in bulk form;

- When U<4, the surface Pu_1 is less oxidized than bulk form, reasonable that the surface atom tends to delocalise its electron to form the surface states
- Meanwhile, the second layer (Pu_2) has the same oxidation level as in the bulk form.

MANCHESTER 1824
The University of Manchester

Summary of section I

- Systematic studied the U value affect on the PuO_2;

experiments	theory	Outcomes
UPS+IPS	Hybrid functional in PEECM method and period condition DFT	Bandgap & work function
ARPES		5f and 2p electrons hybridization
XES		Peaks distance of valence band
	Bader charge	Surface states from surface metal electrons

- **U=3** is the best to mimic the electron characters of the PuO_2;

Section II The individual NO and H_2O molecule reaction on PuO_2 {111} surface

H_2O

Step 1A: H_2O + * → H_2O*; Step 2: H_2O* → HO* + H*

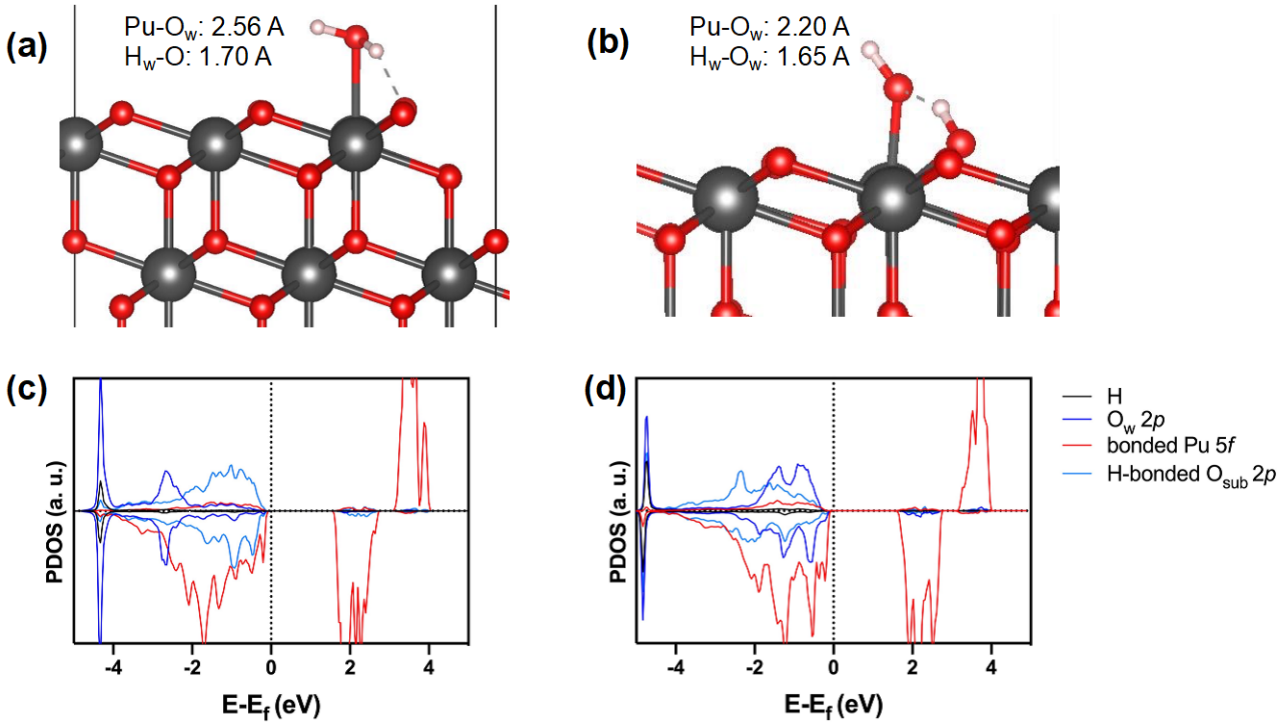

	E_{ad} (eV)	ΔG (eV)
Step 1	-0.66	-0.68
Step 2		-0.12

E_b = 1.15eV

Confirmed our band alignments against water redox potential when U=3

NO major **charge** changes in **water** in both molecular and dissociated forms

O_w is more hybridized with Pu in VB

MANCHESTER 1824
The University of Manchester

NO ⊥ PuO_2

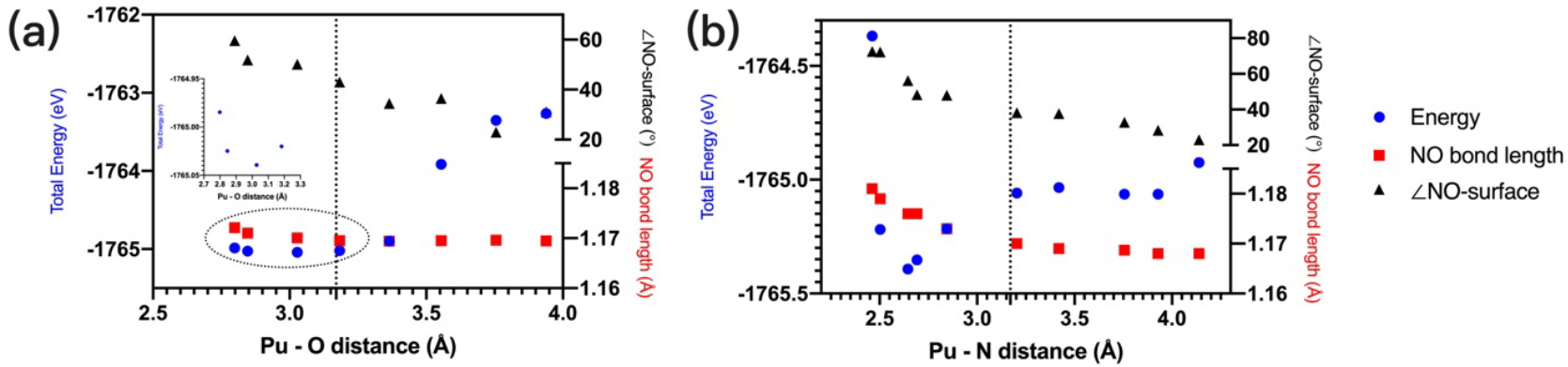

- N pointing down towards Pu is energetic favorable;
- N pointing down also stretched N-O bond length when it reached its energy valley;
- Both experienced from parallel with the surface to perpendicular;

NO//PuO_2

Step 1B NO + * → ON*//

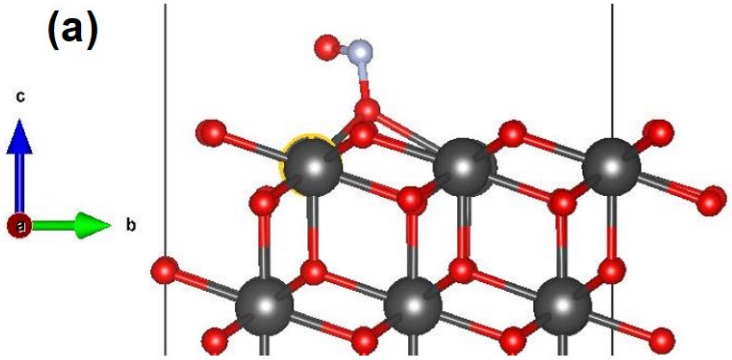

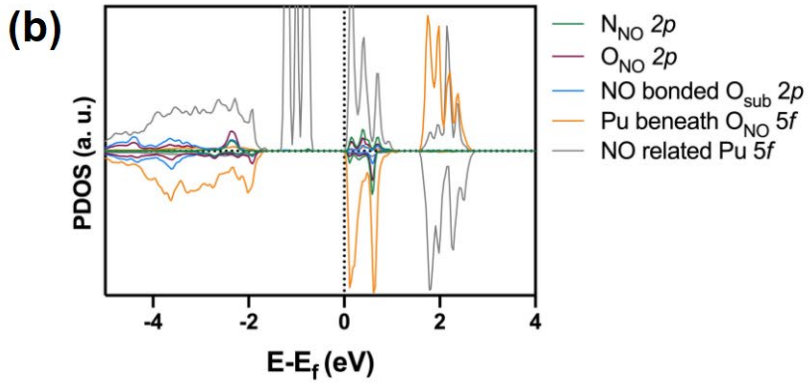

Partial Bader Charge O_{sub} = 0.78e (1.21 e in pristine)

O_{NO} > N_{NO} in bonding states
O_{NO} < N_{NO} in antibonding states

$Pu_{beneath}$ hybrids with NO;
Others contribute to defects states

Section III Sequence reactions: H_2O + NO

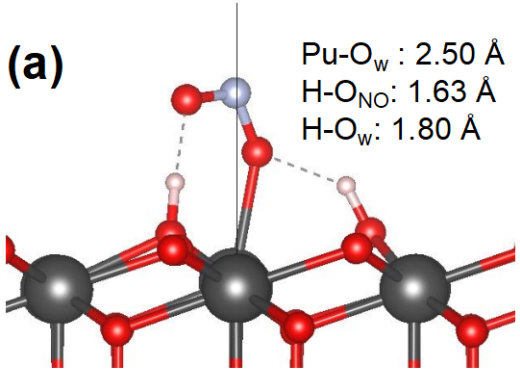

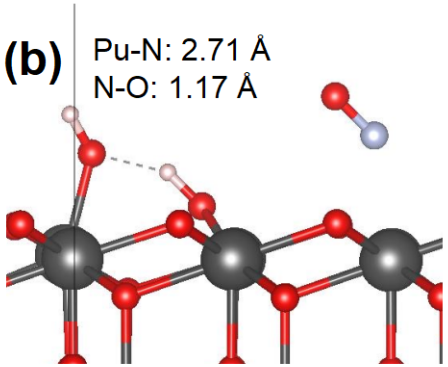

	ΔG (eV)
NO+OH	-1.14
NO	-0.16
NO_2	2.47

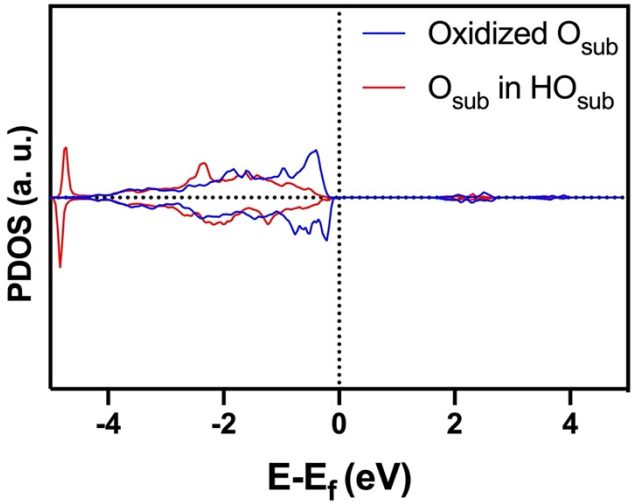

The PDOS of oxidized O_{sub} and O_{sub} in HO_{sub} in the H*+HO*@PuO_2.

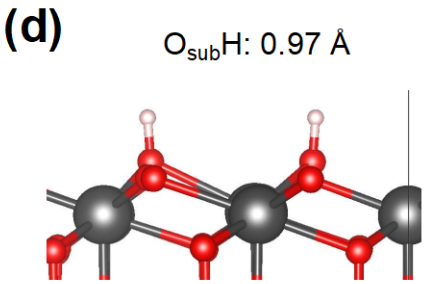

Step 4: NO_2* + 2H*→ 2H* +NO_2

NO favour to react with **OH** but hard to release **NO_2**

	Before NO
O_{sub} pristine	1.21e
O_{sub} in HO_{sub}	1.30e
To be oxidizd O_{sub}	1.18e

The to be oxidized O_{sub} is readily to host H when NO is approaching

Section III Sequence reactions: $NO+H_2O$

$NO^*+H_2O \rightarrow NO^*+H_2O^*$

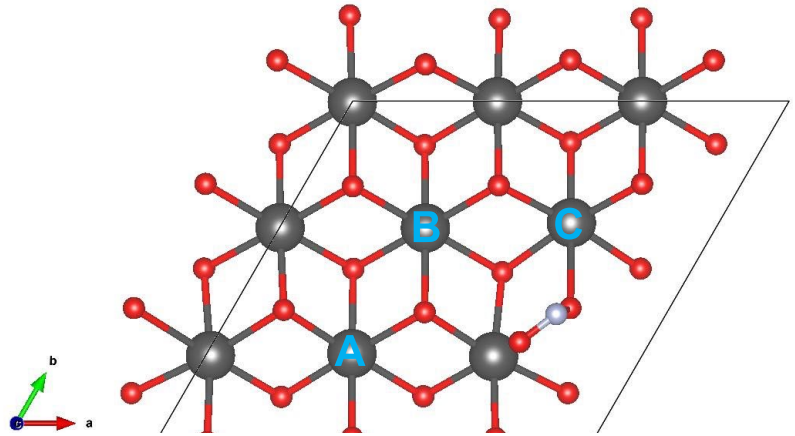

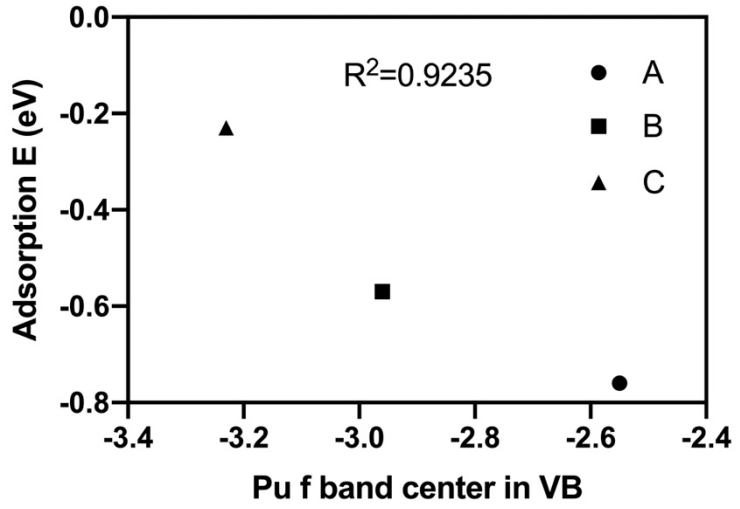

When NO presents, **the adsorption energy is linearly related to Pu f bond center.**

	NO*//	A	B	C
E_{ad}	**-0.64**	**-0.73**	**-0.52**	**-0.23**
NO Bader partial charge	0.017	0.026	0.048	0.034
N-O_{sub} distance	1.362	1.355	1.346	1.353
Pu-O_w distance	N/A	2.559	2.553	2.565
H_2O Bader partial charge	N/A	-0.004	-0.023	-0.004
Pu f band centre in VB	N/A	**-2.55**	**-2.96**	**-3.23**
O_w 2p band centre in VB	N/A	-3.28	-3.59	-3.97
$\Delta G_{1C,2,300K}$	-0.60	-0.71	-0.51	-0.22

competitive reactions

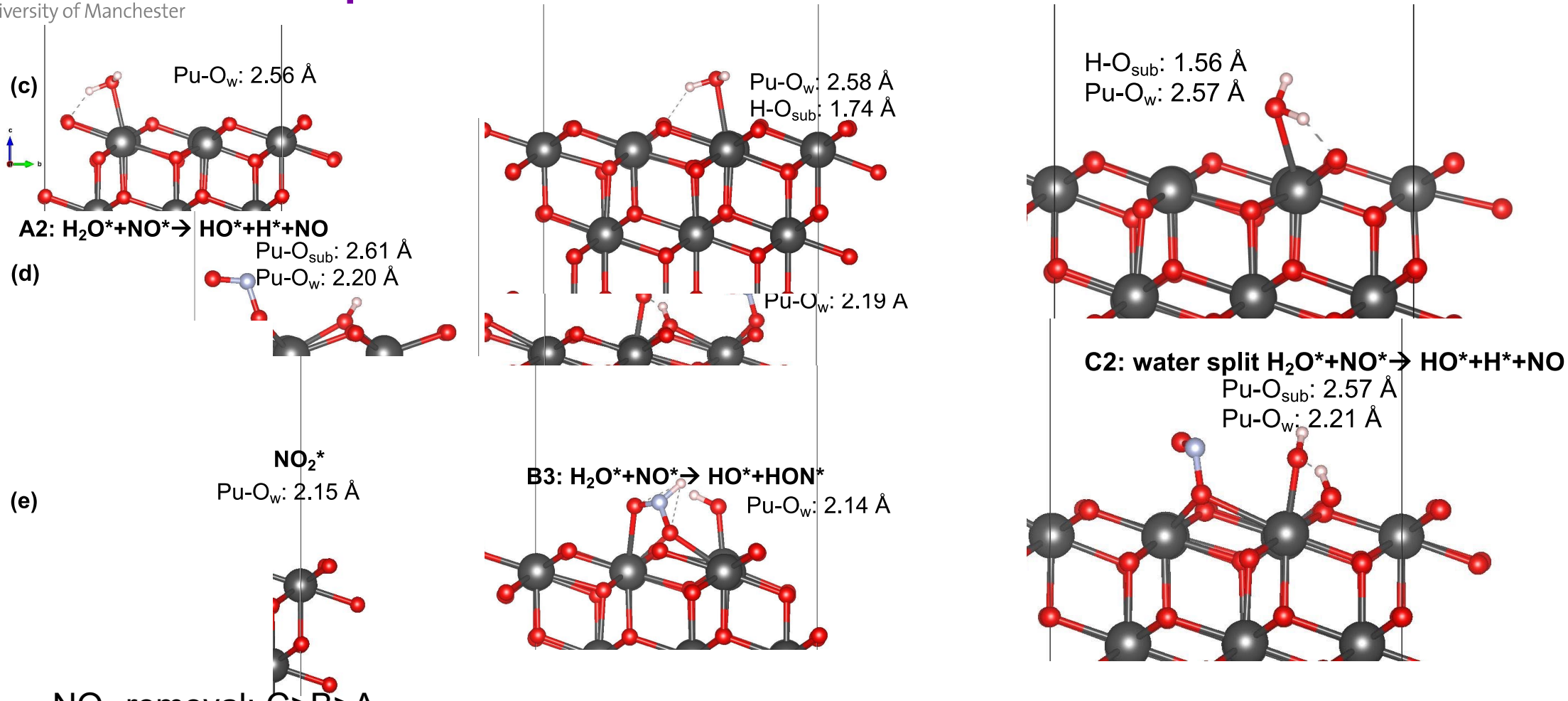

- NO_2 removal: C>B>A
  - While forming nitric acid at A or nitroxyle at B are easier than NO_2 removal
- water splitting: A>B>C
  - A site has lower energy barrier than water splitting on pristine surface

water splitting with NO presents

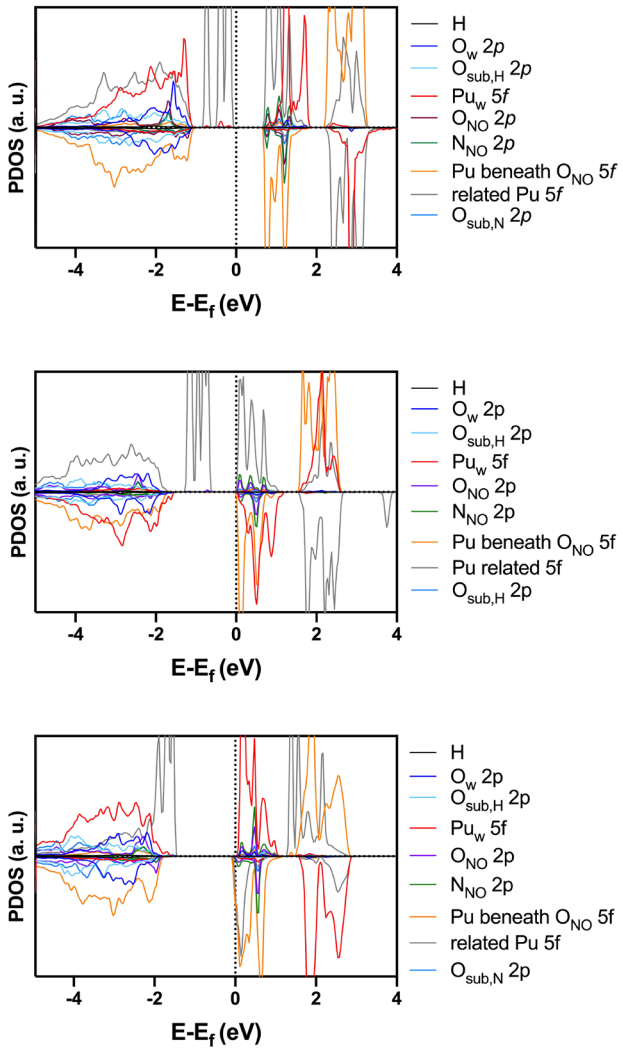

- **the defect states** merged with VB in C sites

	2A	2A2	2B	2B2	2C	2C2
Pu_w	-2.55	-2.29	-2.96	-3.01	-3.23	-3.30
O_w	-3.28	-2.15	-3.59	-2.81	-3.97	-3.60

pristine	H2O*	HO*+H*
Pu_w	-1.63	-1.49
O_w	-2.68	-1.32

H_2O splitting in pristine surface

The reaction of water splitting has controlled by 2 factors:

A) the f band center of Pu_w relative to Fermi Level;
B) the distance of f of Pu_w and p of O_w

Summary

- Collectively on lattice parameter, bandgap, peaks distance on VB, work function and general surface charge, we propose **U=3** is the best setting for PuO_2
- NO and H_2O individually and sequentially reaction on PuO_2
- **the f band centre** is linearly related water adsorption on NO@PuO_2 surface; But more comprehensive studies are needed, especially for other 5f oxides.
- **the water splitting** has been governed by 2 factors:

A) the f band center of Pu_w relative to Fermi Level;

B)the distance of f of Pu_w and p of O_w

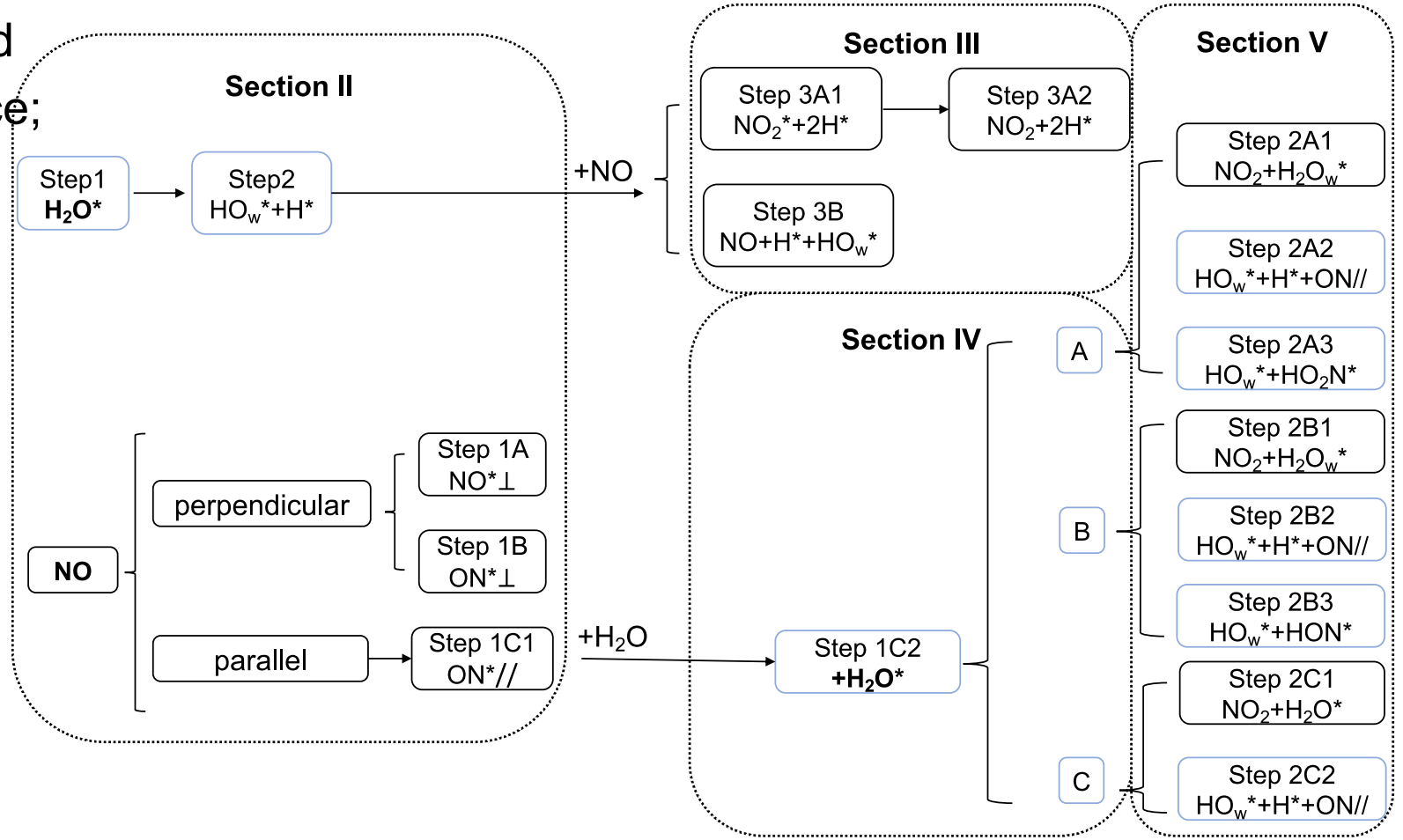

Acknowledgements

Acknowledgements

- Prof. N. Kaltsoyannis and the group members;
- Transcend consortium;
- EPSRC: EP/S01019X/1;
- CSF3, Archer HPC and their associated services;

http://www.mub.eps.manchester.ac.uk/kaltsoyannisgroup/

MANCHESTER 1824
The University of Manchester

Thank you

Sellafield Ltd

The role of drag in sedimentation modelling of flocculated inorganic/organic composite nuclear waste suspensions

TRANSCEND Annual Meeting 1st November 2022

Dr Alex Lockwood, *RSci*: *(He/Him)*

Particles with Fluids Centre of Expertise - Deputy Lead

Particles with Fluids Centre of Expertise

Technical and Strategy

Sellafield Ltd

Pile Fuel Storage Pond

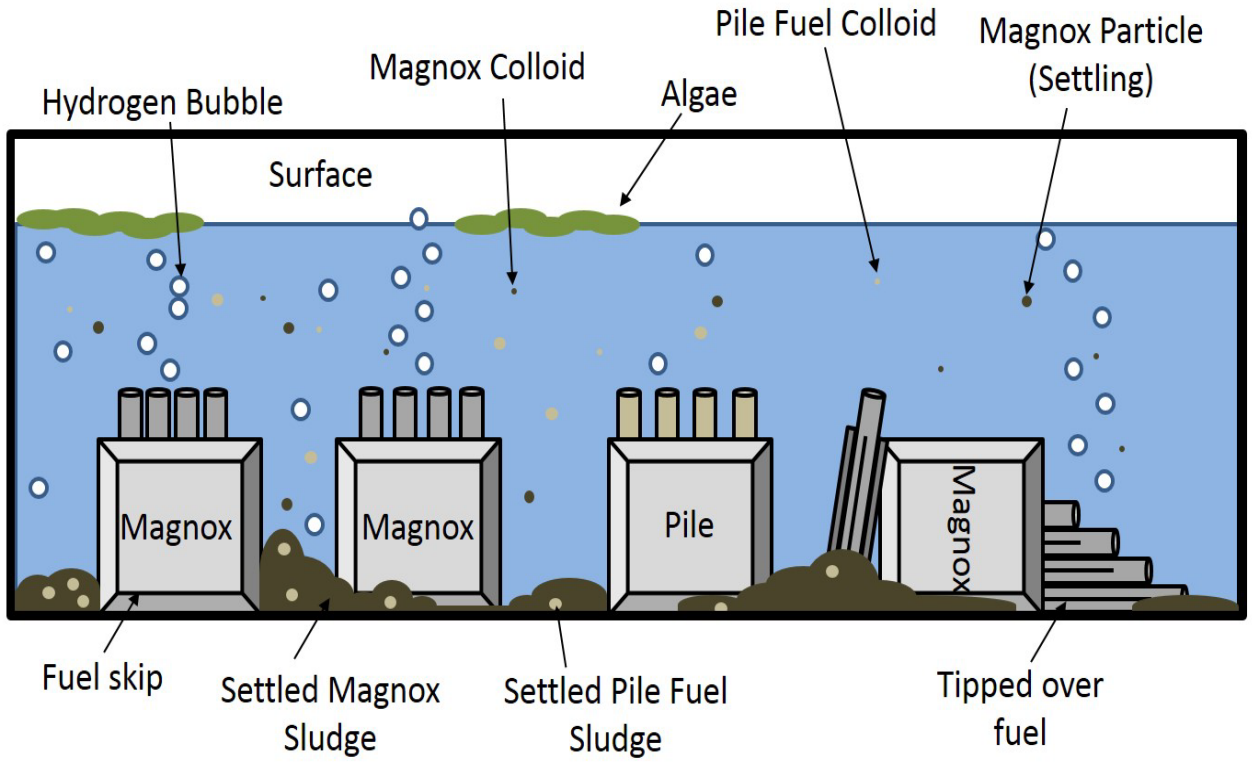

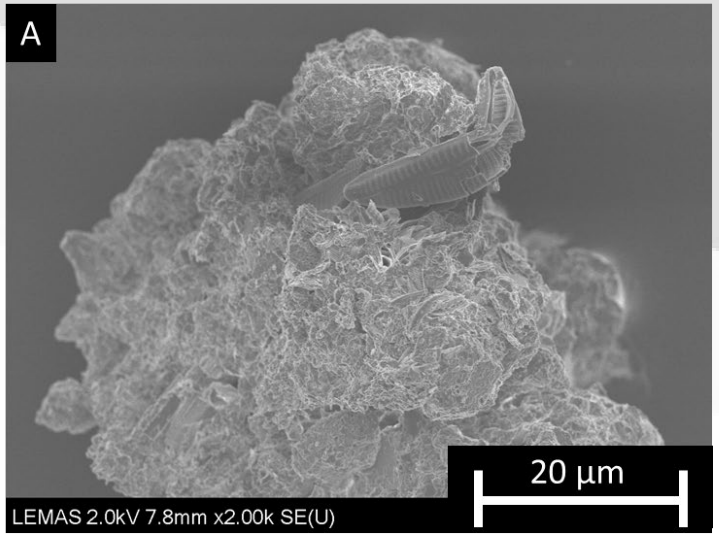

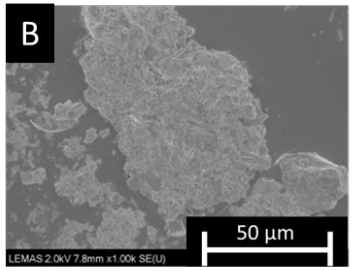

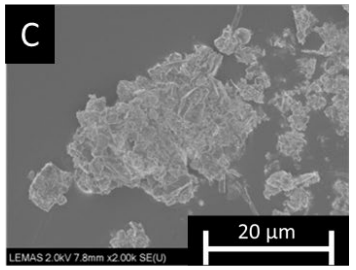

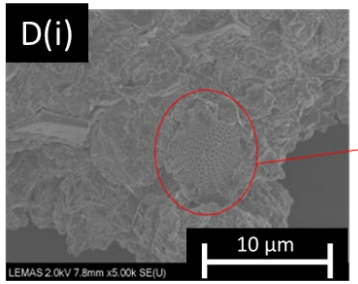

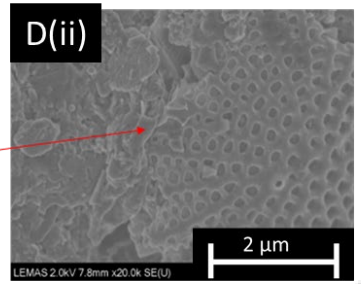

Polymer settling aid dosing in EDT

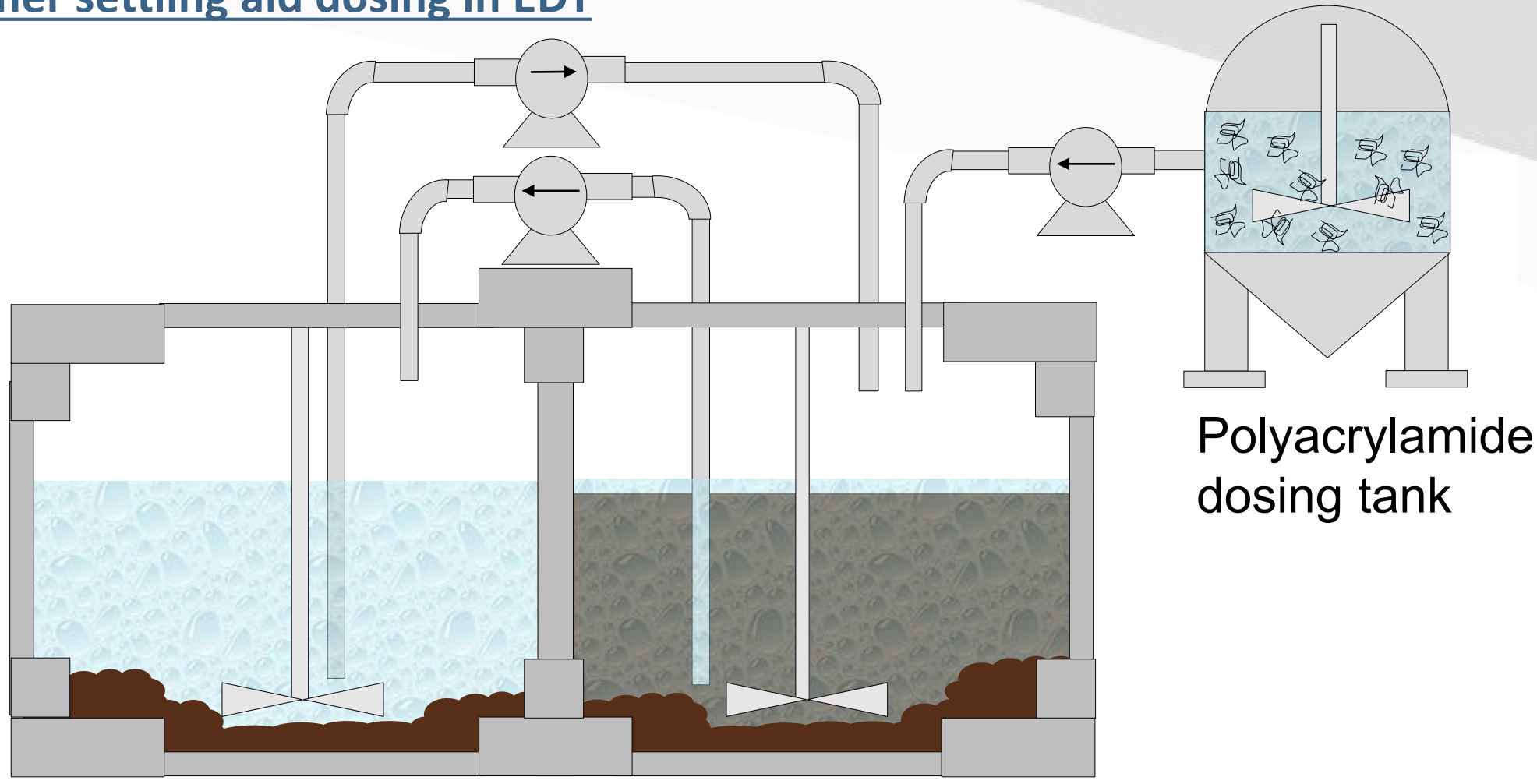

Polymer settling aid dosing in EDT

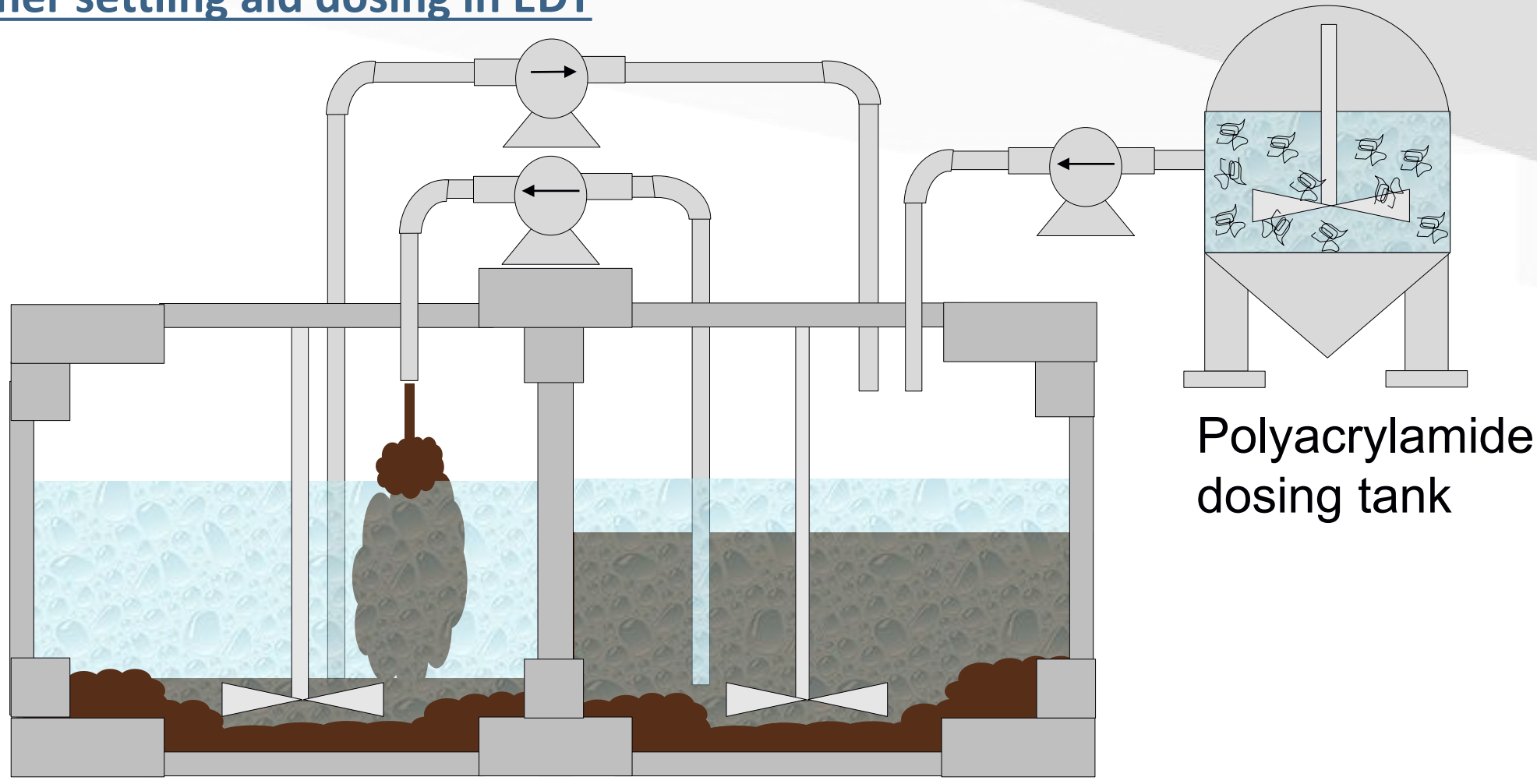

Polymer settling aid dosing in EDT

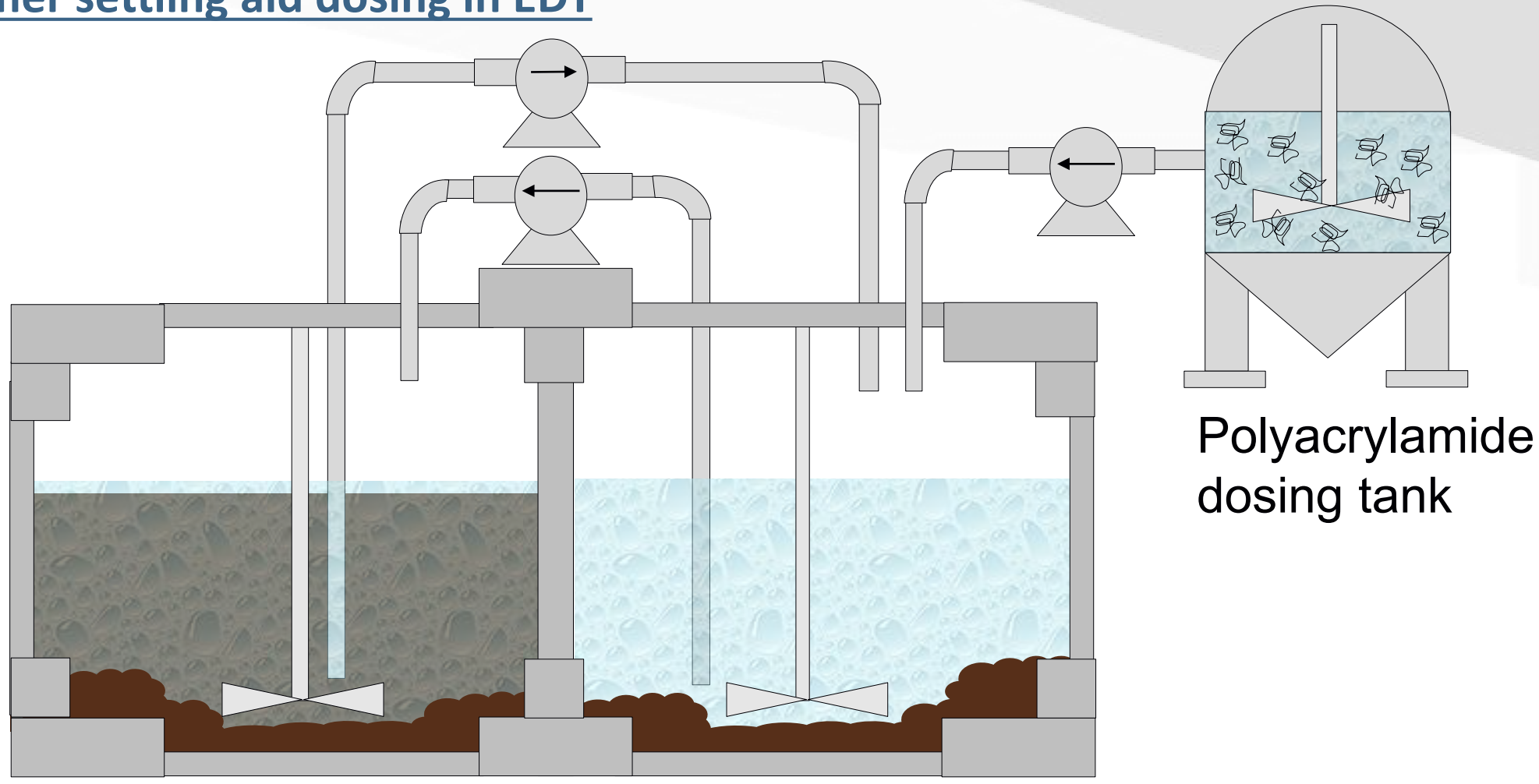

Polymer settling aid dosing in EDT

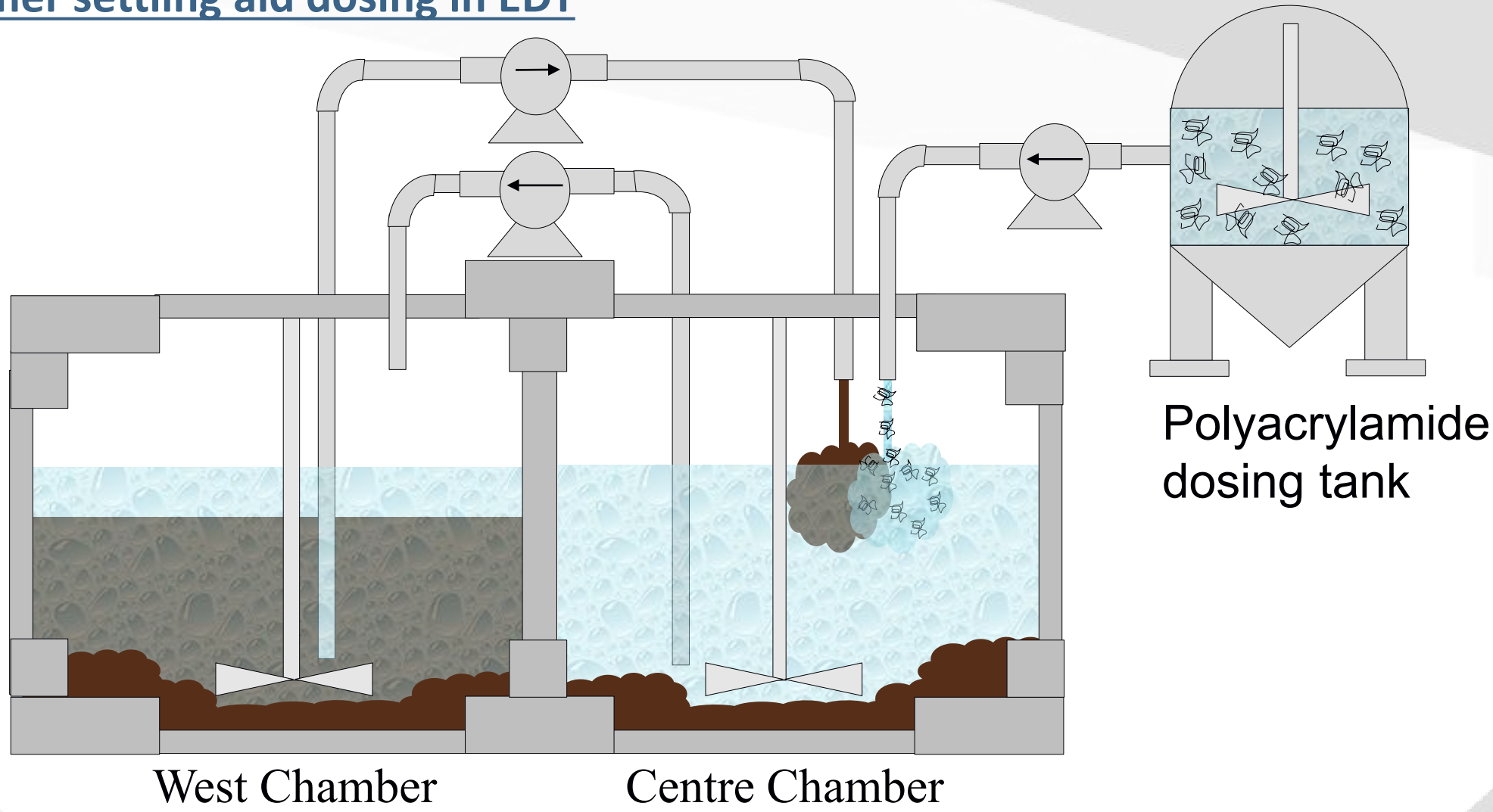

Polymer settling aid dosing in EDT

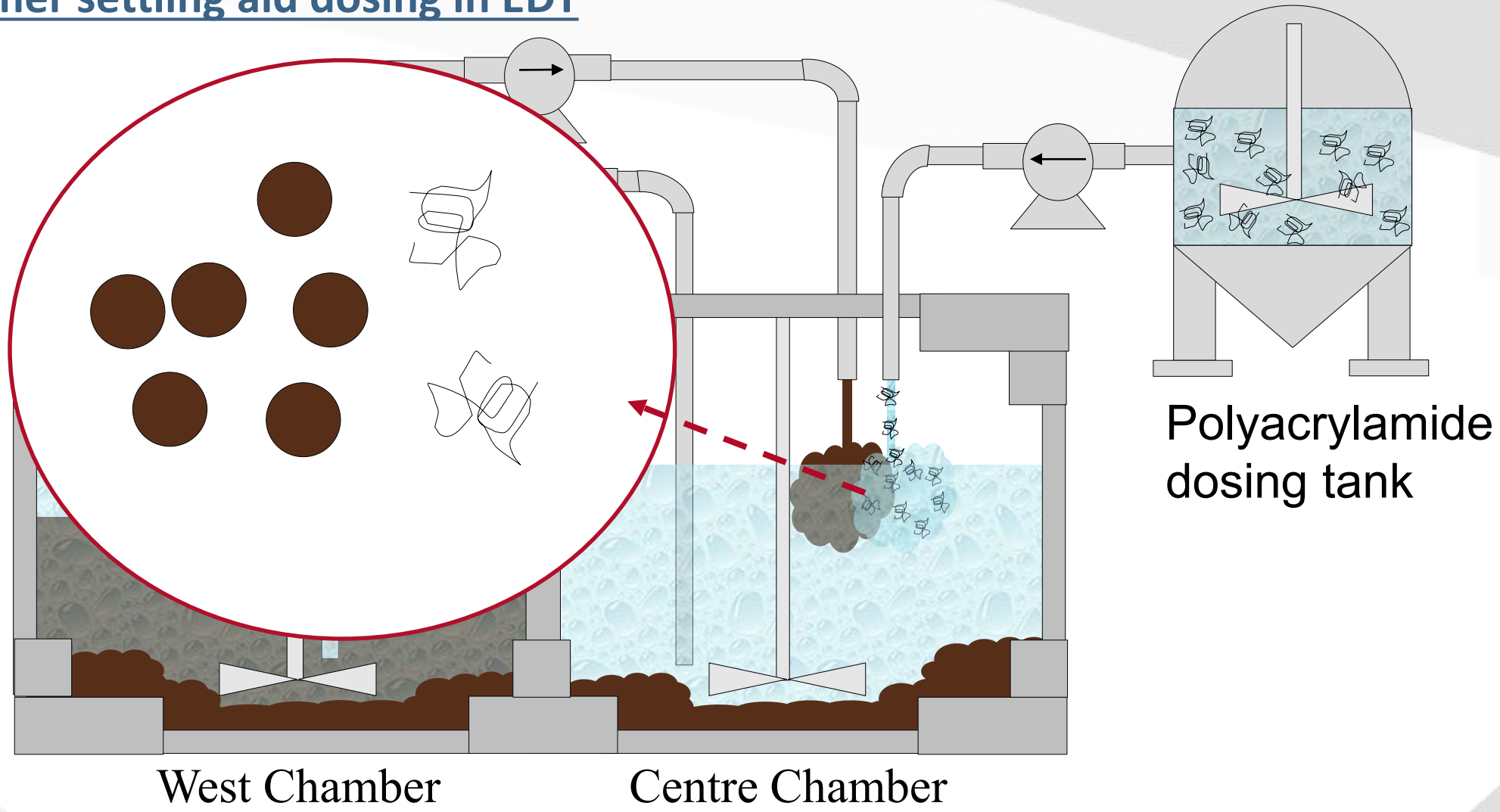

Polymer settling aid dosing in EDT

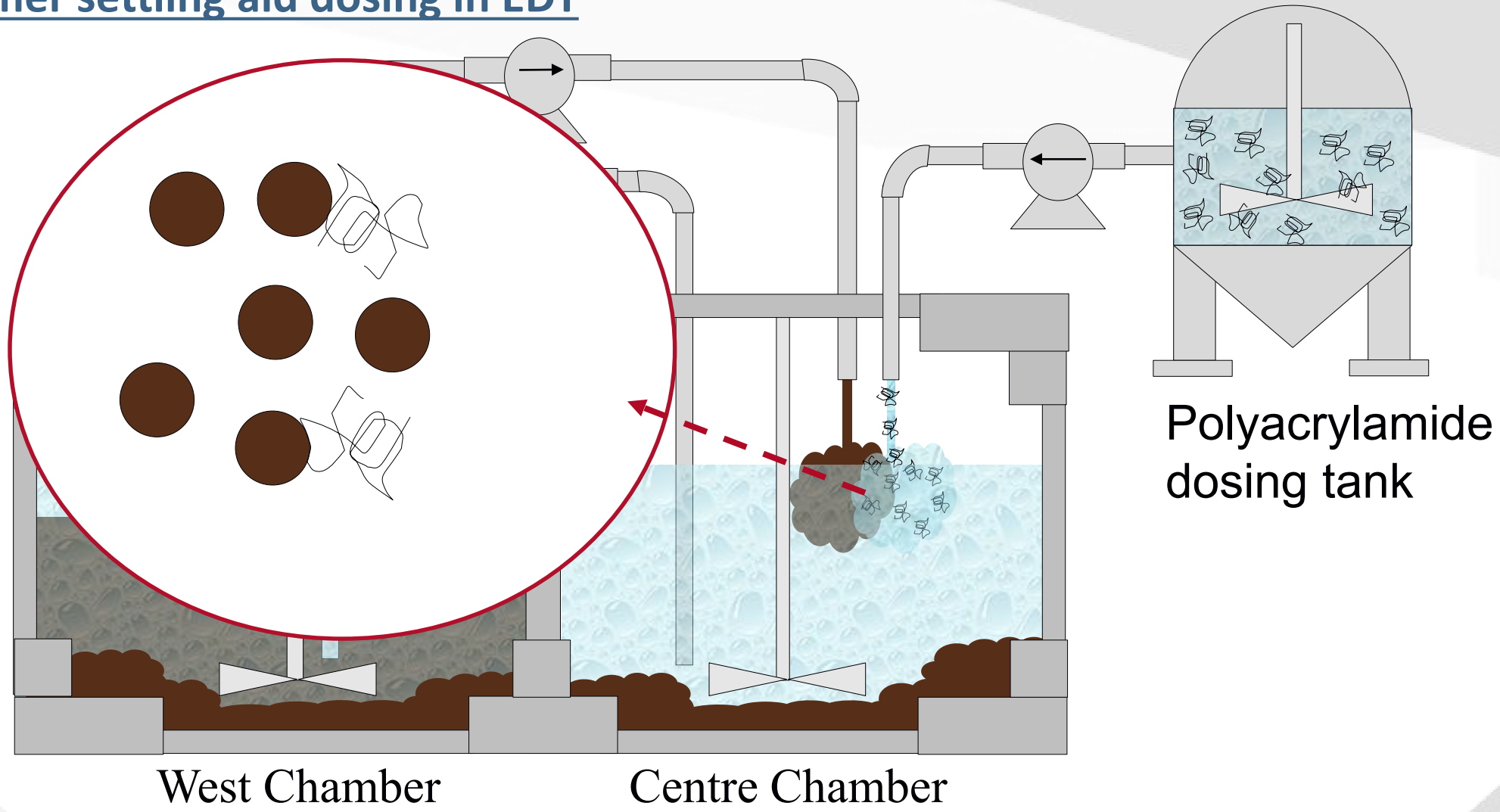

Polymer settling aid dosing in EDT

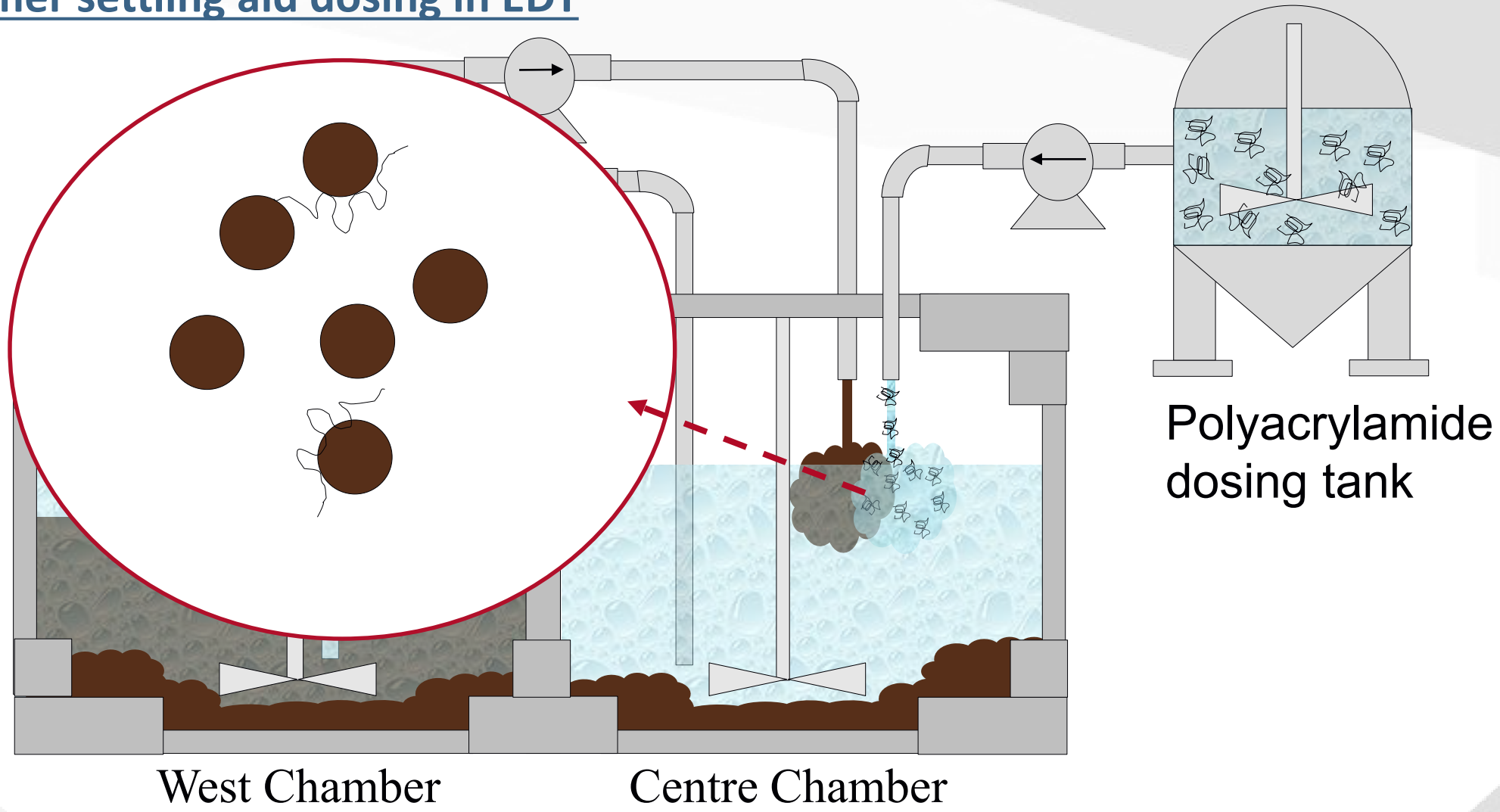

Polymer settling aid dosing in EDT

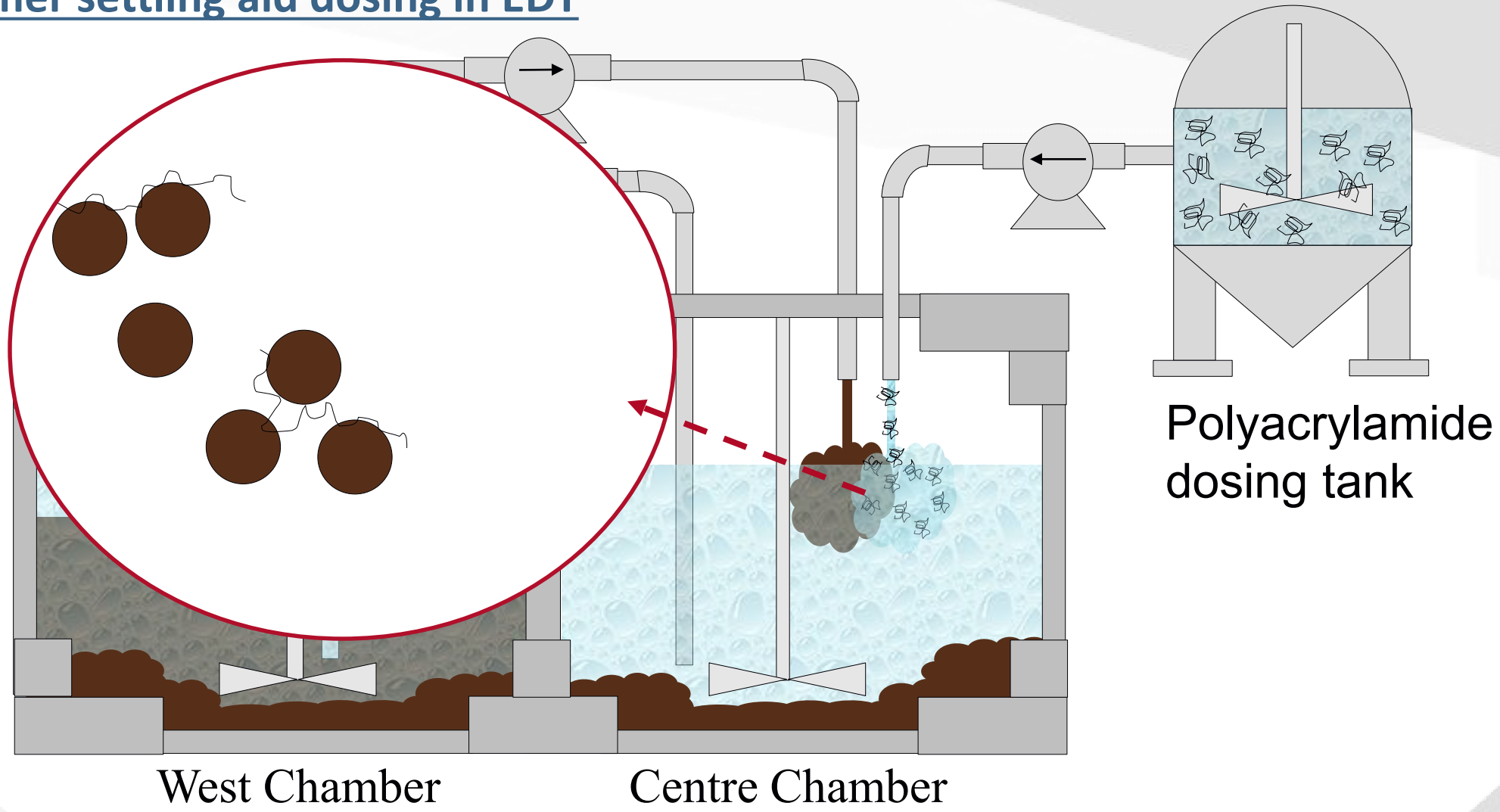

Polymer settling aid dosing in EDT

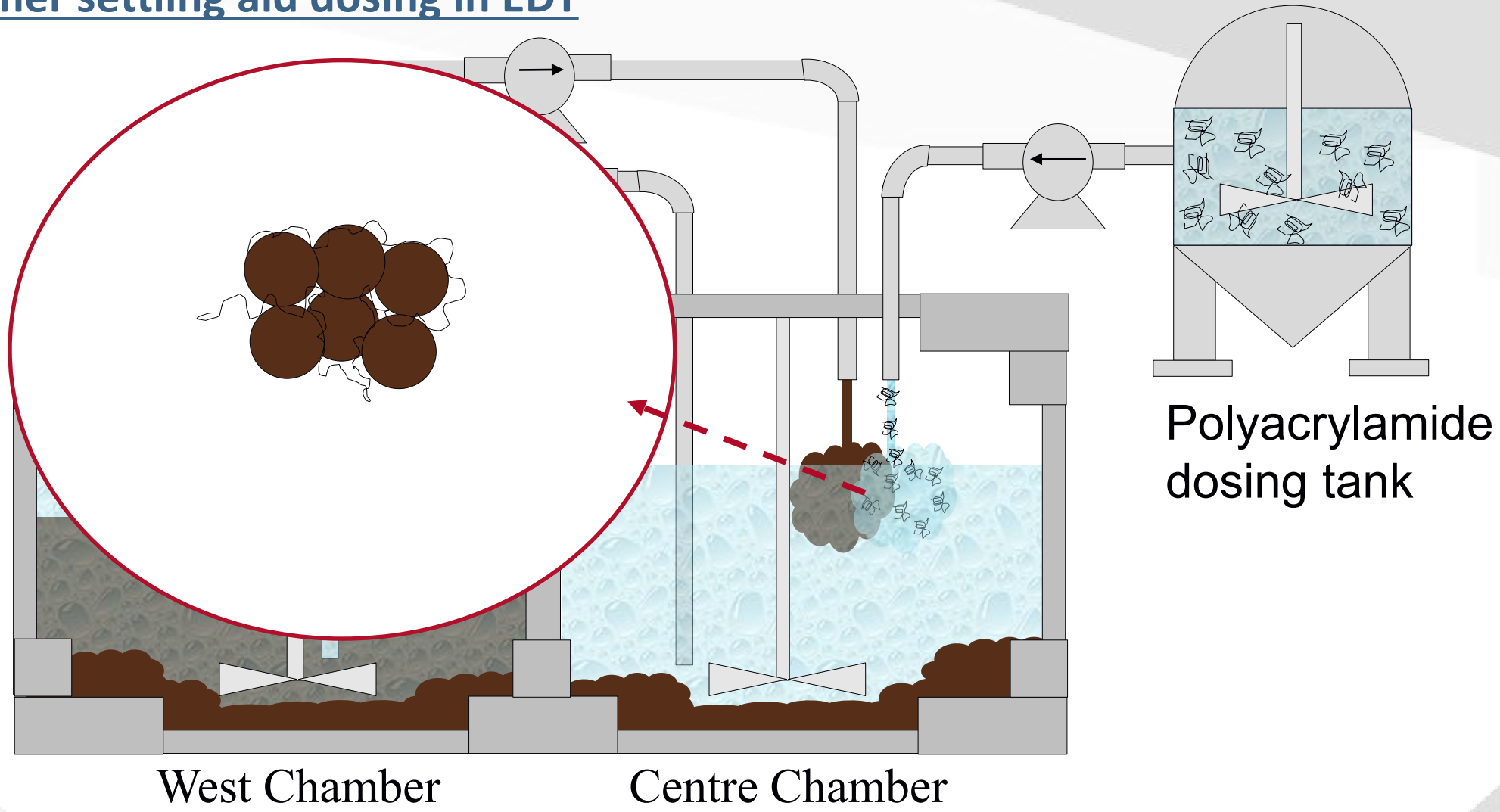

Polymer settling aid dosing in EDT

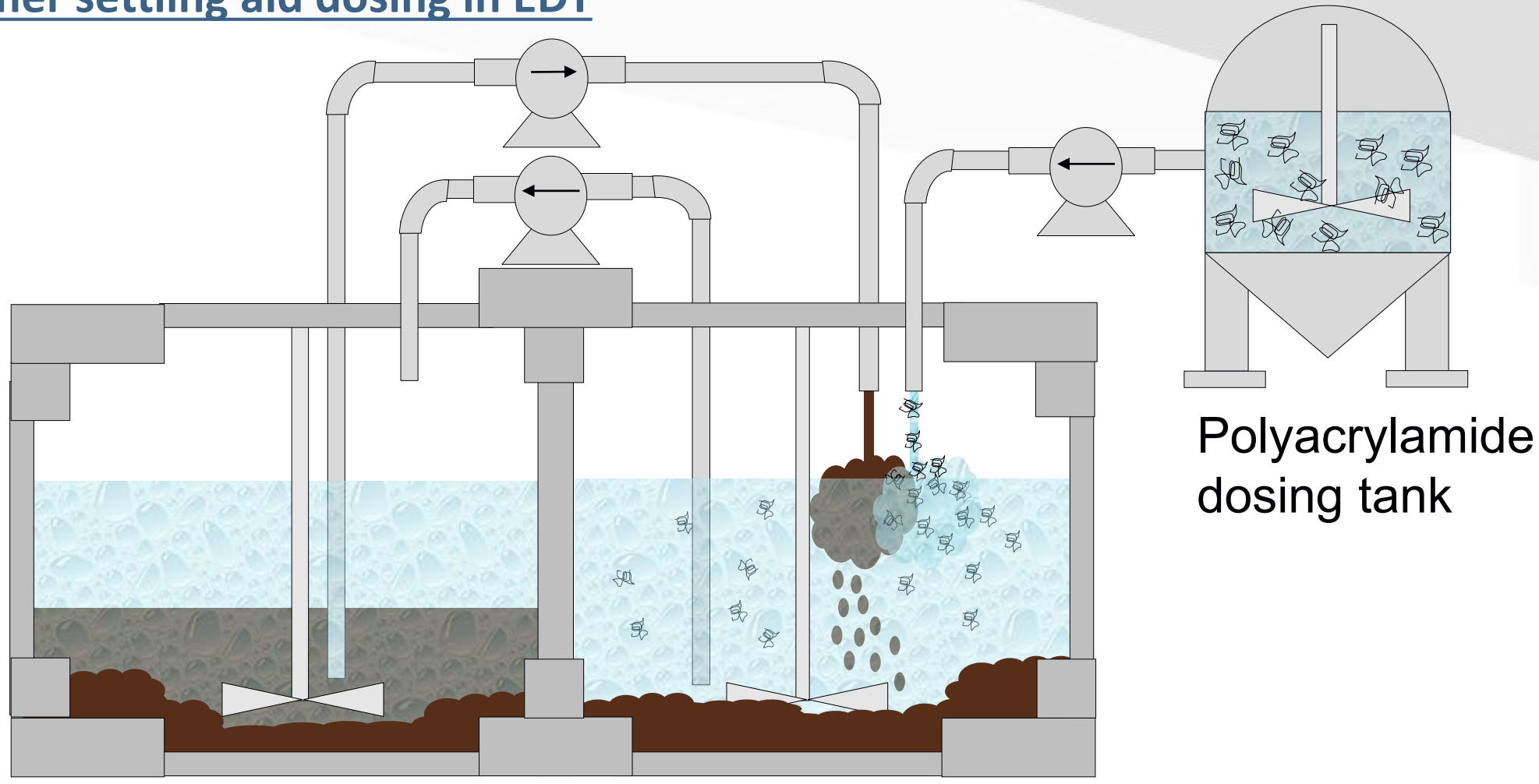

Polymer settling aid dosing in EDT

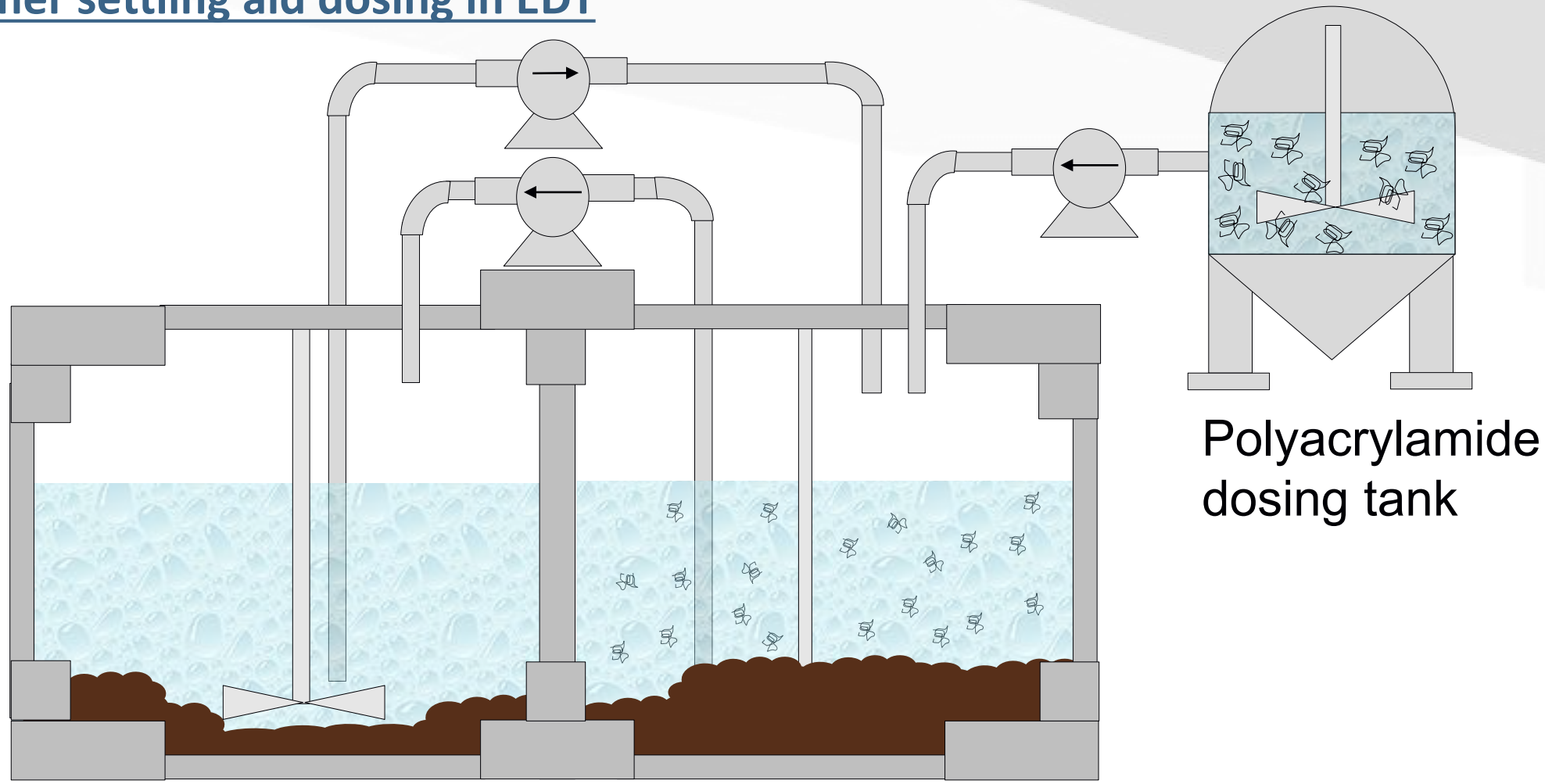

Particles with Fluids Centre of Expertise

Technical and Strategy

Sellafield Ltd

- I proposed a MEng project at the University of Leeds to address poor settling using the FLOPAM polymer in the EDT centre chamber settling programme
- Used University funding and pre-existing stock of PFSP test material
- Negotiated free FLOPAM samples from SNF Ltd.
- Trained MEng student in several analytical techniques and design experimental assay to maximise experiments with minimal test material requirements

Characterising Appleby Sludge

- Sludge was characterised using SEM, EDX, FBRM and electrophoresis
- Presence of silts and organic matter evident from SEM and EDX
- Investigation into surface chemistry required

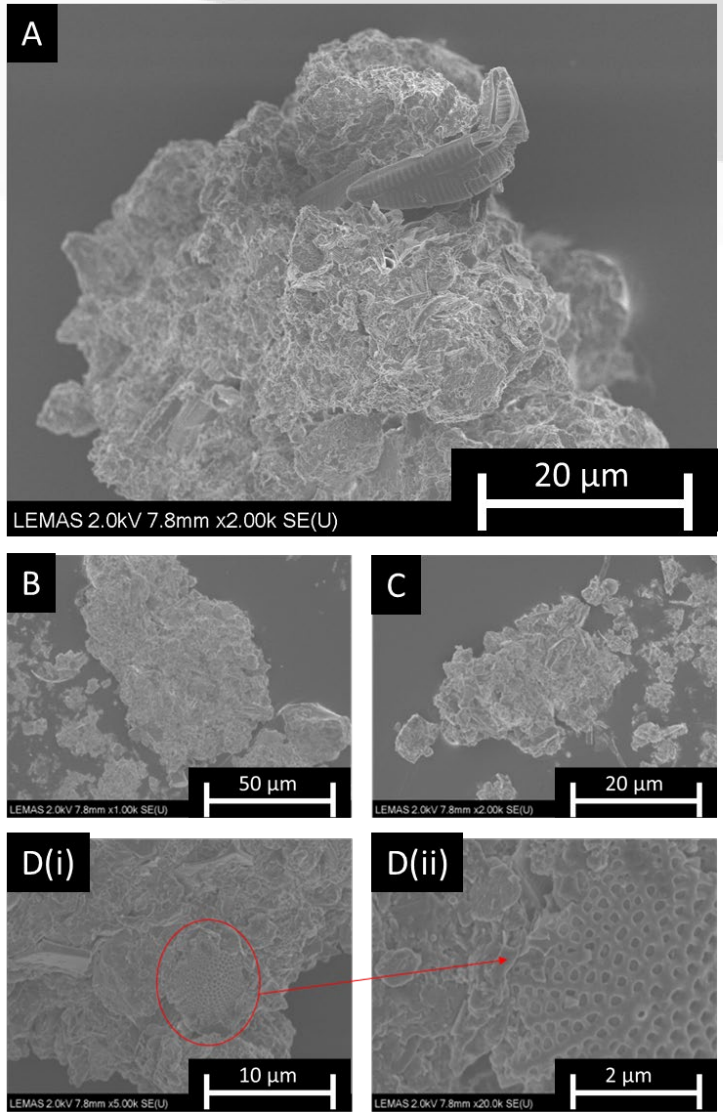

Sellafield Ltd

Characterising Appleby Sludge

- Sludge was characterised using SEM, EDX, FBRM and electrophoresis
- Presence of silts and organic matter evident from SEM and EDX
- Investigation into surface chemistry required

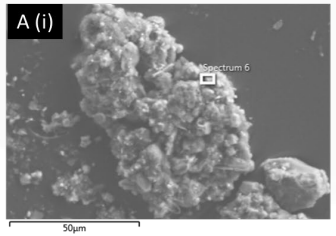

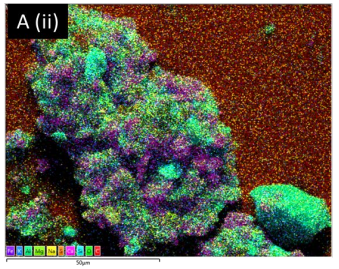

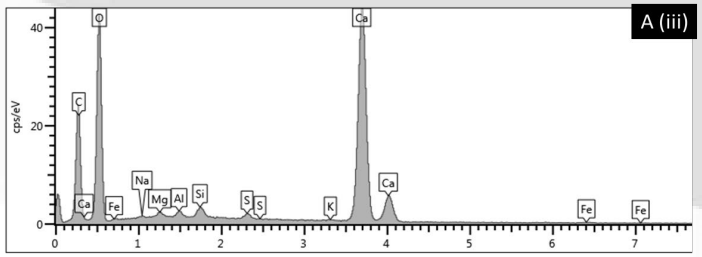

Element	Wt%
C	18.8
O	49.92
Na	0.14
Mg	0.31
Al	0.38
Si	0.61
S	0.42

A (iv)

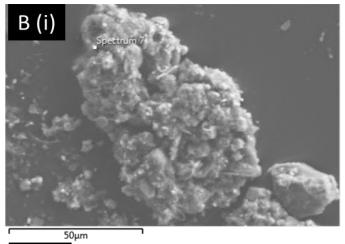

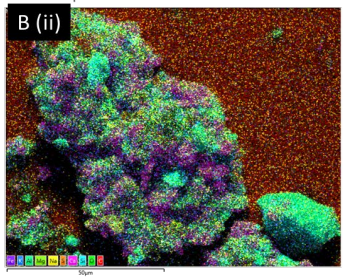

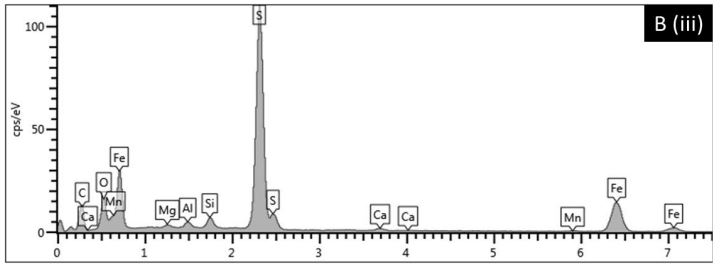

Element	Wt%
C	28.54
O	10.36
Mg	0.33
Al	0.58
Si	1.04
S	29.83
Ca	0.47

B (iv)

Characterising Appleby Sludge

- Sludge was characterised using SEM, EDX, FBRM and electrophoresis
- Presence of silts and organic matter evident from SEM and EDX
- Investigation into surface chemistry required
- Anionic surface charge, high polyacrylamide affinity
- Combination of adsorption mechanisms

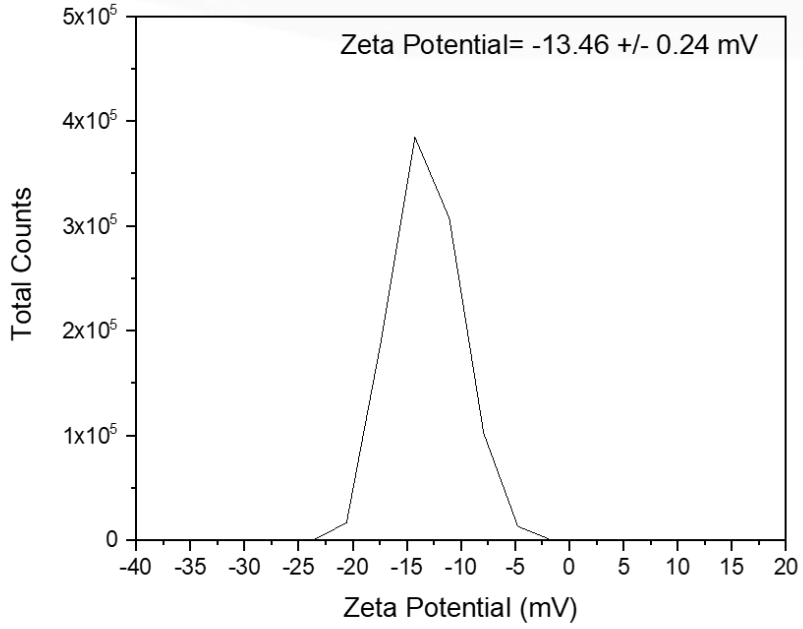

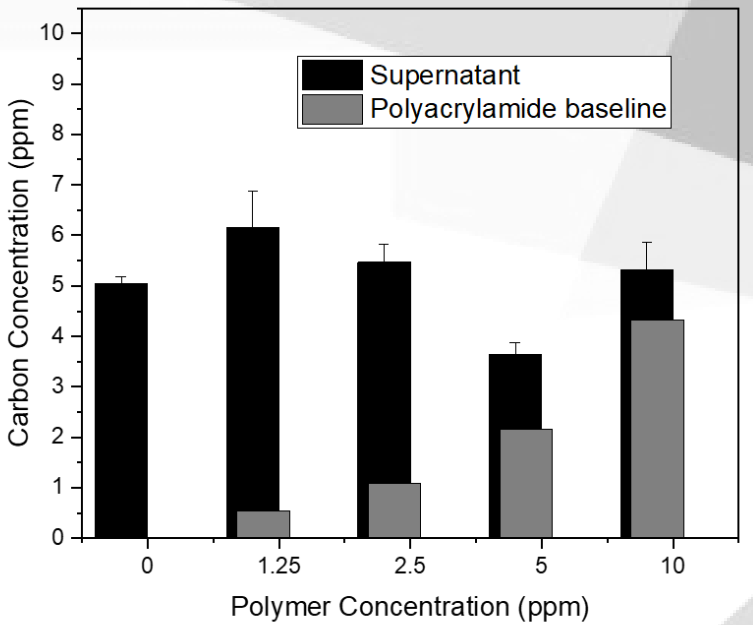

Characterising Appleby Sludge

- Sludge was characterised using SEM, EDX, FBRM and electrophoresis
- Presence of silts and organic matter evident from SEM and EDX
- Investigation into surface chemistry required
- Anionic surface charge, high polyacrylamide affinity
- Combination of adsorption mechanisms

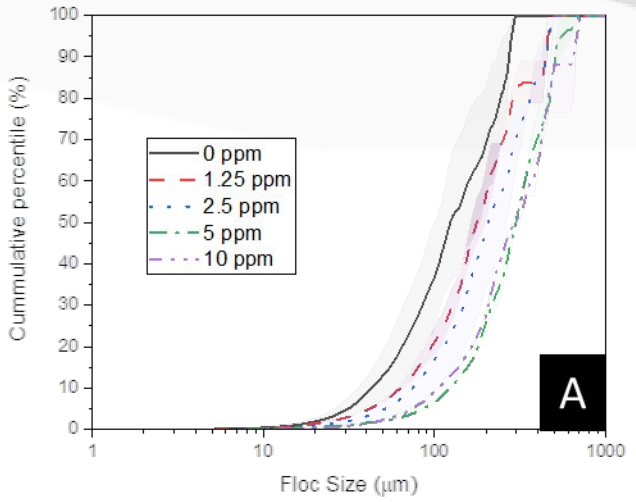

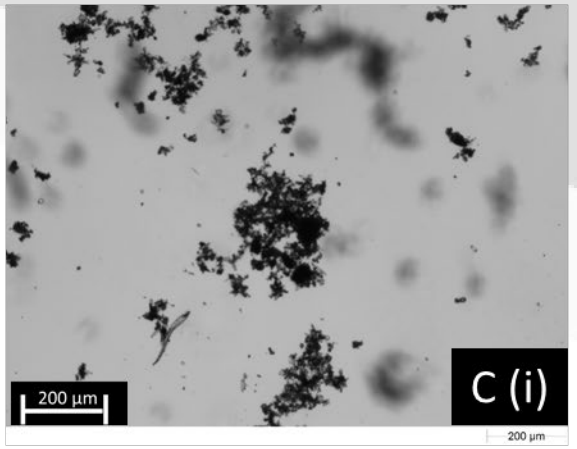

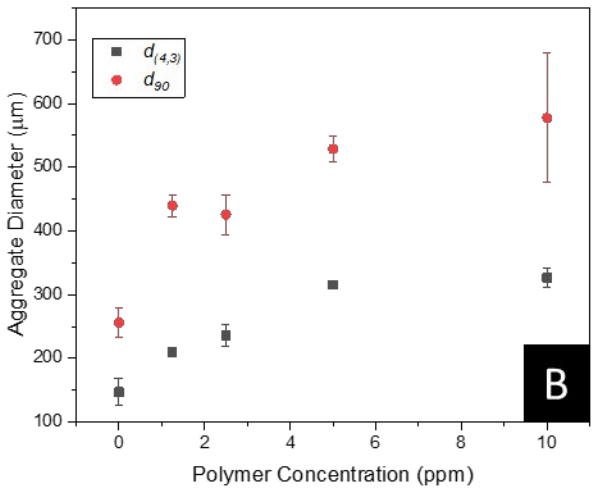

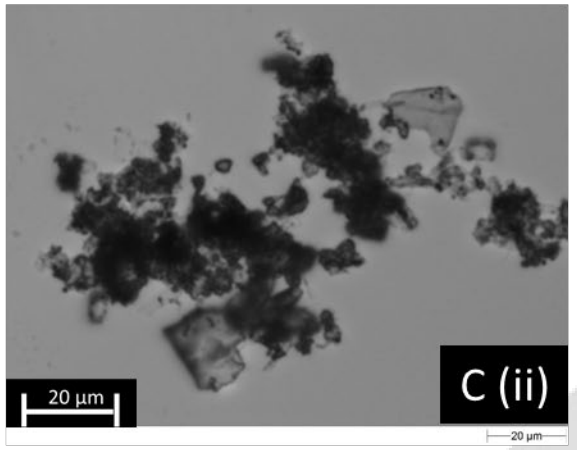

Particles with Fluids Centre of Expertise

Technical and Strategy

Sellafield Ltd

Results

- FLOPAM effectively Flocculated PFSP sludge simulant
- Size of flocs increase significantly
- Settling rate doubles and liquor turbidity drops by a factor of 10
- Data presented to PFSP retrievals
- Opportunity to decrease settler residence times, reduced waste package volumes and improve pond visibility

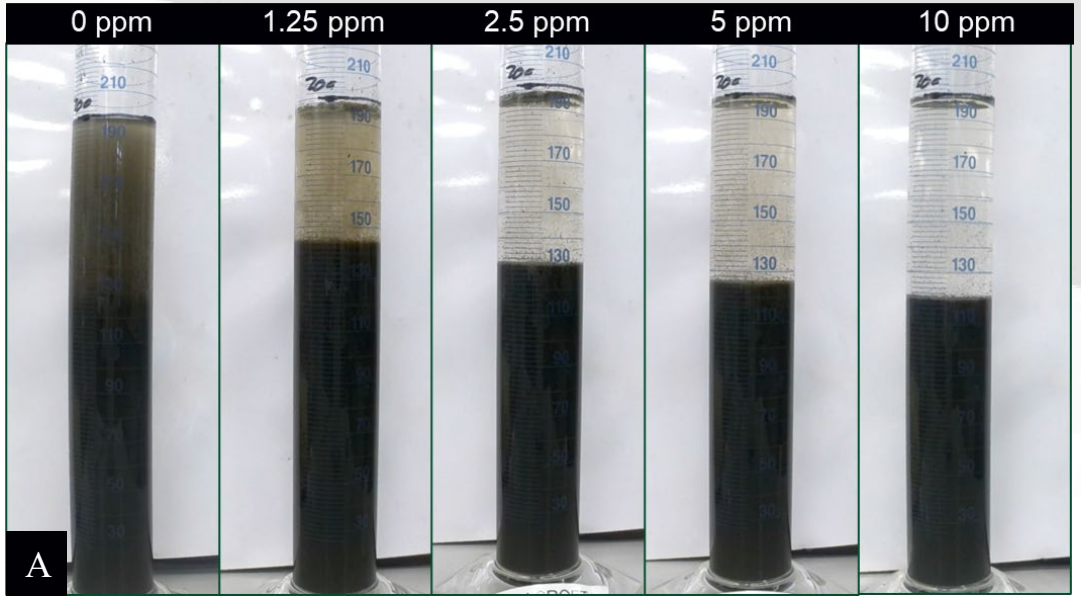

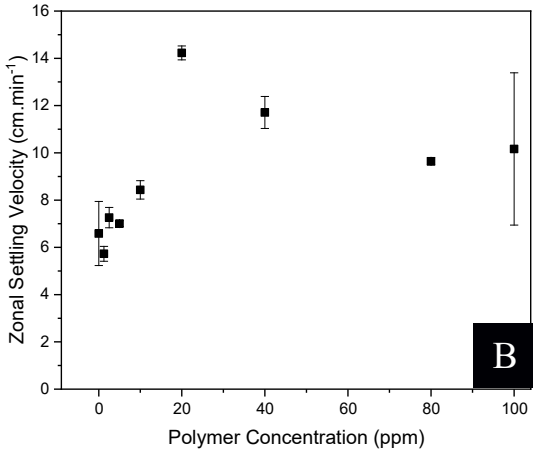

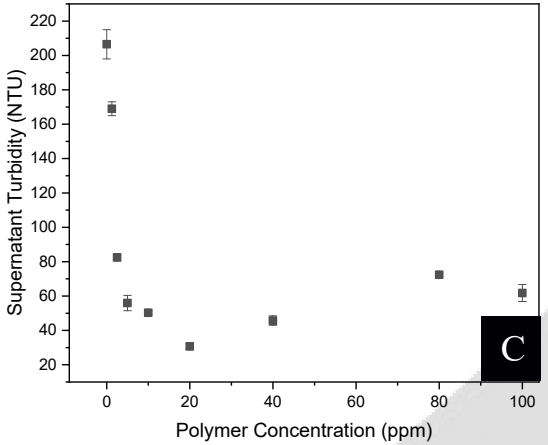

Results cont.

- New floc structure porous in nature
- Low solids concentrations and complex fractal structure complicate settling dynamics
- Typical approaches to residence time models under-predict residence times
- Alternative settling model needed proposing

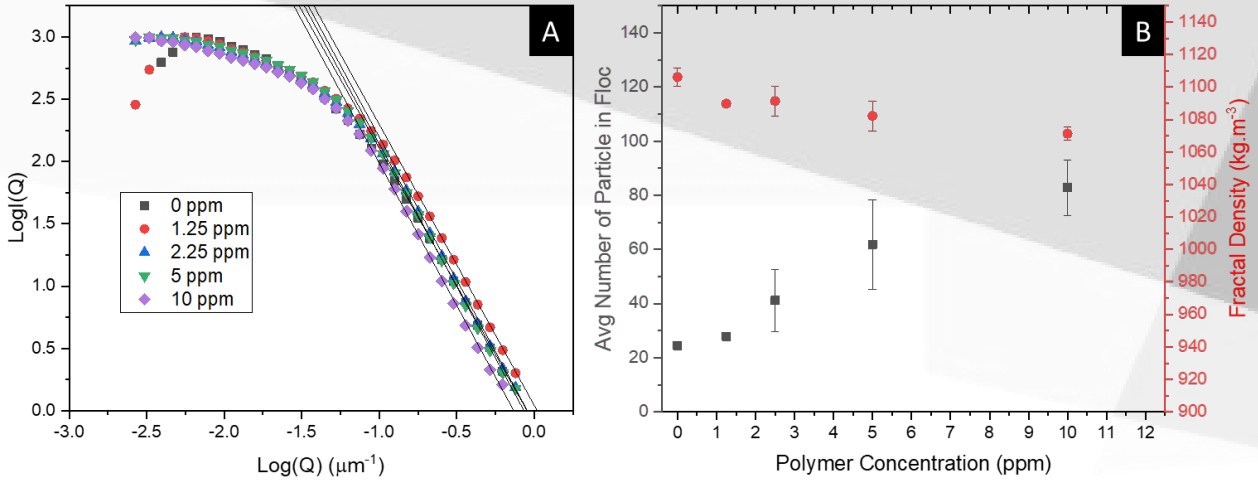

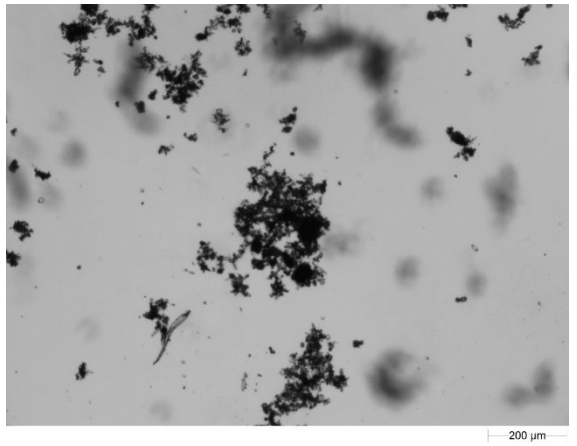

Results Cont.

- Fractal modified hindered settling model (*i*-FMRZ) was further modified to include inertial flow regime considerations (*Re* > 0.3)
- New model was interrogated and scrutinised with via multivariate analysis

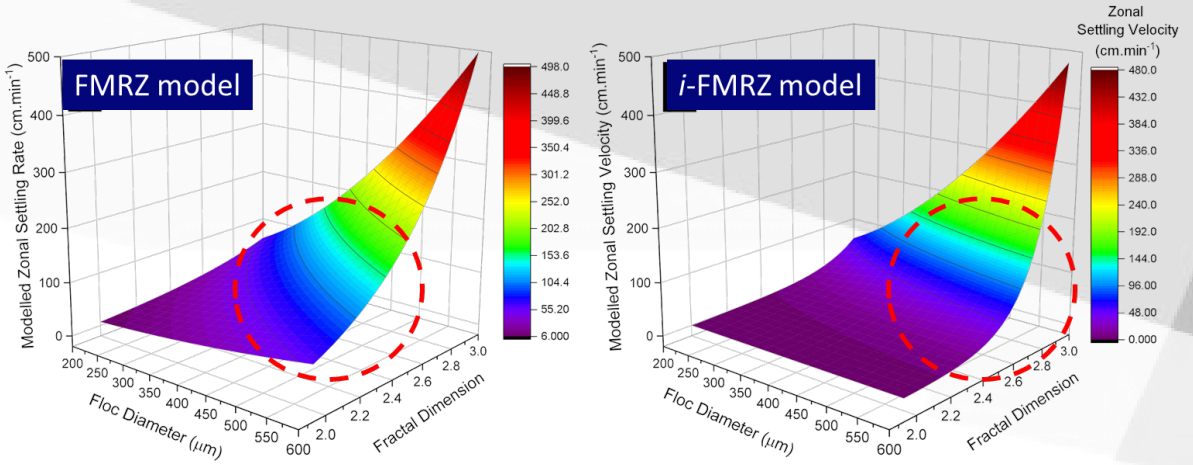

$U_Z = \frac{(\rho_p - \rho_w)\overline{D_f^2}g}{18\mu_w}\left(\frac{D_f}{D_p}\right)^{d_f-3}\left(1-\Phi\left(\frac{D_f}{D_p}\right)^{3-d_f}\right)^{Rz}$	**FMRZ**
$U_Z = \frac{(\rho_p - \rho_w)g}{18\mu_w}D_p^{3-d_f}\frac{\overline{D_f}^{d_f-1}}{1+0.15Re^{0.687}}\left(1-\Phi\left(\frac{D_f}{D_p}\right)^{3-d_f}\right)^{Rz}$	***i*-FMRZ**

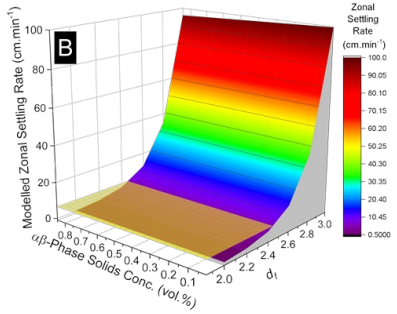

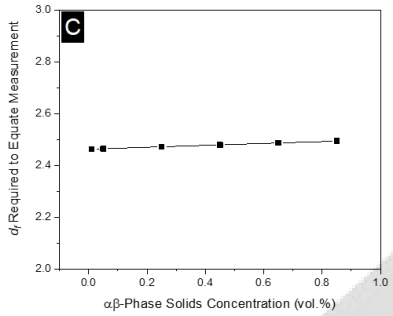

Results Cont.

- i-FMRZ combined with the largest particle size predicted the most accurate zonal settling rates (D)
- Provided more accurate model for developments of digital twins as well as LSTP sludge transfer scheduling

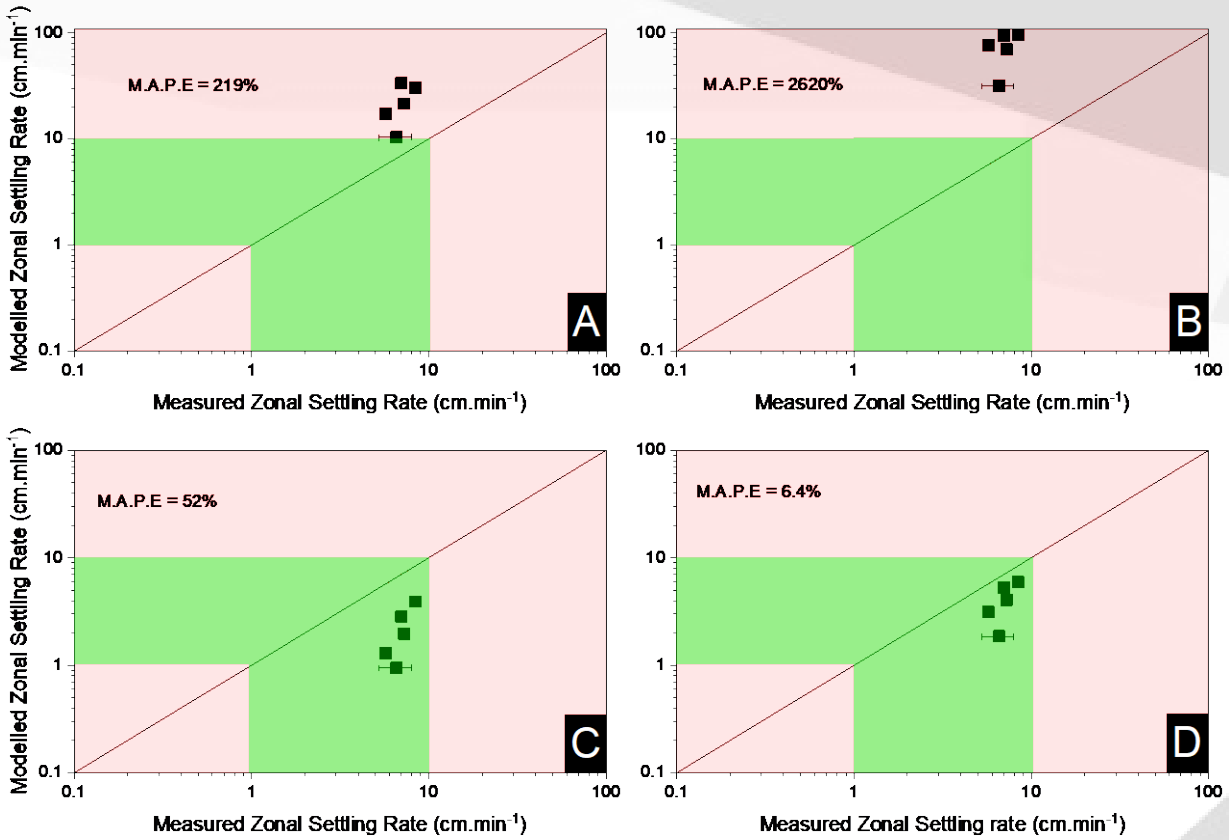

Summary of research impact on Business

- Utilised visiting researcher status for sandboxing exercise delivered through supervision of masters student
- FLOPAM is likely a viable polymer to flocculate PFSP sludges through van der Waals attraction and hydrogen bonding
- Resistance to overdosing complex behaviour
- Settling rates improved drastically
- Inertial modification to FMRZ model effective in predicting settling rates
- Simple jar test to test effectiveness on real sludge
- Work required to identify shear effects and best dosing strategy

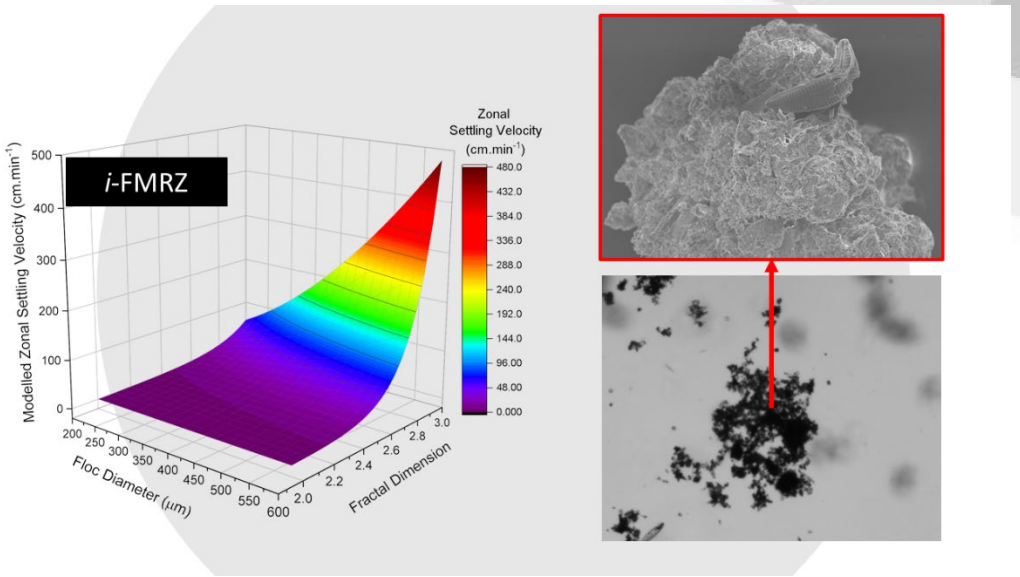

Particles with Fluids Centre of Expertise

Technical and Strategy

Sellafield Ltd

Future Work

- Test on circulation tank samples in Analytical lab
- Engineering considerations (shear rate impact and dosing strategy)
- Technical paper to be taken to RVSTC for endorsement
- Currently under peer review in the Journal of Water Process Engineering

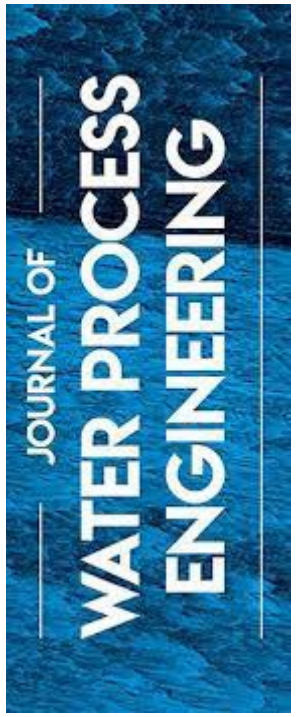

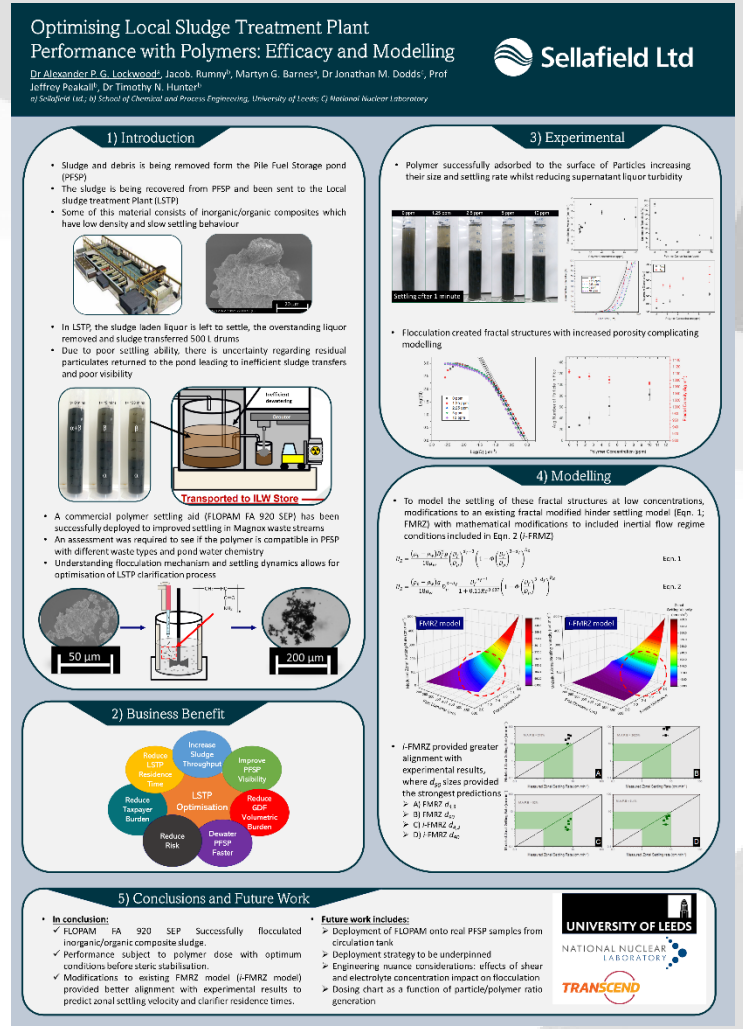

Thank You

Any Questions?

Particles with Fluids Centre of Expertise

Technical and Strategy

Sellafield Ltd

Alex Lockwood: Impact on Business

- Internal pseudo-consultancy with strong supply chain and academic links
- Support for programmes across the value stream and knowledge/ govern through the Particles with Fluids working group
- Various delivery mechanisms with varying delivery manifestations
- £500k academic link with university of Leeds
- Support Postgrad/doctoral research aligned with SL business case
- Utilise visiting researcher status for sandboxing exercise delivered through supervision of masters students

TRANSCEND

Transformative Science and Engineering for Nuclear Decommissioning

Vacuum Drying of Spent AGR Fuel

Thomas Bainbridge

pmtoba@leeds.ac.uk

TRANSCEND Annual Meeting – Glasgow

1/11/2022

Energy

For a Low Carbon Future

Overview

Overview

The UK has decided to cease reprocessing spent nuclear fuel with the preferred option now being to interim store it pending a decision on disposal

Current Strategy

Currently the spent fuel is being interim wet stored in ponds at Sellafield. These ponds are buffered to pH 11.4 to reduce the risk of the cladding corroding

Alternatives

Dry storage is an alternative used by other nations for the interim storage and disposal and is being investigated in the UK as an alternative approach

Why dry the spent fuel?

If the fuel cladding fails while in storage then water can enter causing the production of H_2 and H_2O_2 – these are flammable and corrosive respectively

Nuclear Decommissioning Authority (2021) *Strategy: Effective from March 2021*.

Experimental Work

Drop Evaporation

Pinhole Flow

Experimental Work

Overview

To produce cracks, measure the flow rate of fluid through these cracks & then conduct full vacuum drying to validate the model

Drop Evaporation

To corrode stainless steel samples using chloride solutions with the aim of producing representative cracks

Pinhole Flow Rate

To determine the fluid flow rate through small pinholes and the cracks produced by the drop evaporation experiments

Vacuum Drying

To provide final validation of the process model using samples constructed out of the cracks produced in a vacuum chamber

Drop Evaporation

- 304 stainless steel, sensitised at 600°C for 5 hours and furnace cooled
- Chloride solution used as the corrosive solution. 35 g/L NaCl in de-ionised H_2O
- Exposure durations of 2 and 3 weeks done, 4 weeks ongoing
- Evidence of some pitting corrosion on the 2 week sample with greater damage on the 3 week test

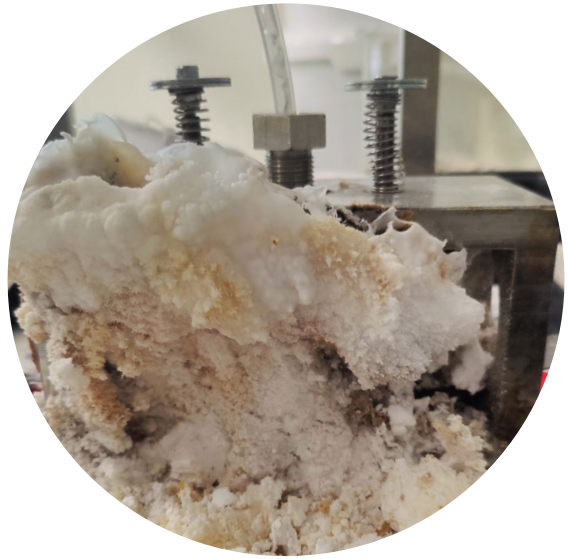

NaCl build-up during operation

Drugli, J. M. and Steinsmo, U. (no date) 'Assessment of Suscetibility to Chloride Stress Corrosion Cracking of Highly Alloyed Stainless Steels. Part II: A New Immersion Test Method', (194).
Jin, L. Z. (1994) 'The chloride stress-corrosion cracking behavior of stainless steels under different test methods', *Journal of Materials Engineering and Performance*, 3(6), pp. 734–739. doi: 10.1007/BF02818373.
Lasek, S., CÍHAL, V. and Blahetová, M. (2002) 'Stress corrosion cracking study of austenitic stainless steels by the drop evaporation test', in *Sb. konf.*
Parrott, R., Pitts, H. and Hill, H. D. (2011) 'Chloride stress corrosion cracking in austenitic stainless steel', *The Health and Safety Laboratory for the Health and Safety Executive: Buxton, UK.*
Pereira, H. B. *et al.* (2019) 'Investigation of stress corrosion cracking of austenitic, duplex and super duplex stainless steels under drop evaporation test using synthetic seawater', *Materials Research*, 22(2), pp. 5–8. doi: 10.1590/1980-5373-MR-2018-0211.

Drop Evaporation - Results

14 days exposure Not sensitised	21 days exposure Sensitised	21 days exposure Sensitised and sanded
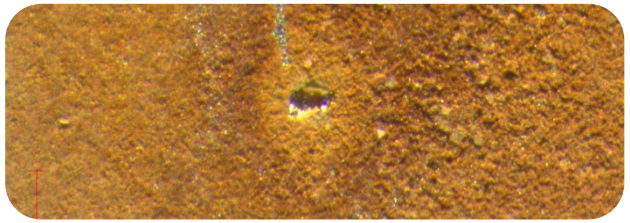	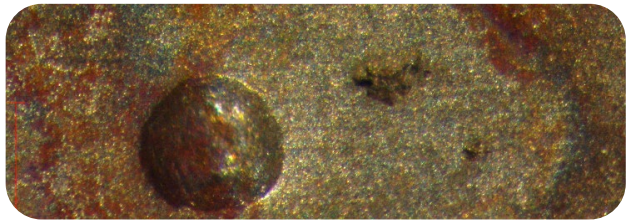	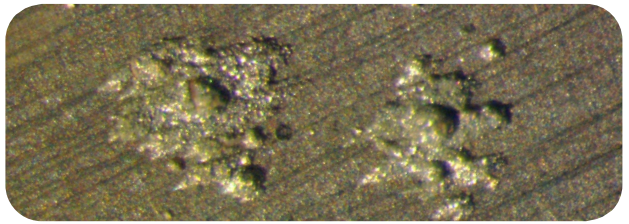
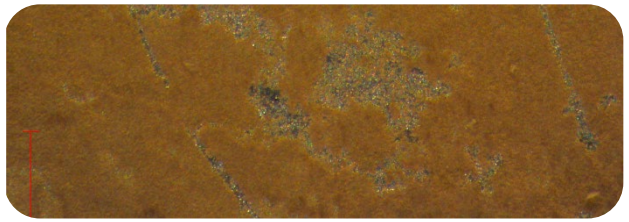	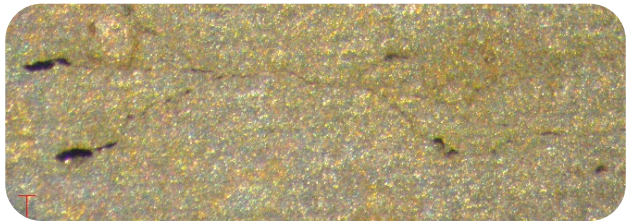	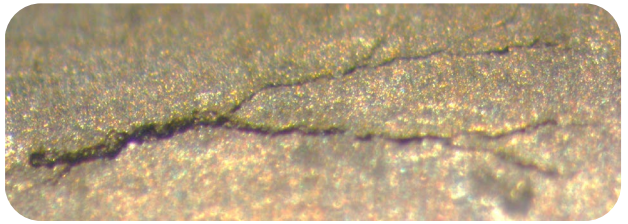
Single pit observed through the corrosion product layer with some scaring	Centre punch used to create areas of stagnant solution. Multiple pits observed and limited fracture networks on the surface	Centre punch again used to create areas of stagnant solution. Multiple pits observed and numerous surface fracture networks

Drop Evaporation Next Steps

- Corrosion of parts has occurred making set up difficult and have since failed
- Two new rigs being built entirely out of 316 and 321 stainless steel to prevent this occurring again
- Tests with other chlorides such as $AlCl_3$ and $MgCl_2$
- Other materials are also being considered with a view towards mechanically cracking the samples

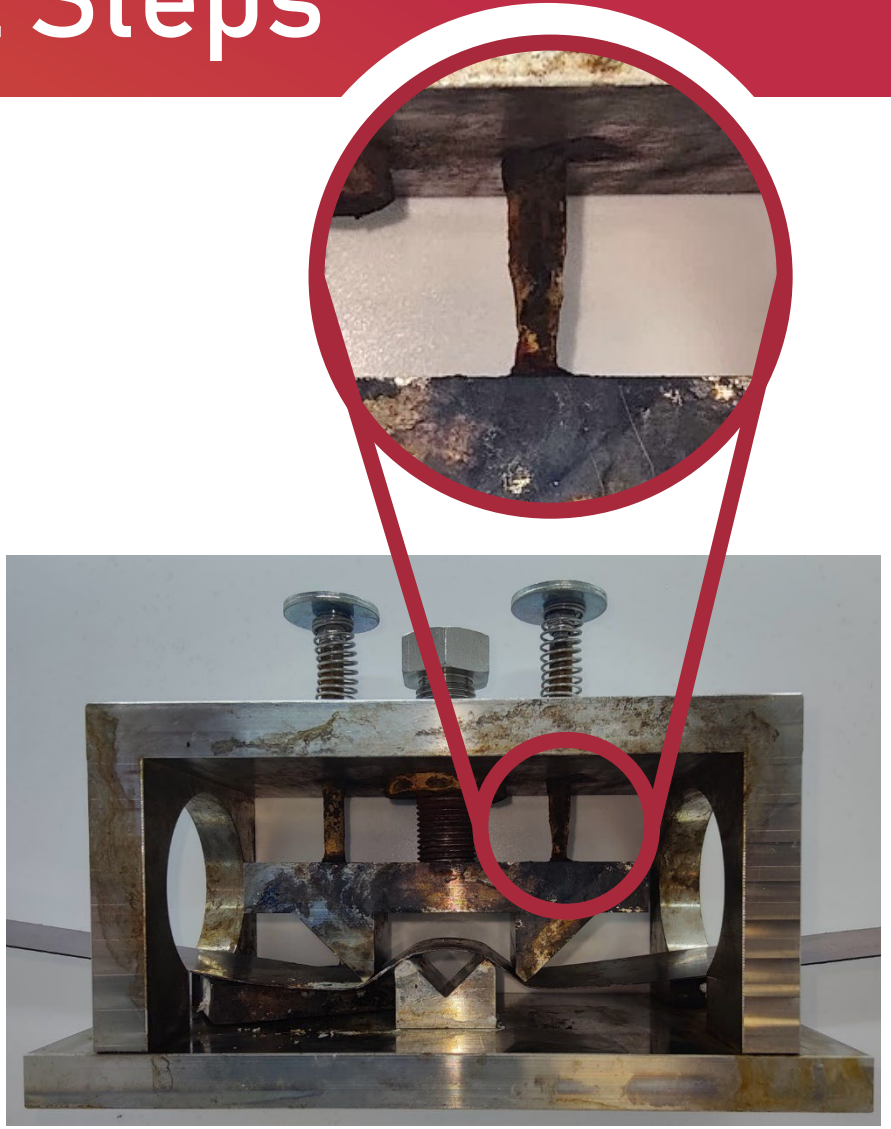

Corrosion on the experimental rig

Pinhole Flow

- Evacuate a gas sample cylinder to act as a reservoir
- Sample discs with pinhole diameters of 1, 5, 10, 20, 50 & 100µm
- Open a valve to let the air back into the cylinder using the disc as a leak path
- Water evaporation under vacuum also possible – testing is underway

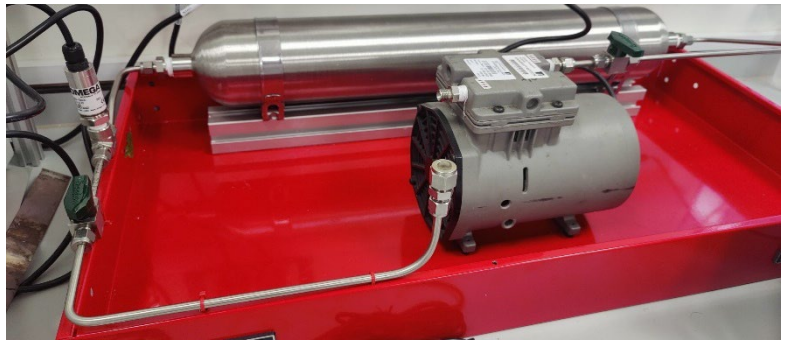

Pinhole flow rig

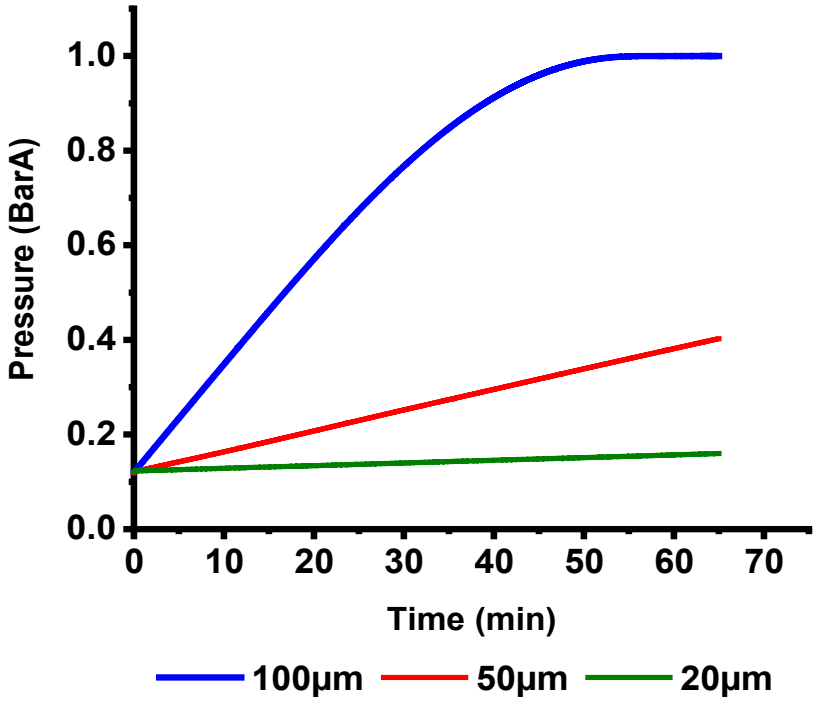

Initial tests done on the pinhole rig

Vacuum Drying

- Allows for a sample to be dried using a process similar to that proposed for the spent fuel
- Pressure, flow rate and dew point are all recorded
- Mass measurements require the experiment to be paused while the reading is taken
- Will be used with pinhole samples as well as the cracks produced

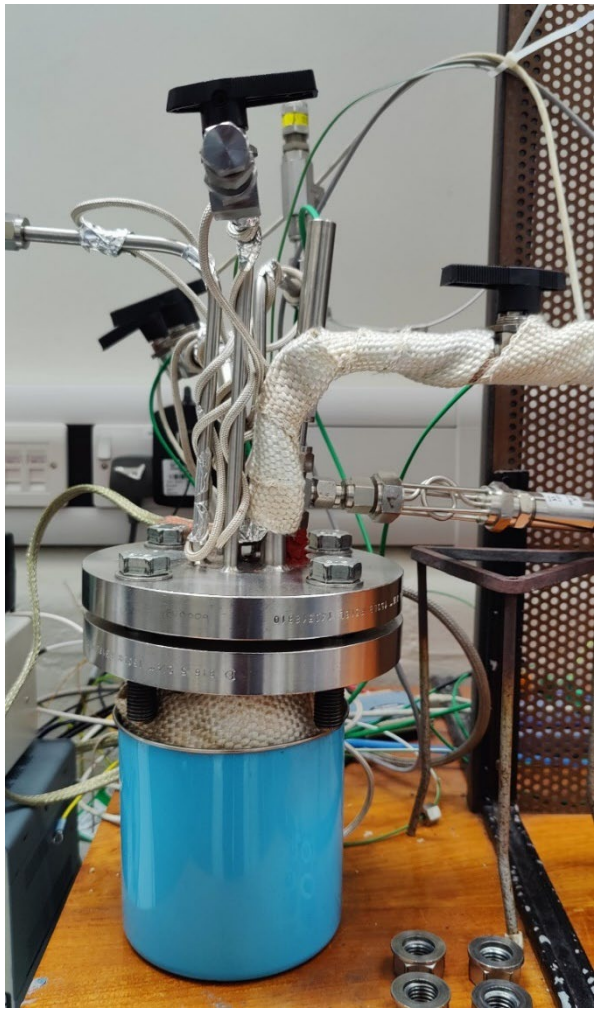

Drying rig vessel

Vacuum Drying - Results

- The pressure, dew point and flow are in step with each other
- The temperature “bounces” due to the heater controller
- Small bumps in pressure etc due to water evaporation
- Final drop marks the last of the water being removed

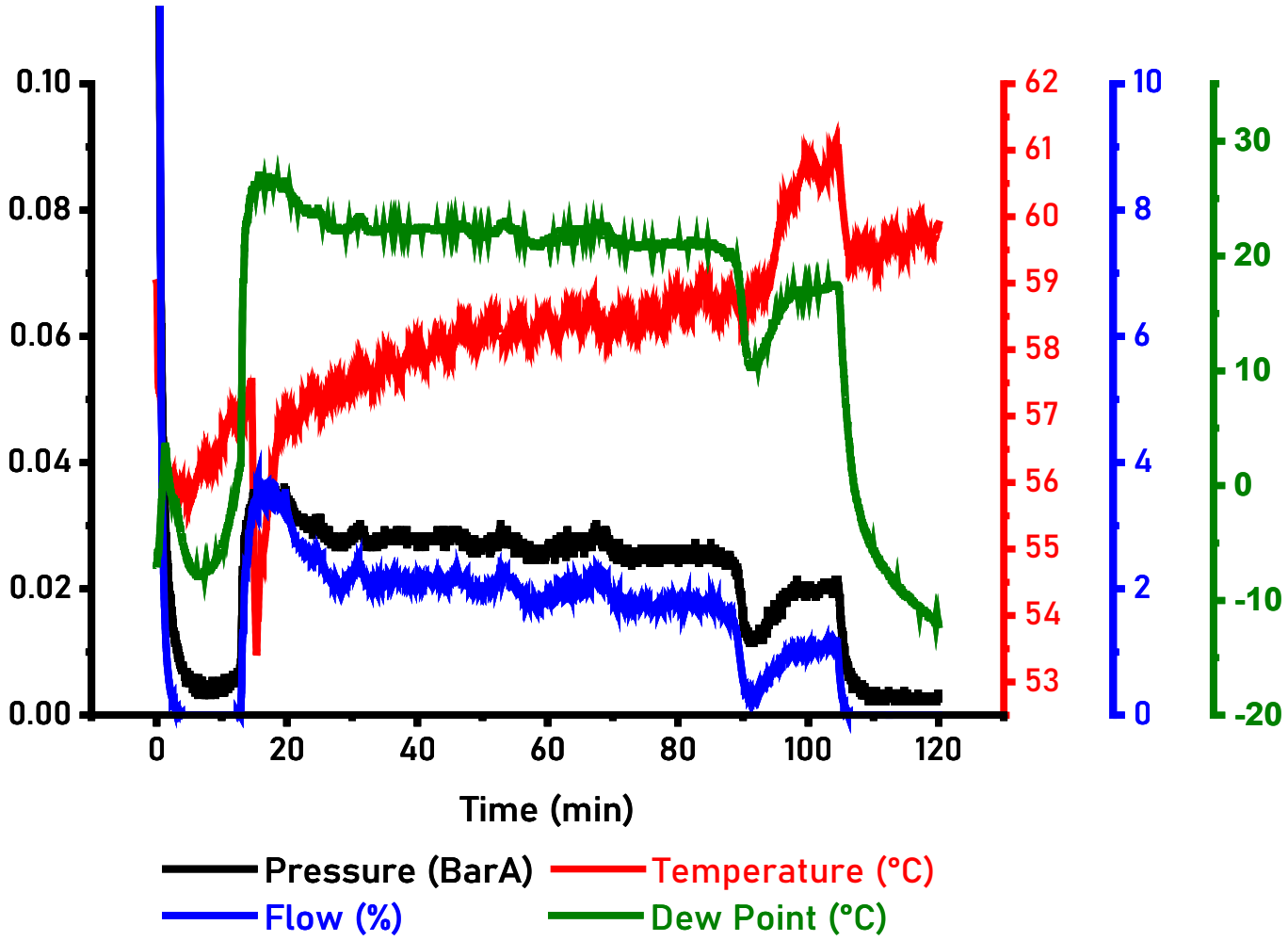

Vacuum Drying - Results

- Taking mass measurements we can see the drying rate
- Unsurprisingly as temperature increases so does the rate
- Heating may not be viable at industrial scale
- Could provide a means to simulate decay heat in pins

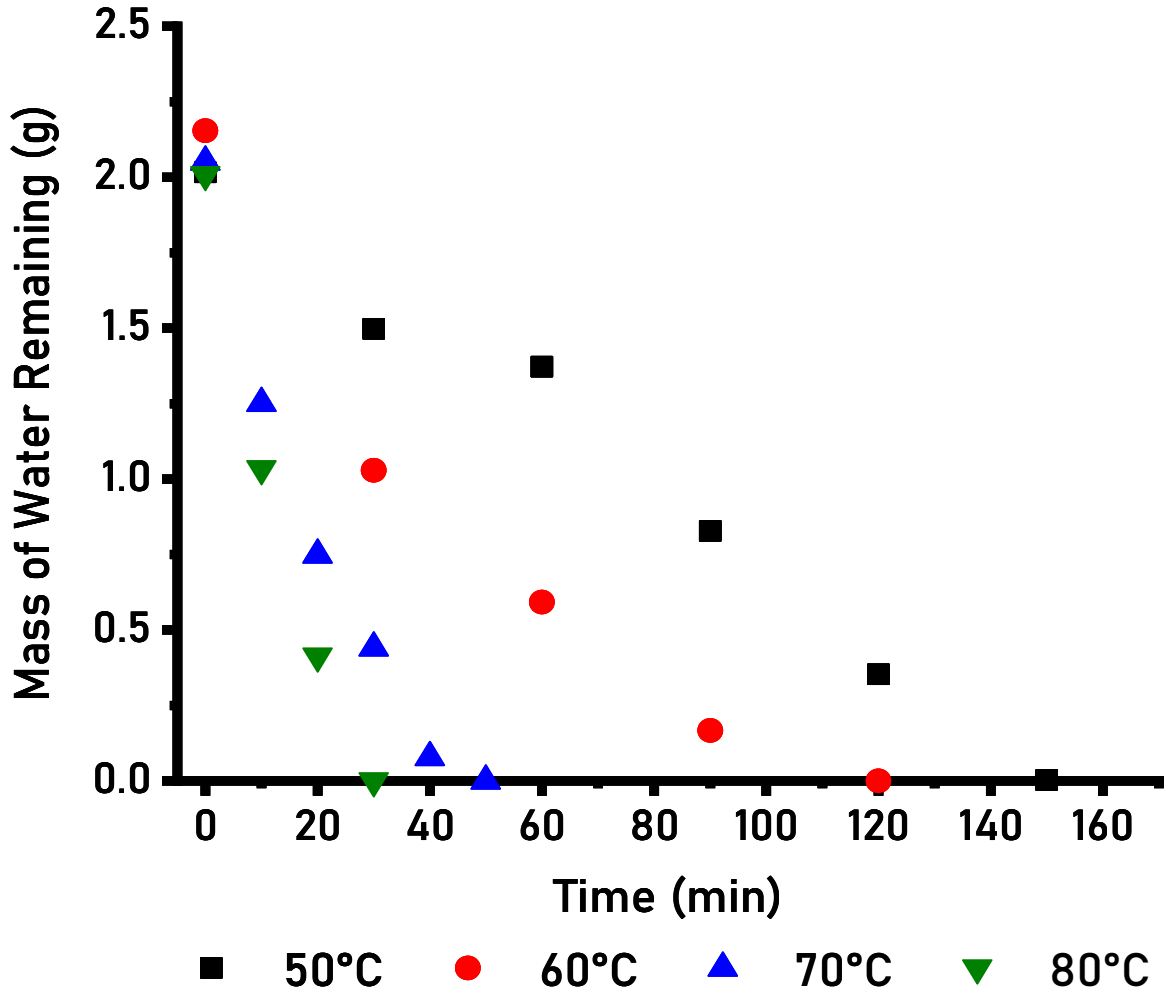

Mass of water left in the sample

Computational Work

Gas Flow

Water at Low Pressure

Computational Work

Overview

To produce cracks, measure the flow rate of fluid through these cracks & then conduct full vacuum drying to validate the model

Image Analysis

To characterise the images of any cracks produced. Length and width of the cracks are required for the flow equations

Pinhole Flow Rate

Various models have been trialled. These include various orifice flow equations as well as more complex crack network equations

Water at Low Pressure

As the work is looking to dry the sample the effect of exposing a quantity of water to a vacuum needs to be modelled

Pinhole Flow Rate

Different models considered. From orifice models to complex leak before break models.

Compared to the experimental data from the pinhole rig – Beck et al was deemed to be the best match

$$) = \frac{\rho u^2}{2}\left[N\left(1-\left(\frac{d_{eff}}{d}\right)^2\right)\right] + \frac{2u}{\rho}\left[\frac{12\mu l_{eff}}{d_{eff}^2}\right] - \Delta P$$

Average of multiple methods also considered however this was not an improvement over the single model.

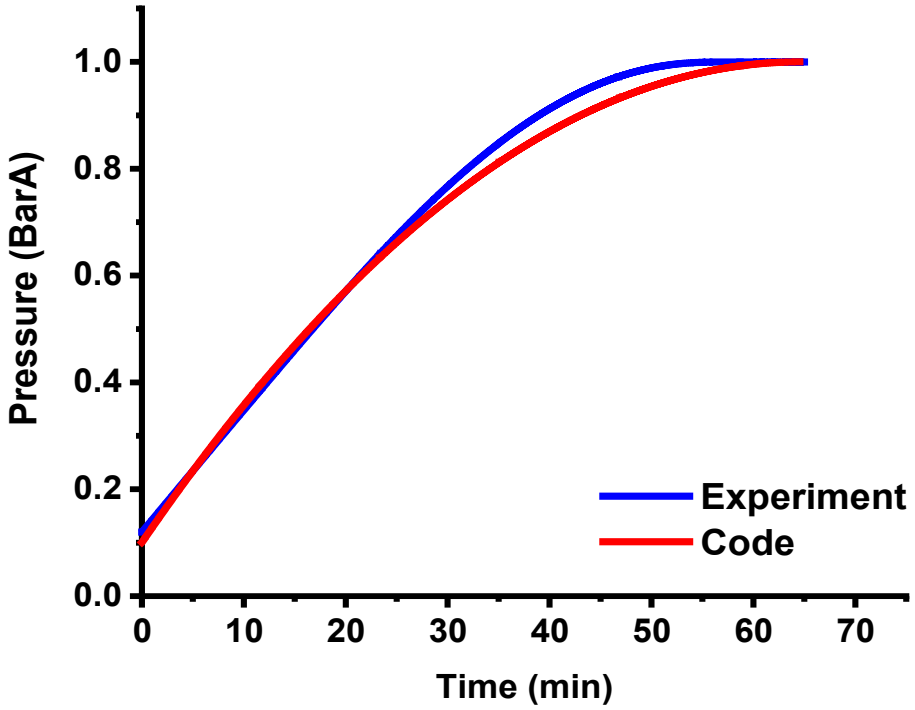

Comparison of the Beck et al method and the experimental data

Water at Low Pressure

From literature there are many approaches however most use a CFD approach which is too complex for this

Two options for modelling the evaporation: Hertz-Knudsen equation and vacuum evaporation

$$j_{HK} = \alpha \frac{1}{\sqrt{2\pi m k_B}} \left(\frac{P_{sat}}{\sqrt{T_{liq}}} - \frac{P_{vap}}{\sqrt{T_{gas}}} \right)$$

$$\Gamma_e = 5.84 \times 10^{-2} \sqrt{\frac{M}{T}} P_v$$

Future Work

- Code water at low pressure equations
- Continue the drop evaporation experiments trying other salts
- Finish the water tests on the pinhole rig
- Full validation of process model

Acknowledgments

Thank you to the NDA for funding this work

Academic supervisors: Prof. Bruce Hanson, Dr Nicole Hondow

Industrial supervisor: Dr Carlos de la Fontaine

NUCLEAR ENGINEERING
University of Leeds

UNIVERSITY OF LEEDS

Thank you for listening
Are there any questions?

TRANSCEND

Transformative Science and Engineering for Nuclear Decommissioning

Computational Studies of Helium Incorporation in PuO_2

Elanor Murray

Cyclife Ltd.

University of Birmingham

NDA

TRANSCEND

Transformative Science and Engineering for Nuclear Decommissioning

Computational Studies of Helium Incorporation in PuO_2

What is the mechanism for bubble formation?

How much helium can the lattice accommodate?

What are the likely trapping sites?

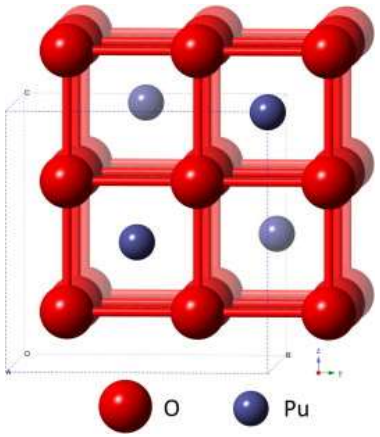

Is helium diffusion vacancy assisted?

How does helium aggregate?

TRANSCEND

Transformative Science and Engineering for Nuclear Decommissioning

Computational Studies of Helium Incorporation in PuO_2

- Bulk PuO_2
- Surface PuO_2
- Static helium in PuO_2
- MD PuO_2
- Helium diffusion
- Helium clustering

TRANSCEND

Transformative Science and Engineering for Nuclear Decommissioning

Bulk PuO_2

Frenkel pair:
- Vacancy
- Self-interstitial

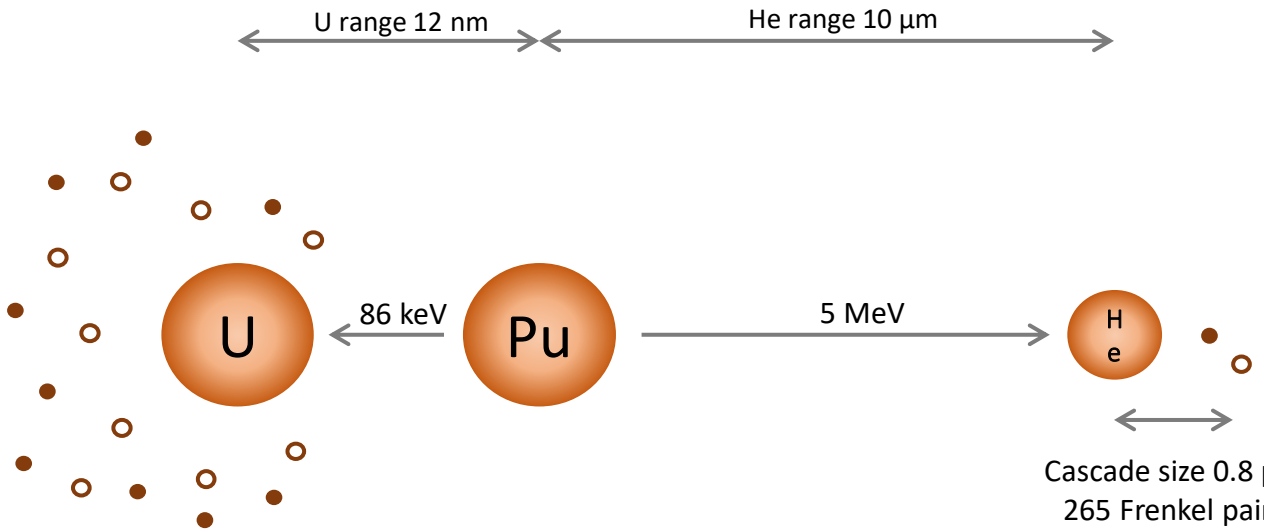

- Plutonium
- Oxygen

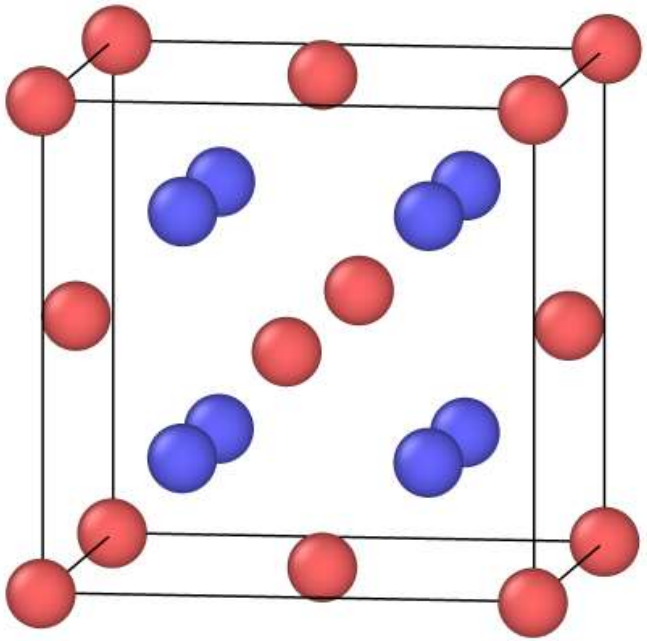

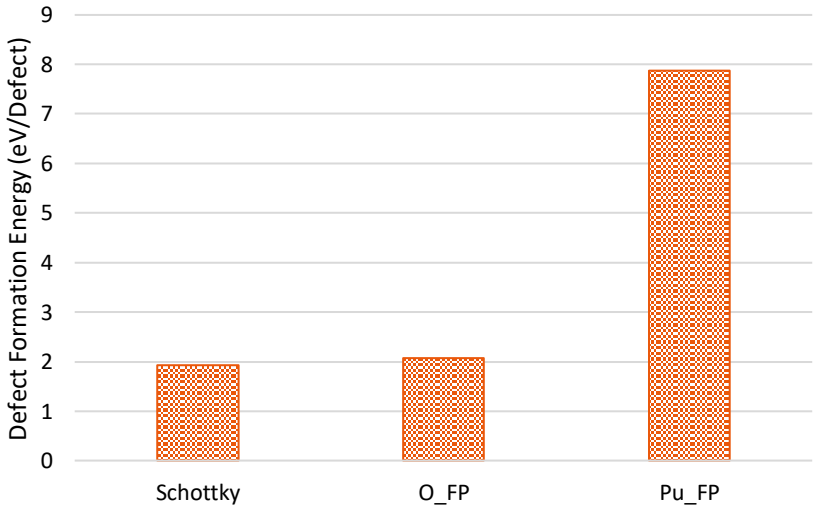

Found Schottky and Oxygen Frenkel Pairs to be most energetically favourable defects

Surface PuO_2

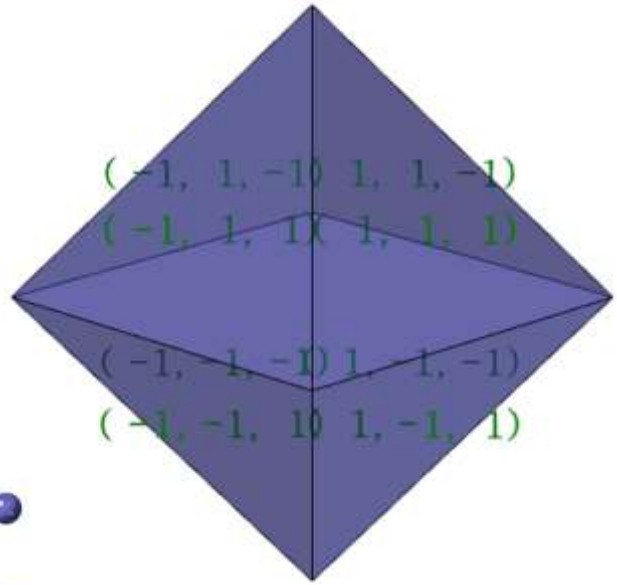

Most stable

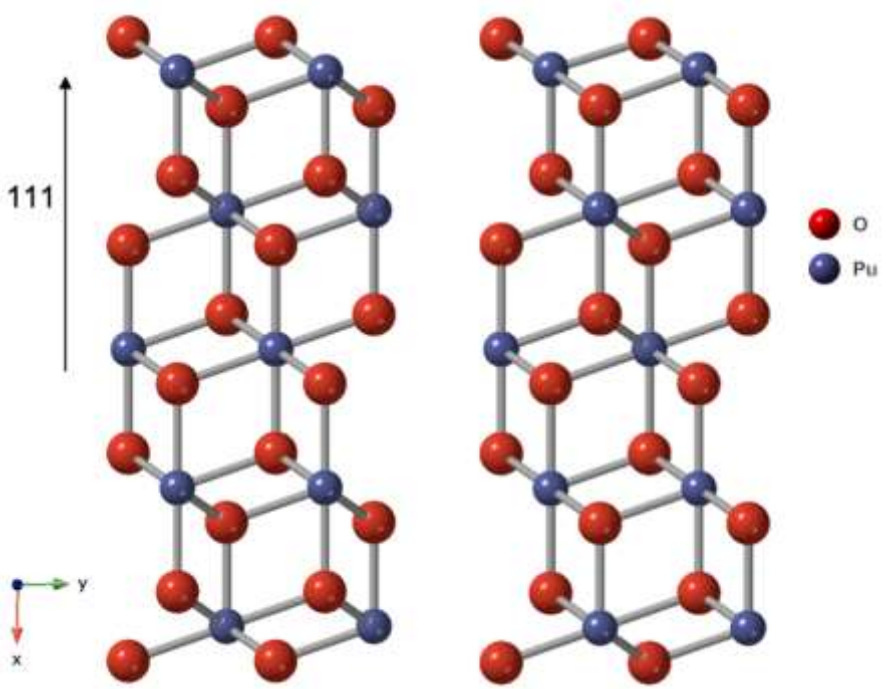

Before relaxation After relaxation

Least stable

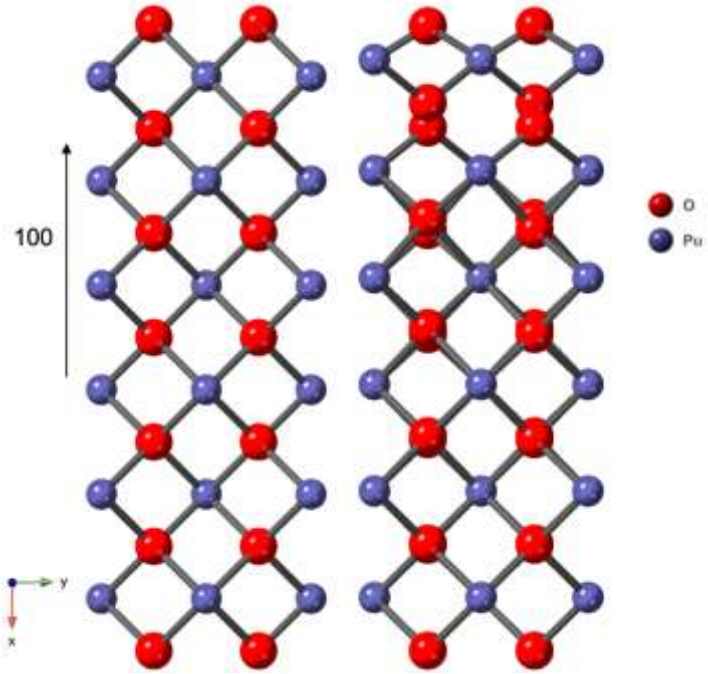

Before relaxation After relaxation

Plutonium vacancies are more stable at the surface

TRANSCEND

Transformative Science and Engineering for Nuclear Decommissioning

Computational Studies of Helium Incorporation in PuO_2

Bulk PuO_2

Surface PuO_2

Static helium in PuO_2

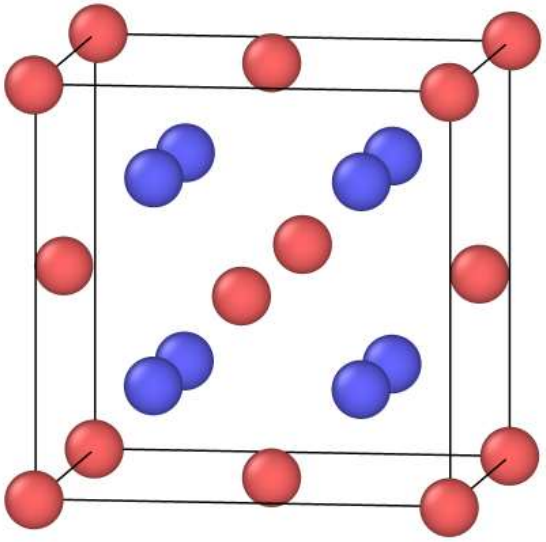

Static helium in PuO_2

Where is He?

Octahedral Interstitial Site (OIS)

Helium
Plutonium
Oxygen

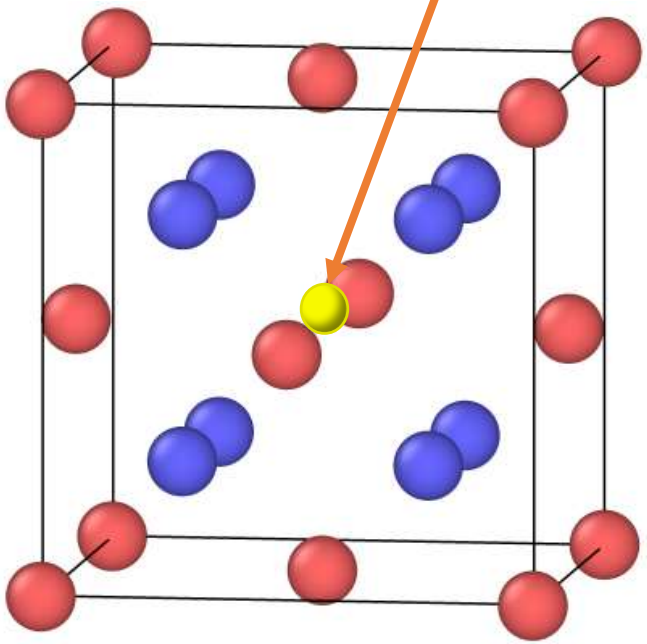

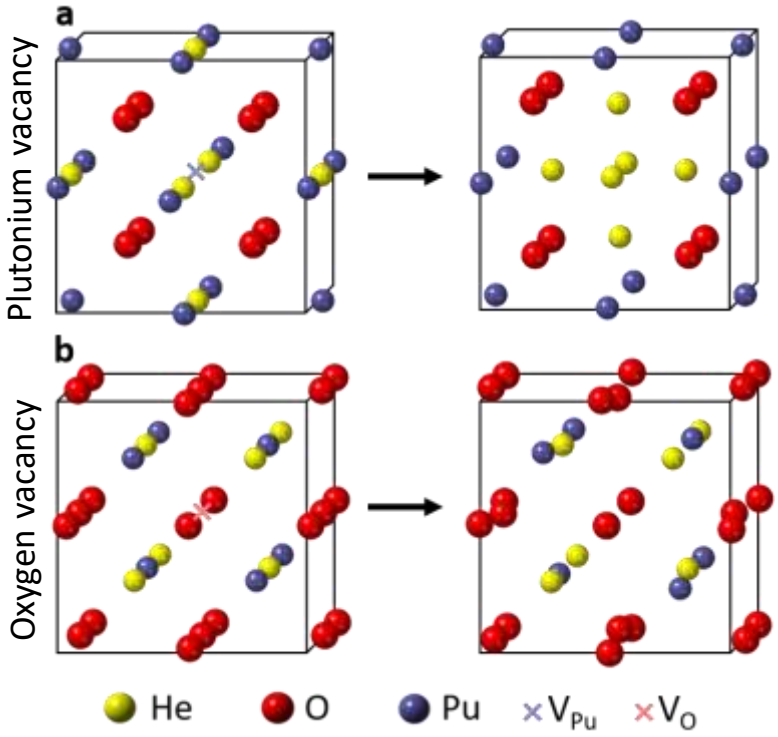

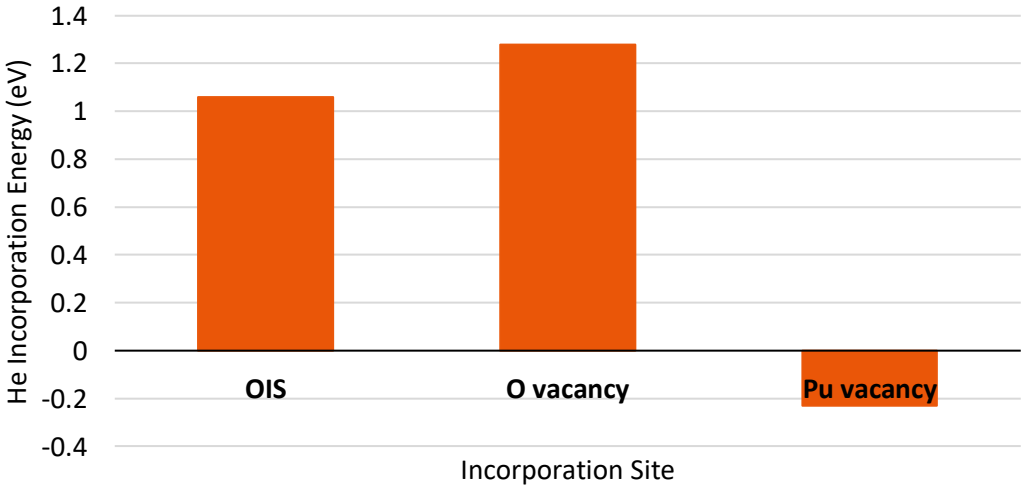

He diffusion

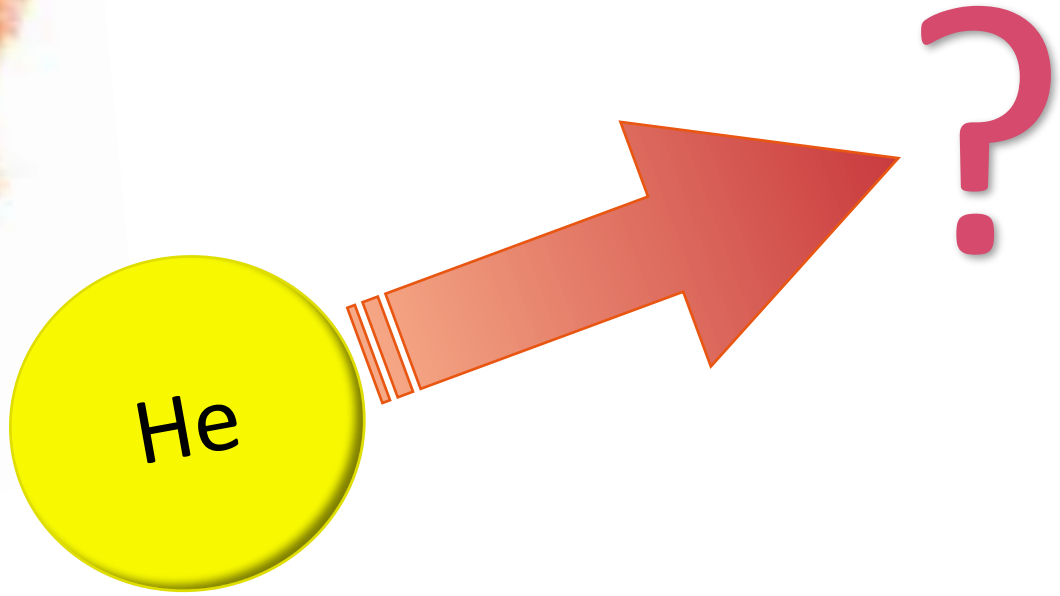

Nudged Elastic Band Calculations

Helium diffusion

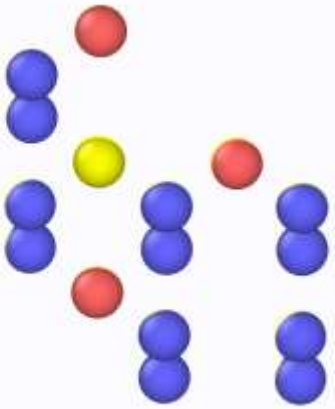

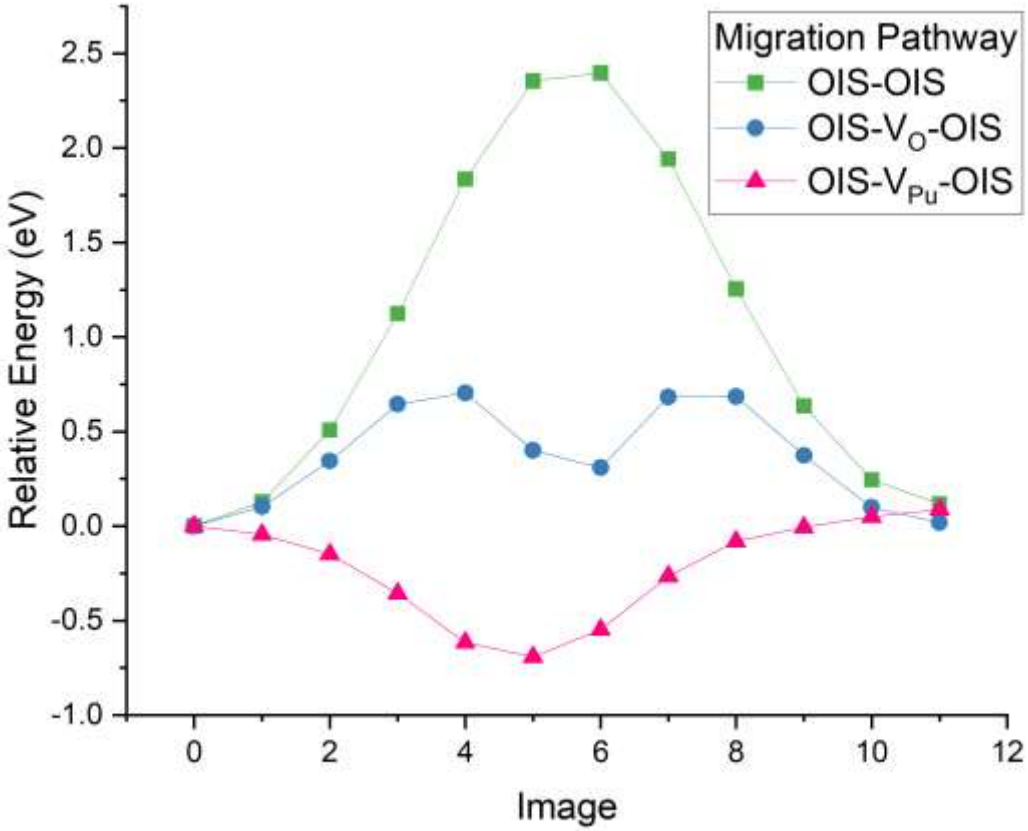

Plutonium
Oxygen
Helium

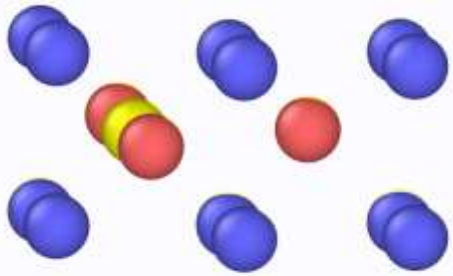

OIS-OIS

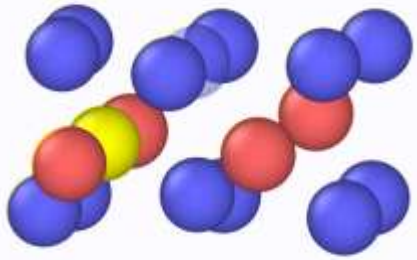

OIS-V$_O$-OIS

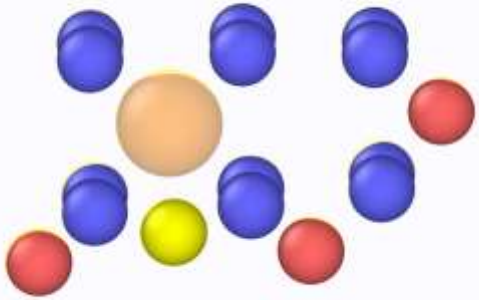

OIS-V$_{Pu}$-OIS

He diffusion

Molecular Dynamics Simulations

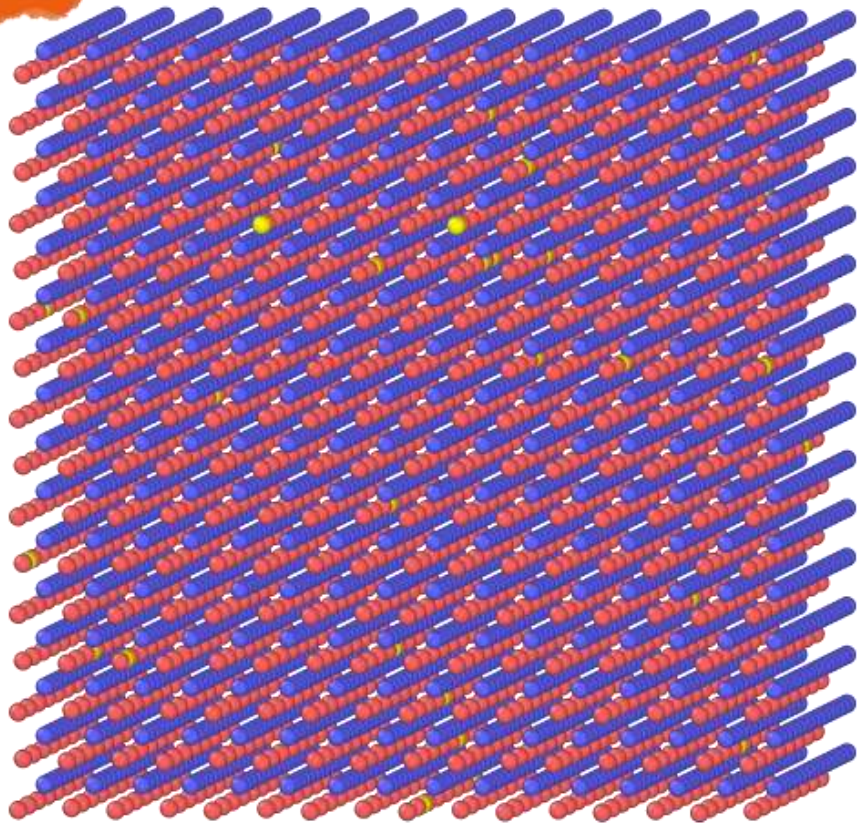

8x8x8 supercell of PuO_2 with 0.5% He

Plutonium
Oxygen
Helium

Molecular dynamics for 5 ns over range of temperatures

1200 K

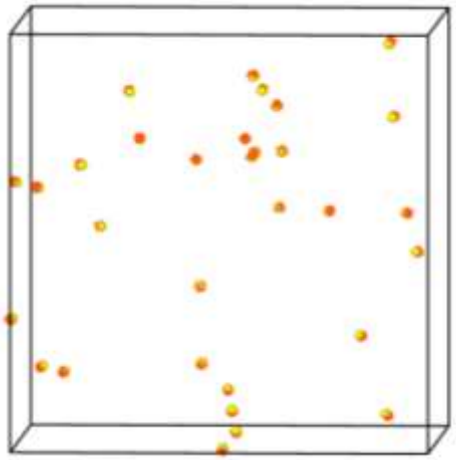

2100 K

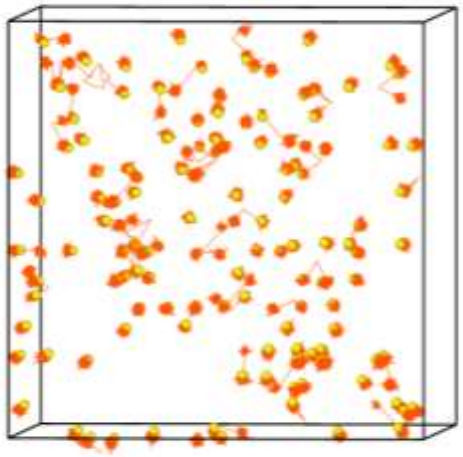

MD PuO_2

R2 (1500-2500 K):
The diffusivity of He and O increases

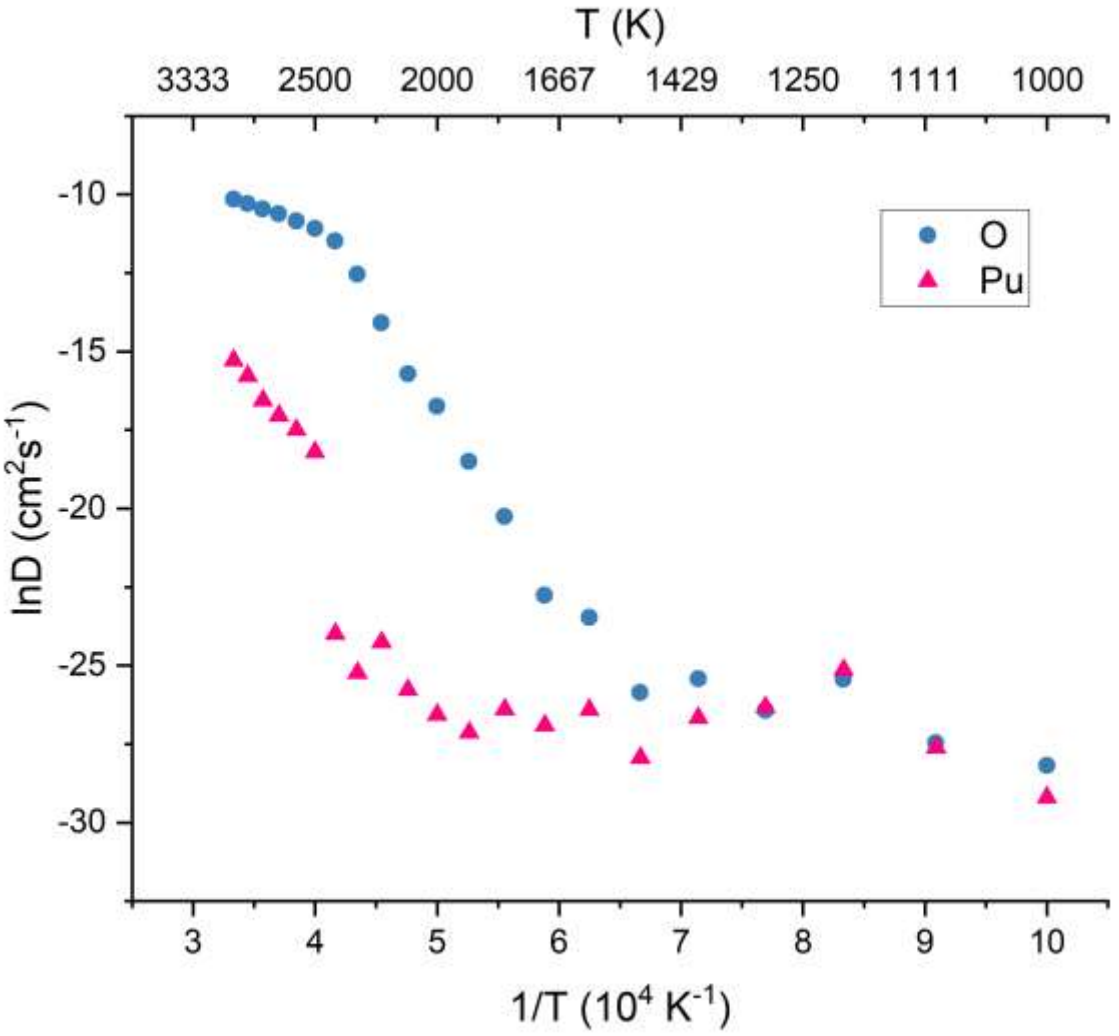

R3 (>2500 K):
Plateau in helium diffusivity and Pu becomes mobile

1 (1000-1500 K):
here is no diffusion

Oxygen is mobile at lower temperatures than plutonium

TRANSCEND

He diffusion

What about intrinsic defects?

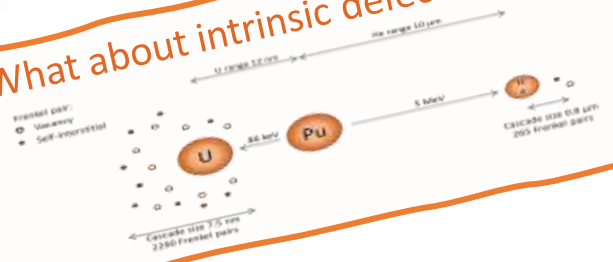

nce and Engineering for Nuclear Decommissioning

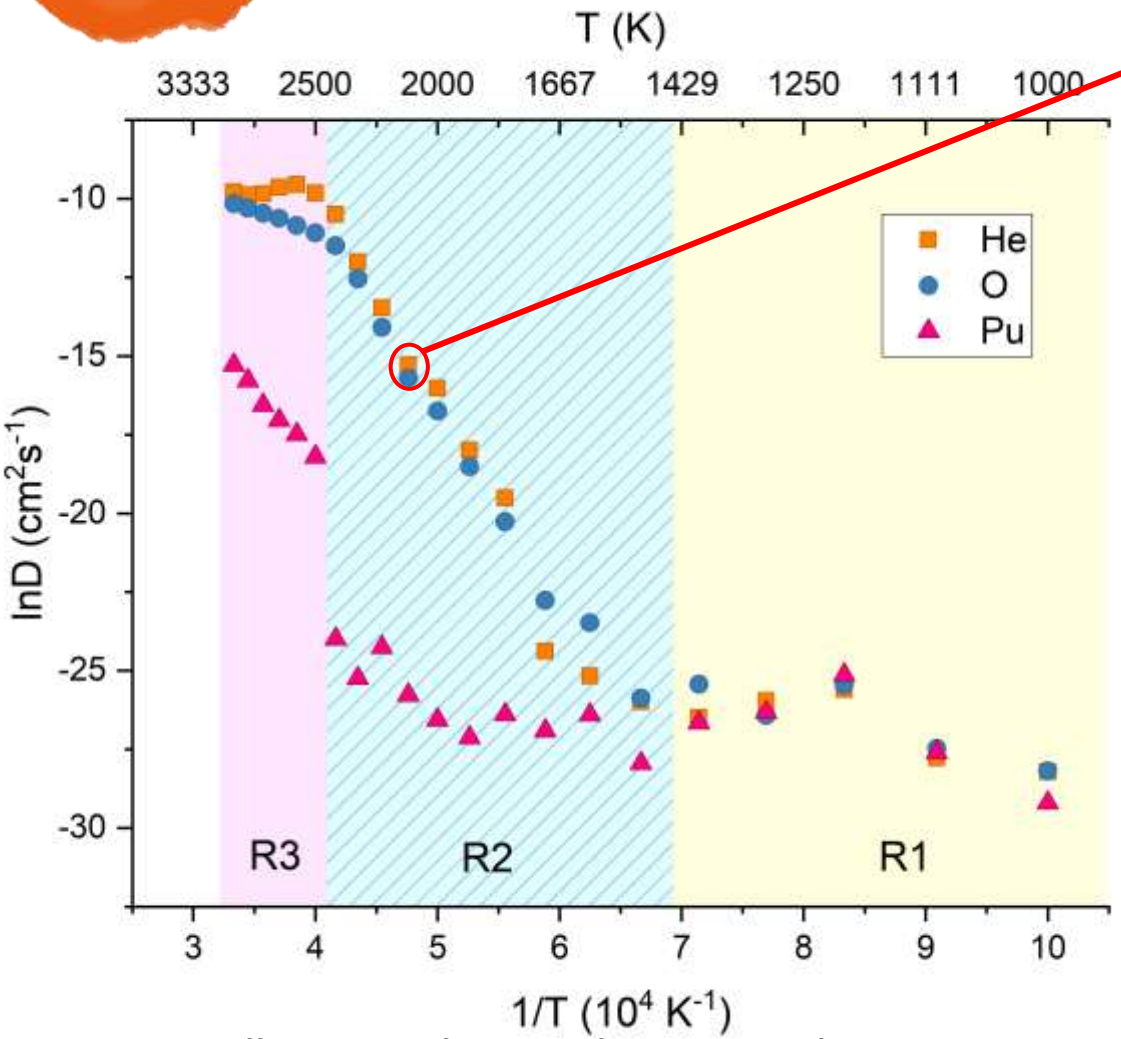

Diffusivity as a function of temperature for He, O and Pu

a

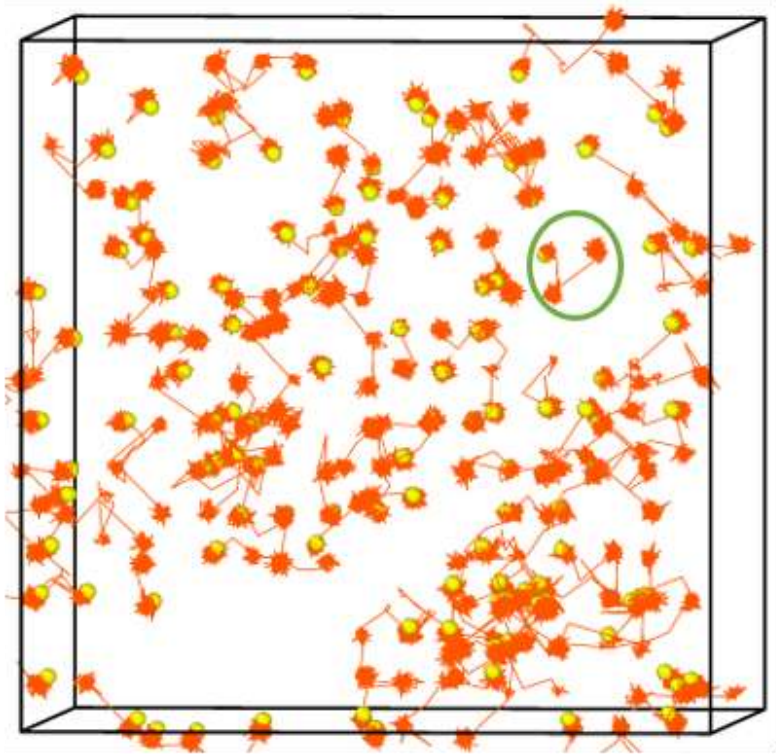

b

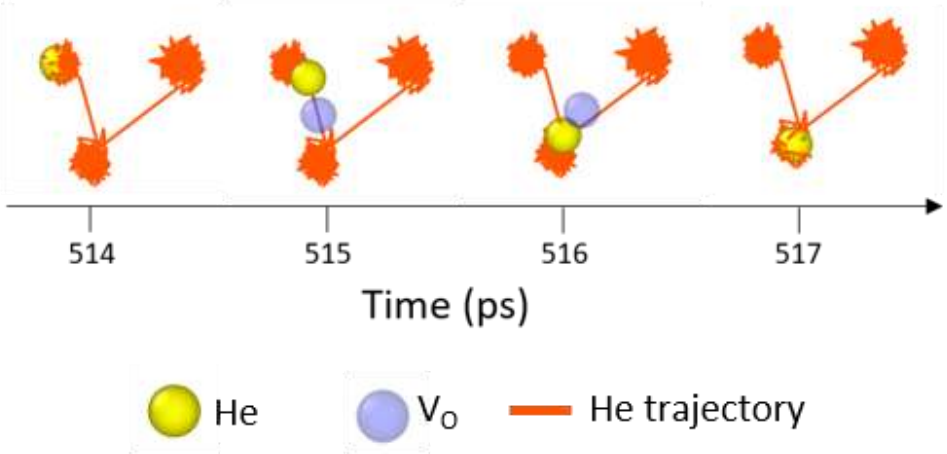

He diffusion

Generate defective lattice

Three Schottky concentrations considered: 0.5, 2 and 4%

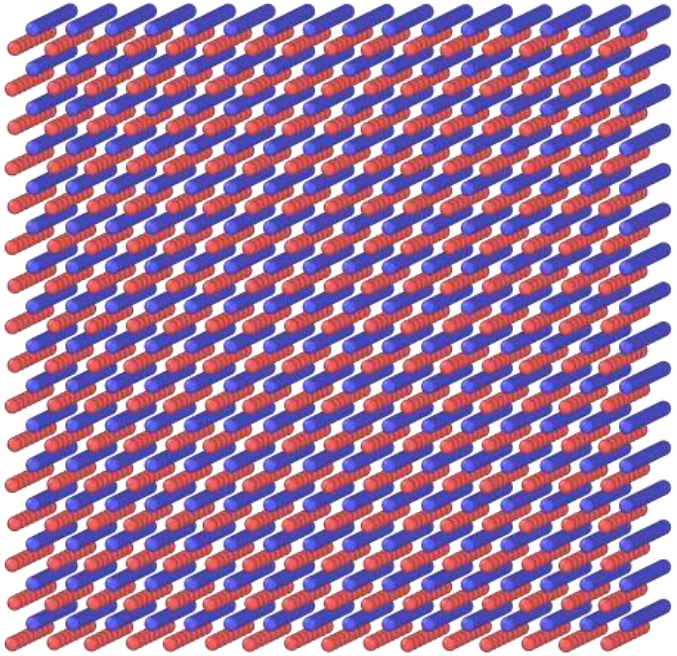

Pure PuO_2

Remove % of atoms

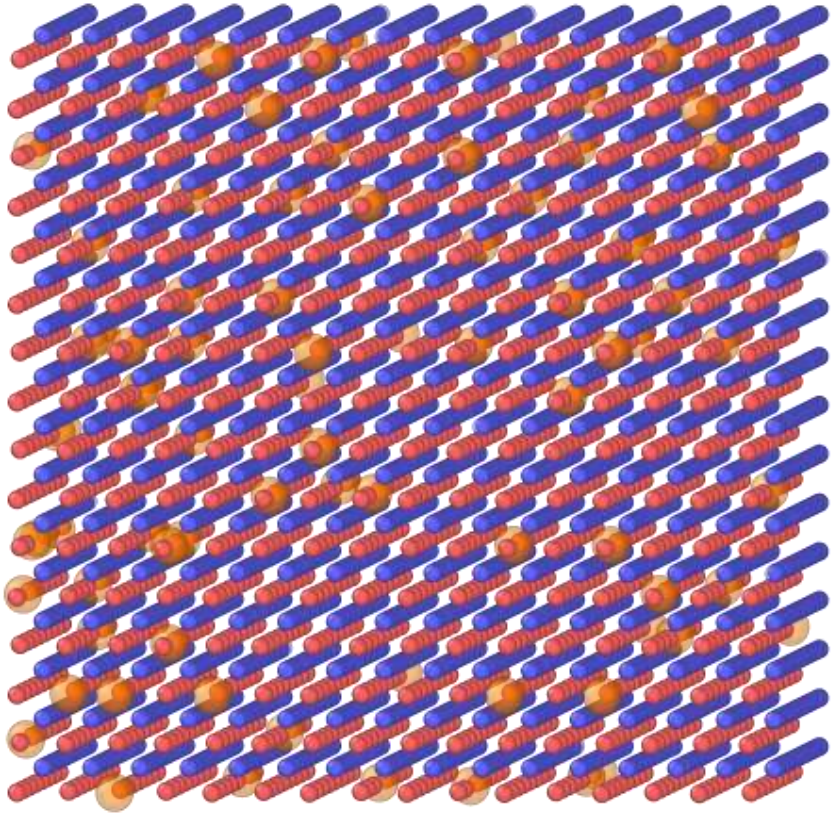

Minimisation, add helium, run MD

He diffusion

Calculate diffusivities

Helium diffusivity

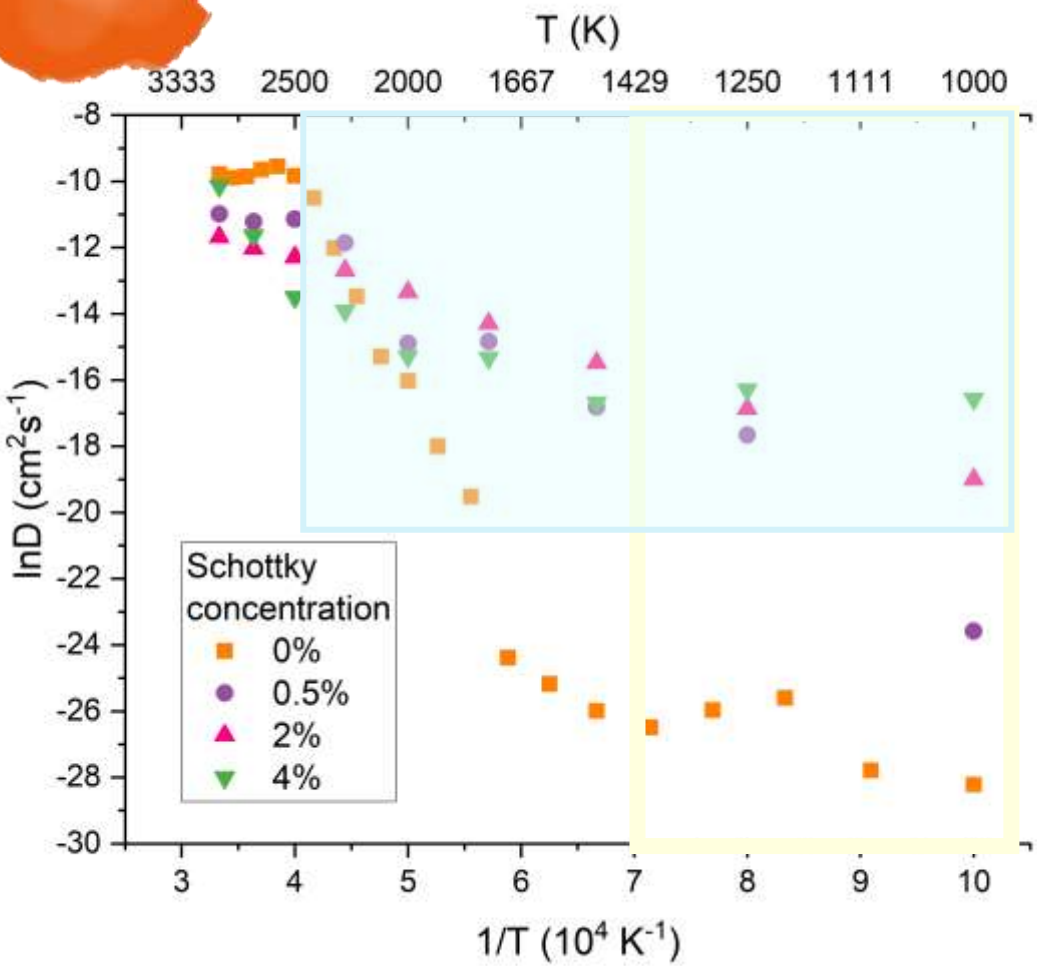

Diffusivity of helium as a function of temperature in PuO_2 with a range of Schottky concentrations, helium input in OIS

Oxygen diffusivity

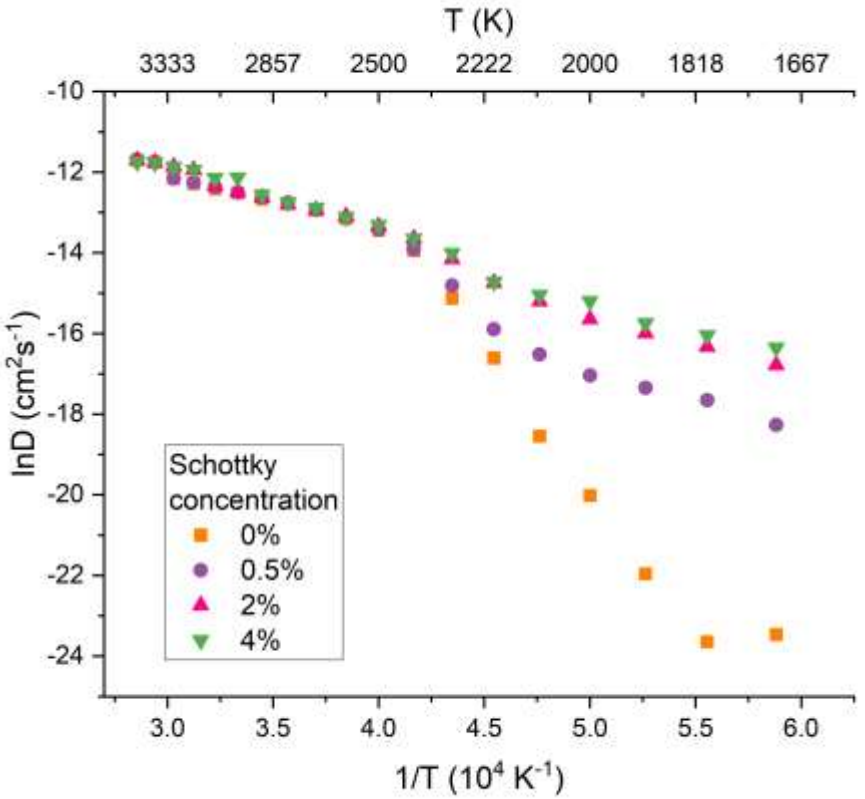

Diffusivity of oxygen as a function of temperature in PuO_2 with a range of Schottky concentrations

When defects are present, helium is mobile at lower temperatures

He diffusion

Does the He input site affect He diffusion?

2% Schottky defect concentration at 2250K, 1ns MD.

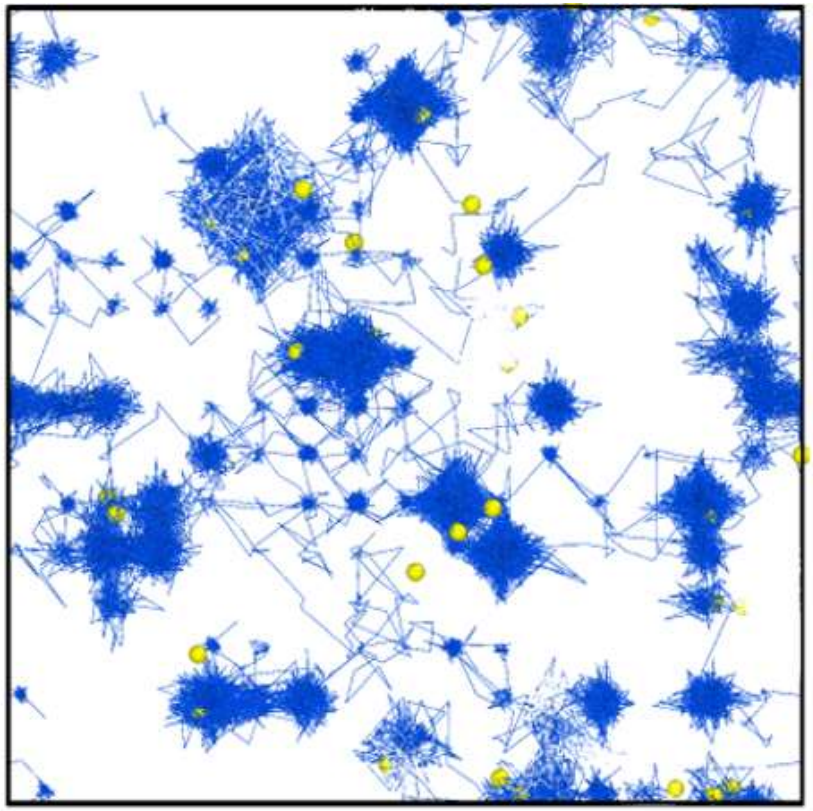

He trajectory V_O starting sites

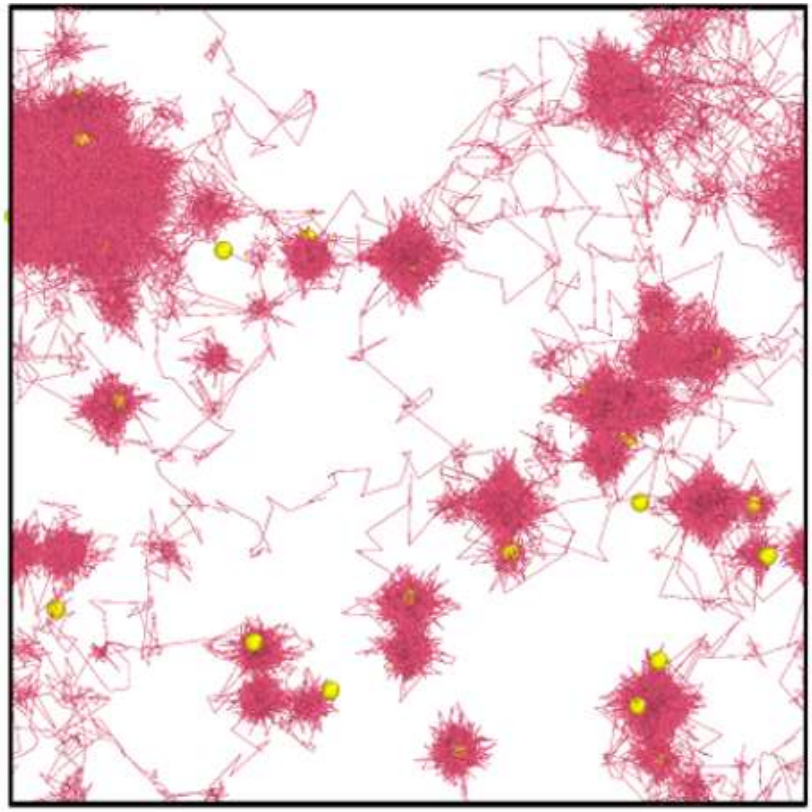

He trajectory V_{Pu} starting sites

Diffusion is reduced when He is input in a V_{Pu}

He cluster analysis

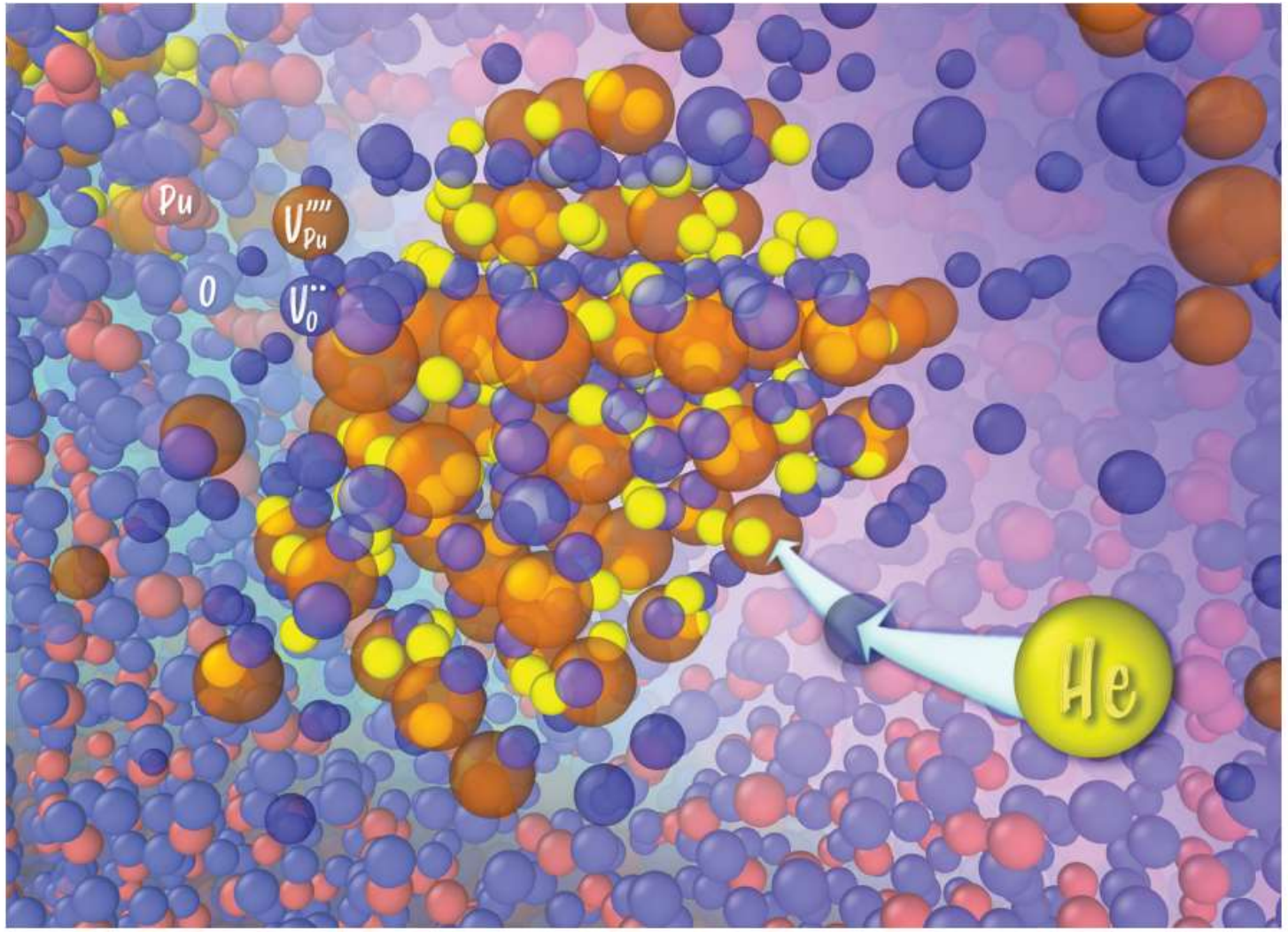

E. Murray, Y. Zhou, P. Slater, R. Smith, P. Goddard and H. Steele, *PCCP,* 2022, **24**, 20709.

He cluster analysis

Helium:vacancy ratio

Schottky trio

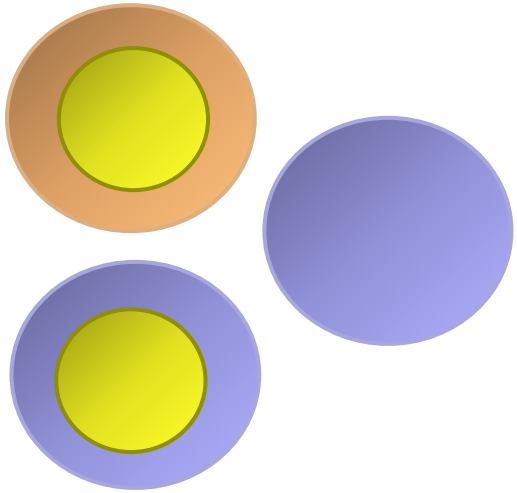

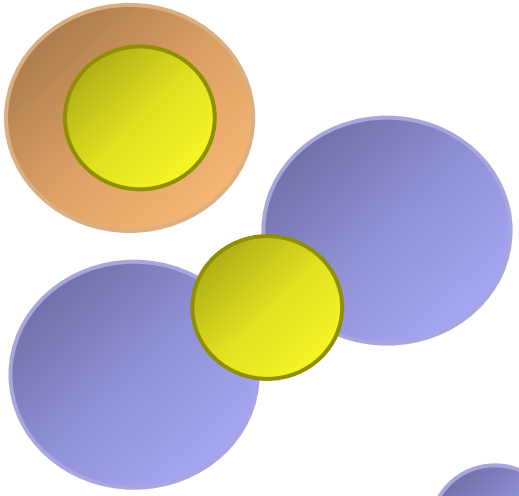

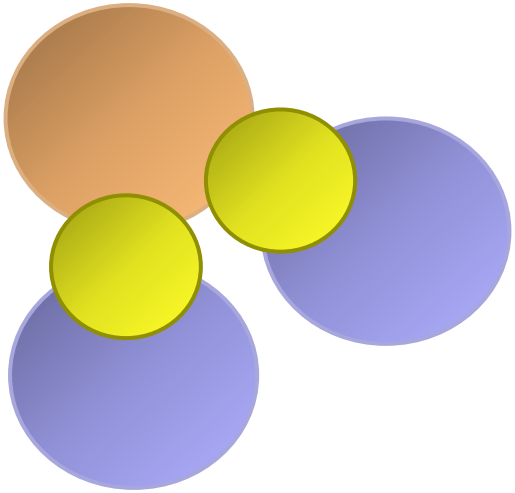

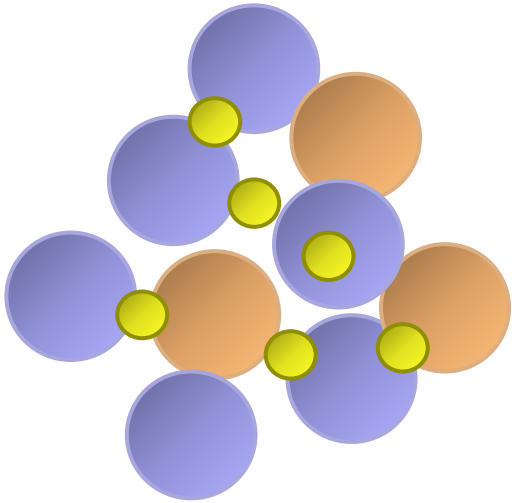

Pu vacancy

O vacancy

He interstitial

He cluster analysis

Static Calculations

Helium Successive Incorporation Energy

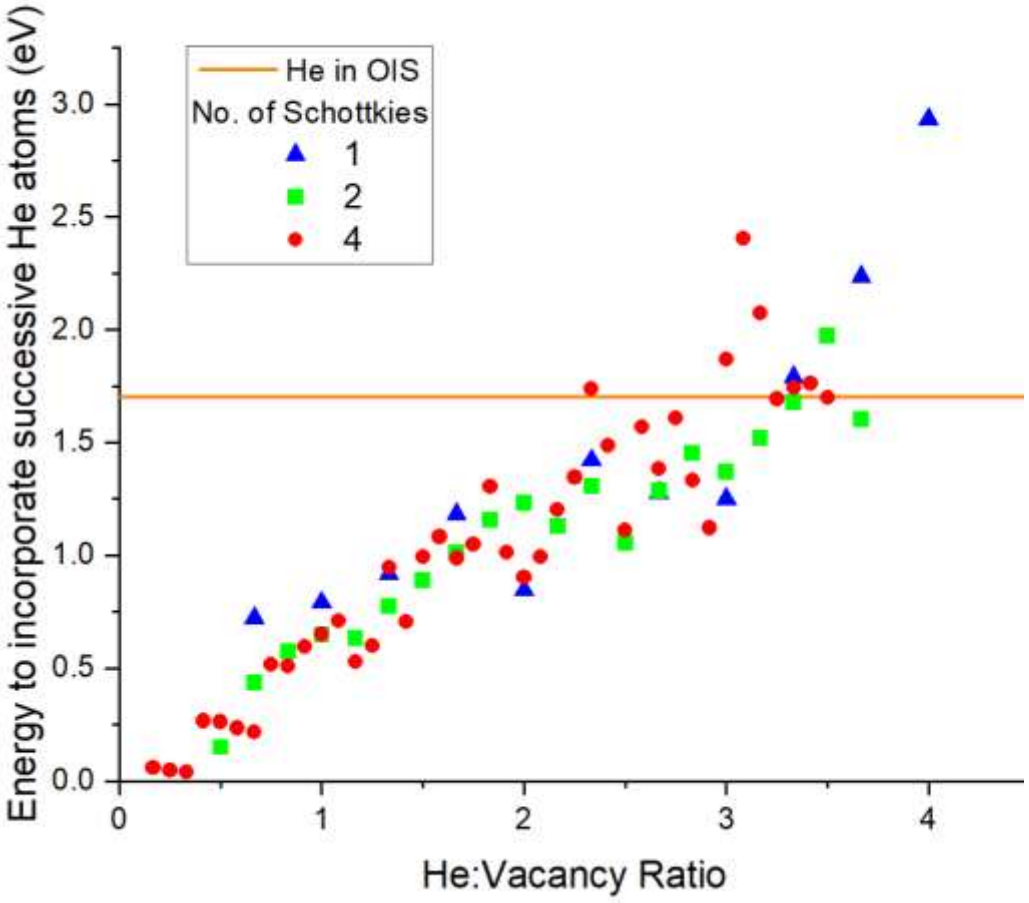

Energy Barrier Difference (Leave – Join)

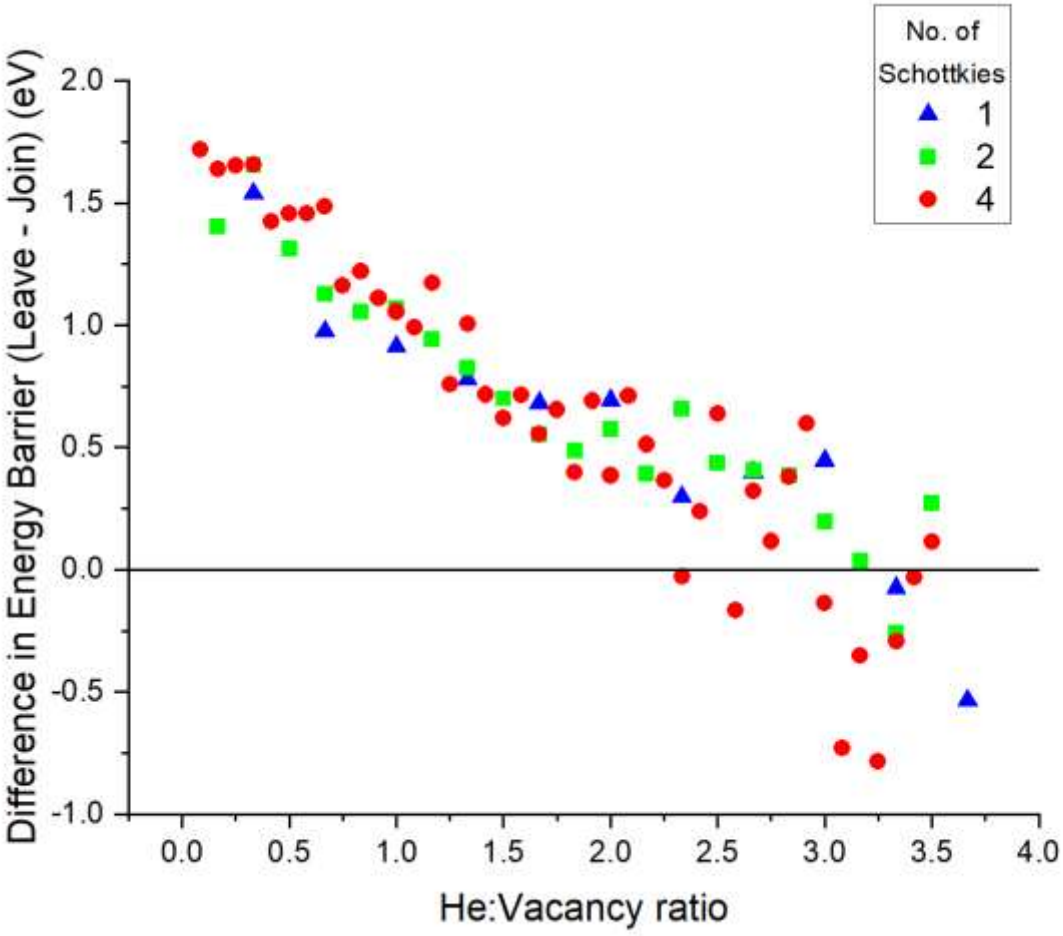

Max cluster has ~ 3.5:1 He:Vacancy ratio

Pu vacancy O vacancy He interstitial

He cluster analysis

Clusters at high temperatures

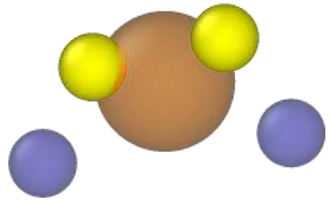

2400 K

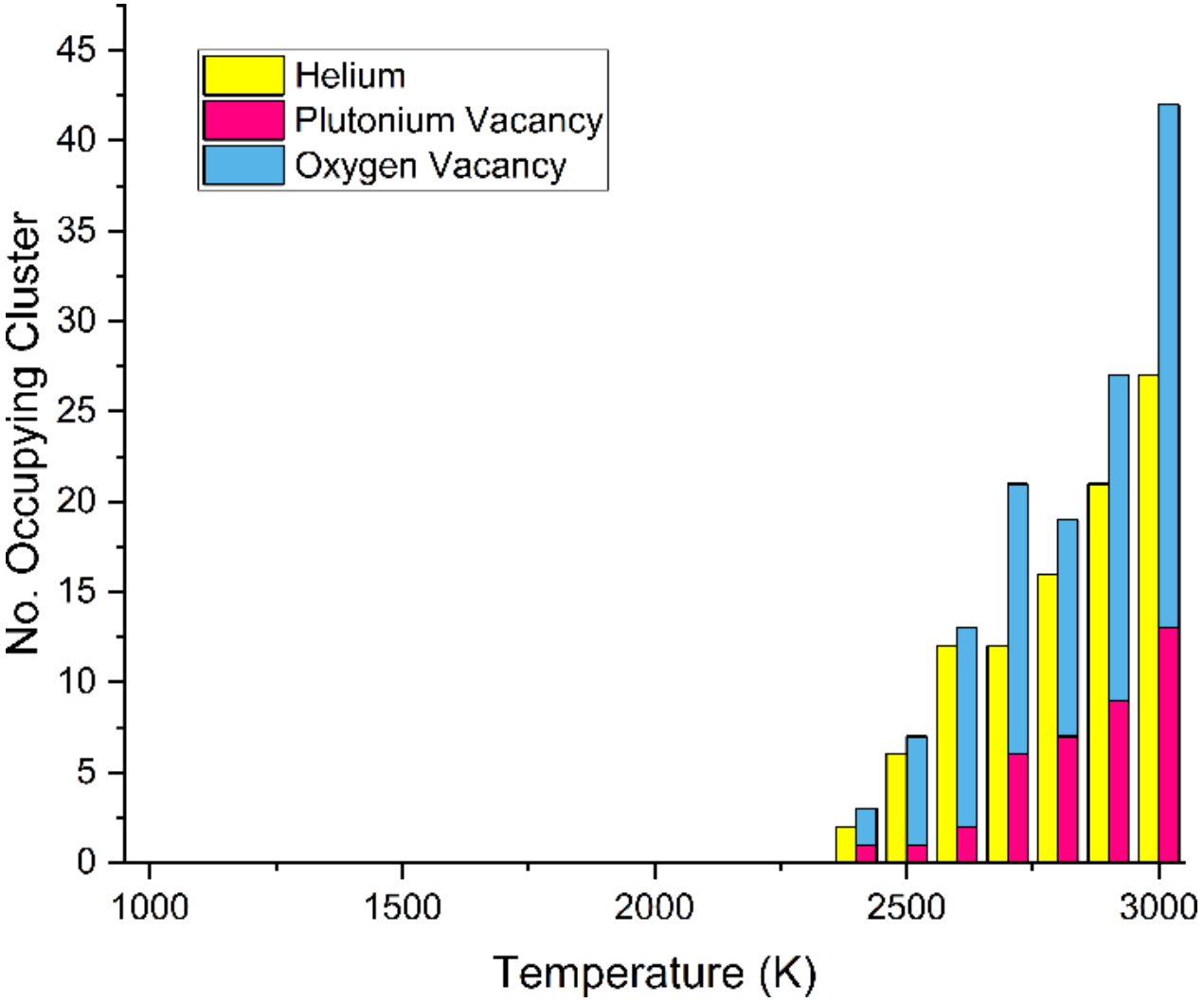

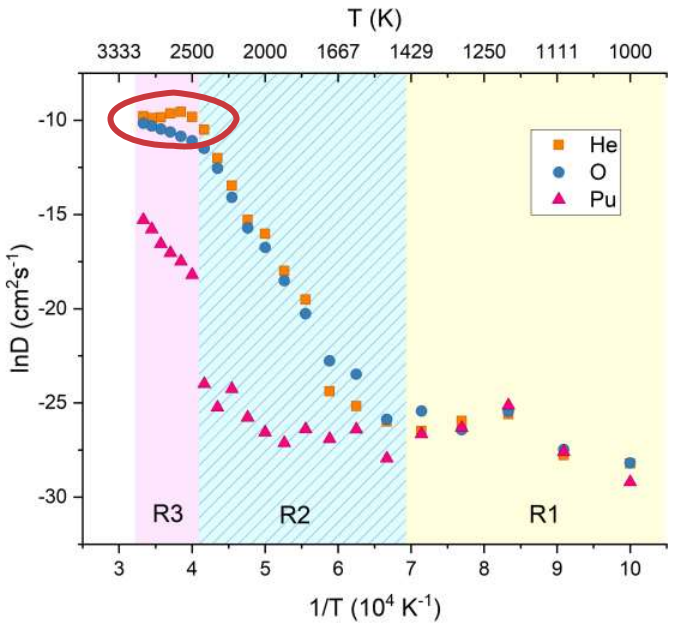

He clustering requires Pu vacancies

TRANSCEND

Transformative Science and Engineering for Nuclear Decommissioning

Pu vacancy O vacancy He interstitial

He cluster analysis

He:Vacancy ratio analysis

Although max theoretical 3.5:1 He:Vacancy, from dynamics find mean < 1:1
Found to remain true at very high He concentrations

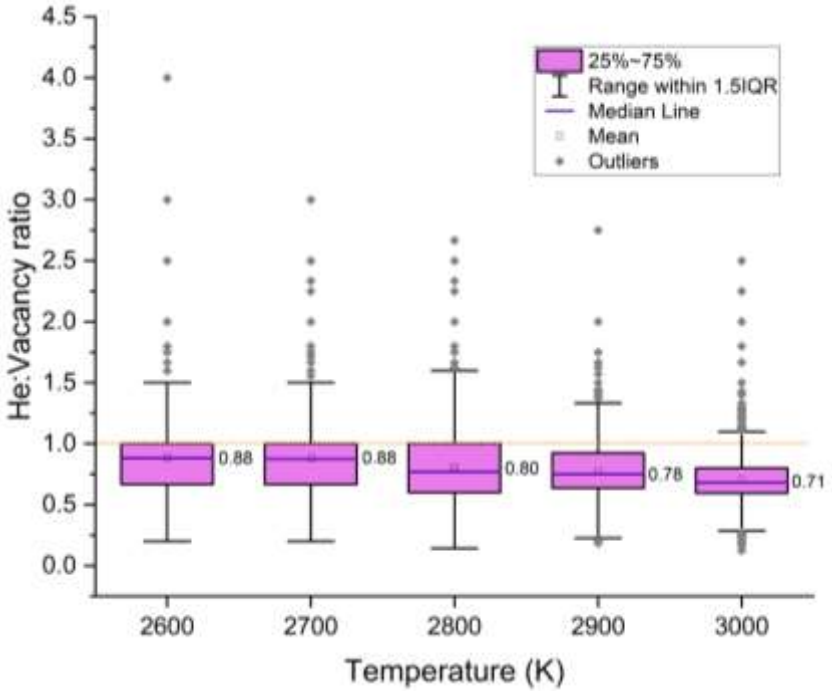

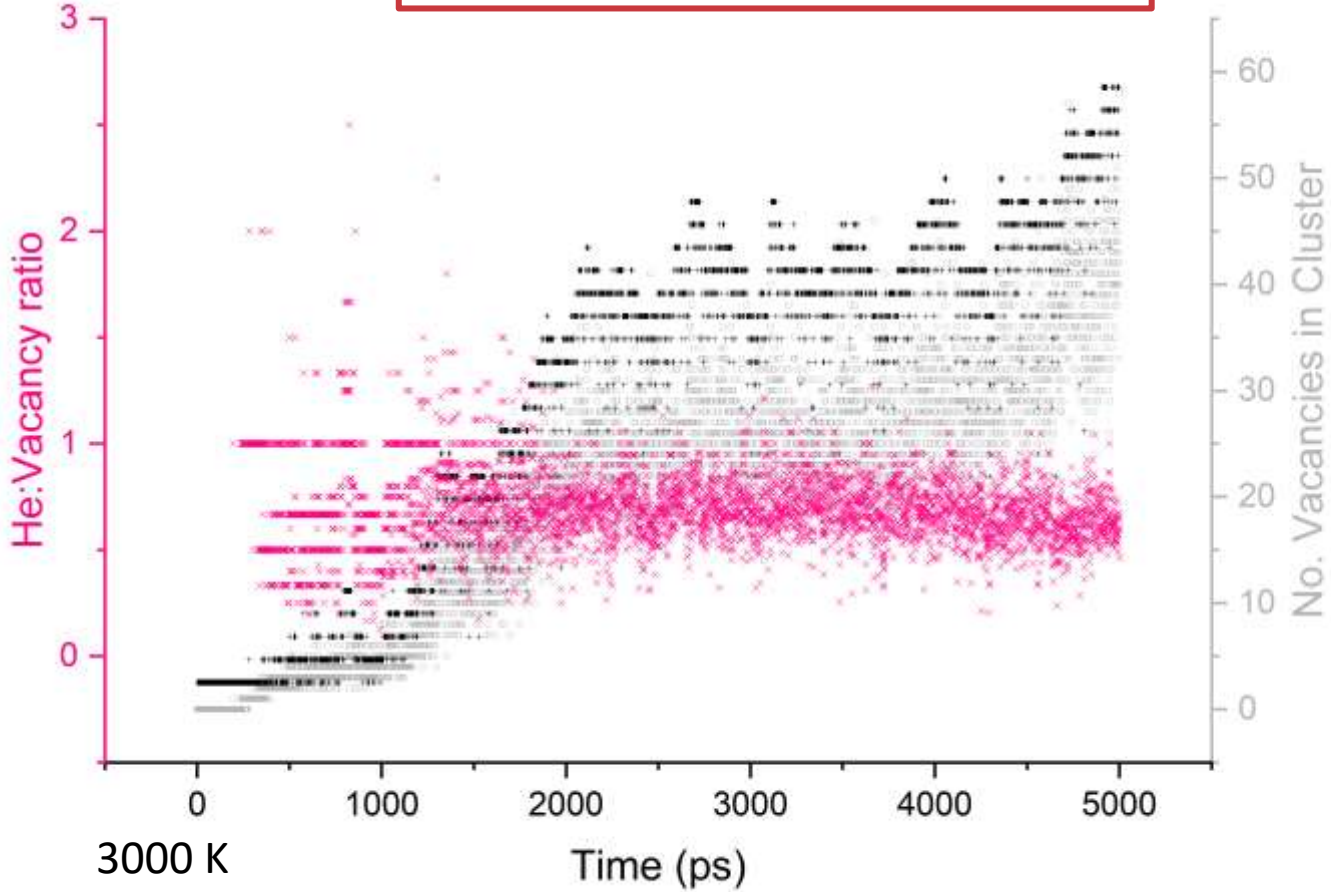

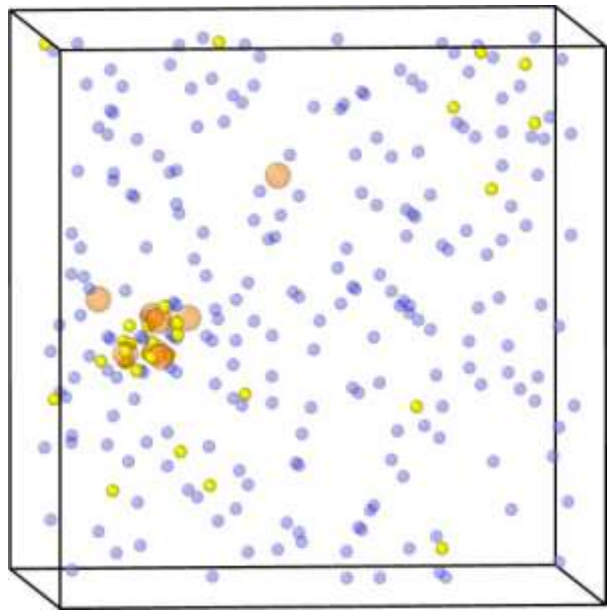

2700 K, $He_{17}V_{24}$

Pu vacancy O vacancy He interstitial

He cluster analysis

Vacancy cluster in centre of lattice – will He migrate?

Input: 2% He, 3 Schottky trios 1500 K 2500 K

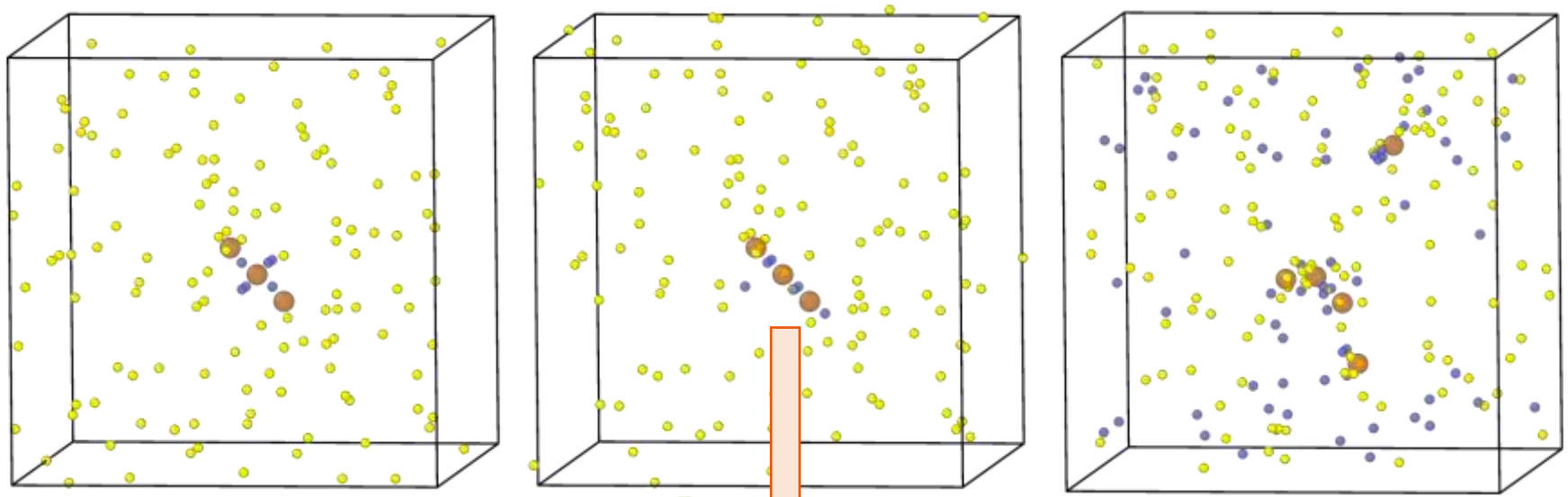

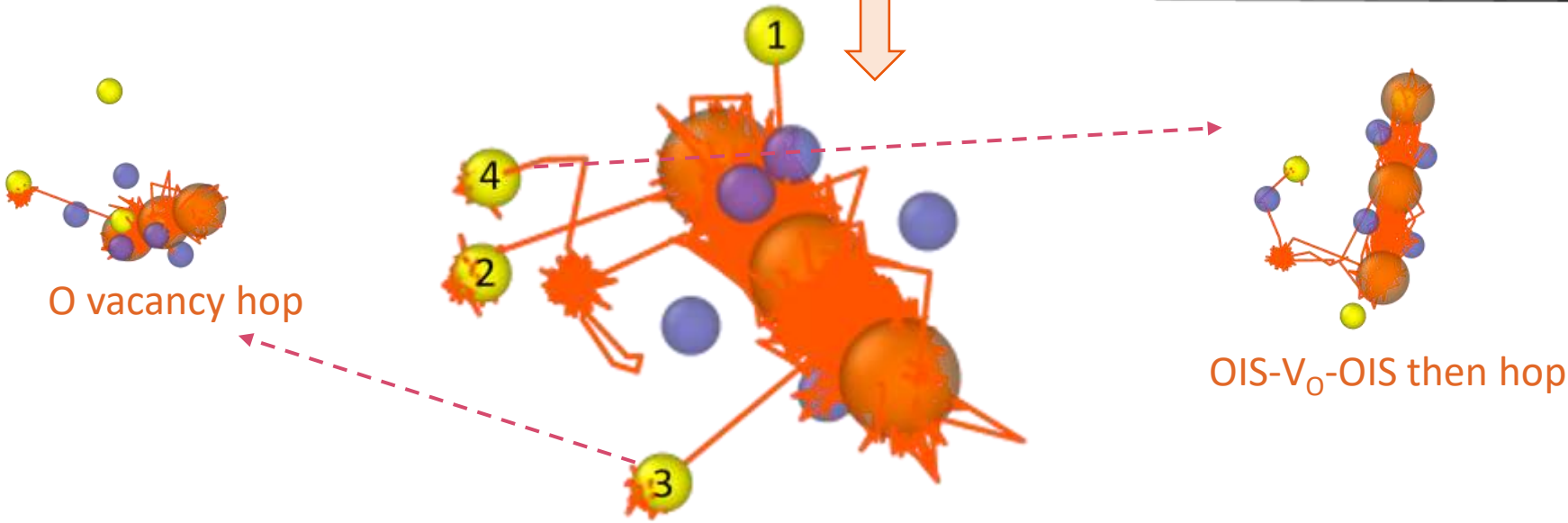

Cluster seeded at lower temperatures as available void space

TRANSCEND

Plutonium

Oxygen

Pu vacancy

O vacancy

He interstitial

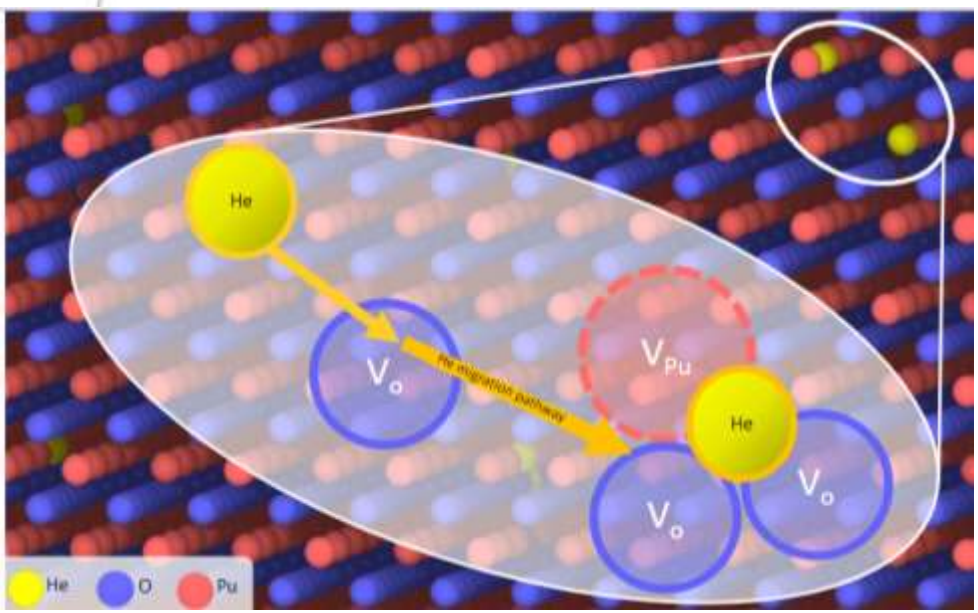

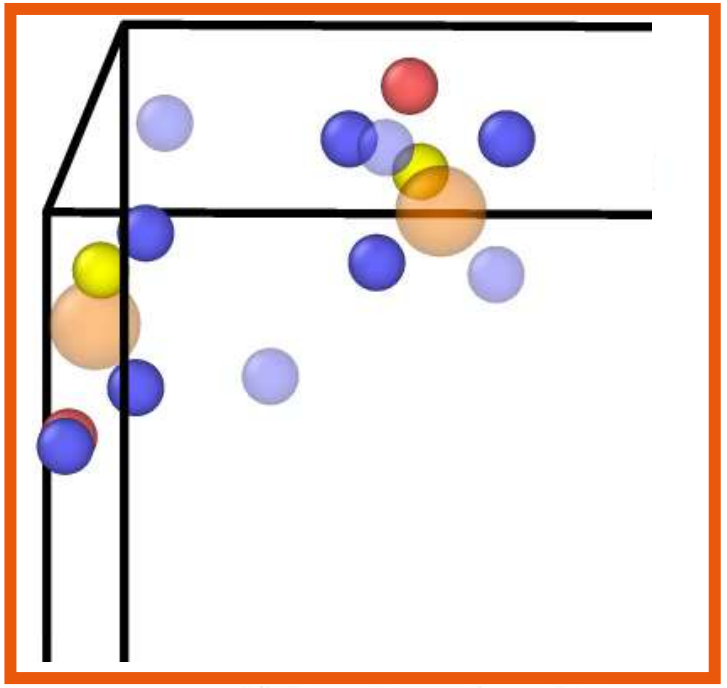

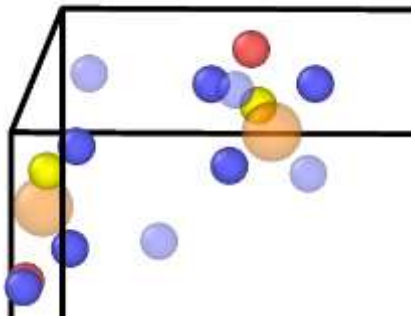

1. 2 He atoms in separate V_{Pu}

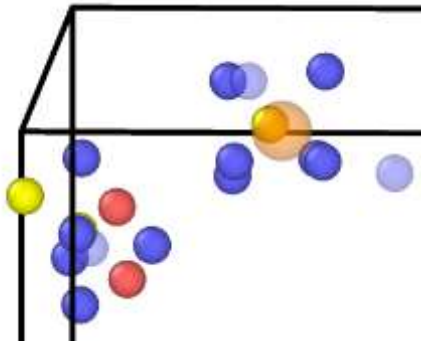

2. He knocked out by Pu interstitial

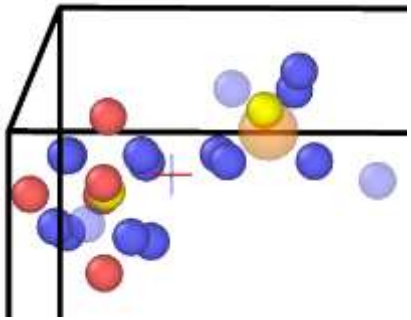

3. He in OIS, stays here for ~5 ps

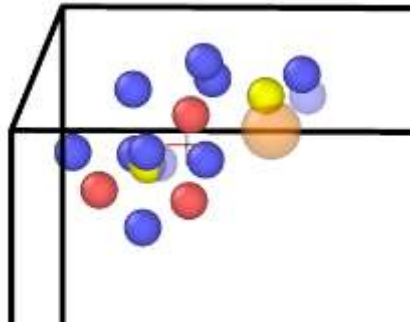

4. Hop to oxygen vacancy

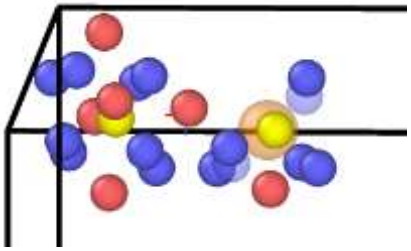

5. To neighbouring OIS (V_O assisted diffusion)

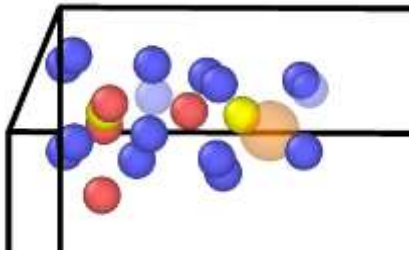

6. Neighbouring Oxygen vacancy

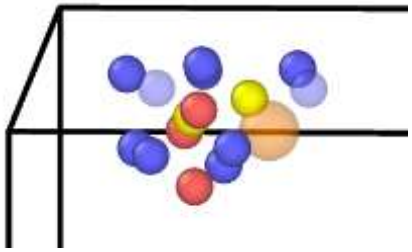

7. OIS jump via V_O

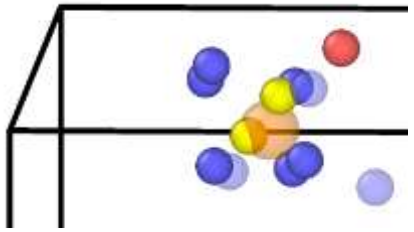

8. 2 He in V_{Pu}

Conclusions

Transformative Science and Engineering for Nuclear Decommissioning

E. Murray, Y. Zhou, P. Slater, R. Smith, P. Goddard and H. Steele, *PCCP,* 2022, **24**, 20709.

Computational Simulations of Helium in PuO_2

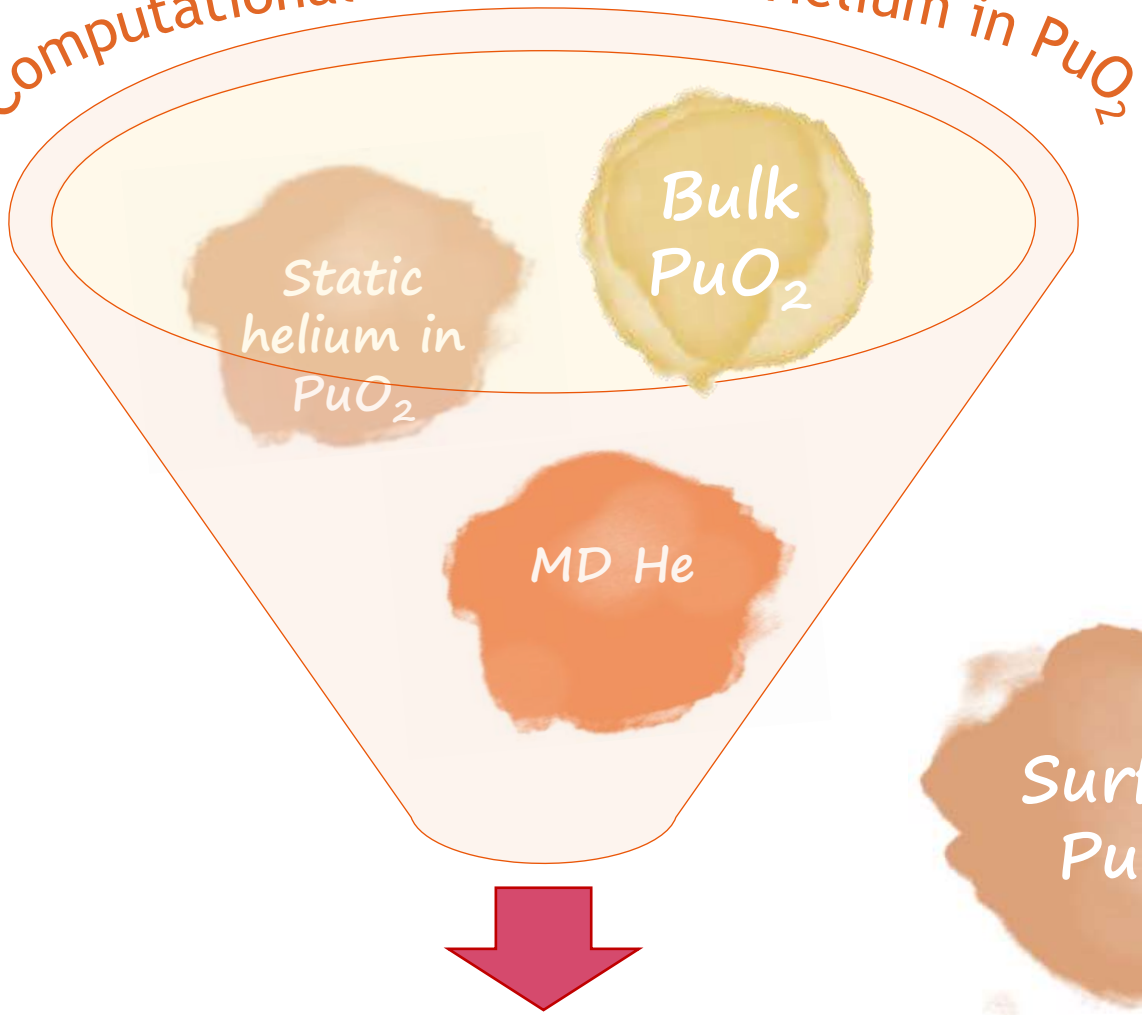

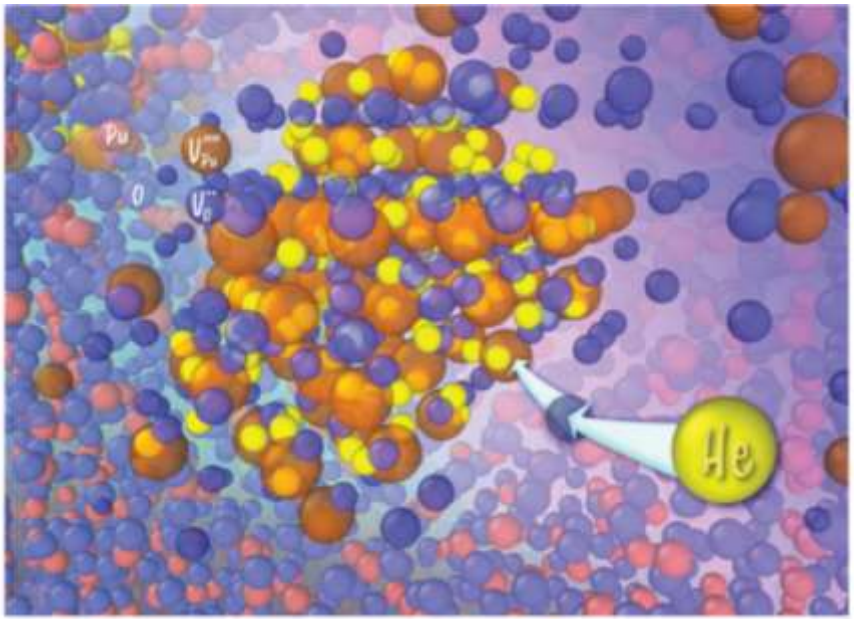

Surface PuO_2

- How He behaves at surface
- Migration of He to surface defects

Translate to low temperature, long timescales?

Acknowledgements

- Peter Slater (University of Birmingham)
- Pooja Goddard, Ying Zhou, Roger Smith (Loughborough University)
- Rob Jackson (University of Keele)
- Helen Steele (SL)
- Robin Orr, Mark Read (NNL)

UNIVERSITY OF BIRMINGHAM

NATIONAL NUCLEAR LABORATORY

Sellafield Ltd

NDA

TRANSCEND

Transformative Science and Engineering for Nuclear Decommissioning

exm350@student.bham.ac.uk

TRANSCEND

Transformative Science and Engineering for Nuclear Decommissioning

Engineering dual-phase zeolite composites for remediation of aqueous nuclear decommissioning waste

James Reed, University of Birmingham

1.11.2022

Energy
For a Low Carbon Future

Introduction

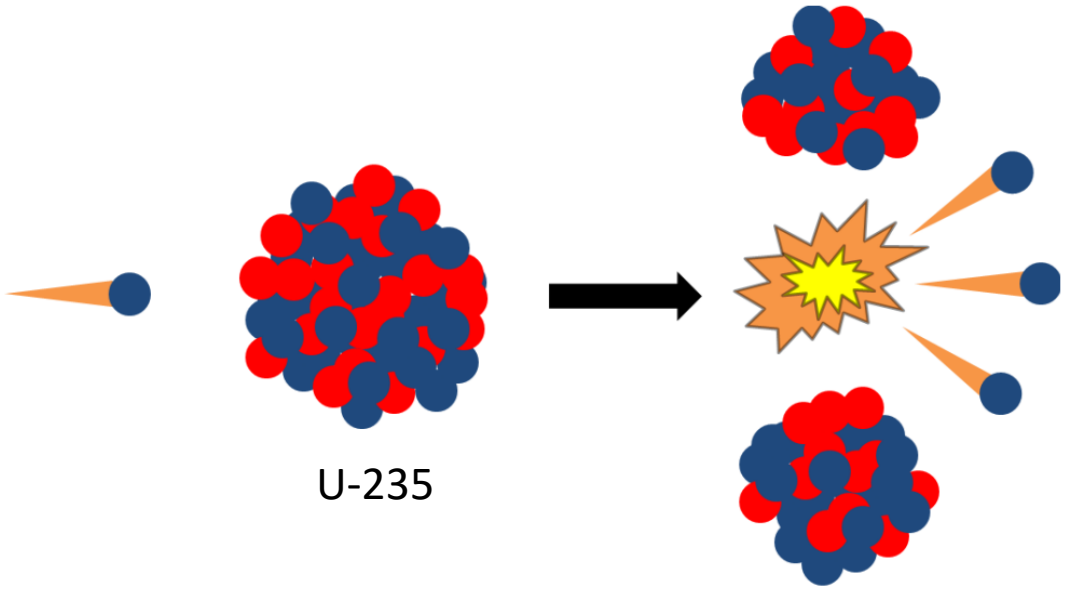

U-235

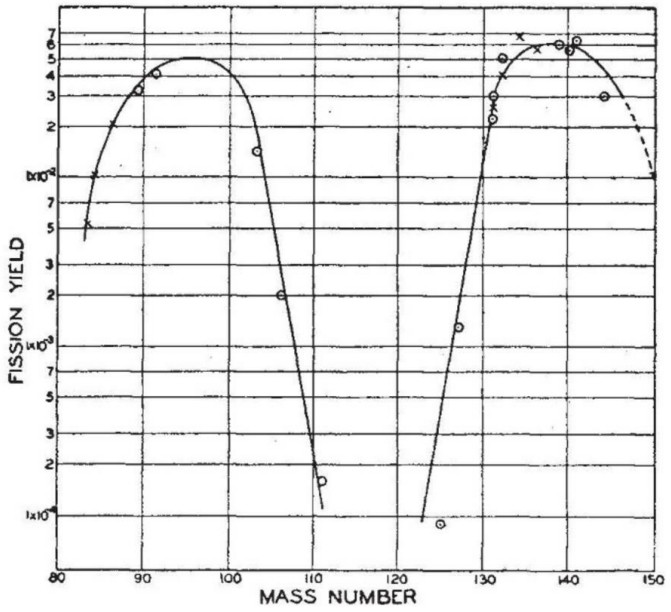

(2)

(3)

- Fission products of U-235 end up in solution.
- Require immobilisation in a solid waste form for long-term storage.

Composition of contaminated wastewater

- Fission products Cs-137 and Sr-90, which account for 99% of medium-lived radioactivity in spent nuclear fuel (highly soluble and ~30 year half-lives).
- Various cations, commonly including (Na, Mg, K, Ca).
- Various pH's.

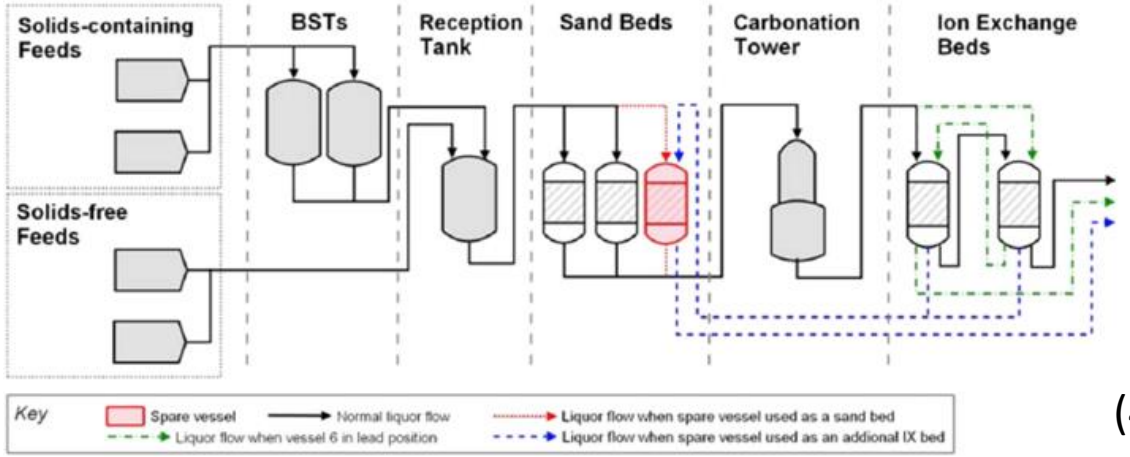

(4)

Current solution at Sellafield

- Encapsulation of Cs-137 and Sr-90 in zeolite clinoptilolite using ion-exchange columns (SIXEP plant).
- Current supply of zeolite forecast to deplete in the 2030s.
- New materials must be sourced to future-proof nuclear decommissioning.

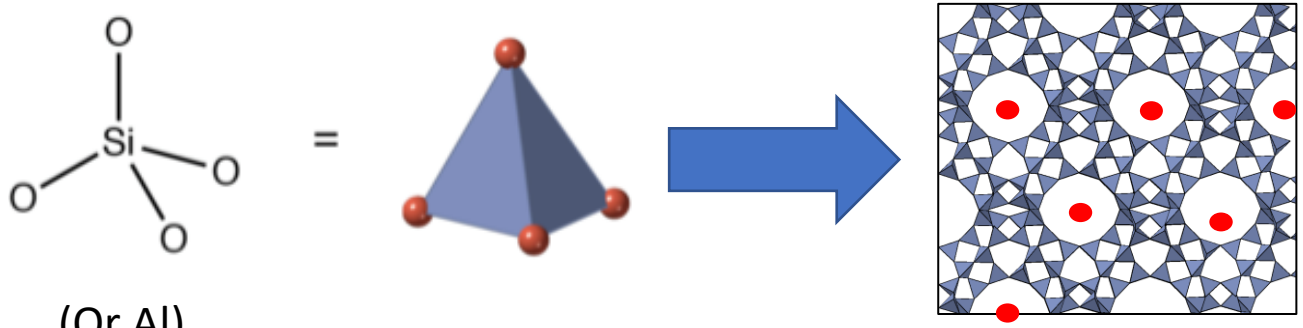

(Or Al)

MOR → GIS controllable transformation

Mordenite (MOR)
- Orthorhombic C m c m
- 12 and 8 ring channels

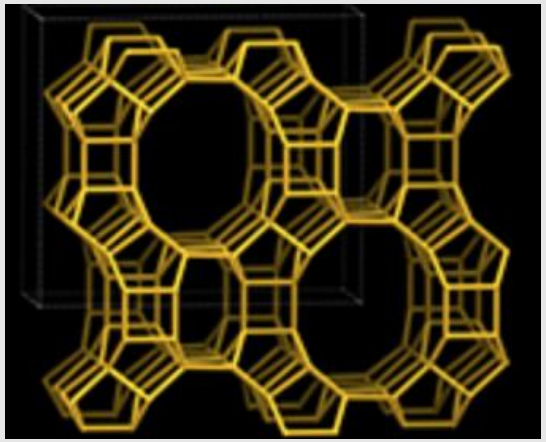

- 1 source: Indonesia
- Si/Al 4.6

0.3-0.8 M NaOH

Zeolite P (GIS)
- Tetragonal I 4_1/a m d
- 8 ring channels

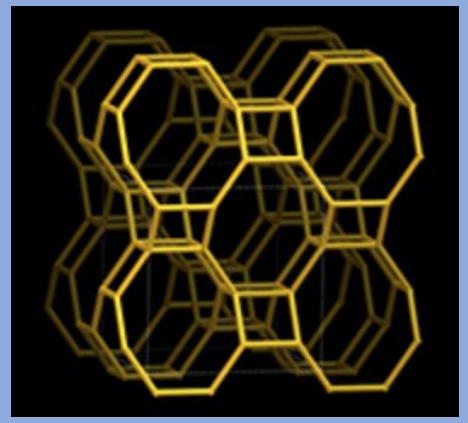

- Si/Al ~2.5

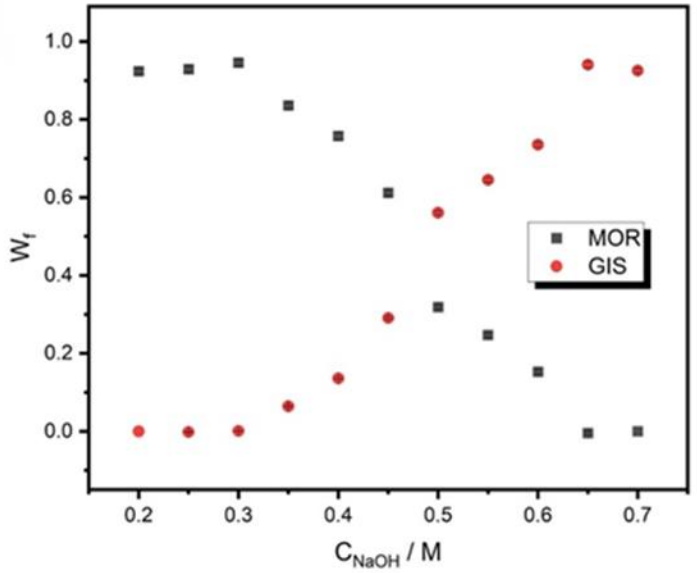

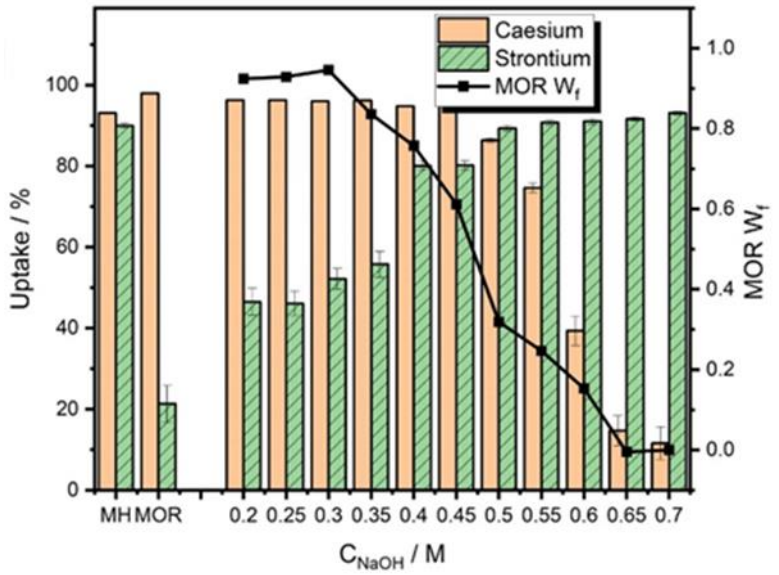

Mordenite → zeolite P transformation by SEM

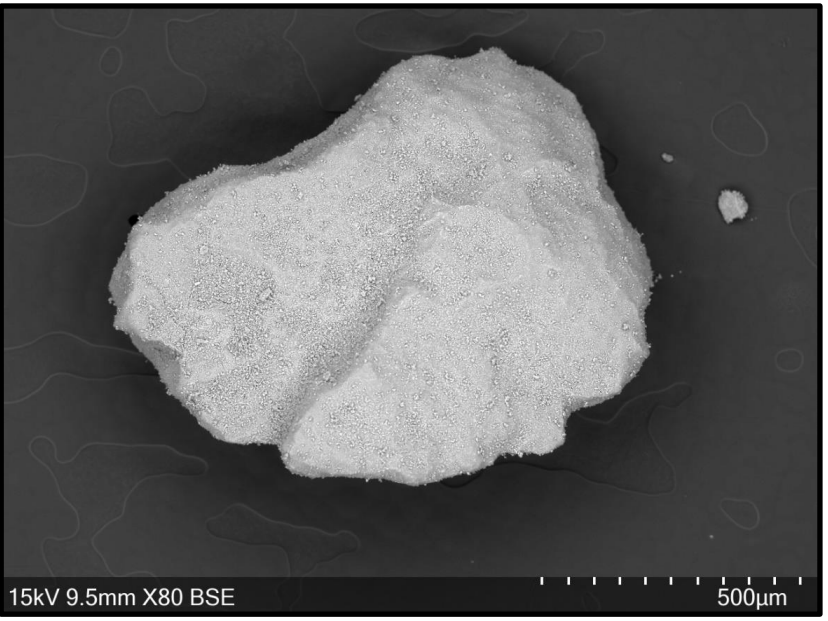

Raw mordenite

- Featureless exterior

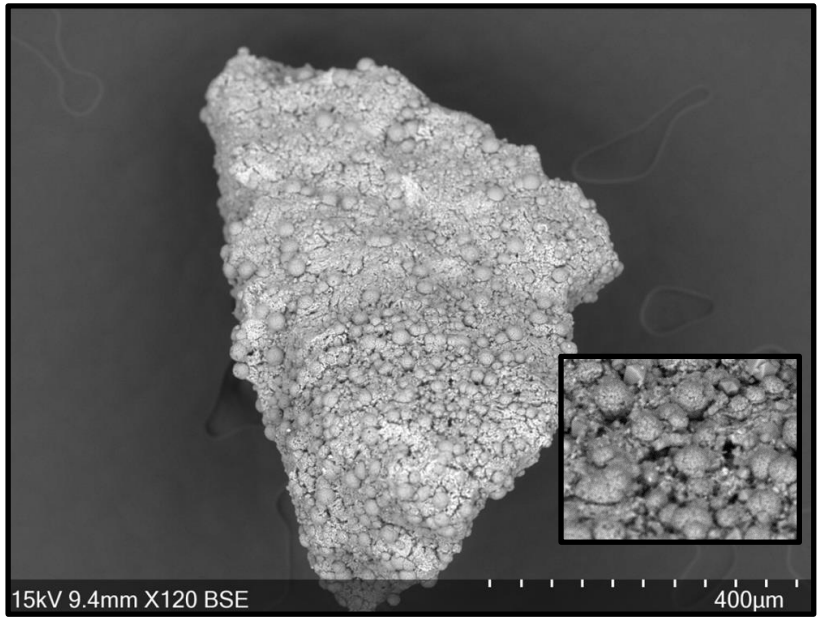

Mordenite / zeolite P composite (55:35)

- Development of new phase on surface of existing particles

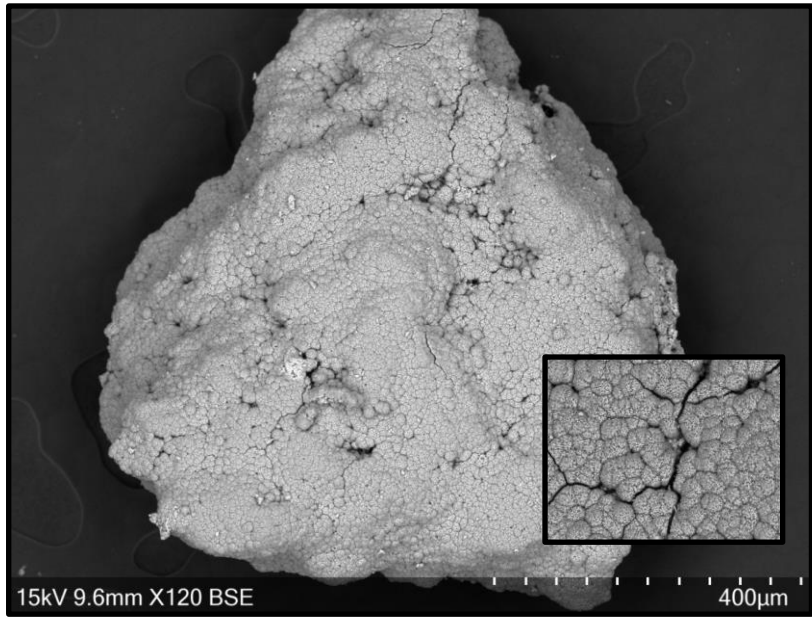

Zeolite P (fully converted mordenite)

- Full coverage
- Particle size maintained

Use of Dual Imaging and Diffraction (DIAD) beamline (5)

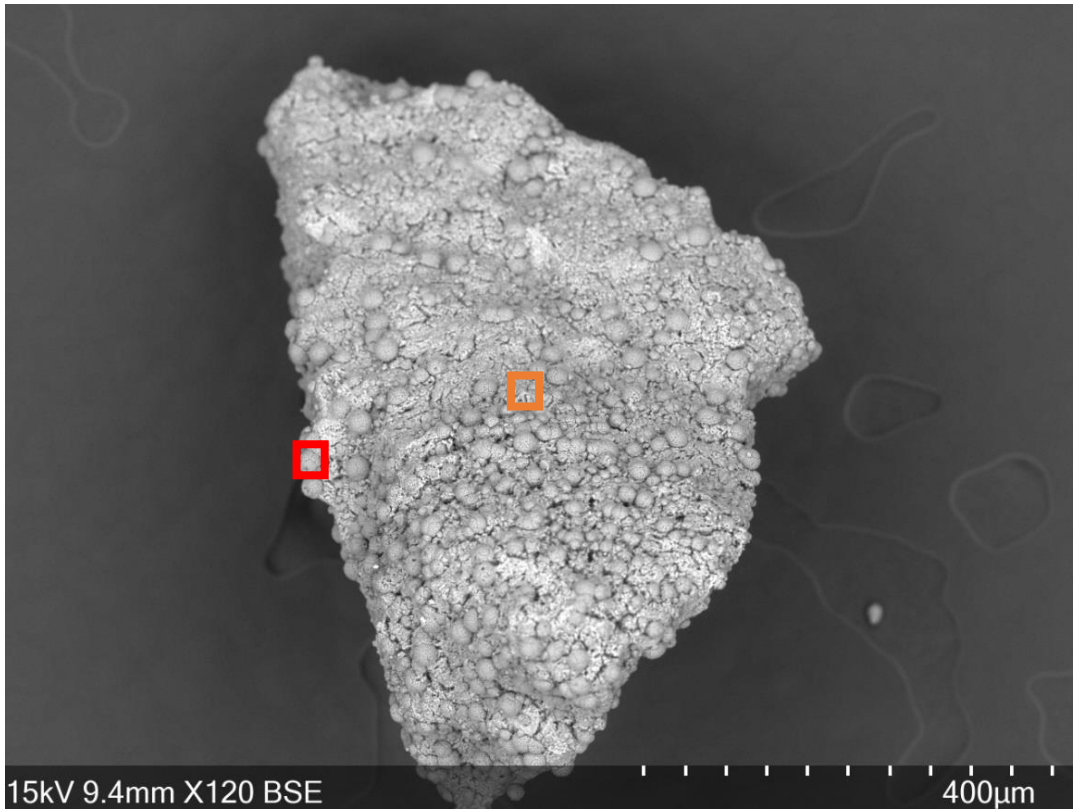

- Could we isolate new phase on exterior and confirm GIS structure?
- What would tomography tell us about the interior of the particle?
- Would a shot down the middle show both phases by XRD?
- Look at diffraction tomography

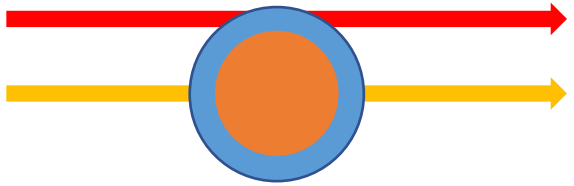

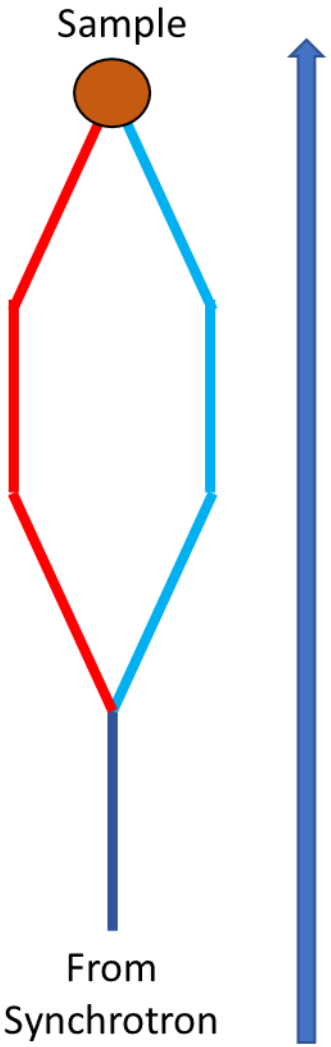

Point and shoot X-ray diffraction of partially converted mordenite (MOR/GIS, 55:35)

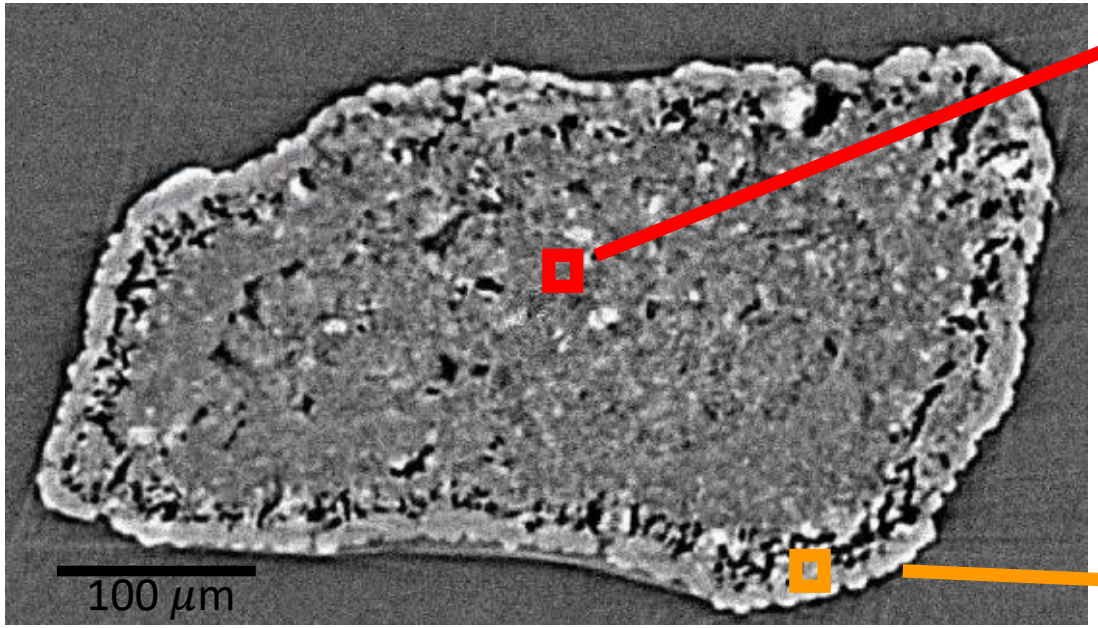

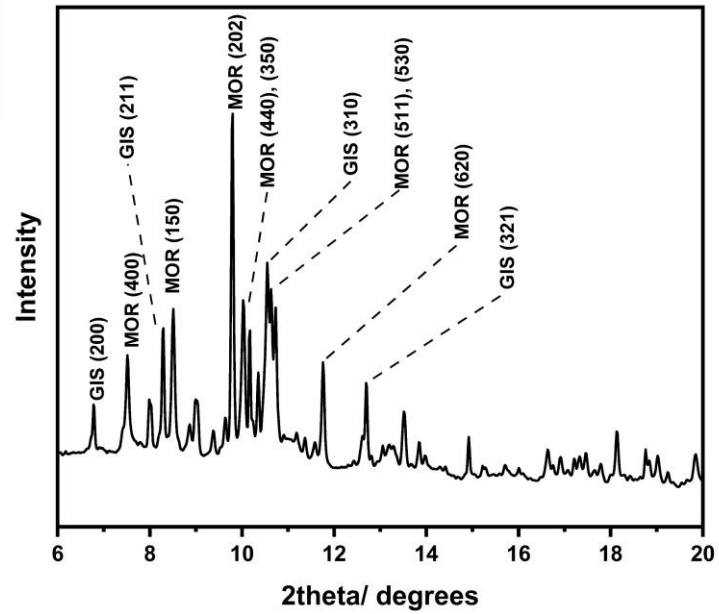

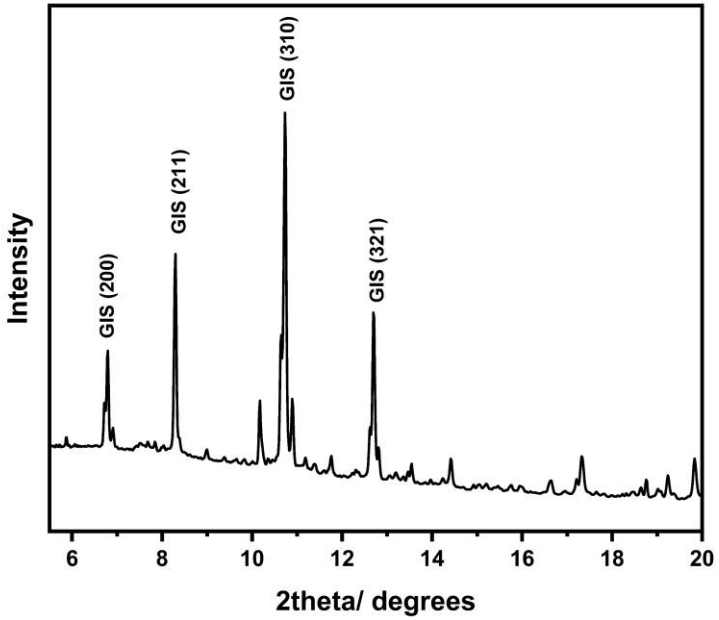

Diffraction tomography of composite particle (55:35)

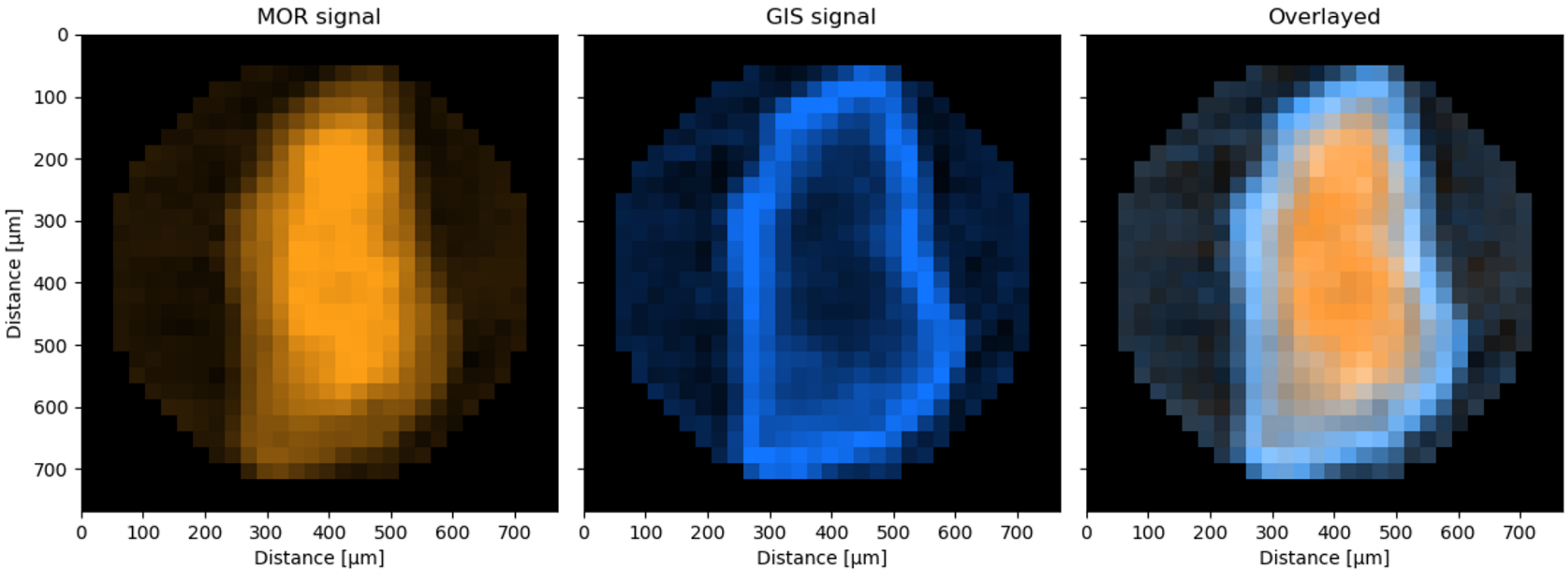

Proposed mechanism of transformation

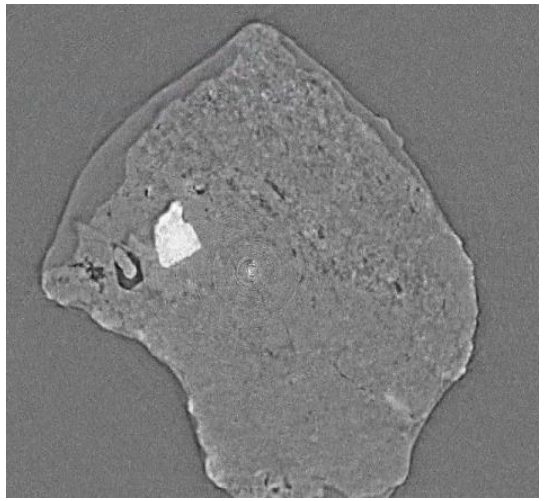

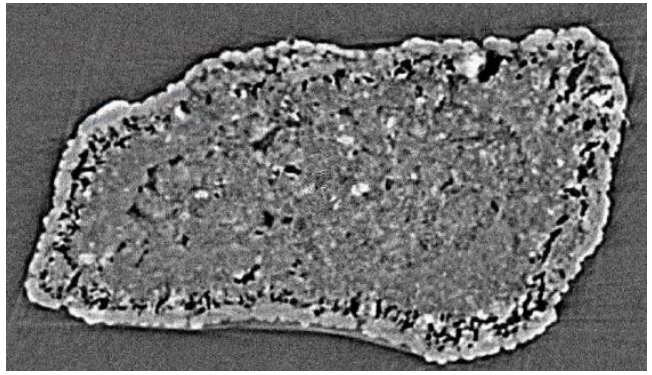

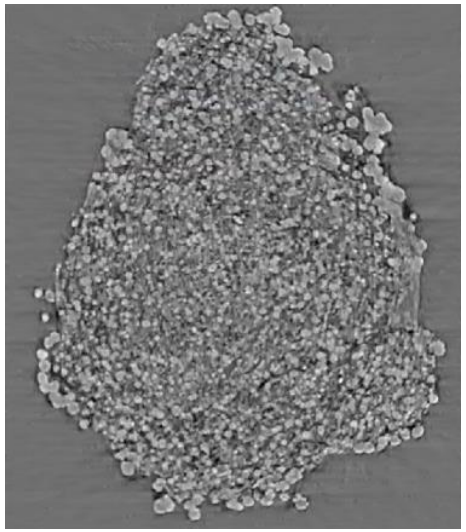

MOR → **GIS**

- **Surface dissolution followed by recrystallization of new phase on existing particles.**
- **Results in outer 'shell' encapsulating partially dissolved interior.**
- **Interior dissolved and recrystalised. Potentially contained by 'shell'.**
- **Whole particle now comprised of GIS spheres. Larger, older spheres on exterior.**

Proposed mechanism of transformation

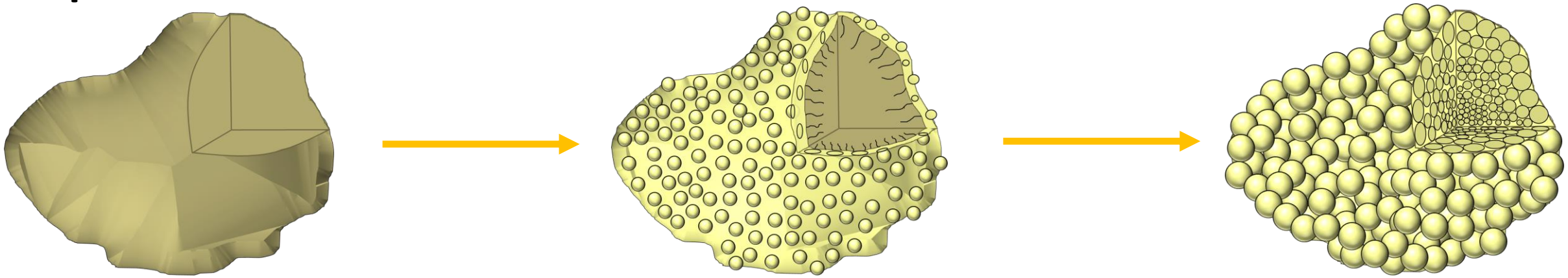

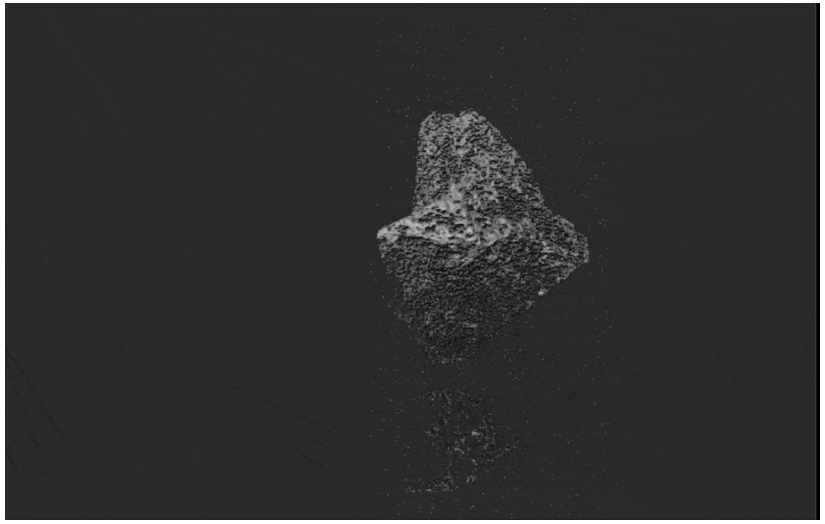

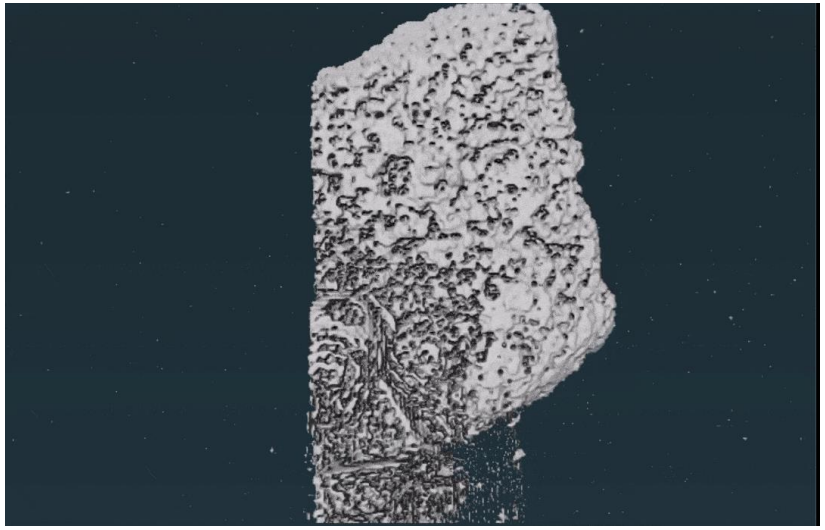

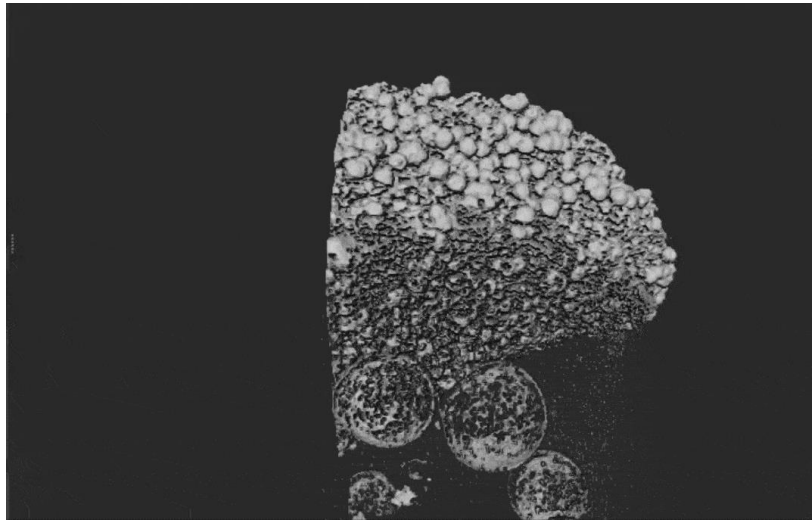

Rapid ion-exchange method (developed by NNL)

NATIONAL NUCLEAR LABORATORY

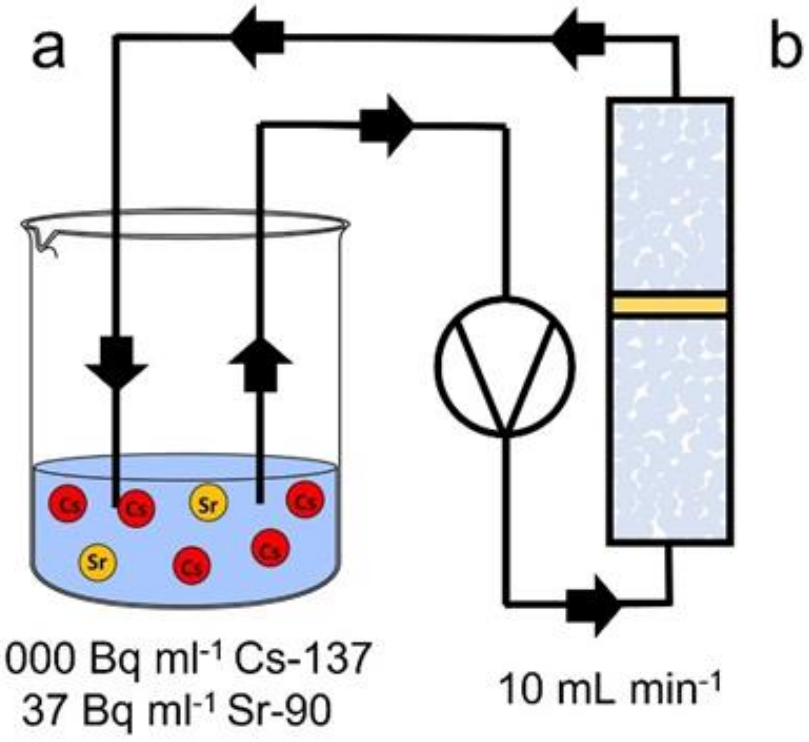

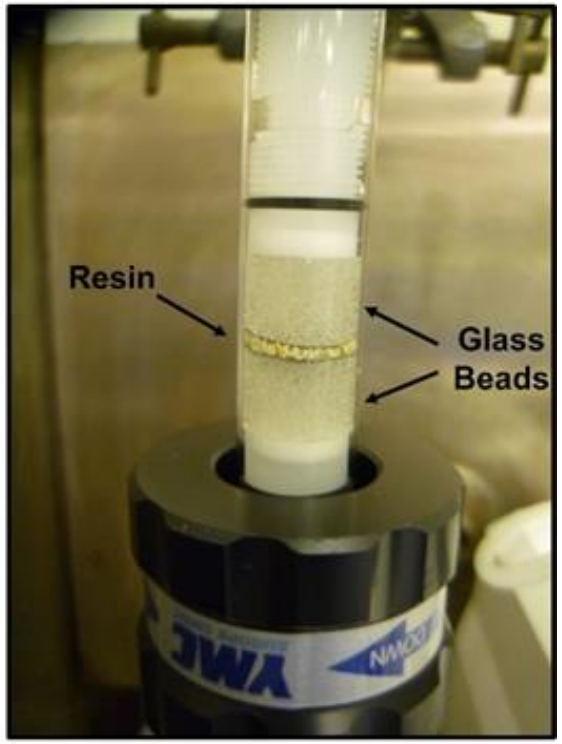

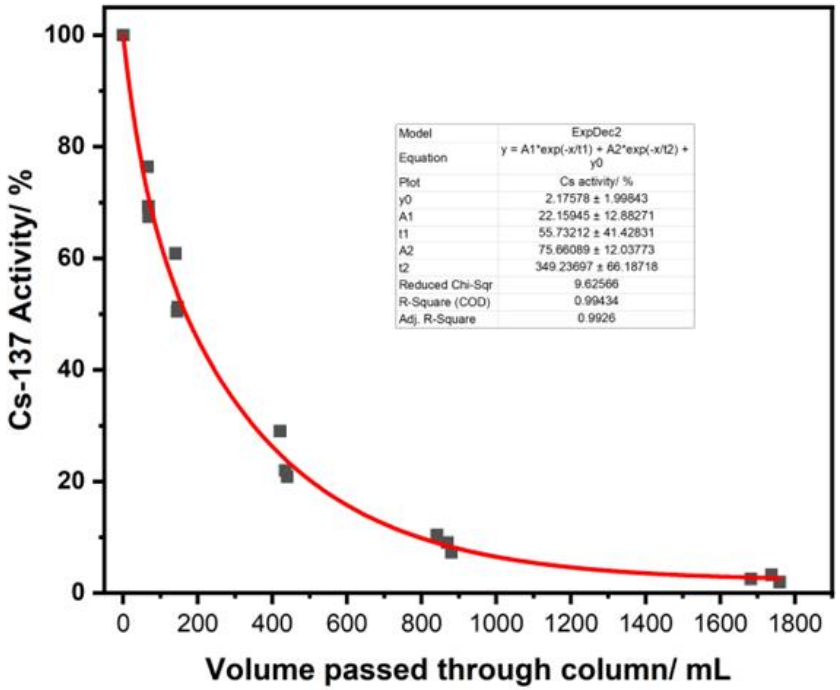

Sr-90 uptake curves

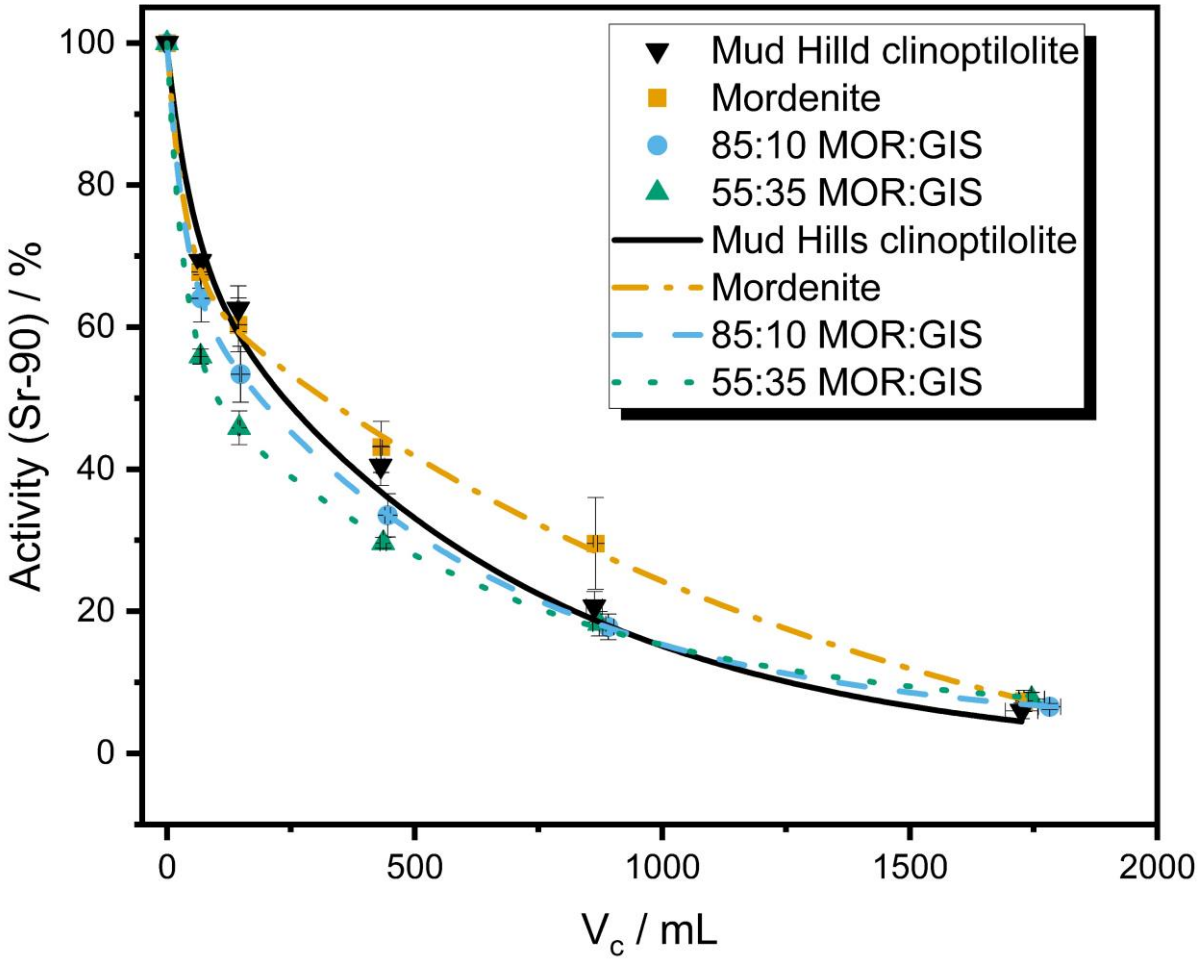

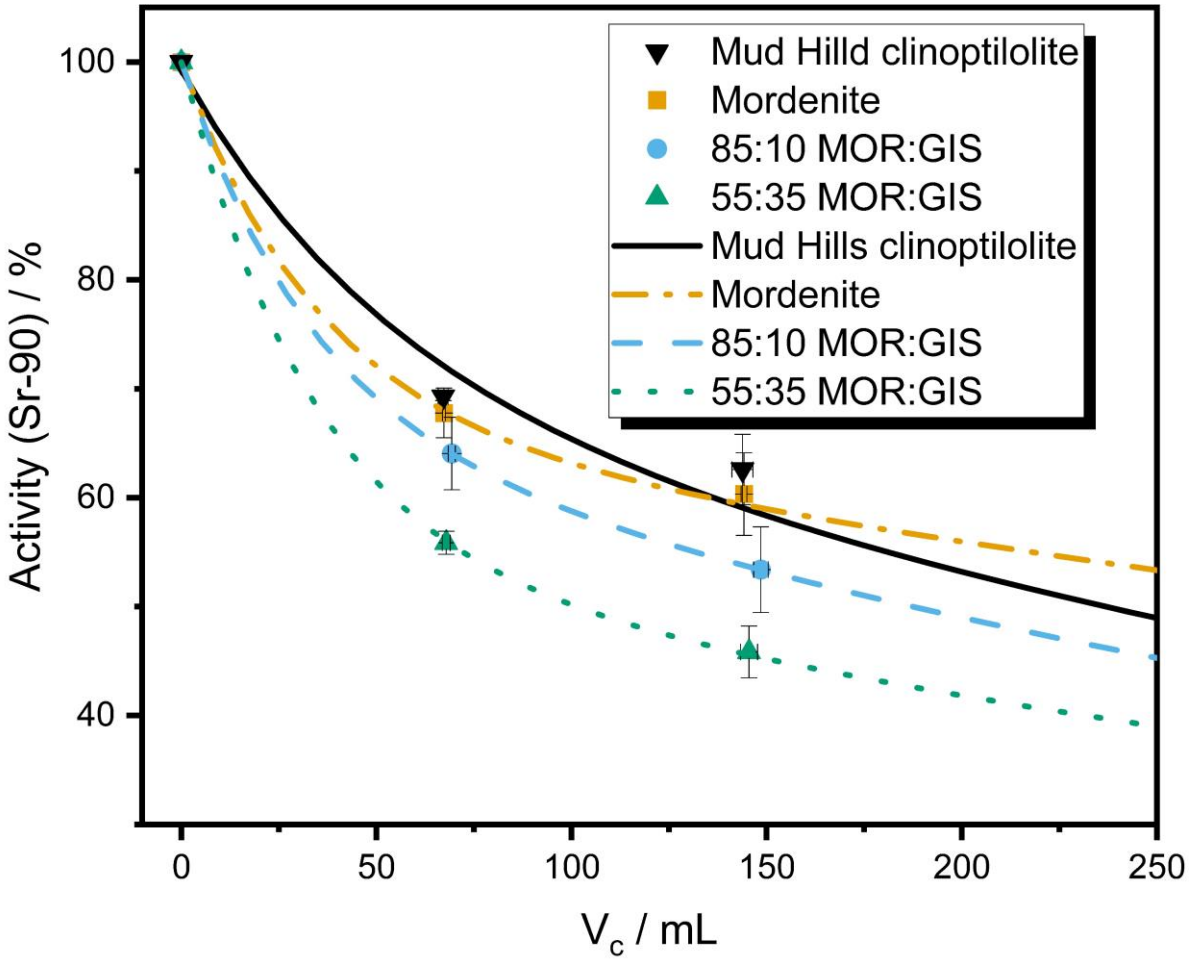

Acknowledgements

- Phoebe, Joe.
- Tom Carey, Neelam and the rest of the M&A team at NNL.
- Hamish.
- Transcend.
- NDA.
- Simon Kellet, Sellafield.
- Andrew James, DLS.
- Antony, Dan and the rest of floor 5/6.
- Norman Day, Chris Stark (Biosciences).

UNIVERSITY OF BIRMINGHAM

NATIONAL NUCLEAR LABORATORY

Sellafield Ltd

TRANSCEND

NDA

diamond

References

1. https://grid.iamkate.com/
2. Grummitt, W. E. and G. Wilkinson (1946). "FISSION PRODUCTS OF U-235." Nature **158**(4005): 163-163.
3. https://www.gov.uk/government/case-studies/ponds-and-silos-at-sellafield
4. Dyer, A., et al. (2018). "The use of columns of the zeolite clinoptilolite in the remediation of aqueous nuclear waste streams." Journal of Radioanalytical and Nuclear Chemistry **318**(3): 2473-2491.
5. Reinhard, C., et al. (2021). "Beamline K11 DIAD: a new instrument for dual imaging and diffraction at Diamond Light Source." Journal of Synchrotron Radiation **28**: 1985-1995.

TRANSCEND

Transformative Science and Engineering for Nuclear Decommissioning

jlr552@student.bham.ac.uk

Point and shoot X-ray diffraction of mordenite (MOR)

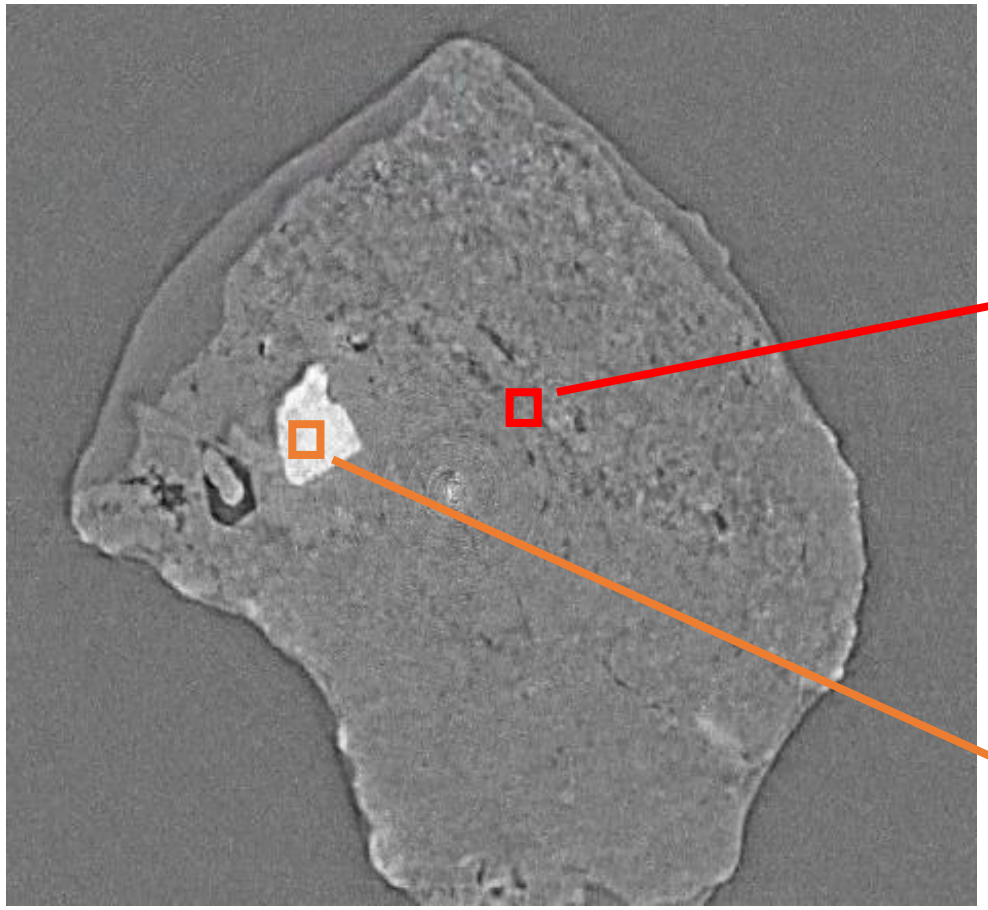

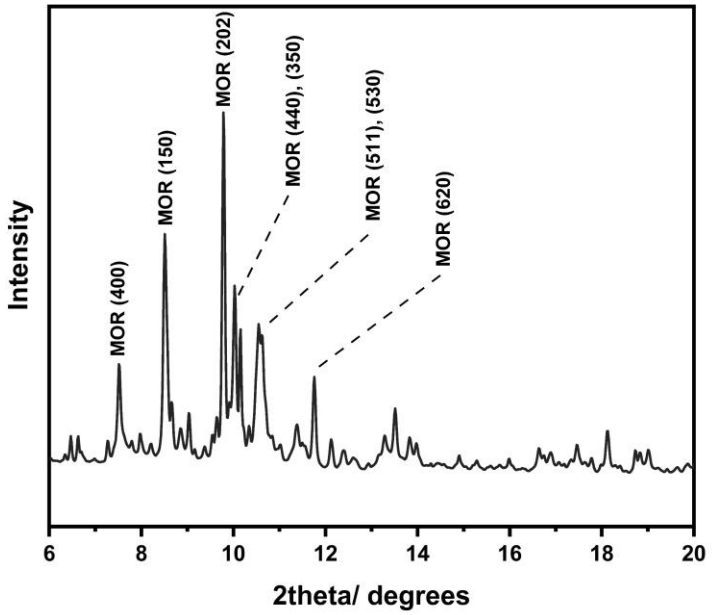

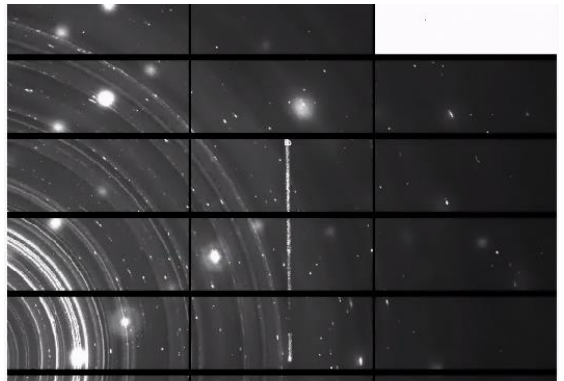

Point and shoot X-ray diffraction of fully converted mordenite

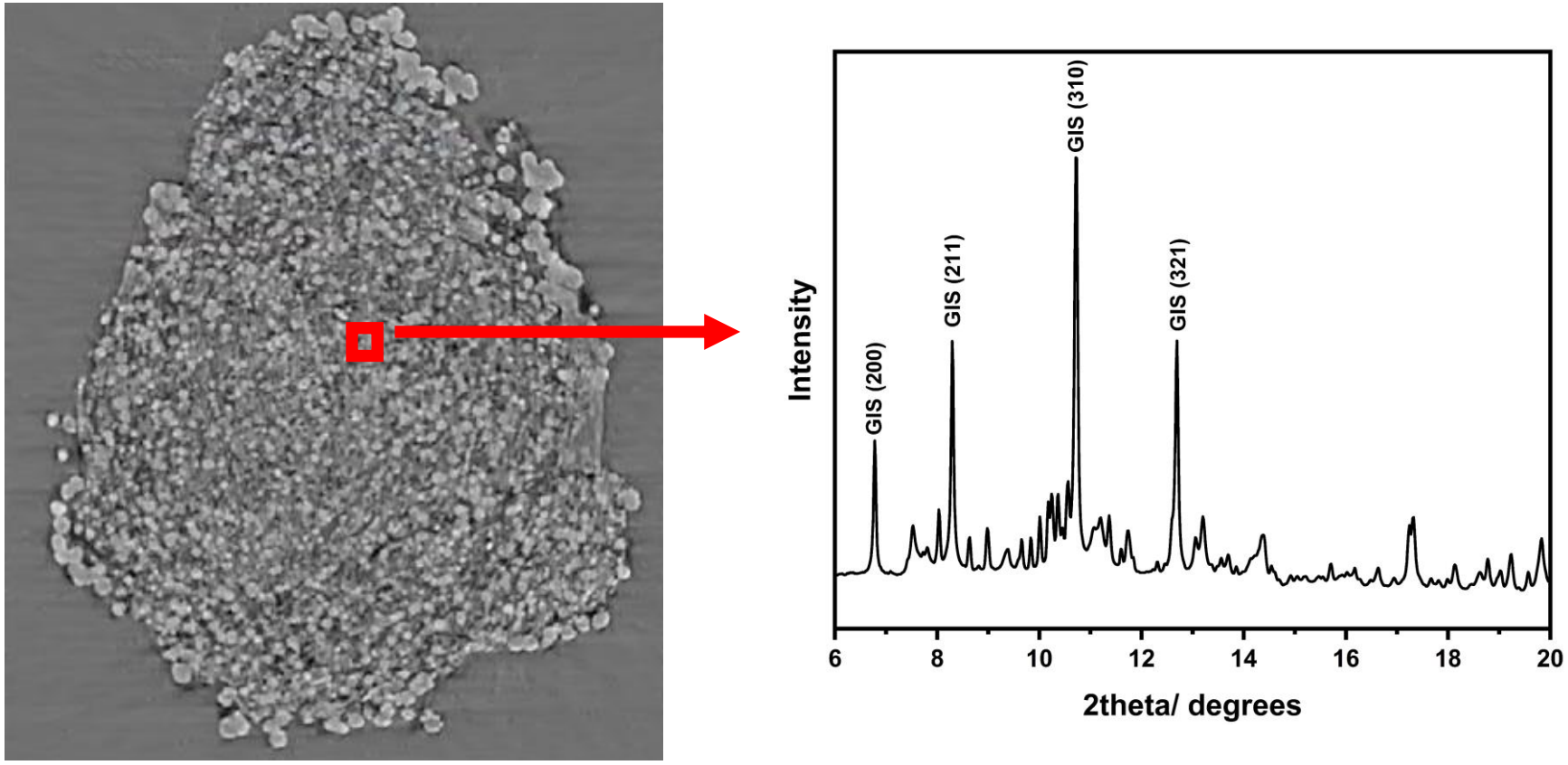

Cs-137 uptake curves

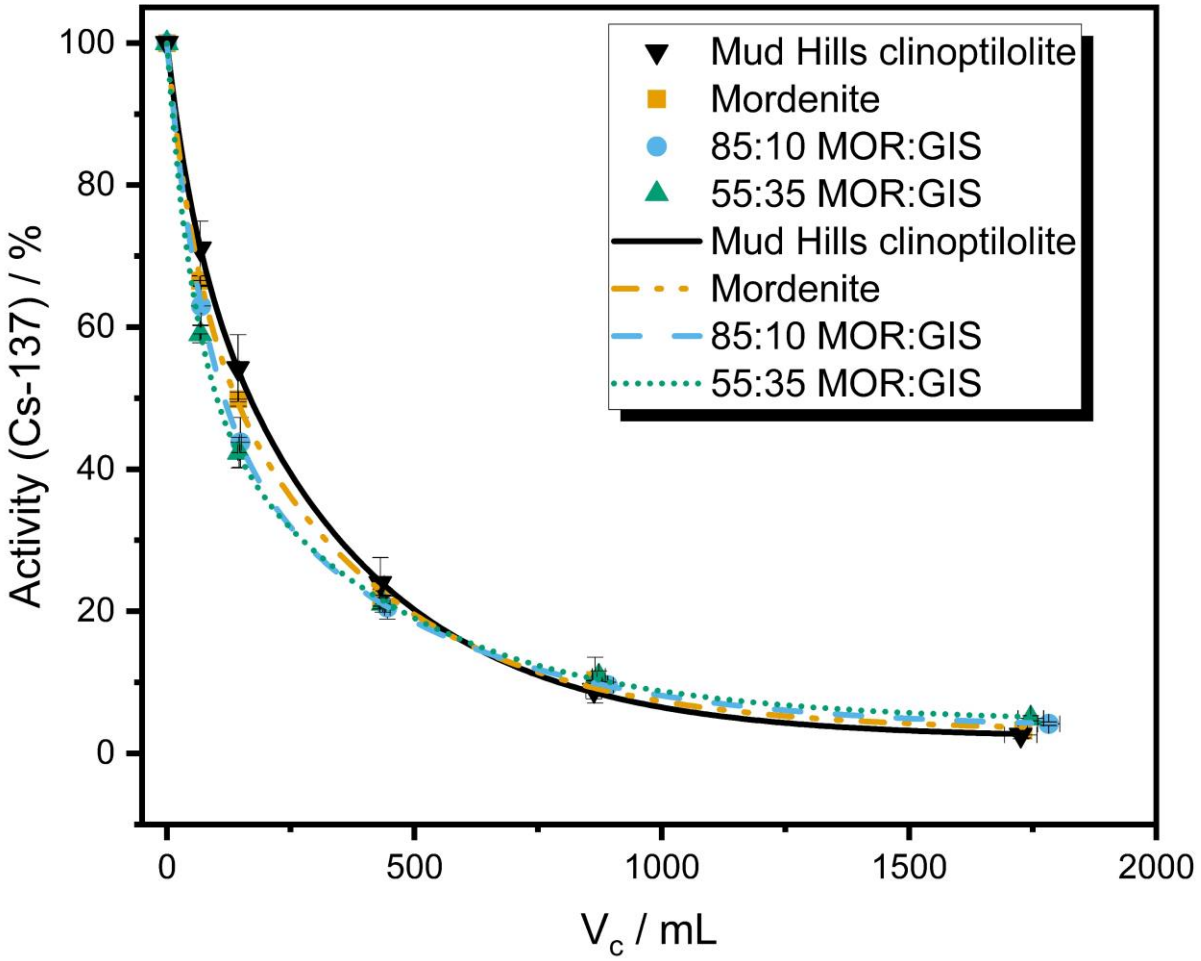

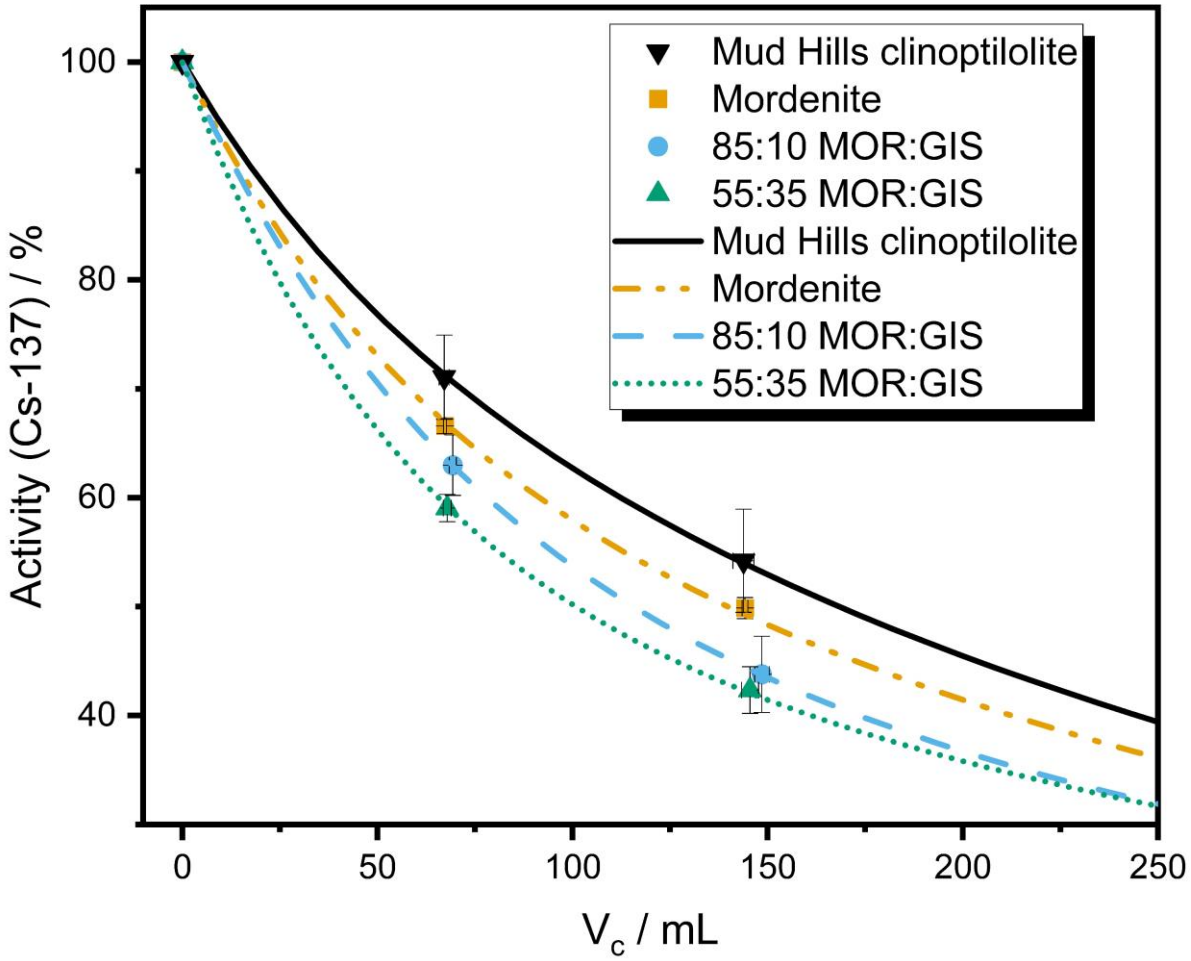

TRANSCEND

Transformative Science and Engineering for Nuclear Decommissioning

Patent: Elísio, S., Joyce, J. M., 29 September 2022, *Method and Apparatus for Determining Attributes of a Source of Radiation*, P347121GB/CAB.

Blind-tube Monitoring Instrument: Point-spread Analysis of Photon-depth Spectra

Soraia Elísio[1] (s.elisio@lancaster.ac.uk); Malcolm J. Joyce[1] (m.joyce@lancaster.ac.uk); James Graham[2] (james.graham@uknnl.com); Tom Calverley[3] (tom.calverley@sellafieldsites.com)

[1]Department of Engineering, Lancaster University, Lancaster (UK); [2]National Nuclear Laboratory Ltd., Central Laboratory, Sellafield (UK); [3]Radiometric Systems Group, Sellafield Ltd., Site Management Centre, Sellafield (UK)

Acknowledgments – This research is supported by NNL and Sellafield Ltd. (UK) via the EPSRC programme TRANSCEND (TRANSformative Science & Engineering for Nuclear Decommissioning), code EP/S01019X/1. M. J. J. acknowledges the support of the Royal Society via a Wolfson Research Merit Award.

Content

- Motivation
- Research focus & challenges
- The concept & hypothesis
- Experimental work:
  - ^{137}Cs & ^{90}Sr detector response
  - ^{137}Cs gamma-ray depth profile
- Future work

Motivation

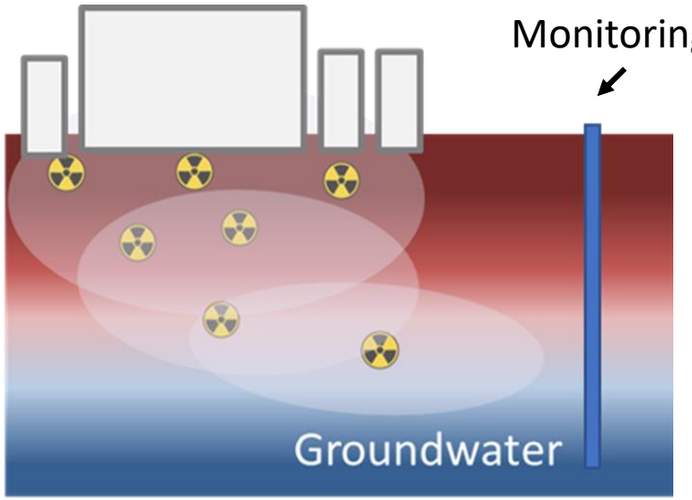

Contamination of groundwater & other water receptors → Radiological risk to public health & environment

Figure 1 – Simplified schematic representing the migration of contaminated water into the ground from legacy nuclear facilities.

Figure 2 – Methods to assess radioactive contaminants underground using monitoring wells.

A. Groundwater sampling

(Taken from Groundwater monitoring at Sellafield: Annual data review, 2016

B. Radiometric logging

(Taken from www.geozentrum-hannover.de/)

Research focus & challenges

- Radiological surveillance at Sellafield site:

Focus: Liquor from the Magnox Swarf Storage silos (MSSS) have leaked into the ground contaminated the land below the silo.

Additional challenges:

- Operational infrastructure and deployment constraints.
- Device has to be deployed in the existing in-ground assets:
  - Narrow carbon steel blind-tubes (ID 75 mm)
- The radioactivity fingerprint in the soil is believed to be dominated by caesium-137 and strontium-90.
- Doses involved can be significant

GAME CHANGERS

Hybrid Instruments

"Characterisation and monitoring using in-ground assets"

www.gamechangers.technology/challenge/Characterisation_and_monitoring_using_in-ground_assets

The concept & hypothesis

Figure 3 – Simplified schematic of the deployment system.

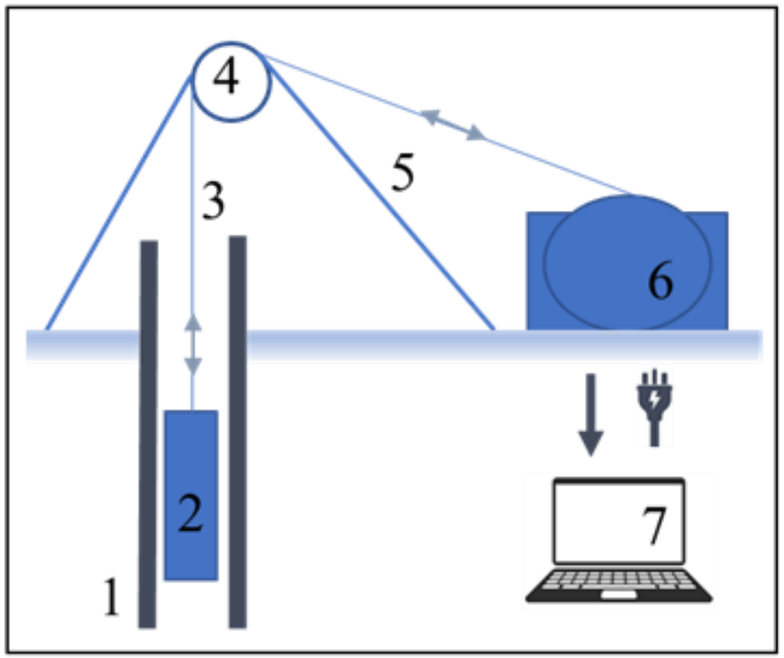

Figure 4 – Demonstration of a radiometric logging in the blind-tube test pit at Lancaster University.

ABACUS GAME CHANGERS Hybrid Instruments

The concept & hypothesis

Figure 5 – *Left:* Developed prototype #1 used for preliminary tests; *Right: D*eveloped prototype #2 ready for site tests.

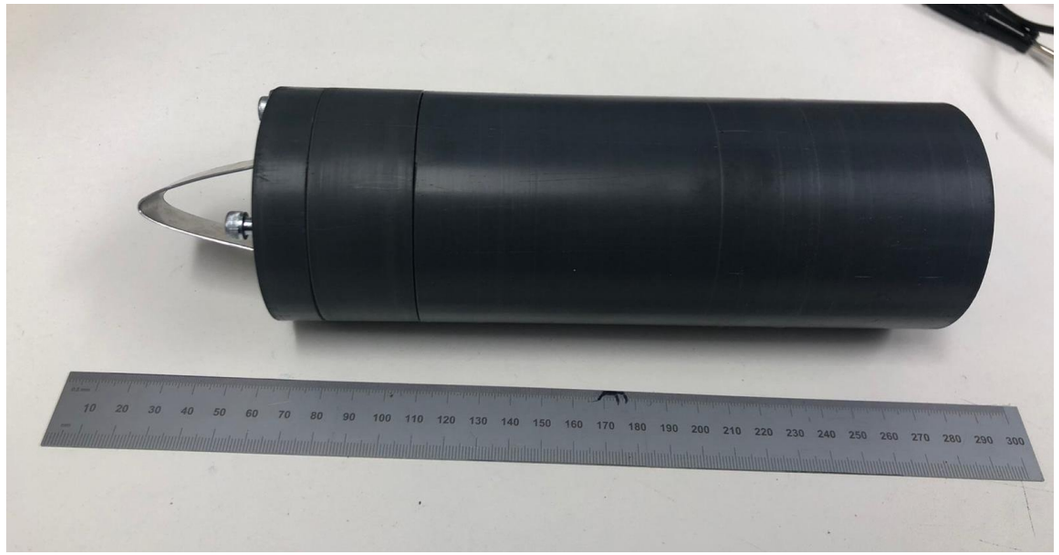

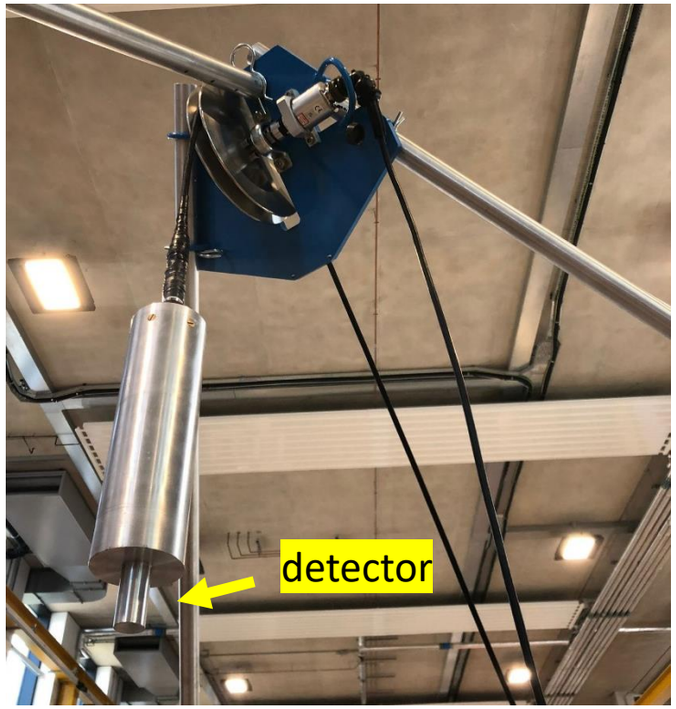

ABACUS project

The concept & hypothesis

Figure 6 – *Left* Schematic diagram of the detector and *right* respective components of the logging probe.

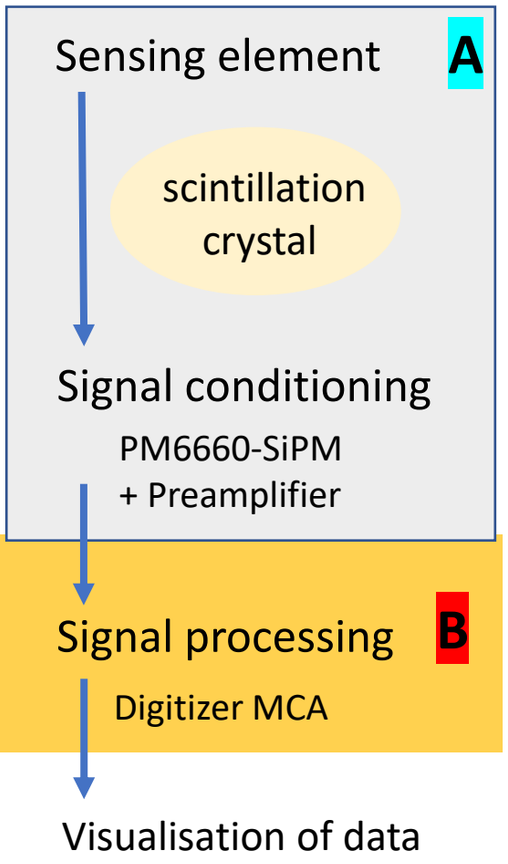

A. Ø10 mm x 9 mm Cerium Bromide ($CeBr_3$) detector

- ✓ Good γ-ray detection efficiency
- ✓ Good energy resolution: 4 % @ 662 keV
- ✓ High count-rate capability: $\tau = 17$ ns
- ✓ High radiation hardness: < 100 kGy

Commercialized by Scionix (Netherlands)

USB output Module Size 7 x 4.5 x 2.6 cm

B. TOPAZ-SiPM digital Multi-Channel Analyser

- ✓ Compact full-featured MCA
- ✓ Compatible with dimensions of typical blind-tubes
- ✓ Designed specially for SiPM detectors
- ✓ 5V low-ripple, low-noise supply
- ✓ Powered from the PC via the USB cable

Commercialized by BrightSpec NV

The concept & hypothesis

Assessment of underground sources in blind-tubes: ^{137}Cs & ^{90}Sr

^{137}Cs → ^{137m}Ba → γ (0.662 MeV) → ^{137}Ba

^{137}Cs → **Direct Detection** ✓

^{90}Sr → β (0.546 MeV) → ^{90}Y → β (2.28 MeV) → ^{90}Zr

^{90}Sr → **Direct Detection** ✗

Detection of produced bremsstrahlung photons

Figure 7 – Schematic diagram of detection of ionizing radiation present in the ground surrounding a blind-tube.

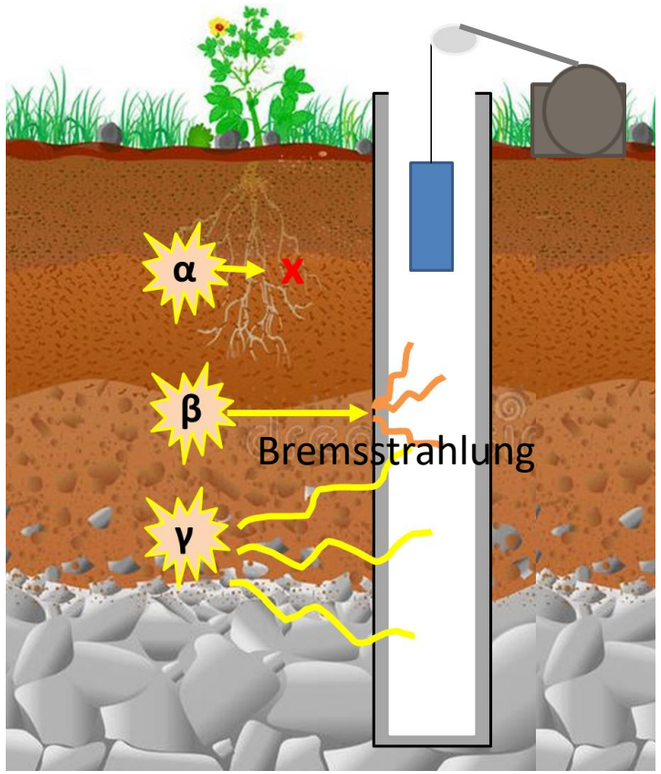

The concept & hypothesis

Assessment of underground sources in blind-tubes: ^{137}Cs & ^{90}Sr

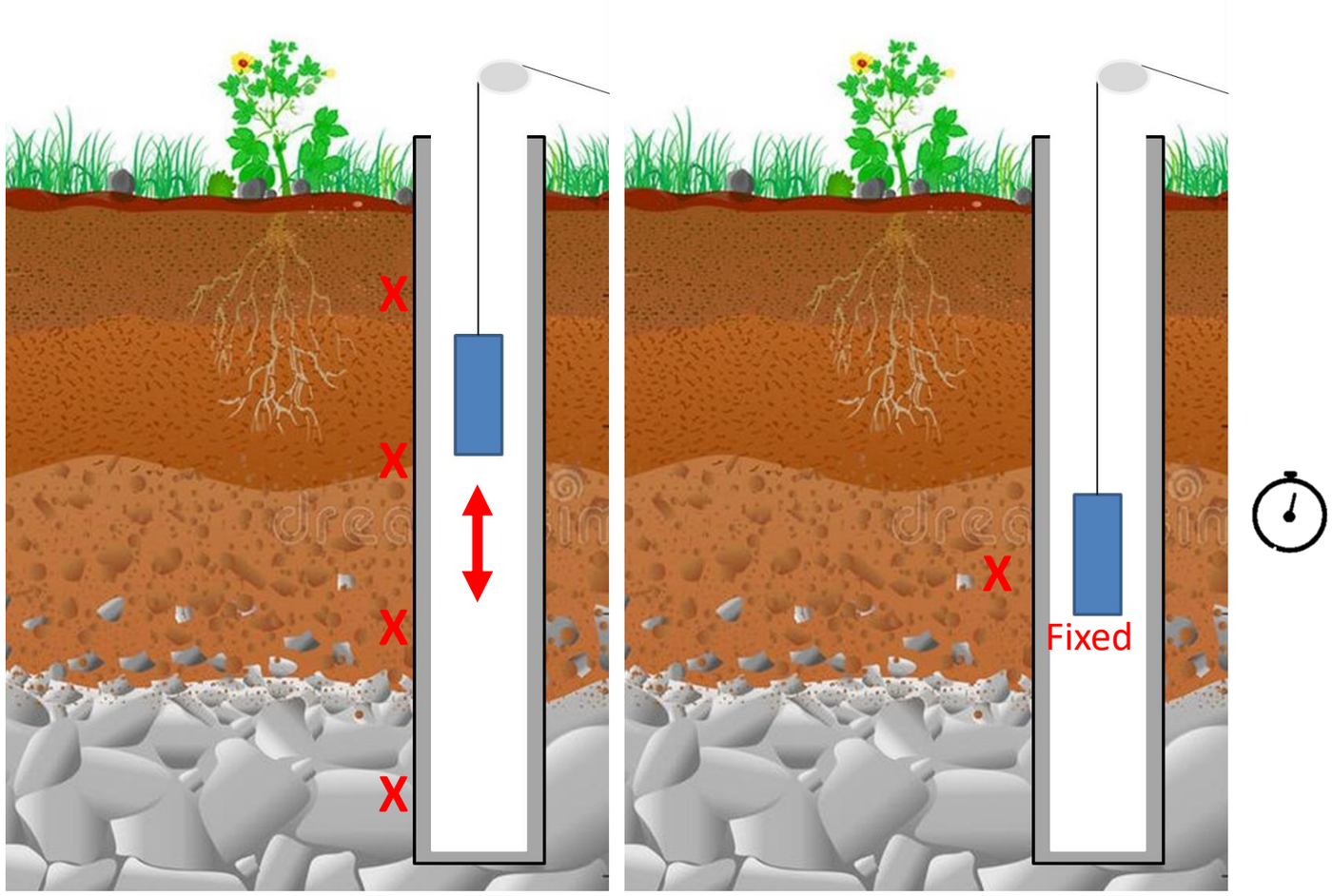

Figure 8 – Schematic diagram of *Left:* probe lowered in the blindtube and data recorded at number of depths; *right:* probe fixed at a specific depth position and data recorded at different times.

The concept & hypothesis

Assessment of underground sources in blind-tubes: ^{137}Cs & ^{90}Sr

Figure 9 – *Left:* Schematic diagram of conceptual spatial distribution of sources underground*; Right:* simplified scenario applied in this study.

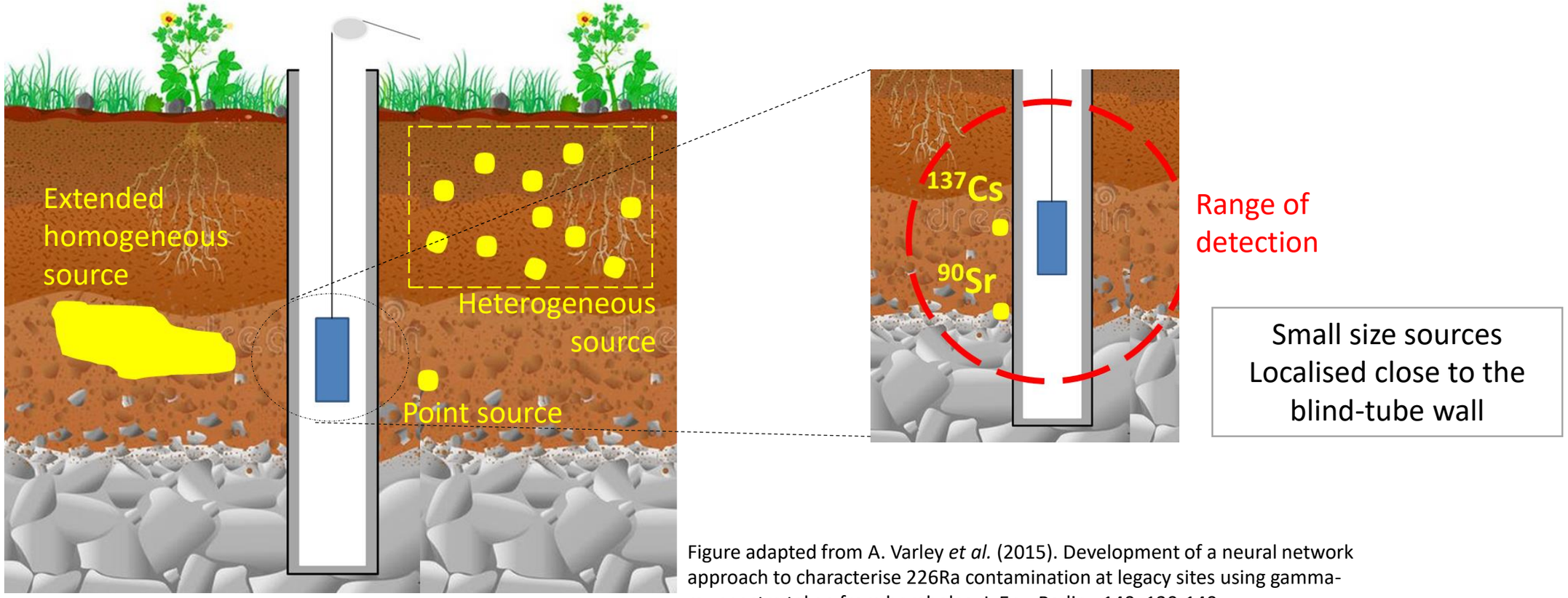

Figure adapted from A. Varley *et al.* (2015). Development of a neural network approach to characterise 226Ra contamination at legacy sites using gamma-ray spectra taken from boreholes. J. Env. Radio., 140, 130-140.

Experimental work

Assessment of underground sources in blind-tubes: ^{137}Cs & ^{90}Sr

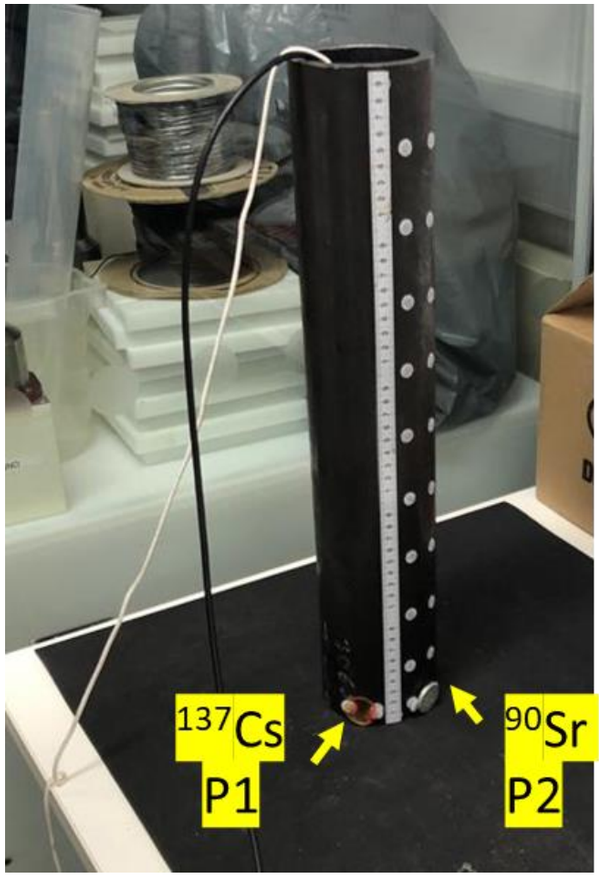

Figure 10 – Experimental setup to test detector response for contamination via ^{137}Cs and/or ^{90}Sr in a source distribution simplified scenario.

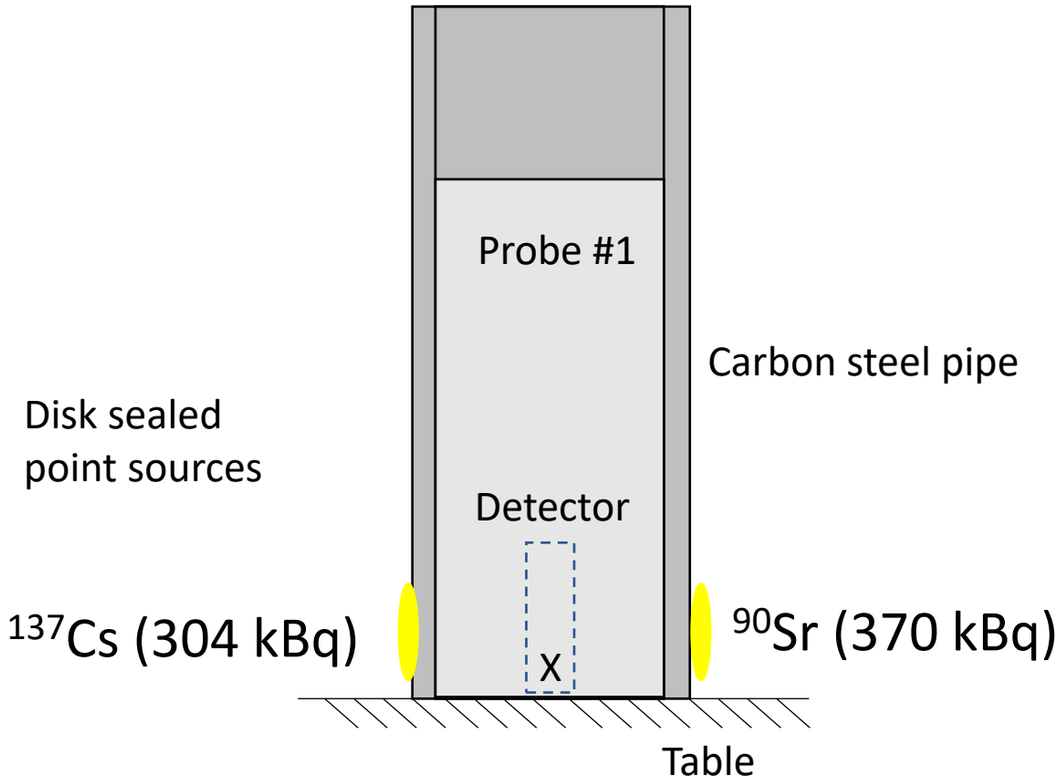

Experimental work

Assessment of underground sources in blind-tubes: ^{137}Cs & ^{90}Sr

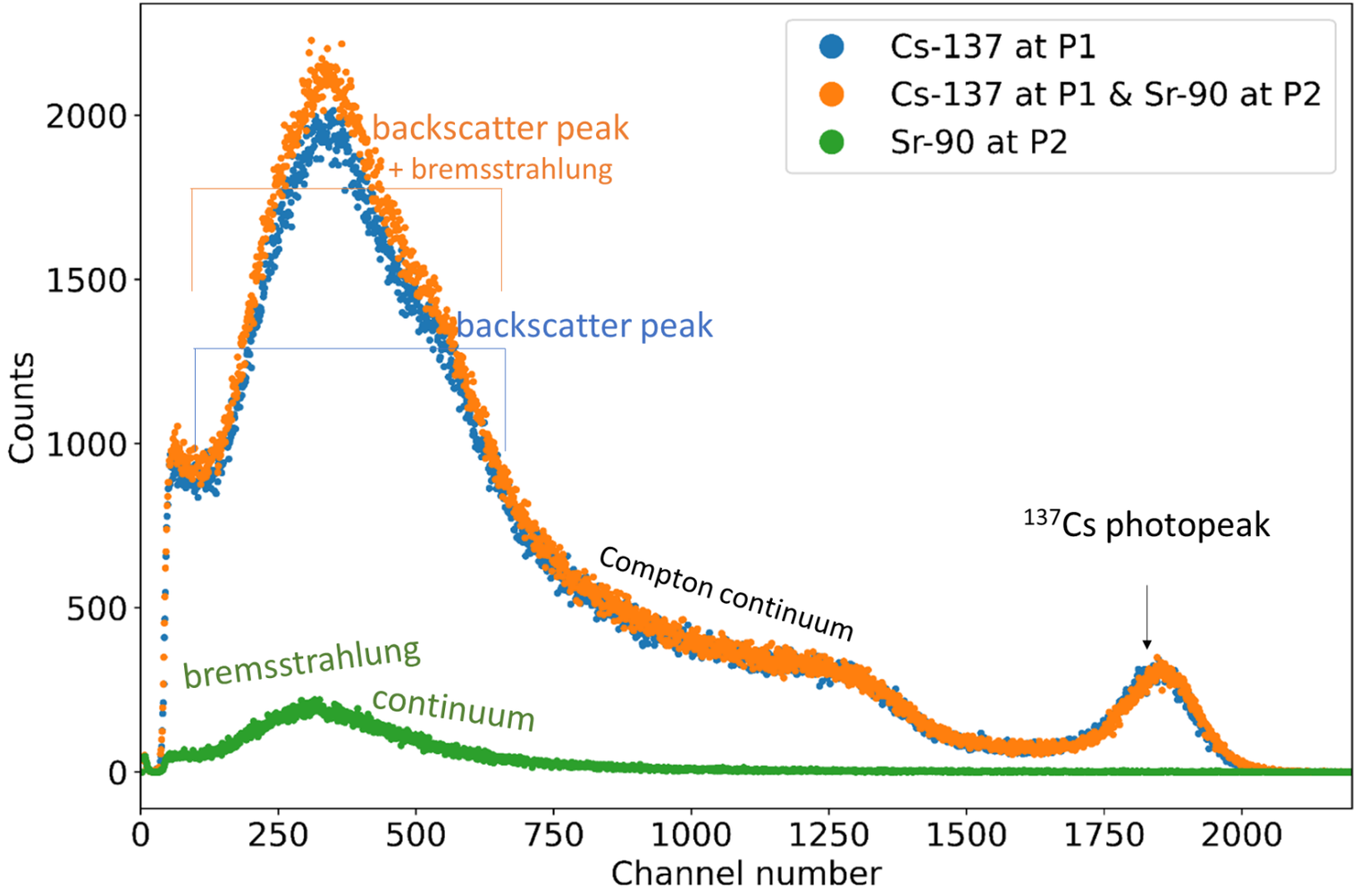

Plot 1 – Gamma-ray spectra obtained for contamination via ^{137}Cs and/or ^{90}Sr in a source distribution simplified scenario (1 h each measurement).

Experimental work

Assessment of underground sources in blind-tubes:

Figure 11 – Experimental setup to obtain a ^{137}Cs gamma-ray depth profile.

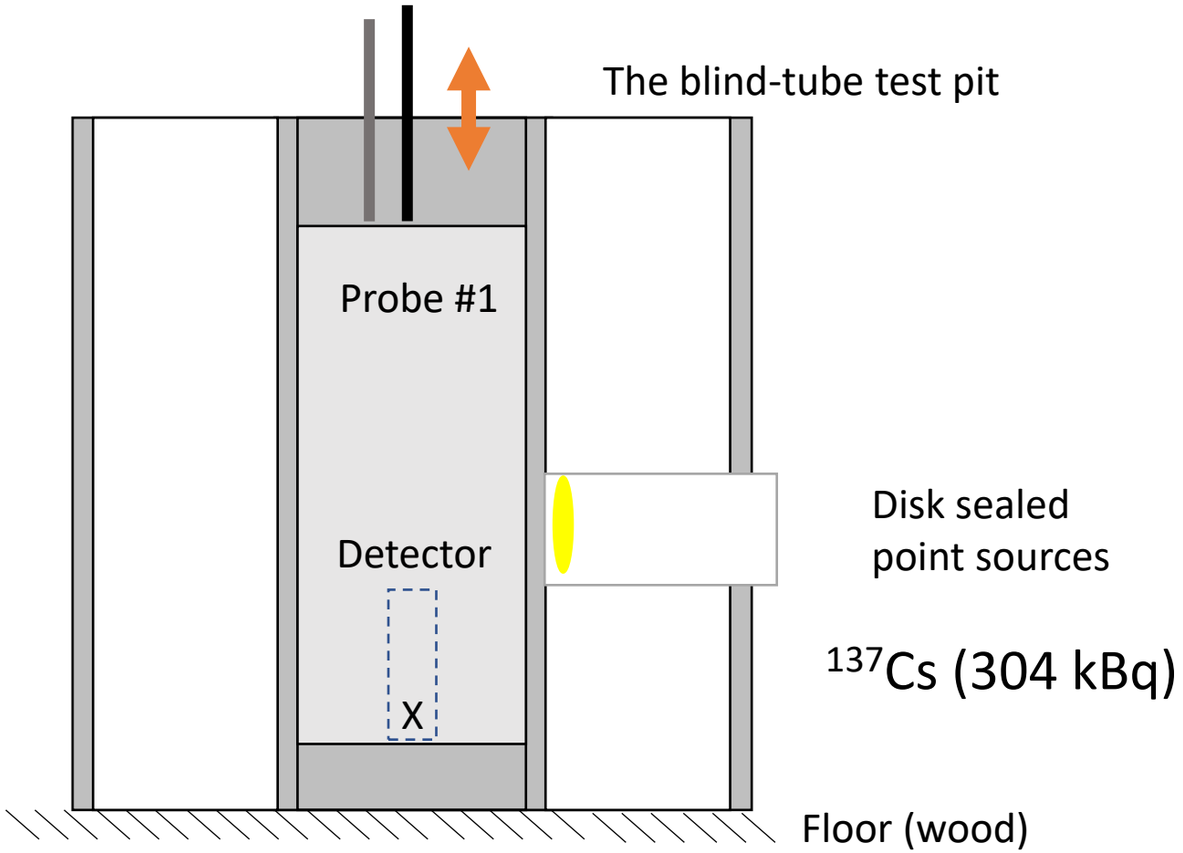

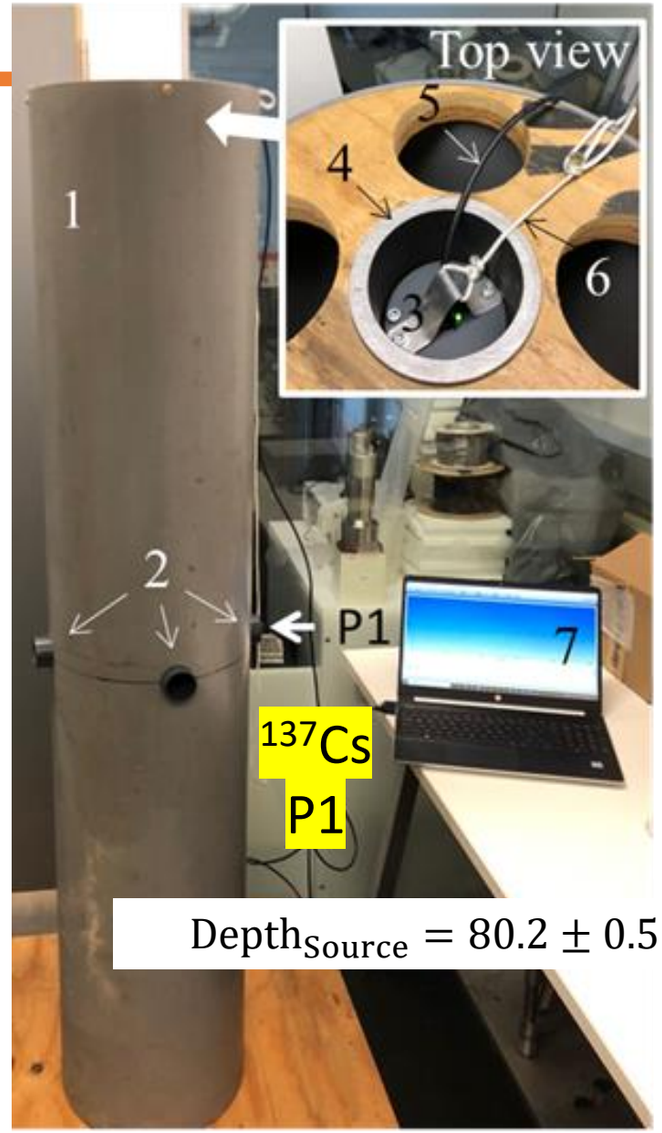

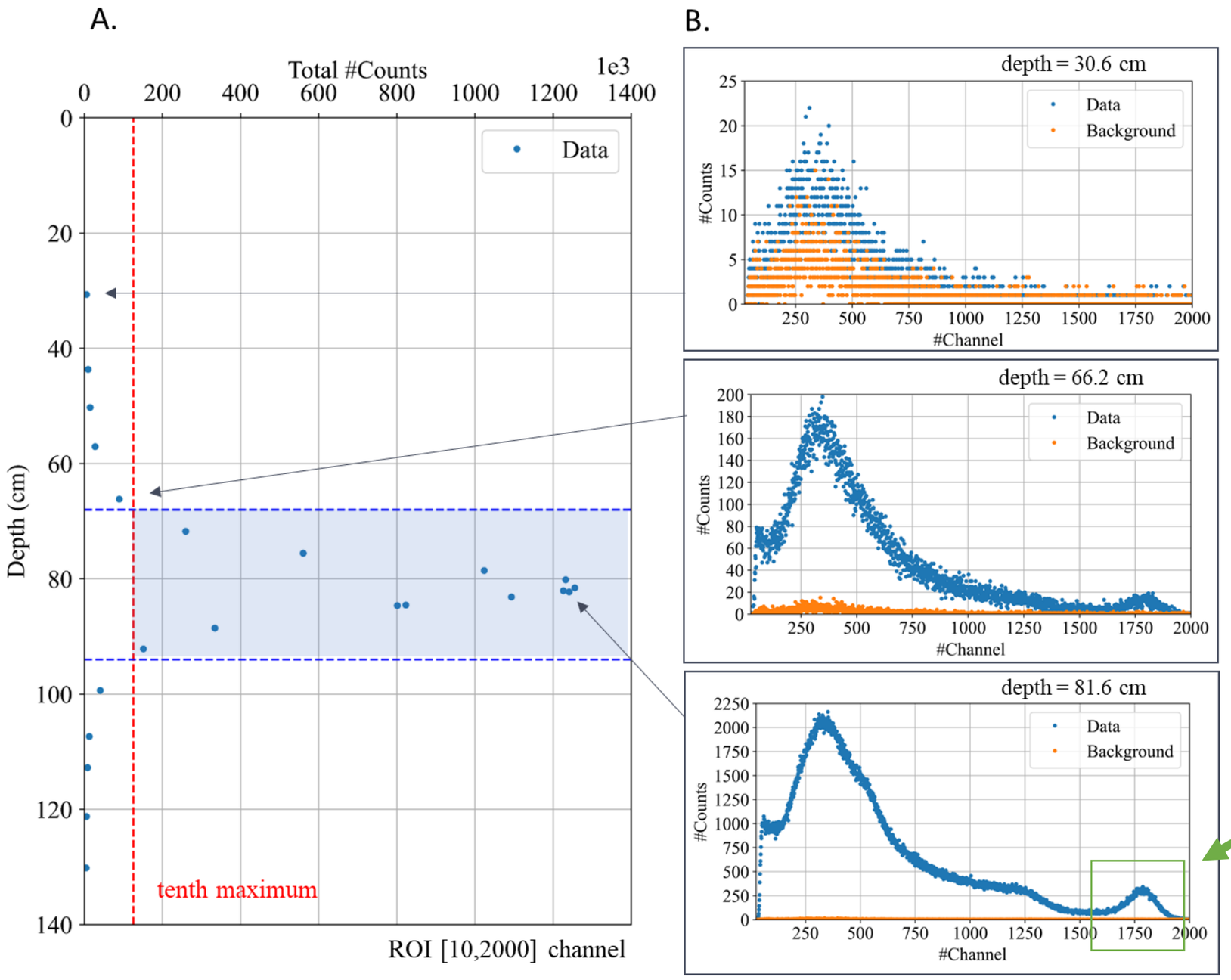

Plot 2 – *Left:* obtained total gamma-ray depth profile for a ^{137}Cs point source; *Right*: obtained gamma-ray spectra at specific depth positions in the rig (1h each point).

Region-of-interest (ROI)

^{137}Cs photopeak

Experimental work

Assessment of underground sources in blind-tubes: ^{137}Cs @ 662 keV gamma-ray depth profile

Plot 3 – Example of an obtained photopeak ^{137}Cs @ 662 keV fitting analysis.

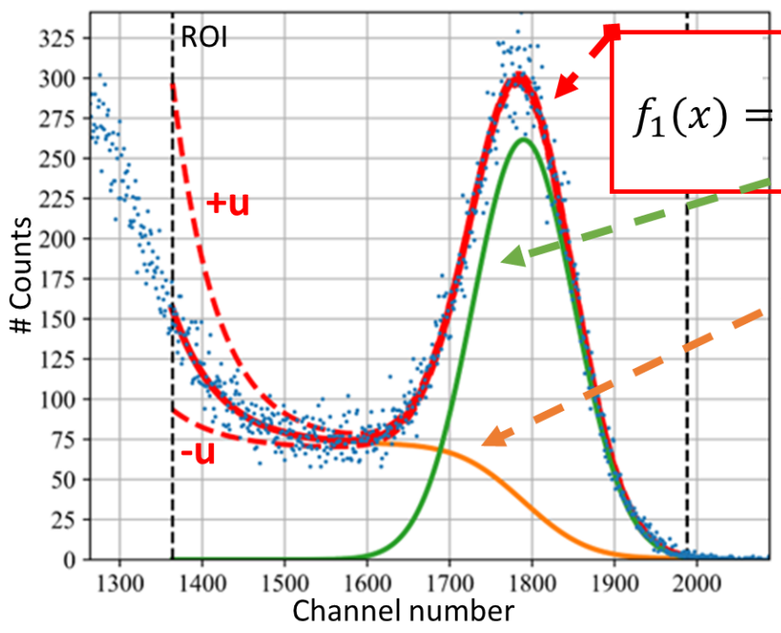

$$f_1(x) = \mathrm{A}e^{-\frac{(x-\mu)^2}{2\sigma^2}} + \mathrm{AB}\,erfc\left(\frac{x-\mu}{\sigma\sqrt{2}}\right) + \mathrm{ACe}^{\frac{x-\mu}{\mathrm{T}\sigma}}\,erfc\left(\frac{x-\mu}{\sigma\sqrt{2}} + \frac{1}{\mathrm{T}\sqrt{2}}\right) + \mathrm{b}$$

$x \equiv$ channel number

ROI = [1364,1988] channel

A = (262 ± 2) counts
μ = (1789.8 ± 0.5) channel
σ = (61.7 ± 0.4) channel
B = (0.135 ± 0.003) 1
C = (0.00009 ± 0.00005) 1
T = (-0.9 ± 0.1) 1
b = (0.7 ± 0.4) counts

$\chi_r^2 = 1.10$
df = 617.0

$$\mathrm{N_i} = \int_{\mu_i - n}^{\mu_i + n} \mathrm{G}_i(x)\mathrm{d}x$$
$$\mathrm{uN_i} = \sqrt{\mathrm{N_i}}$$

Experimental work

Assessment of underground sources in blind-tubes: ^{137}Cs @ 662 keV gamma-ray depth profile

- A typical profile can be described mathematically by a continuum 1D point-spread-function (PSF) model.

Figure 12 – Example of analysis of stellar populations in crowded stellar fields.

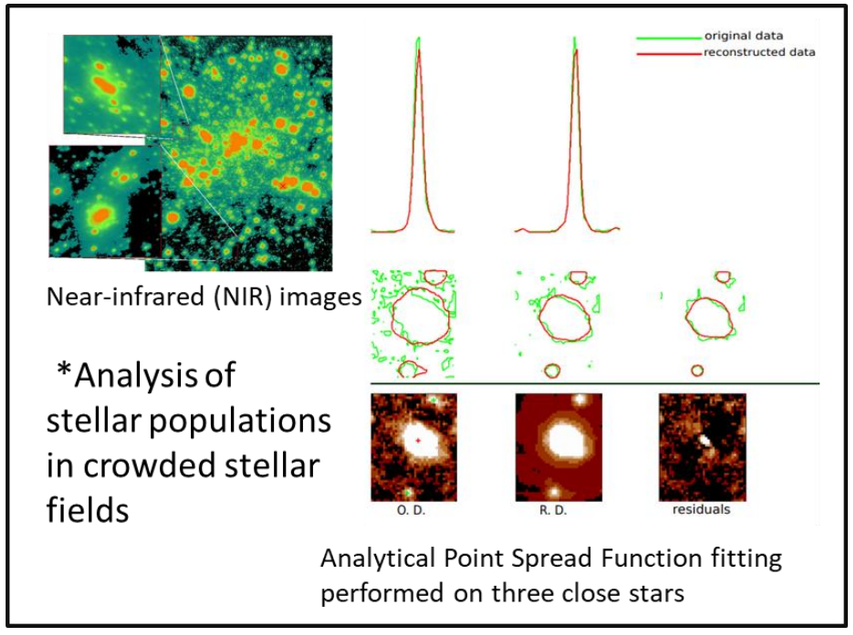

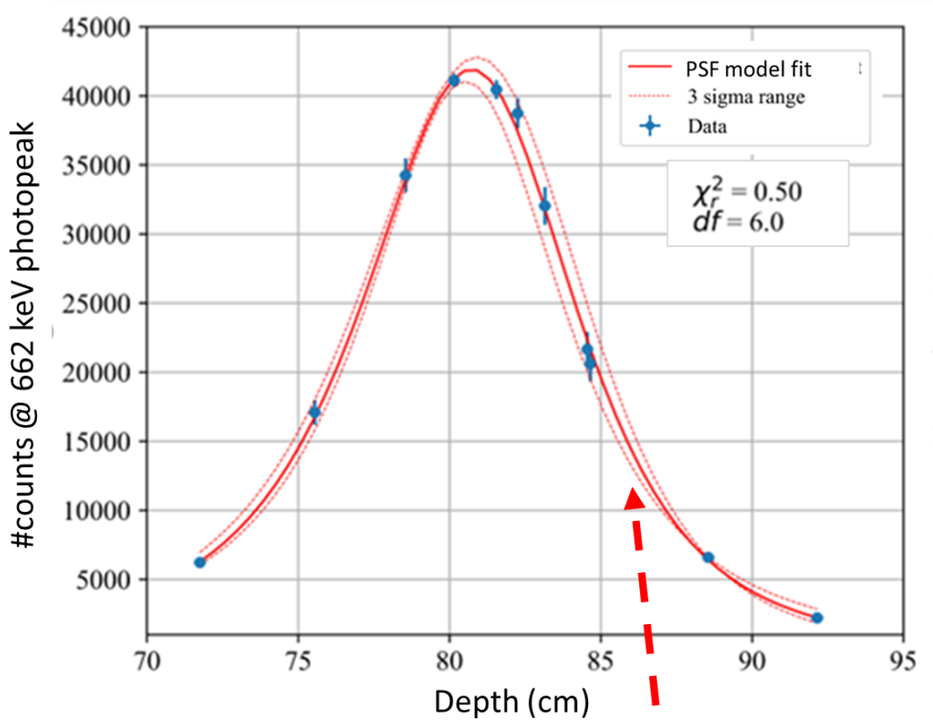

Plot 4 – Obtained photopeak ^{137}Cs @ 662 keV gamma-ray depth profile and 1D PSF fit (1h each point).

$$A = (41923 \pm 293) \text{ counts}$$
$$d = (80.7 \pm 0.1) \text{ cm}$$
$$w = (6.0 \pm 0.4) \text{ cm}$$
$$\beta = (1.7 \pm 0.1)\ 1$$
$$\gamma = (0.015 \pm 0.003) \text{ cm}^{-1}$$

$$f_2(x) = A\left(1 + \frac{(x-d)^2}{s(x)^2}\right)^{-\beta} \quad with \quad s(x) = \frac{2w}{1 + e^{\gamma(x-d)}}$$

Moffatt peak-shape function

$x \equiv$ depth (cm)

Future work

A – Look for complex scenarios:

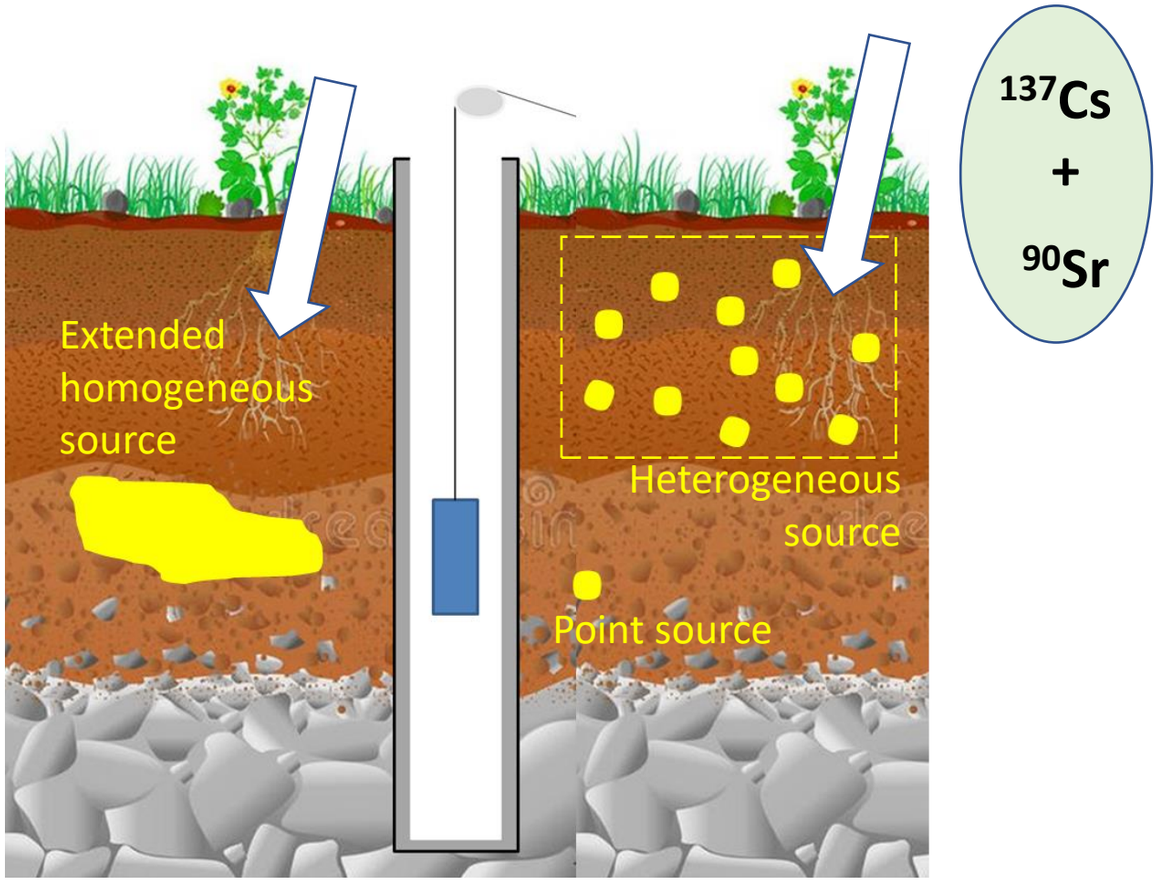

B – In field test trials.

TRANSCEND

Transformative Science and Engineering for Nuclear Decommissioning

Patent: Elísio, S., Joyce, J. M., 29 September 2022, *Method and Apparatus for Determining Attributes of a Source of Radiation*, P347121GB/CAB.

Soraia S. C. Elisio (Lancaster University)
s.elisio@lancaster.ac.uk

Malcolm J Joyce (Lancaster University)
James Graham (NNL)
Tom Calverley (Sellafield Ltd.)

Thank you

Poster “Blind tube monitoring instrument to improve the characterization of underground radioactive plumes”

Future work

A – Look for complex scenarios:

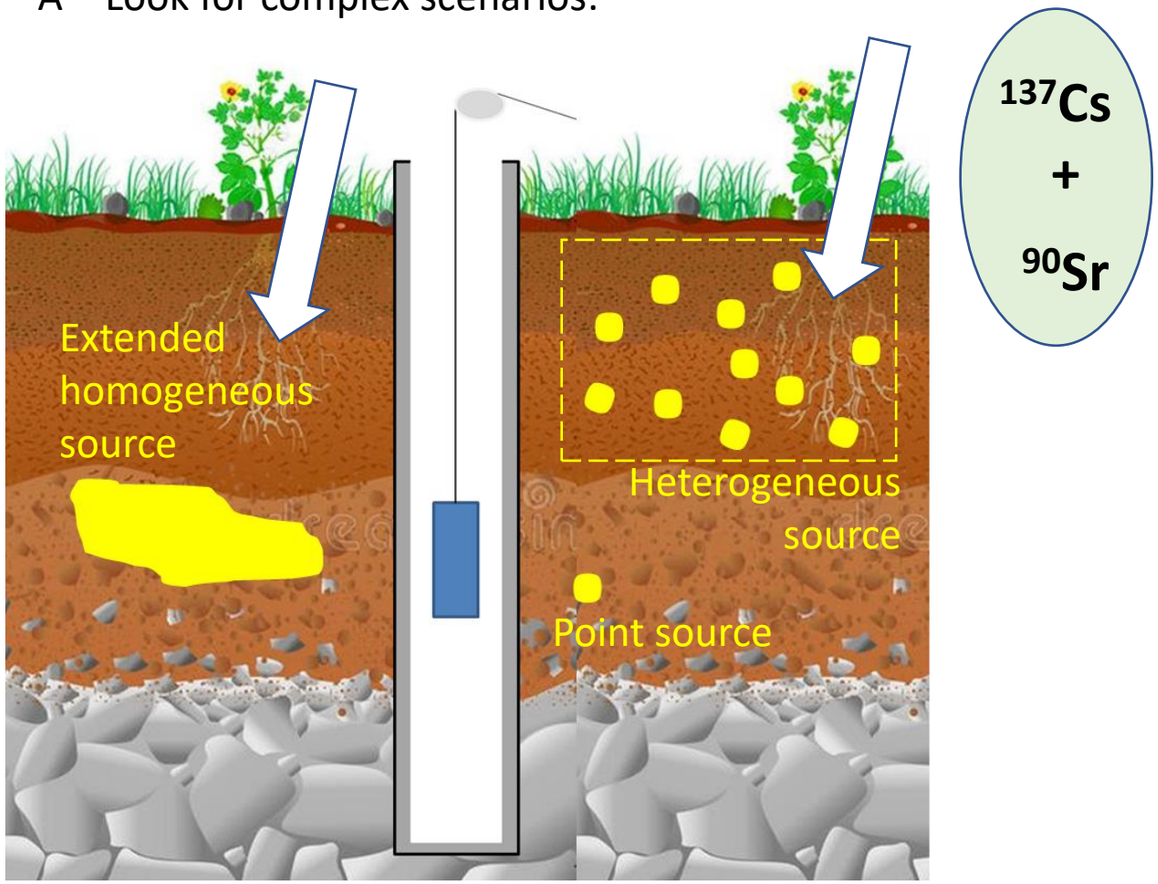

^{137}Cs + ^{90}Sr

B – In field test trials.

Plot 3 – Peak-to-total analysis obtained from gamma-ray spectra with ^{137}Cs + ^{90}Sr point sources.